2012

# Rotationally Inelastic Collisions of Helium with the NaK Molecule

Ruth Fraser Malenda
*Lehigh University*

# Rotationally Inelastic Collisions of Helium with the NaK Molecule

by

Ruth Fraser Malenda

A Dissertation

Presented to the Graduate and Research Committee

of Lehigh University

in Candidacy for the Degree of

Doctor of Philosophy

in

Physics

Lehigh University

September 2012

Approved and recommended for acceptance as a dissertation in partial fulfillment of the requirements for the degree of Doctor of Philosophy.

Ruth Fraser Malenda
Rotationally Inelastic Collisions of Helium with the NaK Molecule

_____
Date

Committee Members:

_____
A. Peet Hickman, Committee Chair

_____
John P. Huennekens

_____
Gary G. DeLeo

_____
Dimitrios Vavylonis

_____
Kamil Klier

# Acknowledgements

I would first like to thank my family. They have been a constant source of love and support throughout all my schooling. My parents have helped me move, had me over every Sunday for dinner and and listened intently to all my trials, triumphs and science speak. My father has shown me by example how to succeed in academia. My mum has been an inspiration as a mother, balancing work, home and family demands. I would also like to thank my sisters for all the joy and happiness they have brought to this journey. Helen reminds me to enjoy life and to take time to see the world. Whenever I am stressed and need to fix a problem, she is the perfect combination of smart and goofy to help me through. Margariete will always be my baby, despite the talented, caring young woman she has grown into. Her love of art and music teach me to appreciate the things in life outside of science. Finally, I would like to thank Stephen. He has been there for me on more days than I can count. He helped me through qualifiers, rescued me from myself on stressful days, and always knew when I needed a sandwich, some Star Trek, or just a hug. Without the endless love and encouragement of these people, I would not be who I am today.

I would also like to thank my research advisor, Dr. Hickman. I began working with Dr. Hickman six years ago as an REU. During this time I have worked on a number of projects, including the dissociative recombination of $N_2H^+$, $C_3H_3^+$ and $HCNH^+$ as well as scattering of He and NaK. Each experience was an opportunity to learn how to approach a new problem. Under his guidance I have learned a great deal about the scientific process, computational techniques, and atomic and molecular physics. His knowledge and insight have been invaluable throughout this process and I cannot thank him enough.

I would also like to thank my Ph.D. committee; Dr. Hickman, Dr. Huennekens, Dr. DeLeo, Dr. Vavylonis, and Dr. Klier, for attending my many meetings, reading and correcting this dissertation, and giving advice and suggestions about how to make this project the best it could be. Dr. Huennekens took great pains to explain

the experimental procedure and results to my non-experimental-self. Dr. DeLeo was my advisor for the NSF GK–12 program during my first two years at Lehigh. He taught me how to make science fun and interesting for children of all ages and gave me the opportunity to explore education in new and exciting ways. I would also like to thank our collaborator Dr. Dahbia Talbi. She has been an invaluable resource, as well as a friend whose visits I look forward to every summer. I must also acknowledge the help and insight of Dr. Fabien Gatti and Dr. Hans-Dieter Meyer. Though I have never had the pleasure of meeting them in person, without their help the lack of agreement between the couple channel and MCTDH methods would have remained a mystery.

Finally I would like to thank all the friends I have made during my time at Lehigh. The members of my research group have always been there with a laugh when things got too serious and frustrating. From the old crew who showed me the ropes Steve Sweeney, Brett McGeehan, Seth Ashman, Chris Wolfe, and especially Dave Kashinski to the new school Josh Jones, Carl Faust, and Kara Richter, I could not have made it through the day-to-day without them. I would also like to thank the other students in my year who helped me through classes and qualifiers, particularly Jon Poplawsky and Daniel Jackson. I learned so much about myself working with them that still gets me by to this day. Finally I would like to thank all the girls I lived with over the years; Amber Marsh, my first grad school roommate, Tina Aragona, Laura Kelley, and (practically) Kara Richter. Thank you for all the wonderful memories, the birthdays, holidays, and all the good times.

Thank you to everyone I mentioned above and those I am sure I forgot. I would not have made it through this journey without you.

This material is based upon work supported by the National Science Foundataion under Grant Number 0968898.

# Table of Contents

# List of Figures

# List of Tables

# Abstract

Cross sections for rotationally inelastic collisions of He with the NaK molecule in the ground ($X^1\Sigma^+$) and first excited ($A^1\Sigma^+$) electronic states have been calculated. Electronic structure calculations were performed with the GAMESS code to determine potential surfaces. For most of the calculations, the NaK bond length was fixed at the equilibrium value. The coupled channel scattering formalism developed by Arthurs and Dalgarno was used with the potential surfaces to calculate cross sections for rotational energy transfer. The computer code was modified to calculate also the collisional transfer of orientation and alignment. These theoretical results have been compared with available experimental measurements of the $A^1\Sigma^+$ state collisional rate constants. Experimental data for the ($A^1\Sigma^+$, $v = 16$, $j = 14$) state show a strong propensity for transitions with even values of $\Delta j$. The theoretical calculations using the potential calculated with the equilibrium bond length of NaK do not show this propensity, but these calculations correspond to an initial state of $v = 0$. Recent calculations have determined the potential surface for several different values of the NaK bond length $r_{\mathrm{v}}$. Preliminary scattering results using a potential averaged over the range of values of $r_{\mathrm{v}}$ appropriate for $v = 15$ show a much greater propensity for even values of $\Delta j$. In addition, the magnitudes of estimated rate constants for several transitions are in good agreement with experiment.

These results suggest that the propensity for even $\Delta j$ rotational transitions of NaK ($A^1\Sigma^+$) may depend strongly on the vibrational level.

In a separate study, the time-dependent MCTDH wavepacket method and the time-independent coupled channel method were compared. Rotationally inelastic cross sections using the same model potential were calculated using both methods, and excellent agreement was obtained.

# Chapter 1

# Introduction

## 1.1 Motivation

An active experimental program at Lehigh University has probed the behavior of heteronuclear alkali molecules [1–6]. Our interest in this project was sparked by experimental results describing inelastic collisions between electronically excited NaK molecules and various collisional partners [2]. Of particular note for the present work are rotationally inelastic collisions between NaK and He or Ar; for example

$$\text{He} + \text{NaK}(v, j, m) \rightarrow \text{He} + \text{NaK}(v, j', m'),$$

where $v$ is the vibrational quantum number, and $j$ and $m$ are the quantum numbers that describe the rotational state of the molecule. The primes indicate the new angular momentum quantum numbers after an inelastic collision occurs. In the experiments at Lehigh [2], the NaK molecule may be either in the ground electronic state ($X^1\Sigma^+$) or the first excited state ($A^1\Sigma^+$) [7]. The focus is on the collisions in which the electronic and vibrational states do not change. In this introduction, we will discuss the experimental methods and results, give a brief background of the

rotational quantum numbers, and discuss future work the experimental group plans to do.

There is a large body of literature on rotationally inelastic collisions [8, 9], but Dr. Huennekens' group has investigated some features that have received less attention. Several aspects of their experimental work are of particular interest. For several electronic and vibrational states of NaK, Dr. Huennekens' group has found a propensity for rotationally inelastic collisions to have even values of $\Delta j$; the odd $\Delta j$ transitions are observed but are less probable than $\Delta j$ even transitions. Homonuclear diatomic molecules have an exact selection rule for $\Delta j$ even. This restriction is based on parity due to the symmetry of the molecule with respect to inversion about the center. The propensity found in NaK may indicate an approximate reflection symmetry. Another aspect of the experimental work is the investigation of how collisions that change $j$ affect the $m$ quantum number. A method known as polarization spectroscopy [10] is used to measure the tendency of the orientation of the NaK molecule to be preserved during collisions. A more precise definition of orientation will be given in Section 1.3, but generally speaking orientation is related to the average value of the $m$ quantum number. This thesis describes the theoretical calculations that are intended to provide a quantitative explanation of the experimental results.

Unless otherwise specified, this work will use atomic units. In particular, units of bohr ($a_0$) will be used for length and hartree ($\mathrm{E_h}$) units will be used for energy. The experimental work discussed here is conducted in a heat pipe oven that is heated to roughly 600 K. The mean thermal energy of this temperature distribution is 0.0020 $\mathrm{E_h}$, an energy which will be reference frequently throughout this dissertation.

## 1.2 Overview of Experimental Method

The recent experimental work of Wolfe *et al.* [2] is based on a pump-probe laser excitation scheme to excite NaK molecules contained within a heat pipe oven (a vessel containing gas phase alkali atoms and molecules and noble gas atoms). The essential features of the pump-probe scheme are illustrated in Figure 1.1, which shows schematic potential curves for the ground and excited states of NaK. A pump laser is fixed on a transition from one rovibrational level of the ground state to a particular $(v, j)$ rovibrational level of the intermediate state. The probe laser is then used to excite the molecule from intermediate state levels to levels of a higher excited state. The probe laser is scanned over a range of wavelengths, and it is absorbed

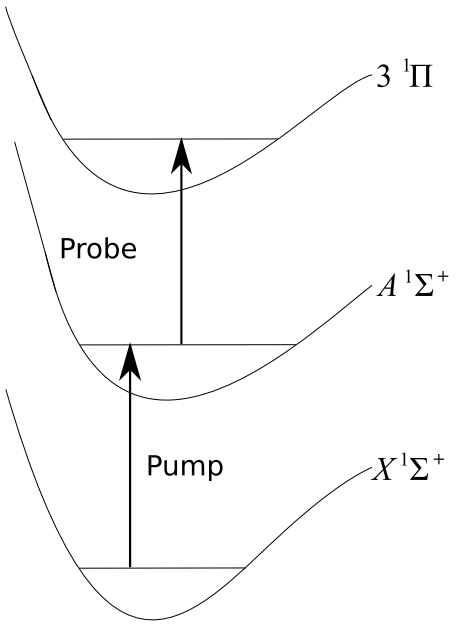


**Figure 1.1:** Diagram of a typical pump and probe scheme for NaK. The pump laser excites transitions out of the ground state to the intermediate state, $A^1\Sigma^+$ $(v,j)$ level. The probe laser excites transitions to the highest state, $3^1\Pi$.

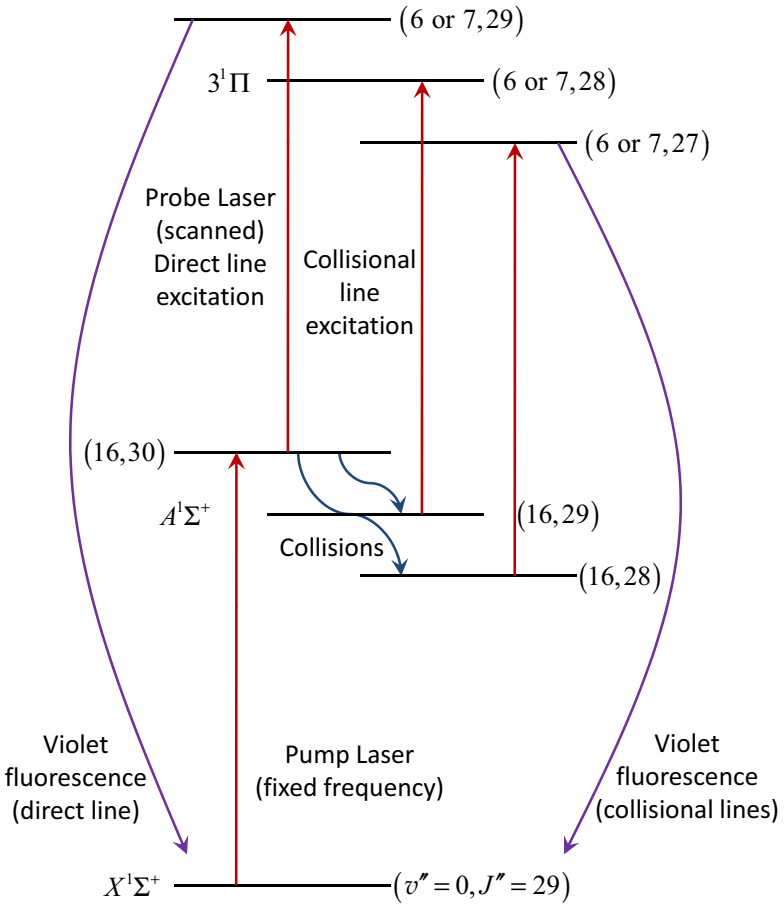


**Figure 1.2:** Diagram of the pump and probe scheme used by Wolfe *et al.* [2]. The pump laser excites transitions out of the ground $X^1\Sigma^+$state of NaK to the $A^1\Sigma^+$ state. While in the intermediate $A^1\Sigma^+$ state the molecule can undergo collisions. The probe laser excites the collisionally populated $A^1\Sigma^+$levels to the highest $3^1\Pi$ state, giving information about the population in the $A^1\Sigma^+$ state. [2]

whenever its frequency matches a transition to an upper state, assuming the lower level of the transition is populated. The absorption is detected by monitoring the fluorescence from the upper electronic state as a function of the probe laser frequency.

The pump-probe method is commonly used to provide information about the

energy level structure of the highest electronic state. An alternative scheme used to study the effect of collisions in the usual pump-probe method is illustrated in Fig. 1.2. In the experiments conducted by Wolfe *et al.* [2], a tunable dye laser was used to excite the NaK from the $X^1\Sigma^+$ground state to the a specific ($v$,$j$) level in the $A^1\Sigma^+$ state and was fixed on this transition. Collisions with the Ar buffer gas populated neighboring levels $A^1\Sigma^+$ ($v$,$j'$) levels. The probe laser was scanned over a range of wavelengths near the direct transition from the $A^1\Sigma^+$ state (16,30) level to the $3^1\Pi$ state. The probe laser also excites transitions from the collisionally populated levels $A^1\Sigma^+$ ($v$,$j'$) to the $3^1\Pi$ state. The violet fluorescence emitted by the NaK molecule as it radiates from the $3^1\Pi$ state back down to the ground state is monitored.

A typical violet fluorescence spectrum (probe laser scan) is shown in Fig. 1.3 for an experiment which excites NaK molecules to the $(v, j)$ = (16,30) level of the $A^1\Sigma^+$ state [7] using the pump laser. The strong peak labeled "Direct" near 12496.4 $cm^{-1}$ corresponds to a transition from the directly pumped level $(v, j)$ = (16,30) of the $A^1\Sigma^+$ state to the (6,29) or (6,31) level of the $3^1\Pi$ state. There are many other peaks in Fig. 1.3. These peaks are weak and are related to collisions of the NaK molecules with atomic perturbers. The perturbers are alkali atoms (potassium and sodium) and atoms of a buffer gas, either helium or argon, which is introduced into the heat pipe oven to keep the ractive alkali vapor away from the windows. Wolfe *et al.* [2] used the full spectra shown in Fig. 1.3, including the satellite peaks, to obtain information about collisions. The fluorescence from the transitions originating from collisionally populated levels in the $A^1\Sigma^+$ state accounts for the weak satellites in Fig. 1.3.

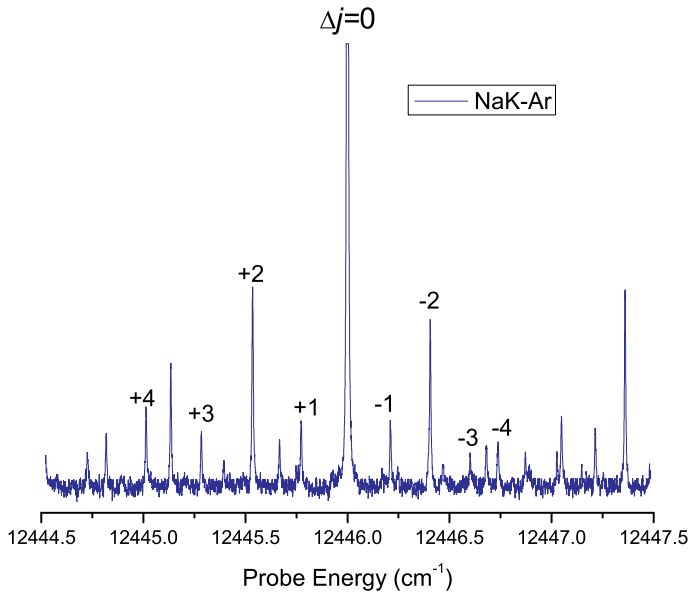


**Figure 1.3:** Scan of fluorescence spectroscopy. The peak labeled "Direct" has a much higher intensity than the others and has been truncated. The smaller peaks are due to fluorescence from the transitions originating from collisionally populated levels in the $A^1\Sigma^+$ state. [2]

The smaller peaks in Fig. 1.3 give information about rotationally inelastic collisions of NaK molecules in the $(v, j)$ rovibrational levels in the $A^1\Sigma^+$ state. Each satellite line corresponds to a transition from a collisionally populated $(v, j')$ level of the $A^1\Sigma^+$ state to the $3^1\Pi$ state. For example, Fig. 1.2 shows a collision that changes the rotational level of the NaK molecule from the directly pumped (16, 30) level to (16, 29). The transition out of this collisionally populated level corresponds to the $\Delta j = -1$ peak shown in Fig. 1.3. The ratio of intensities of the collisional to the direct violet fluorescence is approximately equal to the ratio of the steady-state populations of the rotational levels of the $A^1\Sigma^+$ state populated either by collisions or directly by the pump laser. Experimental spectra can be used to obtain infor-

mation about the amount of population that was transferred to the various $j'$ levels by one collision with an atomic perturber.

Experimental results from Wolfe *et al.* [2] for the rate constant for $j$ changing collisions of NaK with Ar are shown in Fig. 1.4. The initial rotational level was $j = 30$. The data show a clear propensity of transitions with even $\Delta j$, but not a strict selection rule. For a homonuclear diatomic molecule, the rates for transitions with odd $\Delta j$ must be zero. For NaK + Ar, the rate constant for $\Delta j = 2$ is roughly twice that for $\Delta j = 1$ and $\Delta j = 3$.

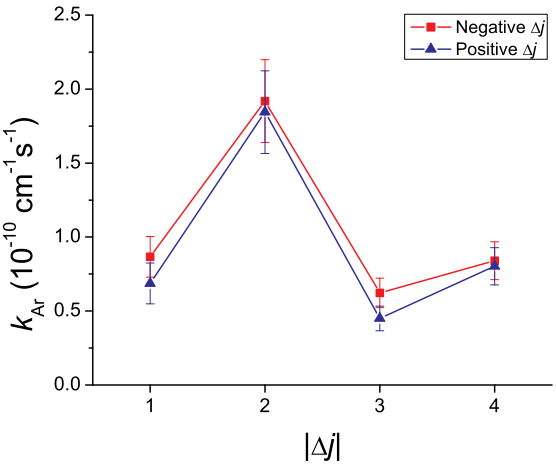


**Figure 1.4:** Rate constant for the transfer of population $j \rightarrow j' = j + \Delta j$ due to collisions of NaK with Ar as a function of $\Delta j$. The initial rotational level was $j = 30$. A propensity for $\Delta j$ even can be seen by the larger rate constant for $\Delta j = 2$.

## 1.3 Orientation and Alignment

Experiments were also conducted to investigate the change in the $m$ sublevels of the NaK molecules due to collisions with atomic partners. Figure 1.5 shows several possible examples of distributions of $m$ for $j = 2$. The height of each bar represents the number of molecules in each of the possible $m$ levels. When there are no other external influences on the system, the angular momenta of all the molecules in the system are randomly oriented in space. Panel (a) shows an $m$ distribution in which all the $m$ sublevels are uniformly populated, indicating the random direction of $j$. Certain experimental techniques [11] can be used to orient the angular momenta in space and populate the $m$ sublevels unevenly. The other panels in Fig. 1.5 show a variety of distributions that will be described below.

Roughly speaking, an ensemble of molecules has an orientation if the angular momentum vectors of all the molecules tend to point in the same direction. The

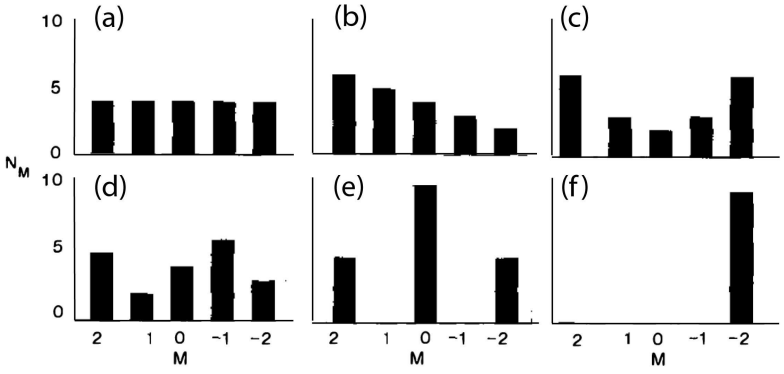


**Figure 1.5:** Various examples of distributions of $m$ for $j = 2$ as discussed by Green and Zare [12]. Panel (a) show a population uniformly distributed among the $m$ sublevels. Panel (b) shows a population with orientation. Panel (c) shows a population with alignment. Panels (d) and (e) show other $m$ distributions of population. Panel (f) shows a linear combination of the distributions in the other panels.

exact definition [12] can be explained using the well-known vector model for angular momentum, which is shown in Fig. 1.6 applied to the NaK molecule. The angular momentum of the NaK molecule is labeled as $j$. This vector has length $\hbar\sqrt{j(j+1)}$ and is precessing around the $z$-axis with fixed cone angle $\theta$. The projection of the angular momentum onto the $z$-axis is $m\hbar$. When studying $m$ changing collisions experimentally, it is important to note how the $z$-axis is defined for a particular setup. There are two main setups commonly used, the beam and the cell experiment. The beam experiment directs a beam of incident particles towards the targets. In this type of experiment, the $z$-axis is defined along the direction of the particle beam. The experiments performed by Huennekens' group more closely resemble a cell environment, in which the incident He atoms may impact the NaK targets from any direction within the heat pipe. In experiments with a circularly polarized pump laser the $z$-axis is taken to be the direction of propagation of the laser beam. The orientation is defined by

$$\langle \cos\theta \rangle = \left\langle \frac{m}{\sqrt{j(j+1)}} \right\rangle, \tag{1.3.1}$$

where the average is over the ensemble of molecules. Panel (b) of Fig. 1.5 shows an ensemble with a non-zero orientation.

Another measure of the distribution of the $m$ levels of an ensemble of molecules is known as the alignment, which is defined [12] as

$$\text{Alignment} = \left\langle \frac{1}{2} \frac{3m^2 - j(j+1)}{\sqrt{j(j+1)\left[j(j+1) - \frac{3}{4}\right]}} \right\rangle. \tag{1.3.2}$$

In the limiting case where $j \gg 1$, one can neglect the $\frac{3}{4}$ inside the square root and

transform Eq. 1.3.2 into

$$\text{Alignment} \approx \frac{1}{2}\left\langle \frac{3m^2}{j(j+1)} - 1 \right\rangle = \left\langle \frac{3\cos^2\theta - 1}{2} \right\rangle . \tag{1.3.3}$$

The distribution in Panel (c) of Fig. 1.5 is a case of population with alignment, which is symmetric. Note that average value of $m$ in this case is zero meaning that the orientation is zero, even though the population distribution is non-uniform.

In general, the distribution of $m$ values may be converted to a distribution of $\theta$ using $\cos\theta = m/\sqrt{j(j+1)}$. Then in the limit of large $j$, this distribution of $\theta$ can be described by an expansion of Legendre polynomials in $\cos\theta$. The orientation and alignment are then just the ensemble averages of the Legendre polynomials $P_1(\cos\theta)$ and $P_2(\cos\theta)$. This idea can be extended to higher moments of the distribution. The remaining panels in Fig. 1.5 show other $m$ distributions of population that can be described by these higher moments. Panels (d) and (e) for instance are representations of linear combinations of population with ensemble averages of $P_3(\cos\theta)$ and $P_4(\cos\theta)$, respectively. Alignment and the other even order moments do not distinguish between $+m$ and $-m$ and are symmetric about $m = 0$. Panel

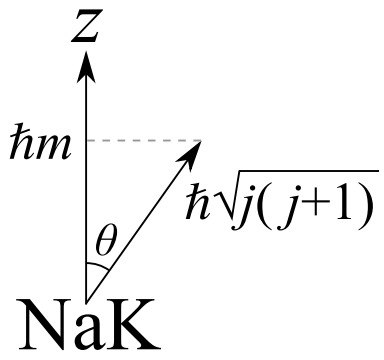


**Figure 1.6:** Vector diagram of rotational angular momentum in NaK.

(f) shows a superposition of the first five moments. These moments will be used to describe the distribution of population among the $m$ sublevels of NaK molecules that have undergone collisions.

## 1.4 Polarization Spectroscopy

Dr. Huennekens' group studies the effect of collisions on orientation of the NaK molecule using the technique of polarization spectroscopy [10]. As explained earlier, molecules are excited to selected rovibrational levels of the $A^1\Sigma^+$ state of NaK. In order to study how orientation is affected by collisions, the system is first given an uneven distribution of $m$ in the $A^1\Sigma^+$ state. To achieve this, the pump beam is circularly polarized. The $z$-axis for a circularly polarized beam is defined in the direction of the laser beam propagation. The arrows in Fig. 1.7 represent the transitions allowed due to selections rules when the pump beam is circularly polarized. The circularly polarized light selectively induces transitions for which $\Delta m = 1$ is positive. Thus, the higher $m$ levels have been selectively populated, creating an average $m$ which is not zero, and therefore an orientation. The ground state is also unevenly depleted, creating an orientation in the ground state as well.

After the orientation is established in the molecules in the $(v, j)$ rovibrational

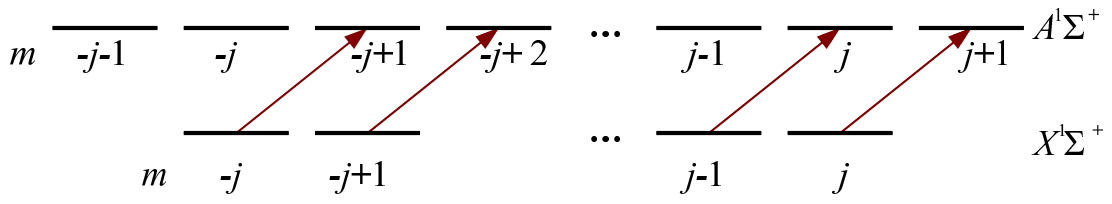


**Figure 1.7:** Circularly polarized beam selectively populates the higher $m$ levels of the intermediate state.

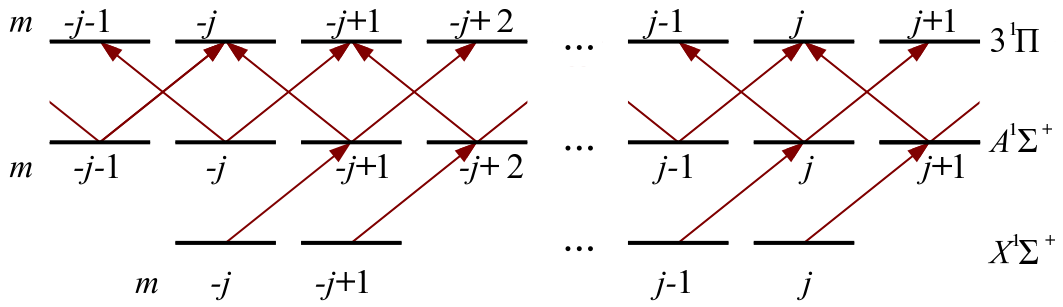


**Figure 1.8:** Selection rules of linearly polarized probe beam. This diagram shows how a linearly polarized probe beam is used to determine the orientation of the intermediate $A^1\Sigma^+$ state. The left circularly polarized pump beam has selectively populated the higher $m$ levels of the $A^1\Sigma^+$ state, as represented by the arrows in the lower transition. The selection rules of the left and right portions of the linearly polarized probe beam are represented as arrows in the higher transition. The uneven population of the $m$ levels causes the right and left component of the probe beam to be absorbed and refracted differently, resulting in a slight ellipticity to the probe beam.

level of the $A^1\Sigma^+$ state, several possible events may occur. Some molecules may be excited to the higher state by the probe; these transitions contribute to the direct line. Other molecules may experience a collision that changes the rovibrational level to $(v, j')$ before being excited to the highest state. These molecules will contribute to a satellite line. We consider those molecules that are transferred to the $(v, j')$ rovibrational levels by collisions and ask what percent of the orientation originally present is retained after the collision.

Polarization spectroscopy measures the amount of orientation that is maintained during a collision. The probe beam passes through a linear polarizer before entering the heat pipe. Linearly polarized light can be thought of as equal parts left and right circularly polarized light. The arrows in the upper transition in Fig. 1.8 represent the selection rules for the transition from the $A^1\Sigma^+$ state to the highest state. Recall that the higher $m$ levels of the intermediate $A^1\Sigma^+$ state have a larger population

due to the selective population by the pump beam. This causes the left and right portions of the probe beam to be absorbed and refracted unequally. Thus, when the probe beam exits the heat pipe, it has a slight elliptical polarization.

Before the probe beam is detected, it passes through a second polarizer oriented at 90° to the original polarizer. If both components of the probe beam were equally attenuated as they passed through the system, then none of the probe beam would reach the detector. However, a probe transition from the directly populated level $(v, j)$, which has an orientation due to the pump beam, will allow some transmission through the second polarizer and,therefore, will be detected. In this instance, the probe beam has been tuned to a transition from a level that has deliberately been oriented. The probe beam acquires a slight elliptical polarization, allowing it to be partially transmitted through the second polarizer. If a collision occurs that causes a change in the rotational level $(j \rightarrow j')$ and also preserves the orientation, the transition from that $(v, j')$ level will also be detected. However, a collision that changes the angular momentum $(j \rightarrow j')$ but destroys the orientation will not cause the probe beam to be elliptically polarized, and will not be detected. The ratio of intensities of the detected probe beam for the collisional to the direct excitation is proportional to the ratio of the product of the population of the levels and the average $m$. By knowing the collisional transfer of population from the fluorescence spectroscopy experiments, the collisional transfer of orientation can be determined.

Figure. 1.9 shows the results of experiments studying collisions of Ar with NaK. The plot shows the fraction of orientation destroyed by these collisions, $f_{\mathrm{Ar}}$. Roughly $40\% - 75\%$ of the orientation created in the direct level of the intermediate $A^1\Sigma^+$ state was transferred to $(v, j')$ levels during collisions with Ar.

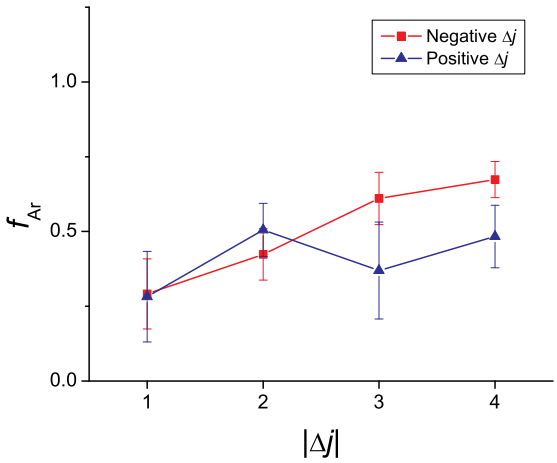


**Figure 1.9:** Experimental results of NaK collisions with Ar. The fraction of orientation destroyed in a collision, $f_{\mathrm{Ar}}$, that transfers population from state $j$ to $j'$ is shown as a function of $\Delta j$. Collisions with Ar cause approximately $40\% - 75\%$ of the orientation to be preserved.

## 1.5 Current Experiments

Wolfe's original experiments [2] involved collisions of NaK molecules in the $A^1\Sigma^+$ state with Ar and K perturbers. Both systems are more difficult to treat theoretically than a simpler system such as He + NaK. For this reason, Dr. Huennekens' group is currently conducting a series of experiments involving collisions of He with NaK molecules in either the $X^1\Sigma^+$ or $A^1\Sigma^+$ states. To conduct these experiments, He is used as a buffer gas in the heat pipe. Performing calculations to compare with experiment will be easier for He as the collisional partner.

Additional modifications must be made to the experimental procedures to study the $X^1\Sigma^+$ state of NaK. The experiments discussed previously involved collisions with NaK in the $A^1\Sigma^+$ state, which was only populated via the pump beam. The $X^1\Sigma^+$ state of NaK is thermally populated within the heat pipe. A V-type laser

method shown in Fig. 1.10 is used to study changes in $j$ of the ground state due to collisions. As before, the pump laser is fixed on a single transition out of the ground state, however in this setup the pump beam is chopped. Chopping modulates the population in a particular $j$ level of the ground state. Other $j$ levels will be thermally populated, but by chopping the pump beam a particular $j$ level is isolated and only signal modulated at the same frequency as the chopper corresponds to the "tagged" level. Any population that is transferred into the other $j'$ levels due to collisions of Ar with NaK molecules in the tagged $j$ level will be modulated at this frequency.

The probe laser is used to excite transitions out of the ground state, and the fluorescence is monitored. Transitions from the ground state include the collisionally populated $j'$ levels, which again appear as satellite lines and are used to determine the amount of population transferred to other $j'$ levels by collisions.

The modifications made to the polarization experiment will be similar to those

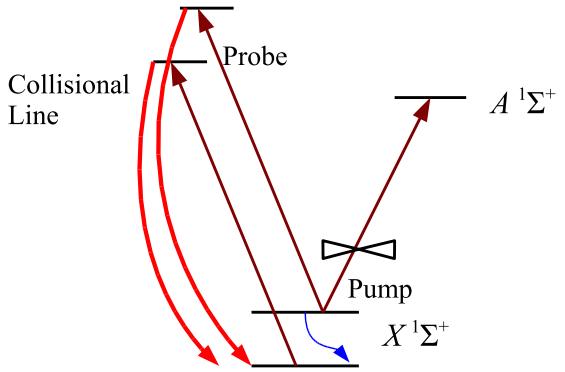


**Figure 1.10:** Diagram of the V-type scheme used by Dr. Huennekens' group to study rotationally inelastic collisions of ground state NaK using fluorescence spectroscopy. The pump beam is chopped so that the population in a particular $j$ level of interest will be modulated at a known frequency. Fluorescence modulated at the same frequency gives information about transitions out of various $j'$ levels excited by the probe beam.

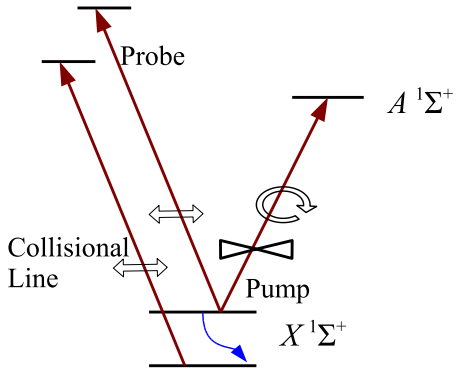


**Figure 1.11:** Diagram of the V-Type scheme used by Dr. Huennekens' group to study orientation transfer during rotationally inelastic collisions of ground state NaK using polarization spectroscopy. The pump beam is left circularly polarized to create an orientation in the ground state and chopped to "tag" a particular $j$ level. Polarization signal detected from the probe beam will only be collected if it is modulated at the same frequency as the chopper.

made to the fluorescence spectroscopy and can be seen in Fig 1.11. In addition to being left circularly polarized, the pump beam is now also chopped. The ground state $j$ level is tagged and oriented using modulated left circularly polarized light of the pump laser. The linearly polarized probe laser is then scanned over transitions from the ground state. Any signal from the probe laser that has been slightly elliptically polarized by the vapor will partially pass through the crossed polarizer where the laser exits the heat pipe, indicating an orientation of the $j$ level. Polarization signal detected from the probe beam will only be collected if it is modulated at the same frequency as the chopper. Again, the relative strength of the direct line to satellite lines gives the relative product of the population and average $m$.

These planned experiments are expected to provide data that can be directly compared with the calculations presented in this dissertation.

# Chapter 2

# Theory

## 2.1 The Schrödinger Equation

The basis for quantum mechanics of atoms and molecules is the Schrödinger equation. The time-independent Schrödinger equation (TISE) is written as

$$\hat{H}\Psi = E\Psi, \tag{2.1.1}$$

where $\hat{H}$ is the Hamiltonian operator, $\Psi$ is the wave function describing the quantum mechanical state of the system, and $E$ is the energy of the system in that state. $E$ are the eigenvalues and $\Psi$ are the eigenvectors of the TISE.

The Hamiltonian is the sum of operators corresponding to the kinetic, potential and any other energy terms in the system. Our work focuses on molecular systems of the general form AB + X. The Hamiltonian that pertains to this system is expressed as

$$\hat{H} = -\frac{\hbar^2}{2}\sum_{\alpha=1}^{3}\frac{\nabla_\alpha^2}{M_\alpha} - \frac{\hbar^2}{2m_e}\sum_{k=1}^{N}\nabla_k^2 + U(\mathcal{R}, \mathbf{r}_1, \ldots, \mathbf{r}_N). \tag{2.1.2}$$

The first term is the kinetic energy operator for the nuclei, where $M_\alpha$ is the mass of the $\alpha^{\text{th}}$ nucleus. The second term is the kinetic energy operator of the $N$ electrons, where $m_e$ is the electron mass. The final term $U(\mathcal{R}, \mathbf{r}_1, \ldots, \mathbf{r}_N)$ is the Coulomb potential describing the interaction between particles, where $\mathcal{R}$ collectively represents the coordinates of all the nuclei, $\mathbf{R}_1$, $\mathbf{R}_2$, and $\mathbf{R}_3$, and $\mathbf{r}_k$ $(k = 1, \ldots, N)$ describes the coordinates of the $N$ electrons. Solving Eq. 2.1.1 for this Coulomb interaction is a nontrivial task that involves treating the nuclear and electronic motion simultaneously. For all but the simplest systems, the complexity of the interactions between the particles makes finding the exact solution impossible. However, the Born-Oppenheimer approximation allows for the decoupling of the electronic and nuclear motions, which makes solving this equation managable.

### 2.1.1 Born-Oppenheimer Approximation

The physical basis of the Born-Oppenheimer approximation is the significant difference between the masses of the nuclei and electrons [13]. This mass difference allows us to make the approximation that the relatively light electrons move instantaneously compared to the relatively massive nuclei. Treating the nuclear particles as stationary allows the separation of the nuclear and electronic motion. The nuclear and electronic problems can thus be solved independently.

The Hamiltonian in Eq. 4.1.2 can be separated into nuclear and electronic parts:

$$\hat{H} = -\frac{\hbar^2}{2} \sum_\alpha \frac{\nabla_\alpha^2}{M_\alpha} + \hat{H}_{\text{elec}}(\mathcal{R}, \mathbf{r}_1, \ldots, \mathbf{r}_N). \tag{2.1.3}$$

As before, the first term is the nuclear kinetic energy operator. The second term $\hat{H}_{\text{elec}}(\mathcal{R}, \mathbf{r}_1, \ldots, \mathbf{r}_N)$ is referred to as the electronic Hamiltonian. $\hat{H}_{\text{elec}}$ describes the

motion of the electrons for a fixed set of nuclear coordinates $\mathcal{R}$:

$$\hat{H}_{\text{elec}} = -\frac{\hbar^2}{2m_e}\sum_k^N \nabla_k^2 + U(\mathcal{R}, \mathbf{r}_1, \ldots, \mathbf{r}_N). \tag{2.1.4}$$

Now it is possible to solve the electronic form of the Schrödinger equation,

$$\hat{H}_{\text{elec}}\psi_n(\mathcal{R}, \mathbf{r}_1, \ldots, \mathbf{r}_N) = E_n(\mathcal{R})\psi_n(\mathcal{R}, \mathbf{r}_1, \ldots, \mathbf{r}_N), \tag{2.1.5}$$

for a set of electronic wave functions $\psi_n$ and energies $E_n(\mathcal{R})$ for any fixed $\mathcal{R}$.

Though the problem has been significantly simplified, it is still not simple. Another point of consideration is that the electronic Schrödinger equation must be solved for all relevant nuclear positions. The total molecular wave function can be written as an expansion involving the $\psi_n$ wave functions, which are orthogonal for each fixed $\mathcal{R}$,

$$\Psi(\mathcal{R}, \mathbf{r}_1, \ldots, \mathbf{r}_N) = \sum_{n=1}^{M} \chi_n(\mathcal{R})\psi_n(\mathcal{R}, \mathbf{r}_1, \ldots, \mathbf{r}_N), \tag{2.1.6}$$

where the nuclear wave functions $\chi_n(\mathcal{R})$ will be determined by substitution into the Schrödinger equation.

Eq. 2.1.6 is now substituted into Eq. 2.1.1. The result is then multiplied by $\psi_m$ and integrated over the electronic coordinates $\mathbf{r}_k$ to yield

$$\begin{aligned}\int \psi_m(\mathcal{R}, \mathbf{r}_1, \ldots, \mathbf{r}_N)\left[-\frac{\hbar^2}{2}\sum_\alpha \frac{\nabla_\alpha^2}{M_\alpha} + \hat{H}_{\text{elec}}\right]\sum_{n=1}^{M}\chi_n(\mathcal{R})\psi_n(\mathcal{R}, \mathbf{r}_1, \ldots, \mathbf{r}_N)d\mathbf{r}_1 \ldots d\mathbf{r}_N \\ = E\int \psi_m(\mathcal{R}, \mathbf{r}_1, \ldots, \mathbf{r}_N)\sum_{n=1}^{M}\chi_n(\mathcal{R})\psi_n(\mathcal{R}, \mathbf{r}_1, \ldots, \mathbf{r}_N)d\mathbf{r}_1 \ldots d\mathbf{r}_N. \end{aligned} \tag{2.1.7}$$

The orthogonality of the electronic wave functions $\psi_m(\mathcal{R}, \mathbf{r}_1, \ldots, \mathbf{r}_N)$ and the fact that they are eigenfunctions of the electronic Hamiltonian $\hat{H}_{\text{elec}}$ allows us to write

$$\int \psi_m(\mathcal{R}, \mathbf{r}_1, \ldots, \mathbf{r}_N)\hat{H}_{\text{elec}}\psi_n(\mathcal{R}, \mathbf{r}_1, \ldots, \mathbf{r}_N)\, d\mathbf{r}_1 \ldots d\mathbf{r}_N$$
$$= \langle \psi_m(\mathcal{R}, \mathbf{r}_1, \ldots, \mathbf{r}_N)|\hat{H}_{\text{elec}}|\psi_n(\mathcal{R}, \mathbf{r}_1, \ldots, \mathbf{r}_N)\rangle = E_n(\mathcal{R})\delta_{mn} \quad (2.1.8)$$

where the $\delta_{mn}$ is the Kronecker delta function. Eq. 2.1.8 can be used in Eq. 2.1.7 to obtain

$$\frac{\hbar^2}{2}\sum_\alpha \frac{1}{M_\alpha}\sum_{n=1}^{M}\langle \psi_m(\mathcal{R}, \mathbf{r}_1, \ldots, \mathbf{r}_N)|\nabla_\alpha^2|\chi_n(\mathcal{R})\psi_n(\mathcal{R}, \mathbf{r}_1, \ldots, \mathbf{r}_N)\rangle$$
$$= [E_m(\mathcal{R}) - E]\chi_n(\mathcal{R}) \quad (2.1.9)$$

The kinetic energy operator on the right hand side of Eq. 2.1.9 acting on the wave function gives

$$\begin{aligned}
&\nabla_\alpha^2\left[\chi_n(\mathcal{R})\psi_n(\mathcal{R}, \mathbf{r}_1, \ldots, \mathbf{r}_N)\right] \\
&= \nabla_\alpha\cdot\left[\{\nabla_\alpha\chi_n(\mathcal{R})\}\psi_n(\mathcal{R}, \mathbf{r}_1, \ldots, \mathbf{r}_N) + \chi_n(\mathcal{R})\nabla_\alpha\psi_n(\mathcal{R}, \mathbf{r}_1, \ldots, \mathbf{r}_N)\right] \\
&= \left[\nabla_\alpha^2\chi_n(\mathcal{R})\right]\psi_n(\mathcal{R}, \mathbf{r}_1, \ldots, \mathbf{r}_N) + 2\left[\nabla_\alpha\chi_n(\mathcal{R})\right]\cdot\nabla_\alpha\psi_n(\mathcal{R}, \mathbf{r}_1, \ldots, \mathbf{r}_N) \\
&\qquad + \chi_n(\mathcal{R})\nabla_\alpha^2\psi_n(\mathcal{R}, \mathbf{r}_1, \ldots, \mathbf{r}_N).
\end{aligned} \quad (2.1.10)$$

Substituting this expansion into Eq. 2.1.9 and rearranging terms yields a set of

coupled differential equations:

$$\left[-\frac{\hbar^2}{2}\sum_{\alpha}\frac{1}{M_\alpha}\nabla_\alpha^2 + E_m(\mathcal{R}) - E\right]\chi_m(\mathcal{R}) = \frac{\hbar^2}{2}\sum_{\alpha}\frac{1}{M_\alpha}\sum_{n=1}^{M}\left[2\nabla_\alpha\chi_n(\mathcal{R})\cdot\langle\psi_m|\nabla_\alpha|\psi_n\rangle + \chi_n(\mathcal{R})\langle\psi_m|\nabla_\alpha^2|\psi_n\rangle\right] \quad (2.1.11)$$

Eq. 2.1.11 represents an exact set of coupled equations for the functions $\chi_m(\mathcal{R})$, $m = 1, \ldots, M$ defined in Eq. 2.1.6. The solution $\chi_m(\mathcal{R})$ for any one of these functions depends on all of the others because of the coupling on the right hand side of Eq. 2.1.11. Each of the coupling terms involves derivatives of the electronic wave functions $\psi_n$ with respect to the nuclear coordinates. This is the point at which the Born-Oppenheimer Approximation is applied. As was stated previously, the electronic wave functions $\psi_n$ often depend very weakly on the nuclear coordinates. In those cases, the terms that include $\nabla_\alpha\psi_n$ can be neglected. This approximation leaves us with a set of separated, uncoupled equations for each nuclear wave function $\chi_m(\mathcal{R})$ that correspond to nuclear motion on a single potential surface $E_m(\mathcal{R})$:

$$\left[-\frac{\hbar^2}{2}\sum_{\alpha}\frac{1}{M_\alpha}\nabla_\alpha^2 + E_m(\mathcal{R}) - E\right]\chi_m(\mathcal{R}) = 0. \quad (2.1.12)$$

In summary, the Born-Oppenheimer approximation has yielded a set of uncoupled equations for the nuclear motion. Each of these equations uses the electronic energy solutions $E_m(\mathcal{R})$ to the electronic Schrödinger equation Eq. 2.1.5 as a potential energy surface. Qualitatively speaking, one can say that the massive nuclei move very slowly, allowing the individual electrons to react instantaneously to the nuclear motion. Thus, the electron cloud affects the nuclei as potential energy.

The potential surface is formed by finding a set of energies $E_m(\mathcal{R})$ for systematically varied values of $\mathcal{R}$, which form a grid of nuclear positions. This potential surface is then used to solve the uncoupled equations in Eq. 2.1.12. Though the Born-Oppenheimer approximation has greatly simplified solving the Schrödinger equation by separating the electronic and nuclear parts, the individual tasks are still quite formidable.

## 2.2 Electronic Structure Calculations

To solve the electronic Schrödinger equation Eq. 2.1.5, we employ the General Atomic and Molecular Electronic Structure Systems (GAMESS)[14] code. GAMESS is one of many available *ab initio* quantum chemistry codes used to calculate the wave functions and energy of a system. This section will give a brief overview of how these codes work.

### 2.2.1 Formation of the Molecular Orbitals

In a molecule, the multi-electron wave function is constructed from separate, single particle wave functions for each electron called molecular orbitals (MOs). The MOs are linear combinations of atomic orbitals (LCAO) [15]. This form is an obvious choice when certain limiting cases of the system are considered. When the atoms are well separated, each atom will have electrons that occupy atomic orbitals. At closer internuclear separations, the interaction of the electrons and nuclei will cause the orbitals to deform. The inclusion of multiple atomic orbitals provides a means of describing this deformation. Thus, an LCAO method with enough atomic orbitals sufficiently represents the MO for all possible separation limits.

The first step is to determine which basis functions (called primitive basis functions) will be used to describe the atomic orbitals. There are two common types of primitive basis sets used in electronic structure calculations; Slater-type orbitals (STOs) and Gaussian-type orbitals (GTOs). Atomic $s$ type STOs have the form [16]

$$g_{\mathrm{STO}}(\mathbf{r}) = \left(\frac{\zeta^3}{\pi}\right)^{\frac{1}{2}} e^{-\zeta r}. \tag{2.2.1}$$

Atomic $s$ type GTOs have the form [17]

$$g_{\mathrm{GTO}}(\mathbf{r}) = \left(\frac{2\gamma}{\pi}\right)^{\frac{3}{4}} e^{-\gamma r^2}. \tag{2.2.2}$$

STOs have the same form as the exact solution for the hydrogen $1s$ orbital. However, STOs are not often used because many of the integrals necessary for polyatomic molecules cannot be evaluated analytically. While integrals involving GTOs can be evaluated analytically, GTOs do not properly describe the long range behavior of the hydrogen atomic orbitals. This deficiency can be addressed by using a linear combination of GTOs, called contracted GTOs, as shown in Eq.2.2.3.

$$g(\mathbf{r}) = \sum_{j=1}^{L} c_j \left(\frac{2\gamma_j}{\pi}\right)^{\frac{3}{4}} e^{-\gamma_j r^2} \tag{2.2.3}$$

The contracted GTOs are comprised of normalized primitive GTOs and are used as the atomic orbitals for the expansion of the molecular orbitals. Over the years, extensive work has been done to determine the best possible basis sets for each type of atom by optimizing the number of terms $L$, the expansion coefficients $c_j$, and the exponents $\gamma_j$.

The example of Gaussian-type primitive basis functions given in Eq. 2.2.2 is representative of $s$ type atomic orbitals. To describe the electrons in higher atomic orbitals, other forms of GTOs must be used. These functions have the same radial form as the $s$ type orbitals, but must include an angular dependence. For example, the $p_x$ type orbitals have the form

$$g_{p_x}(\mathbf{r}) = \left(\frac{2^7\gamma^5}{\pi^3}\right)^{\frac{1}{4}} xe^{-\gamma r^2} \tag{2.2.4}$$

and $d_{xy}$ type orbitals have the form

$$g_{d_{xy}}(\mathbf{r}) = \left(\frac{2^{11}\gamma^7}{\pi^3}\right)^{\frac{1}{4}} xye^{-\gamma r^2}. \tag{2.2.5}$$

Other forms of contracted GTOs shown in Eq. 2.2.3 can be created using these and other GTOs.

As previously stated, the contracted basis functions are used to construct optimized atomic orbitals for each element. The chosen contracted GTOs are then used as a basis set to calculate the MOs of the molecule in question. The general form of any molecular orbital $\phi$ is

$$\phi(\mathcal{R}, \mathbf{r}) = \sum_{j=1}^{M} \xi_j g_j(\mathbf{r} - \mathbf{R}_{\alpha(j)}) \tag{2.2.6}$$

where $\xi_j$ is a weighting coefficient, $g_j$ is a contracted GTO of type $s$, $p_x$, $p_y$, $p_z$, etc. and $\mathbf{R}_{\alpha(j)}$ is the position of the $\alpha^{\text{th}}$ nucleus about which the $j^{\text{th}}$ contracted GTO is centered. The number of linearly independent MOs is the same as the number of atomic orbitals, $M$, included in the basis set. Note that the GTO's dependence on

$\mathbf{R}_{\alpha(j)}$ causes the molecular orbitals to be dependent on the position of the nuclei of the atoms as well.

Thus far, we have only considered the spatial portion of the molecular orbitals necessary to solve the Schrödinger equation. We must also incorporate spin to describe the electronic states properly. The spin functions $\alpha$ and $\beta$ will be used to represent spin up and spin down, respectively. The spin functions are orthonormal. With the inclusion of the spin functions, each spatial orbital yields two possible spin orbitals $\chi$

$$\chi_i(\mathcal{R}, \mathbf{r}) = \begin{cases} \phi(\mathcal{R}, \mathbf{r})\alpha \\ \phi(\mathcal{R}, \mathbf{r})\beta \end{cases} \tag{2.2.7}$$

Another condition the multi-electron wave function must satisfy is the Pauli Exclusion Principle, which states that an exchange of all coordinates of any two electrons must produce a change in sign of the total wave function. Thus, the total electronic wave function $\psi$ must have the property

$$\psi(\mathbf{r}_1, \ldots, \mathbf{r}_i, \ldots, \mathbf{r}_j, \ldots, \mathbf{r}_N) = -\psi(\mathbf{r}_1, \ldots, \mathbf{r}_j, \ldots, \mathbf{r}_i, \ldots, \mathbf{r}_N). \tag{2.2.8}$$

To meet this requirement, the total electronic wave function is written as a determinant of spin orbitals, known as a Slater Determinant, which has the form

$$\Phi(\mathcal{R}, \mathbf{r}_1 ... \mathbf{r}_N) = (N!)^{-\frac{1}{2}} \begin{vmatrix} \chi_1(\mathcal{R}, \mathbf{r}_1) & \chi_1(\mathcal{R}, \mathbf{r}_2) & \cdots & \chi_1(\mathcal{R}, \mathbf{r}_N) \\ \chi_2(\mathcal{R}, \mathbf{r}_1) & \chi_2(\mathcal{R}, \mathbf{r}_2) & \cdots & \chi_2(\mathcal{R}, \mathbf{r}_N) \\ \vdots & \vdots & & \vdots \\ \chi_N(\mathcal{R}, \mathbf{r}_1) & \chi_N(\mathcal{R}, \mathbf{r}_2) & \cdots & \chi_N(\mathcal{R}, \mathbf{r}_N) \end{vmatrix}. \tag{2.2.9}$$

In the Slater determinant, each row corresponds to a particular spin orbital and

each column corresponds to each electron. The $(N!)^{-\frac{1}{2}}$ term is a normalization factor. The total electronic wave function has $\mathcal{R}$ dependence due to the fact that each GTO basis function is centered at the nucleus of a specific atom. The Slater determinant can also be written in a more compact form using the antisymmetrizer operator

$$\Phi(\mathcal{R}, \mathbf{r}_1 ... \mathbf{r}_N) = \mathcal{A}\left\{\chi_1(\mathcal{R}, \mathbf{r}_1) \cdots \chi_N(\mathcal{R}, \mathbf{r}_N)\right\}. \tag{2.2.10}$$

The important feature of the Slater determinant is that it automatically satisfies the antisymmetry requirement. An exchange of electrons $i$ and $j$ corresponds to an exchange of columns $i$ and $j$, which due to the mathematical nature of the determinant changes the sign. The Slater determinant also ensures that no two electrons will have exactly the same quantum numbers, because if two electrons occupy the same spin orbital ($\chi_m(\mathcal{R}, \mathbf{r}_i) = \chi_m(\mathcal{R}, \mathbf{r}_j)$) two columns will be identical, and the determinant will be zero.

### 2.2.2 Variational Principle

Now that the basic form of the MOs have been reviewed, we will discuss finding the optimal orbitals for a molecular system. The Variational Principle states that for any approximate solution to the Schrödinger equation, $\psi_0^{\text{approx}}$, the expectation value of the energy, $E_0^{\text{approx}}$ must be greater than or equal to the exact ground state energy, $E_0^{\text{exact}}$:

$$E_0^{\text{approx}} = \int (\psi_0^{\text{approx}})^* \ \hat{H}_{\text{elec}} \ \psi_0^{\text{approx}} \ d\mathbf{r} = \langle \psi_0^{\text{approx}} \ | \hat{H}_{\text{elec}} \ | \psi_0^{\text{approx}} \ \rangle \geq E_0^{\text{exact}} \ . \tag{2.2.11}$$

This result is due to the fact that the approximate wave function $\psi_0^{\text{approx}}$ can be written as a linear combination of the exact wave functions, $\psi_m^{\text{exact}}$;

$$\psi_0^{\text{approx}} = \sum_m c_m \psi_m^{\text{exact}}, \tag{2.2.12}$$

because the exact wave functions form a complete, orthonormal basis set. The form of the approximate wave function Eq. 2.2.12 allows the approximate expectation energy Eq. 2.2.11 to be written as

$$\begin{aligned} E_0^{\text{approx}} &= \left\langle \sum_m c_m \psi_m^{\text{exact}} \mid \hat{H}_{\text{elec}} \mid \sum_n c_n \psi_n^{\text{exact}} \right\rangle \\ &= \sum_m \sum_n \langle c_m \psi_m^{\text{exact}} \mid \hat{H}_{\text{elec}} \mid c_n \psi_n^{\text{exact}} \rangle \\ &= \sum_m \sum_n c_m^* c_n E_n^{\text{exact}} \langle \psi_m^{\text{exact}} \mid \psi_n^{\text{exact}} \rangle \\ &= \sum_n |c_n|^2 E_n^{\text{exact}} \geq E_0^{\text{exact}} . \end{aligned} \tag{2.2.13}$$

If the wave function is exactly the ground state wave function, the energy will be the actual ground state energy, which is the lowest possible energy. Any other wave functions will result in an energy higher than the ground state energy. The variational principle is usually implemented by selecting a physically appropriate trial wave function that has one or more adjustable parameters. The best approximate wave function is found by selecting the values of the parameters that minimizes $E_0^{\text{approx}}$. The best parameters are often found using linear variational theory, which is described in the next section.

### 2.2.3 Linear Variational Theory

The electronic structure calculations used in this research are based on the linear variational theory. A complete description of the method is provided in McQuarrie [18]. Linear variational theory applies to cases where one wants to find the best solution to

$$(\hat{H} - E)\Psi = 0 \tag{2.2.14}$$

by using a trial wave function $\Psi^{\text{trial}}$ that is a linear combination of known functions $f_i$:

$$\Psi^{\text{trial}} = \sum_i c_i f_i, \tag{2.2.15}$$

where the $c_i$ are adjustable parameters that are varied to minimize $\langle E \rangle$, the expectation value of the energy. Using the trial wave function and the Hamiltonian $\hat{\text{H}}_{\text{elec}}$ we can define matrix elements

$$H_{ij} = \langle f_i | \hat{H} | f_j \rangle \text{ and } S_{ij} = \langle f_i | f_j \rangle. \tag{2.2.16}$$

Substituting the normalized trial wave function into the Schrödinger equation, multiplying on the left by the complex conjugate of the wave function, and integrating over all space yields

$$\langle E \rangle = \frac{\sum_{ij} c_i^* c_j H_{ij}}{\sum_{ij} c_i^* c_j S_{ij}}. \tag{2.2.17}$$

Eq. 2.2.17 is rearranged and differentiated with respect to the $c_i$ coefficients to obtain the minima of the expectation energy. This yields the set of equations

$$\sum_j (H_{ij} - E S_{ij}) c_j = 0 \tag{2.2.18}$$

where the energies $E$ are the eigenvalues and the $c_j$ are the eigenvectors. The energies can be found by solving the secular determinant $\det(H_{ij} - ES_{ij}) = 0$. The eigenvector $c_j$ corresponding to the lowest eigenvalue gives the coefficients for an approximate ground state wave function in Eq. 2.2.15. This lowest eigenvalue gives $E_0^{\text{approx}}$ for the chosen trial wave function.

Generally speaking, the functions $f_i$ used to form the trial wave function are chosen or mathematically manipulated to be orthonormal [14]. For orthonormal functions, $S_{ij}$ becomes the Kronecker Delta function $S_{ij} = \delta_{ij}$. This choice of orthonormal functions simplifies Eq. 2.2.18 to a standard eigenvalue equation:

$$\sum_j (H_{ij} - E\delta_{ij})c_j = 0. \tag{2.2.19}$$

Again, the determinant of Eq. 2.2.19 is set equal to zero, used to solve for the lowest energy, which is in turn used to produce the coefficients of the wave function.

### 2.2.4 Hartree-Fock Approximation

Solving the electronic Schrödinger equation can be achieved with varying degrees of accuracy. In all cases, some form of approximation must be used. One of the most fundamental approaches is the Hartree-Fock (HF) approximation [15]. The simplest form of this method applies only to closed shell systems, for which the number of electrons $N$ is even. The trial wave function used in the HF method is a single Slater determinant of the form in Eq. 2.2.9. The total electronic wave function can be written as

$$\psi_{\text{HF}}(\mathcal{R}, \mathbf{r}_1 ... \mathbf{r}_N) = \mathcal{A}\chi_1(\mathcal{R}, \mathbf{r}_1) \cdots \chi_N(\mathcal{R}, \mathbf{r}_N). \tag{2.2.20}$$

There are a total of $\frac{N}{2}$ spatial molecular orbitals, each doubly occupied, which is why this is sometimes called the closed-shell method.

The main difficulty in solving the Schrödinger equation is treating the electron-electron interactions. The approximation made in the Hartree-Fock approach is to assume that each electron experiences the average electric field caused by all the other electrons. In the mathematical formulation of this approach, one defines an effective one-electron Schrödinger equation,

$$(\hat{h} + \hat{V})\phi(\mathbf{r}) = E\phi(\mathbf{r}), \tag{2.2.21}$$

where $\hat{h}$ is a one-electron operator that includes the kinetic energy plus the Coulomb interaction of the electron with each nucleus, and $\hat{V}$ is a nonlocal operator representing the average potential that has an effect on one electron. Linear variational theory is then used to solve for the optimum electron orbitals that can be constructed within a given basis set. If the set has $M$ basis functions $g_j$, where $M \geq \frac{N}{2}$ and $N$ is the number of electrons, then there are $M$ orbitals $\phi_i(\mathbf{r}), i = 1, \ldots, M$ defined by

$$\phi_i(\mathcal{R}, \mathbf{r}) = \sum_{j=1}^{M} c_{ji} g_j(\mathbf{r} - \mathcal{R}_{\alpha(j)}) \tag{2.2.22}$$

where the rows of the matrix $\mathbf{c}_{ji}$ correspond to the $M$ eigenvectors discussed earlier in section 2.2.3. The $\frac{N}{2}$ occupied spatial molecular orbitals in the HF approximation are given by orbitals defined in Eq. 2.2.22, corresponding to the lowest $\frac{N}{2}$ eigenvalues determined by linear variational theory.

Because the operator $\hat{V}$ in Eq. 2.2.21 depends on the molecular orbitals, it is necessary to solve Eq. 2.2.21 iteratively. An initial set of orbitals is chosen and used

to compute a potential field felt by each electron. This field is in turn used to find a new set of orbitals by varying the coefficients of the LCAO. This iterative process is repeated until the orbitals result in the same field used to find them. This method is also called the Self-Consistent Field (SCF) method in reference to the properties of the solution.

While the Hartree-Fock method is appropriately accurate in some cases, it may not be sufficient in all cases. Approximating all the electron-electron interactions with a potential field can cause unrealistic behavior. To account for the instantaneous repulsion between electrons, a method must be used that correlates the motion of the electrons.

### 2.2.5 Configuration Interaction

The HF calculations use a single Slater determinant. The key advantage of the Configuration Interaction (CI) calculations is that the wave function is a linear combination of Slater determinants,

$$\psi(\mathcal{R}, \mathbf{r}_1 ... \mathbf{r}_N) = \sum_j \vartheta_j \Phi_j(\mathcal{R}, \mathbf{r}_1 ... \mathbf{r}_N) \tag{2.2.23}$$

In many cases some of the $\Phi_j$ may be linear combinations of Slater determinants chosen to be eigenfunctions of the total spin. The general term for the $\Phi_j$ in Eq. (2.2.23) is configuration state function (CSF).

In Eq. 2.2.23 the first CSF is the Hartree-Fock ground state, which is formed by having electrons occupy the $\frac{N}{2}$ lowest orbitals of a $\frac{N}{2} \times \frac{N}{2}$ determinant. Those occupied orbitals are referred to as the ground state orbitals, and unoccupied orbitals above the ground state are referred to as virtual orbitals. Higher energy CSFs can

be formed by promoting one or more electrons from the ground state orbitals to the virtual orbitals. These excited CSFs are included in the CI wave function. Including multiple configurations leads to a more accurate treatment of the electron-electron interaction. In CI calculations, the molecular orbitals are held constant. The coefficients $\vartheta$ of Eq. 2.2.23 are the adjustable parameters of a CI calculation and are varied according to linear variational theory.

The most complete form of the wave function would include all possible excitation states, formed by promoting every electron in the ground state to every possible virtual orbital, in every possible combination. The total number of configurations can be determined with a binomial coefficient

$$\binom{K}{N} = \frac{K!}{N!(K-N)!}, \tag{2.2.24}$$

where $K$ is the total possible number of spin orbitals define in Eq. 2.2.7 and $N$ is the number of electrons in the molecule [18]. As an illustrative example, the He atom + the NaK molecule system has $N = 32$ electrons and a typical basis includes $K = 76$ spin orbitals. This results in $2.695 \times 10^{21}$ possible configurations. Using this many configurations in a calculation is not possible and in most cases unneccesary.

By only considering excited determinants in which at most two electrons are promoted to a virtual orbital, one can still obtain reliable results. This is referred to as a Singles and Doubles CI (SDCI) or a Second Order CI (SOCI). However, calculations of this nature are very large. Further approximations can be used to reduce the computer resources needed, but care must be taken to find a balance between the desired accuracy and available computing resources.

Electrons in higher occupied orbitals are more likely to be promoted from the

ground state than those in lower energy core occupied orbitals. The electrons in low energy orbitals will not be allowed to be promoted; those orbitals are called the frozen core. The orbitals above those occupied in the ground state are called the virtual orbitals. The orbitals that have electrons that can be promoted are known as the active space. The electrons in the active space are then excited in single and double excitations. Finally, promoting any of the electrons to the highest virtual space orbitals is also very unlikely. Thus, some of the upper virtual space orbitals can also be frozen. The number of frozen core orbitals is the same number of virtual space orbitals frozen in our calculations.

### 2.2.6 Multi-Configuration Self Consistent Field

In systems with open shell atoms or molecules, the single Slater determinant of the HF method may not sufficient. The Multi-Configuration Self Consistent Field method also uses a linear combination of Slater determinants. However, in MCSCF calculations both the coefficients of the molecular orbitals ($\xi_{ij}$) and the coefficients of the CSFs ($\vartheta_i$) are optimized. The molecular orbitals calculated using the MCSCF method and those that correspond to the single and double excitations can then be used in the CI calculations, discussed in subsection 2.2.5.

### 2.2.7 Concluding Remarks

The needs and restrictions of each individual calculation will determine the size and type of procedure applied. The calculations in this work include scattering of helium with both the ground and excited state of NaK. The methods used for each of the electronic structure calculations will be discussed further in Chapter 3.

# Chapter 3

# Calculations of the Potential

Experimental data are available for helium collisions with NaK in the first excited ($A^1\Sigma^+$) electronic state and will hopefully be available soon for He collisions with ground state ($X^1\Sigma^+$) NaK [19]. The first step in performing calculations that can be compared with these experiments is to determine potential energy surfaces for the interaction of helium with the ground and first excited states of NaK. The potential energy depends on the bond length of the NaK, $r_\mathrm{v}$, the distance of the helium from the center of mass of the NaK molecule, $R_\mathrm{d}$, and the angle $\theta$ as shown in Fig. 3.1. This work fixed the NaK internuclear distance, $r_\mathrm{v}$, at the equilibrium separation. To determine a full potential surface, calculations must be performed at multiple values of $R_\mathrm{d}$ and $\theta$.

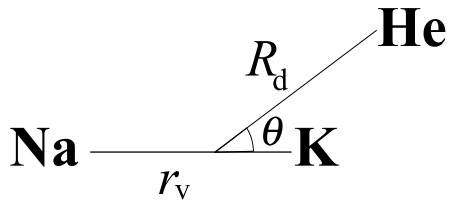


**Figure 3.1:** The Jacobi coordinate system used to describe He + NaK.

## 3.1 Ground State of NaK

### 3.1.1 Electronic Structure Calculations for the Ground State

We determined the potential energy surface (PES) of the ground state of He + NaK using standard techniques of electronic structure calculations, as implemented using the GAMESS code [14]. For the closed-shell ground electronic state of He + NaK we performed a restricted Hartree Fock calculation and then a configuration interaction (CI) calculation. The basis set is shown in Table 3.1. A $5s2p/3s2p$ basis set was used for He [20] and 6-311$G$++(3$d$) (triple zeta plus three $d$ polarization functions) for Na [20, 21] and K [22]. For the CI calculations, the six lowest core orbitals were frozen and the six highest orbitals of the virtual space were closed to excitation. With single and double excitations from the reference state, the total number of configurations state functions (CSFs) was 160,021.

The NaK separation, $r_{\mathrm{v}}$, was fixed at the equilibrium value of the ground state, 6.612 $a_0$, which was determined experimentally by Russier-Antoine *et al.* [23]. This corresponds approximately to the $v = 0$ vibrational level of the $X^1\Sigma^+$ state. The calculations described above were performed for various combinations of $R_{\mathrm{d}}$ and $\theta$. For the ground state, calculations were done at intervals of 0.50 $a_0$ for $R_{\mathrm{d}}$ = 4.00–6.00 $a_0$ and 11.00–20.00 $a_0$. For $R_{\mathrm{d}}$ = 6.00–11.00 $a_0$, calculations were done at 0.25 $a_0$ intervals. Addtional potential energies were calculated at $R_{\mathrm{d}}$ = 21.00, 22.00, 23.00, 24.00, 25.00, 26.00, 27.50, 29.00, and 30.00 $a_0$.

Calculations were performed for a greater number of $\theta$ in regions of $R_{\mathrm{d}}$ where the potential was particularly sensitive to the angular position. Depending on the value of $R_{\mathrm{d}}$, calculations were performed for angles $\theta$ between 0° and 180° with

**Table 3.1:** Gaussian type basis functions used for HeNaK. Column three gives the coefficients of the normalized GTO in the contracted orbital. The $d$ functions are polarization functions.

| He AOs | Exponent | Coefficient |
|---|---|---|
| $s$ | 98.1243000 | 0.0287452 |
| | 14.7689000 | 0.2080610 |
| | 3.3188300 | 0.8376350 |
| $s$ | 0.8740470 | 1.0000000 |
| $s$ | 0.2445640 | 1.0000000 |
| $p$ | 1.5000000 | 1.0000000 |
| $p$ | 0.3750000 | 1.0000000 |

| Na AOs | Exponent | Coefficient |
|---|---|---|
| $s$ | 36166.40000 | 0.00103 |
| | 5372.58000 | 0.00807 |
| | 1213.21000 | 0.04213 |
| | 339.62300 | 0.16979 |
| | 109.55300 | 0.51462 |
| | 38.77730 | 0.37982 |
| $s$ | 38.77730 | 0.37476 |
| | 14.57590 | 0.57577 |
| | 5.26993 | 0.11293 |
| $s$ | 1.82777 | 1.00000 |
| $s$ | 0.61995 | 1.00000 |
| $s$ | 0.05724 | 1.00000 |
| $s$ | 0.02405 | 1.00000 |
| $p$ | 144.64500 | 0.01149 |
| | 33.90740 | 0.08238 |
| | 10.62850 | 0.31966 |
| | 3.82389 | 0.70130 |
| $p$ | 1.44429 | 0.63851 |
| | 0.55262 | 0.42537 |
| $p$ | 0.18872 | 1.00000 |
| $p$ | 0.04650 | 1.00000 |
| $p$ | 0.01629 | 1.00000 |
| $d$ | 0.70000 | 1.00000 |
| $d$ | 0.17500 | 1.00000 |
| $d$ | 0.04375 | 1.00000 |

| K AOs | Exponent | Coefficient |
|---|---|---|
| $s$ | 182594.00000 | 0.00053 |
| | 27369.00000 | 0.00408 |
| | 6229.17000 | 0.02123 |
| | 1764.58000 | 0.08649 |
| | 577.05100 | 0.28183 |
| | 210.24900 | 0.69044 |
| $s$ | 82.61780 | 0.60152 |
| | 33.23320 | 0.43432 |
| $s$ | 8.10649 | 1.00000 |
| $s$ | 3.33403 | 1.00000 |
| $s$ | 0.84554 | 1.00000 |
| $s$ | 0.32822 | 1.00000 |
| $s$ | 0.03640 | 1.00000 |
| $s$ | 0.01765 | 1.00000 |
| $p$ | 891.05400 | 0.02294 |
| | 211.01600 | 0.18469 |
| | 67.67140 | 0.85867 |
| $p$ | 25.27150 | 0.26380 |
| | 10.13900 | 0.46604 |
| | 4.20186 | 0.38914 |
| $p$ | 1.62507 | 1.00000 |
| $p$ | 0.64377 | 1.00000 |
| $p$ | 0.24613 | 1.00000 |
| $p$ | 0.04544 | 1.00000 |
| $p$ | 0.01616 | 1.00000 |
| $d$ | 13.37000 | 0.06259 |
| | 3.42100 | 0.31072 |
| | 1.06300 | 0.77361 |
| $d$ | 0.68700 | 1.00000 |
| $d$ | 0.22900 | 1.00000 |
| $d$ | 0.07633 | 1.00000 |

an angular separation of 5°, 15°, and 30°. The table in Appendix A lists all the results of the GAMESS calculations preformed for the ground state of He + NaK. Calculations were performed for $R_{\mathrm{d}} = 10000.00\ a_0$ to obtain the asymptotic limit of $-764.216454654\ \mathrm{E_h}$. For the calculations of the potential surface, this value was subtracted from all the calculated potential energies to obtain values relative to the asymptotic limit.

### 3.1.2 General Considerations for Fitting the PES

The PES was fit with a Legendre polynomial expansion of the form

$$V(R_{\mathrm{d}}, \theta) = \sum_{\lambda=0}^{\lambda_{\max}} v_\lambda(R_{\mathrm{d}}) P_\lambda(\cos\theta). \tag{3.1.1}$$

This form of the expansion is required for the coupled channel scattering that will be discussed in Chapter 4. To determine the $v_\lambda(R_{\mathrm{d}})$ coefficients at each value of $R_{\mathrm{d}}$, we must fit the points calculated for various $\theta$ values at that $R_{\mathrm{d}}$ using Legendre polynomials. Several factors play a roll in determining the details of this fit.

If we regard the potential $V(R_{\mathrm{d}}, \theta)$ to be a function of $R_{\mathrm{d}}$ and $\cos\theta$, then the Legendre polynomial expansion of the $\theta$ dependence is essentially equivalent to a polynomial expansion in terms of $\cos\theta$. [$P_\lambda(\cos\theta)$ is a polynomial in $\cos\theta$ whose maximum power is $(\cos\theta)^\lambda$]. This equivalence allows us to use standard, readily-available polynomial least squares fitting routines [24] to find a suitable fit. However, before performing the fit, one must still decide how many terms ($\lambda_{\max}+1$) to include. The simplest approach would be based on the fact that a polynomial of maximum degree $\lambda_{\max}$ (that is, $\lambda_{\max} + 1$ terms) can be found that will exactly fit $\lambda_{\max} + 1$ points. For example, Fig. 3.2(a) shows that for $R_{\mathrm{d}} = 25\, a_0$, an exact fit to five

calculated points is completely satisfactory. For this value of $R_{\mathrm{d}}$, more calculated points are available, and 3.2(b) shows that a five term fit to thirteen calculated points is still satisfactory. The rms deviation of the five term fit to all thirteen points is $9 \times 10^{-9}$ $\mathrm{E_h}$ (0.002 $\mathrm{cm^{-1}}$), which is very small compared to the probable uncertainty in the calculation itself.

The situation is not always so simple. For example, Fig. 3.3 shows a 13 term fit to 13 angular points calculated for $R_{\mathrm{d}} = 6.50\, a_0$. In this case, the oscillations in the fit are obviously unphysical. The reason for this unsatisfactory fit is that the potential becomes very repulsive for values of $\theta$ near 180° ($\cos\theta \sim -1$). This behavior occurs because the He atom is very close to the Na nucleus, and the potential rises exponentially. A polynomial expansion is not well suited to this case. Fortunately, a reasonable expansion can still be obtained if we recognize that a perfect fit to the highly repulsive portion of the PES is not essential. Since the ultimate goal of our work is to perform scattering calculations that can be compared with the experimental data, we may take into consideration the energy range of the planned scattering calculations. The experiments take place in a heat pipe whose temperature is about 600 K [2]. Knowing this fact allows us to identify the range of collision energies that should be included in the scattering calculations. The value of the PES is not critical at molecular geometries for which the PES significantly exceeds the collision energy, and we can tolerate large deviations of the fit at those points. Based on this idea, at each $R_{\mathrm{d}}$ we fit only the subset of the angular points for which the PES was less than a specified energy.

Fig. 3.4 illustrates how the strategy discussed above led to more appropriate fits for $R_{\mathrm{d}} = 6.50\, a_0$. Compared to Fig. 3.3, Fig. 3.4 shows a much smaller energy range

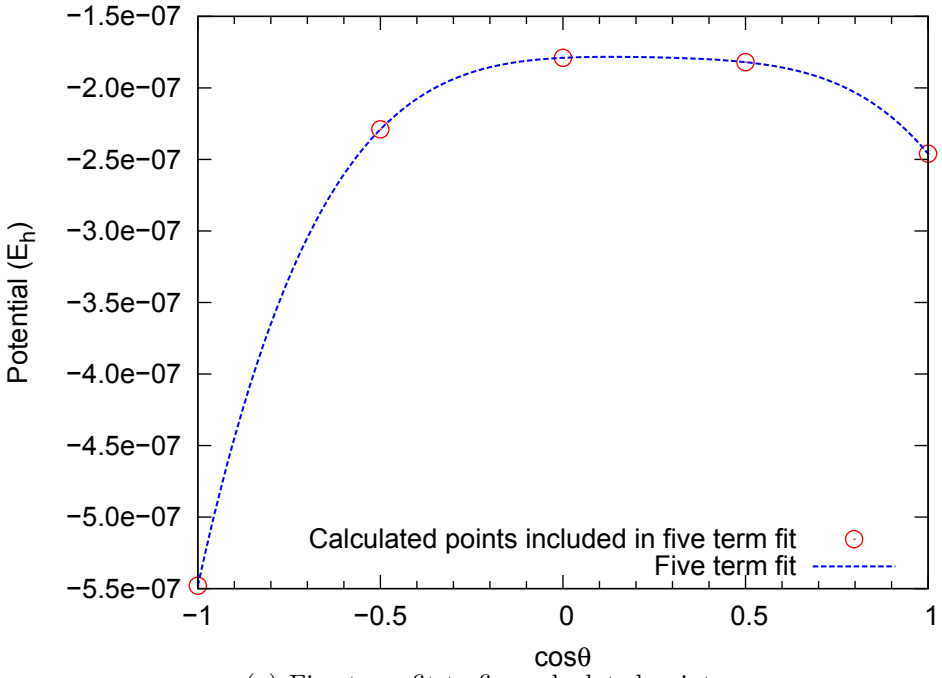


(a) Five term fit to five calculated points

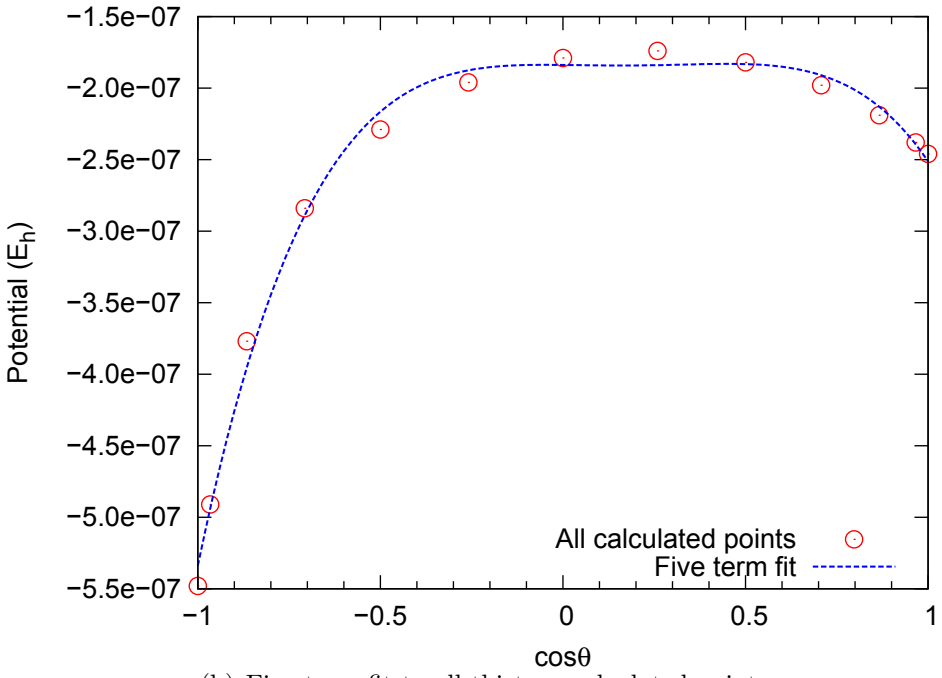


(b) Five term fit to all thirteen calculated points

**Figure 3.2:** Five term fits to the ground state at $R_{\mathrm{d}} = 25.00\ a_0$. Panel (a) shows a five term fit to five calculated points. Panel (b) shows that a five term fit to all the calculated points is also satisfactory at this value of $R_{\mathrm{d}}$.

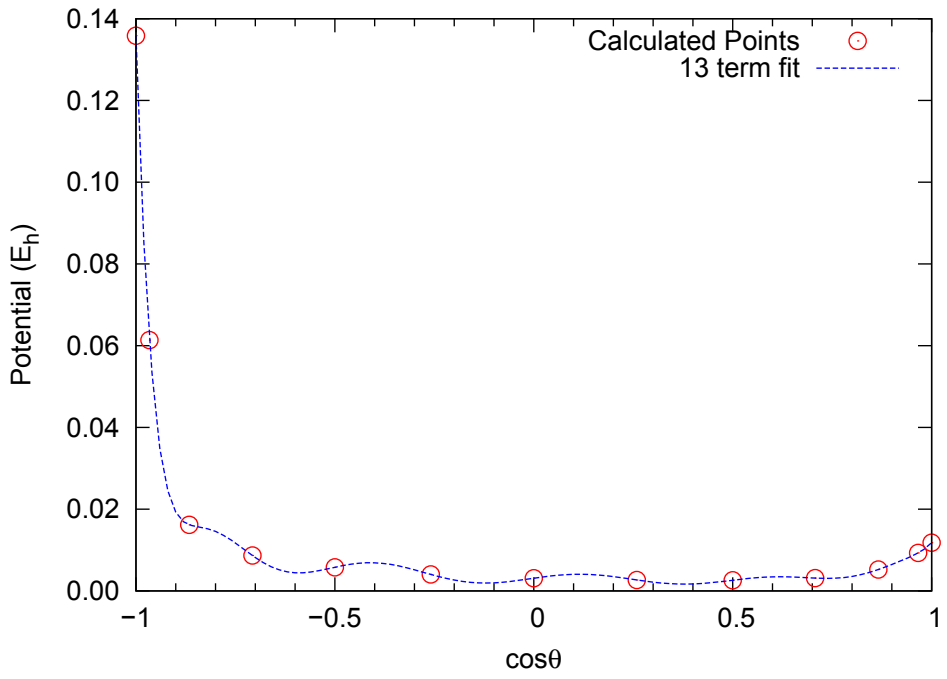


**Figure 3.3:** Thirteen term fit to thirteen calculated points of the ground state at $R_{\mathrm{d}} = 6.50\ a_0$. Though the function fits every point exactly, the strongly repulsive wall causes unphysical oscillations.

because energies higher than 0.012 $\mathrm{E_h}$ are omitted. Panel (a) shows a nine term fit to the angular values such that $E \leq 0.012\ \mathrm{E_h}$. This fit is smooth and accurate for the portion of the PES needed for scattering calculations at the upper end of the thermal distribution at 600 K. We also performed a seven term fit to the angular values such that $E \leq 0.004\ \mathrm{E_h}$. This fit is adequate for calculations at or below the mean thermal energy at 600 K. Both fits are shown in panel (b); it can be seen that in this region both fits agree well with the calculated values. The rms deviations for the nine and seven term fits are 5.05 and 2.33 $\mathrm{cm^{-1}}$, respectively. The number of terms in the fit and the range of energies considered is based on finding a balance between an accurate fit and physically realistic behavior. The final fits to the PES in this work typically had an rms deviation in the range 2–20 $\mathrm{cm^{-1}}$, which is a range

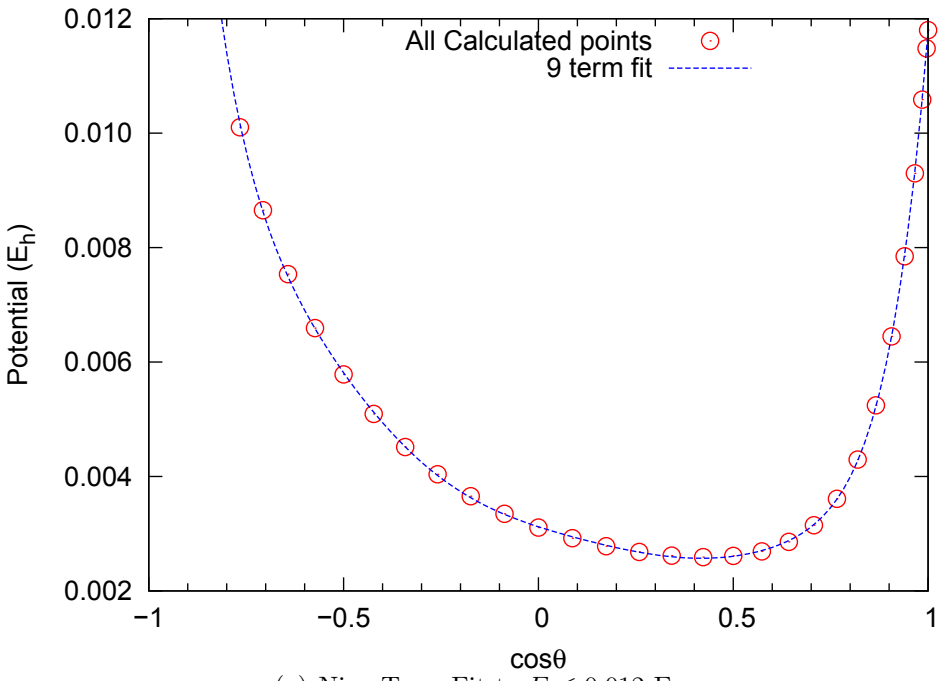


(a) Nine Term Fit to $E \leq 0.012$ $E_h$

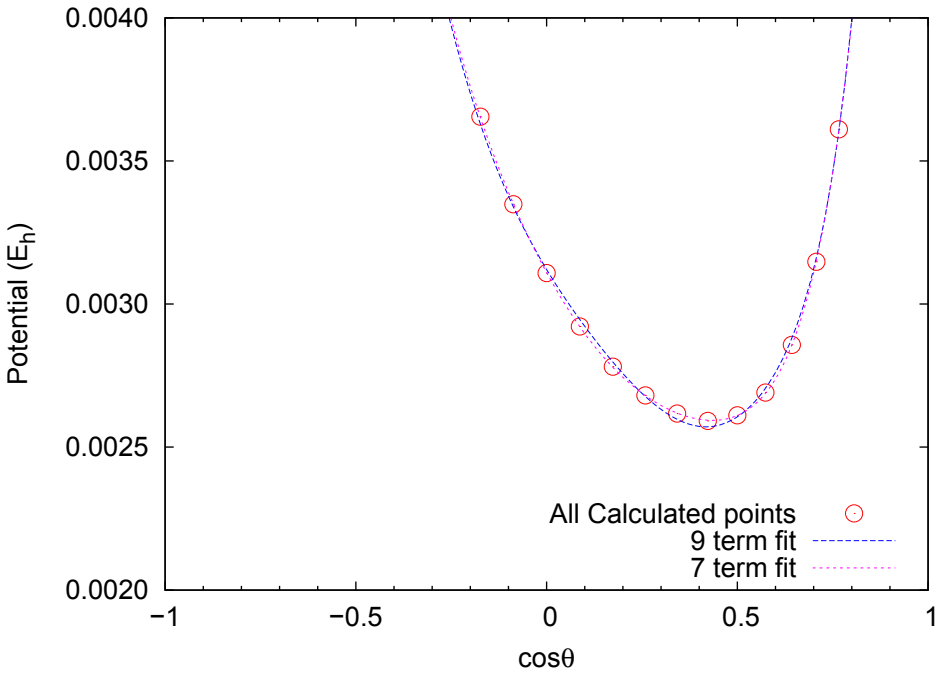


(b) Nine and Seven Term Fits to $E \leq 0.004$ $E_h$

**Figure 3.4:** Seven and nine term fits to the ground state at $R_d = 6.50\ a_0$. Panel (a) shows a nine term fit to five calculated points with energies below 0.012 $E_h$. Panel (b) shows that the seven and nine term fits both sufficiently describe the calculated points below energies of 0.004 $E_h$.

consistent with the probable uncertainty in the determination of the PES.

### 3.1.3 Legendre Expansion of the Ground State Potential

For the ground state, at each fixed $R_{\mathrm{d}}$, the calculated potentials up to an energy of 0.004 $\mathrm{E_h}$ were fit as a function of $\cos\theta$ using a seven term polynomial function. For certain $R_{\mathrm{d}}$ distances, some of the calculated values of the potential for several angles were above this energy and were omitted from the fit. For $R_{\mathrm{d}} \leq 6.00\ a_0$, all the calculated values were above 0.004 $\mathrm{E_h}$. To continue the potential smoothly to smaller $R_{\mathrm{d}}$, the same angular range used for the fit at $R_{\mathrm{d}} = 6.00\ a_0$ was used to fit $R_{\mathrm{d}} \leq 6.00\ a_0$. For values of $R_{\mathrm{d}} \geq 8.75\ a_0$, the potential energy at every angle was below 0.004 $\mathrm{E_h}$ and all values were included in the fits. A second fit with nine terms was done to describe higher energies up to 0.012 $\mathrm{E_h}$ in regions where the potential was more repulsive. As with the seven term fit, any energies higher than this cutoff were omitted. Table 3.2 specifies which of the calculated values were included in the fits for each $R_{\mathrm{d}}$. Fig. 3.5 graphically shows the included values for the seven and nine term polynomial fits. The figure shows that both the seven and nine term fits accurately fit low energies below both energy cutoffs. The nine term fit has the correct behavior for the repulsive wall up to 0.012 $\mathrm{E_h}$, but has some oscillations at low energies. The seven term fit can be used for scattering calculations at low energies, but does not include energies above 0.0040 $\mathrm{E_h}$ and thus does not accurately represent the repulsive region. Using the appropriate fit in each energy region allows us to perform scattering calculations that are accurate for all the energies expected in the experimental setup.

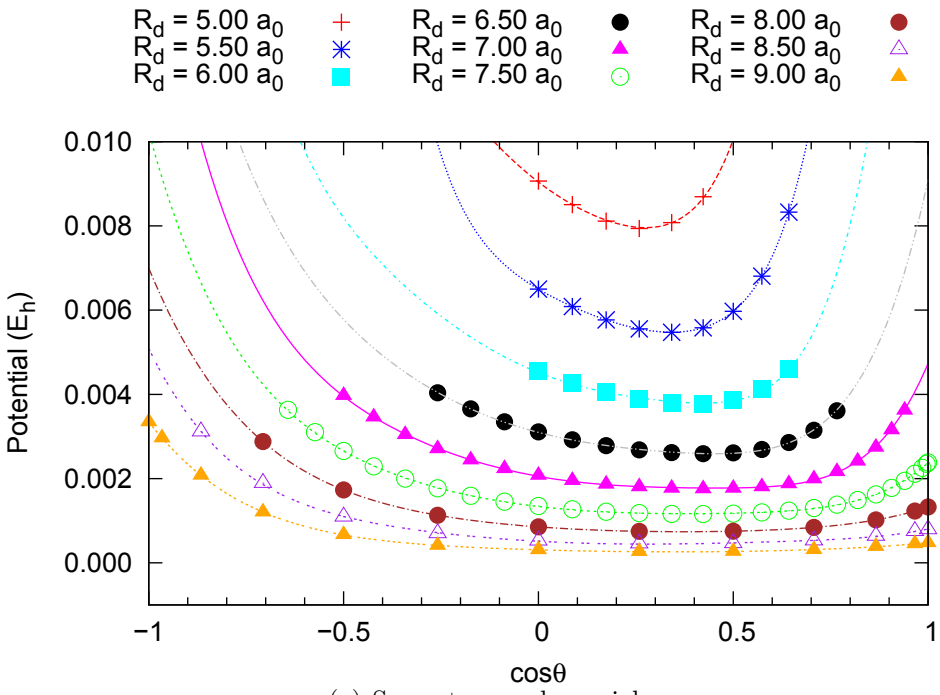


(a) Seven term polynomial

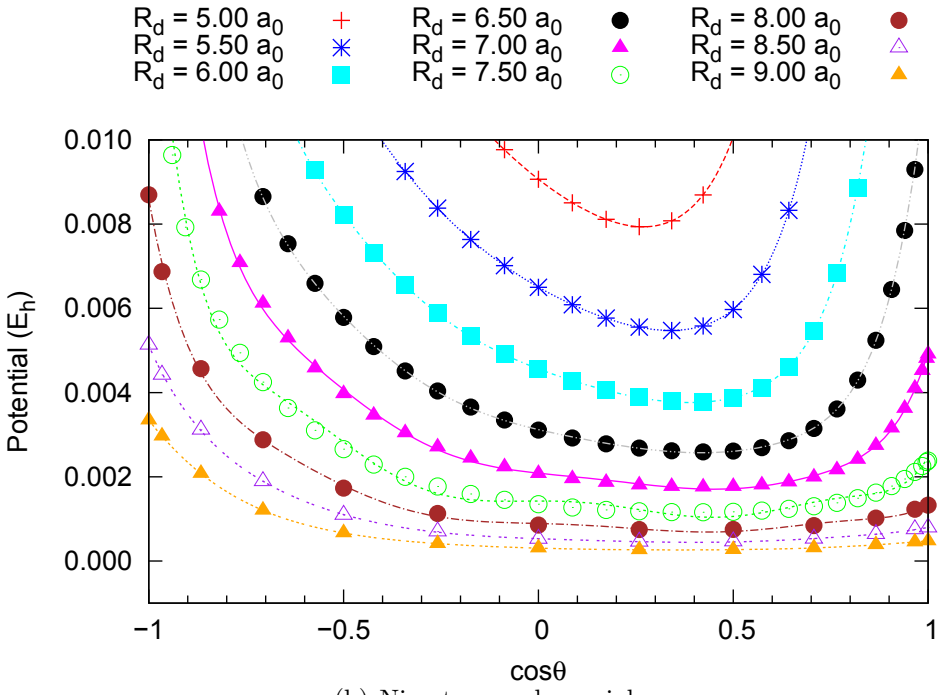


(b) Nine term polynomial

**Figure 3.5:** Calculated values of the ground state within the desired energy ranges that were included in the seven and nine term polynomial fits. The points indicate the calculated values included in the fit, and the lines represent the polynomial fits.

**Table 3.2:** Range of $\theta$ used to fit the calculated ground state potential energies with seven and nine term polynomials for each $R_d$. $R_d$ is given in $a_0$, $\theta$ in degrees and rms deviation in $cm^{-1}$.

| | | 7 Term Expansion | | 9 Term Expansion | |
|---|---|---|---|---|---|
| $R_d$ | $\Delta\theta$ | $\theta$ Range | rms deviation | $\theta$ Range | rms deviation |
| 4.00 | 5 | 50–90 | 4.4 | 60–120 | 0.09 |
| 4.50 | 5 | 50–90 | 4.0 | 60–120 | 0.29 |
| 5.00 | 5 | 50–90 | 4.7 | 50–130 | 0.69 |
| 5.50 | 5 | 50–90 | 5.2 | 40–130 | 0.88 |
| 6.00 | 5 | 50–90 | 6.3 | 25–140 | 3.8 |
| 6.25 | 5 | 45–95 | 2.1 | 15–145 | 8.3 |
| 6.50 | 5 | 40–105 | 2.3 | 0–145 | 5.1 |
| 6.75 | 5 | 30–110 | 3.8 | 0–150 | 9.6 |
| 7.00 | 5 | 20–120 | 4.2 | 0–155 | 16.4 |
| 7.25 | 5 | 0–125 | 2.8 | 0–160 | 21.1 |
| 7.50 | 5 | 0–130 | 3.0 | 0–165 | 22.5 |
| 7.75 | 5 | 0–135 | 0.61 | 0–180 | 30.2 |
| 8.00 | 15 | 0–135 | 0.12 | 0–180 | 16.5 |
| 8.25 | 15 | 0–150 | 4.4 | 0–180 | 7.7 |
| 8.50 | 15 | 0–150 | 5.5 | 0–180 | 3.3 |
| 8.75 | 15 | 0–180 | 1.7 | 0–180 | 1.1 |

We now briefly describe our procedure for converting the polynomial fit to the Legendre expansion. For each fixed $R_d$, the seven term polynomial fit was used to generate seven equally spaced points as a function of $\cos\theta$. These points were then fit exactly by a seven term Legendre expansion, using a computer code written some time ago [25] that solves a set of linear algebraic equations to find the expansion coefficients. Similarly, the nine term polynomial fit was used to generate nine equally spaced points, which were in turn fit exactly by a nine term Legendre expansion. A more direct approach is to use known formulas [26] for the Legendre polynomial

expansion of arbitrary powers:

$$x^{2n} = \frac{1}{2n+1}P_0(x) + \sum_{k=1}^{\infty}(4k+1)\frac{2n(2n-2)\ldots(2n-2k+2)}{(2n+1)(2n+3)\ldots(2n+2k+1)}P_{2k}(x)$$
$$x^{2n+1} = \frac{3}{2n+3}P_1(x) + \sum_{k=1}^{\infty}(4k+3)\frac{2n(2n-2)\ldots(2n-2k+2)}{(2n+3)(2n+5)\ldots(2n+2k+3)}P_{2k+1}(x). \tag{3.1.2}$$

(For any given $n$, the sum over $k$ contains only a finite number of nonzero terms.) We checked that both methods produced the same Legendre expansions.

For both fits, the calculated values of $v_\lambda$ can be interpolated using cubic splines. Figures 3.6 and 3.7 show the Legendre polynomial coefficients as a function of $R_\mathrm{d}$. The points correspond to values of $R_\mathrm{d}$ for which GAMESS calculations were performed and the lines are the cubic splines used to interpolate between the calculations. The (b) panels show the coefficents over a larger range of $R_\mathrm{d}$.

The Legendre expansion coefficients for the seven and nine term expansions are very different. The seven term expansion $\lambda$ = odd coefficients are negative and the $\lambda$ = even coefficients are positive. The nine term expansion coefficients are all greater than zero, except for a few very shallow wells around $R_\mathrm{d} = 6.00\ a_0$. Also, the absolute values of the seven term expansion coefficients are greater than those of the nine term expansion. Despite these differences, both the seven and nine term Legendre expansions produce values of the potentials that agree with the GAMESS calculations. Fig. 3.8 compares the potential produced by the seven and nine term Legendre expansions to the calculated points for several values of $\theta$. Potentials produced by both Legendre expansions agree with the calculated values of the potential for $E \leq 0.004\ \mathrm{E_h}$. For some angles, the seven term expansion is

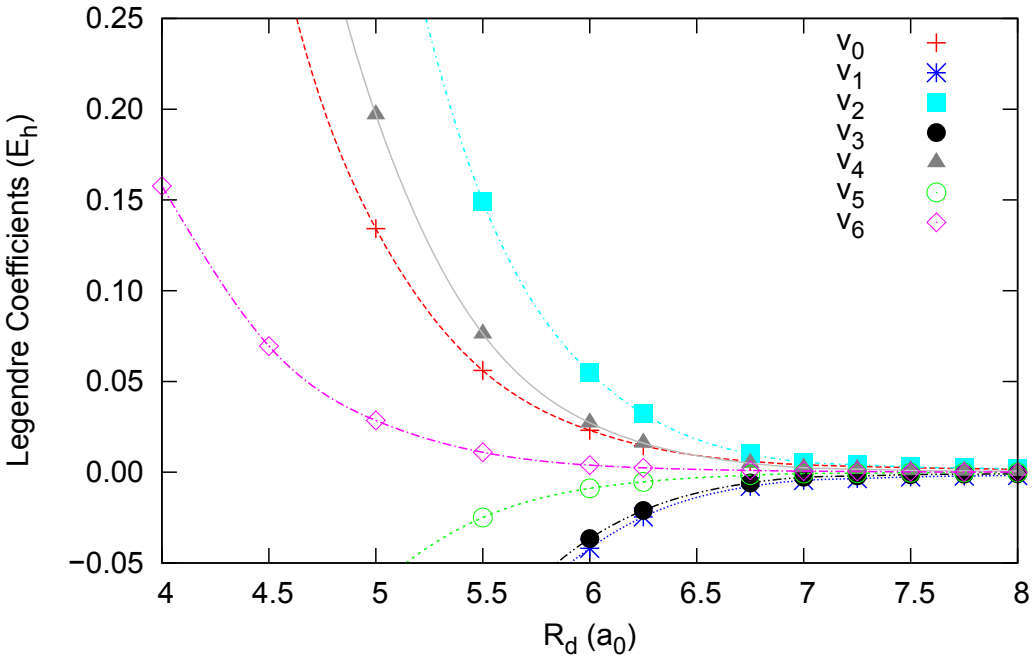


(a) Seven term Legendre polynomial expansion coefficients of the ground state

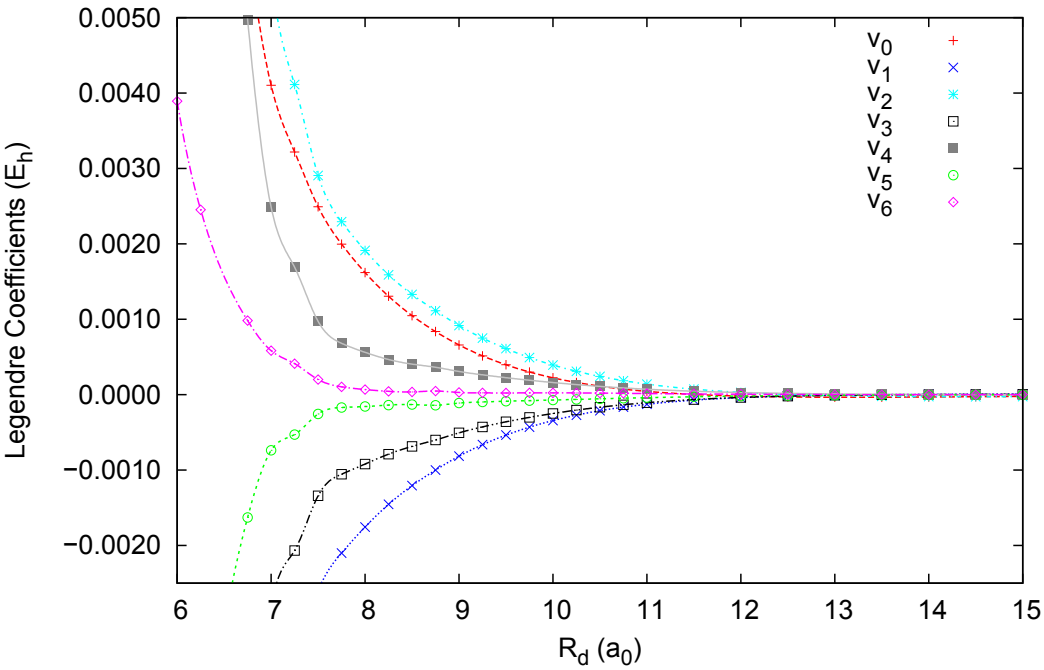


(b) Seven term Legendre polynomial expansion coefficients of the ground state: Long range

**Figure 3.6:** Seven term Legendre polynomial expansion coefficients of the ground state as a function of $R_{\mathrm{d}}$. The points represent Legendre coefficients for calculated points. The lines are the cubic splines between the data. The coefficients are given in atomic units.

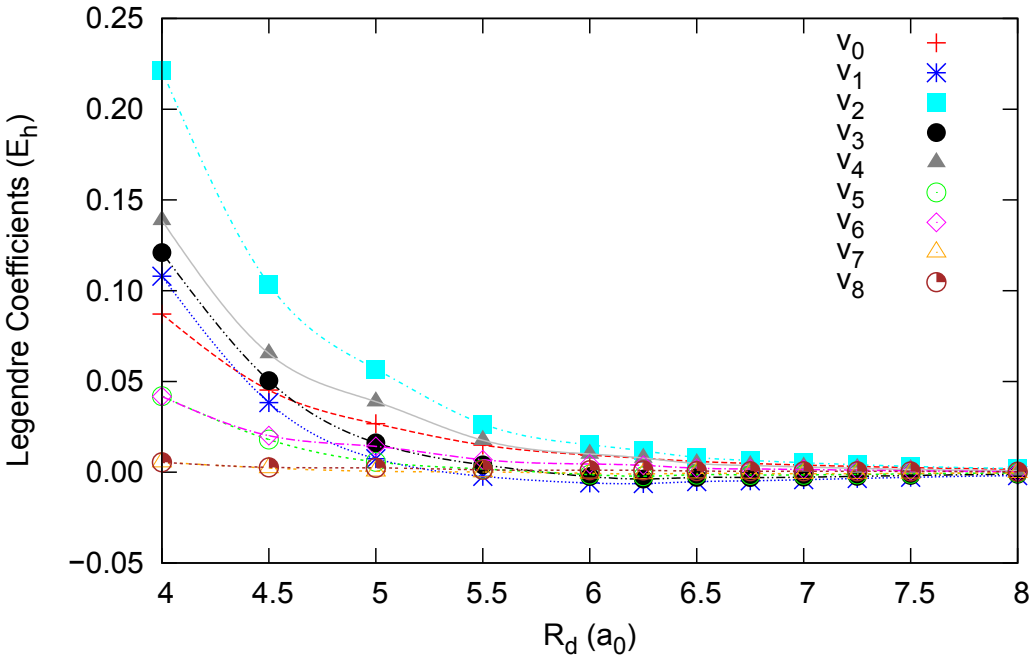


(a) Nine term Legendre polynomial expansion coefficients of the ground state

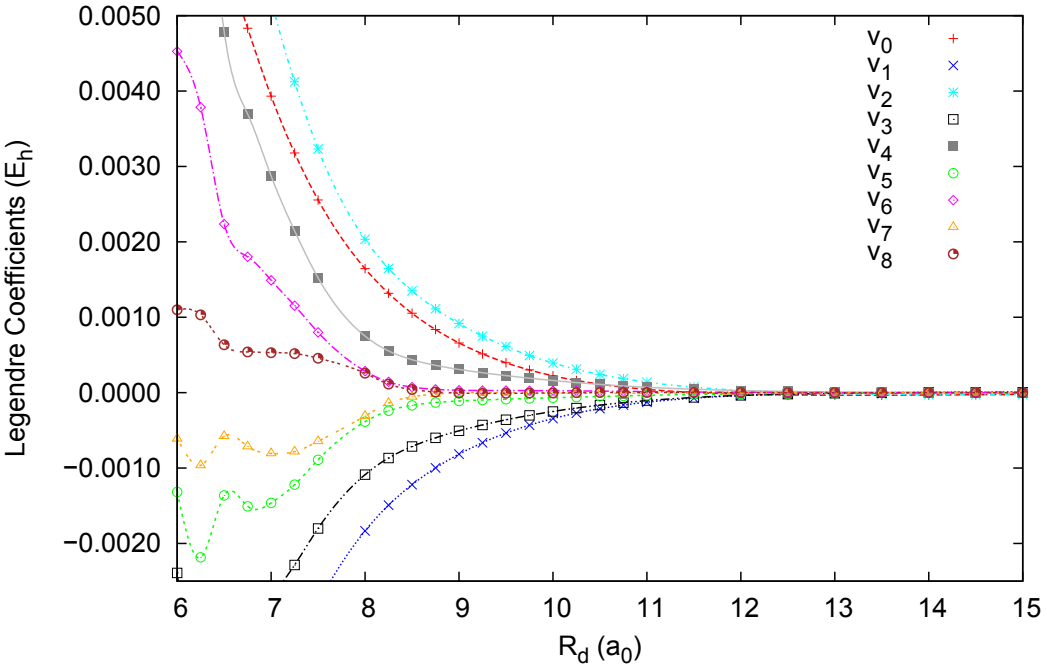


(b) Nine term Legendre polynomial expansion coefficients of the ground state: Long range

**Figure 3.7:** Nine term Legendre polynomial expansion coefficients of the ground state as a function of $R_{\mathrm{d}}$. The points represent Legendre coefficients for calculated points. The lines are the cubic splines between the data. The coefficients are given in atomic units.

nearly as good as the nine term expansion up to 0.012 $E_h$. At other angles, the seven and nine term expansions can be seen to diverge above $E = 0.004$ $E_h$, which is expected given the fitting procedure discussed earlier in this section. As can be seen in Fig. 3.5, values of the potential for $R_d \leq 6.00$ $a_0$ were fit with the seven term polynomial using angles $50° - 90°$. Thus, the seven term expansion for those angles is accurate for $E \geq 0.004$ $E_h$. The potential generated by the nine term expansion agrees well with the calculated values for all $E \leq 0.012$ $E_h$ for all angles.

The splines can be used to generate values of the $v_\lambda$ coefficients for any value of $R_d$; interpolated values will be needed for the scattering calculations. The interpolated $v_\lambda$ can also be used to evaluate the potential for any position specified by $R_d$ and $\theta$ coordinates. This capability allows us to transform the PES to a form that is more easily visualized. Since the NaK internuclear distance is fixed, we may regard the PES as a function of the position of the He atom in a plane containing the NaK. The origin is the center of mass of NaK, and the $x$ and $y$ coordinates specifying the He position are

$$x = R_d \cos\theta \quad \text{and} \quad y = R_d \sin\theta.$$

These formulas can be used to determine the PES on a rectangular cartesian grid for use in a graphics program. A representation of the surface produced by the nine term Legendre polynomial expansion is shown in Fig. 3.9. As $R_d$ decreases, the helium is closer to the NaK molecule, and the interaction between the particles becomes a steep repulsive wall. Larger values of $R_d$ represent the helium at farther distances from the NaK molecule. As $R_d$ increases, the potential is less repulsive and has less angular variation. For very large $R_d$, we expect the Legendre polynomial coefficients for $\lambda > 2$ to fall off very rapidly. Figures 3.6 and 3.7 show that the

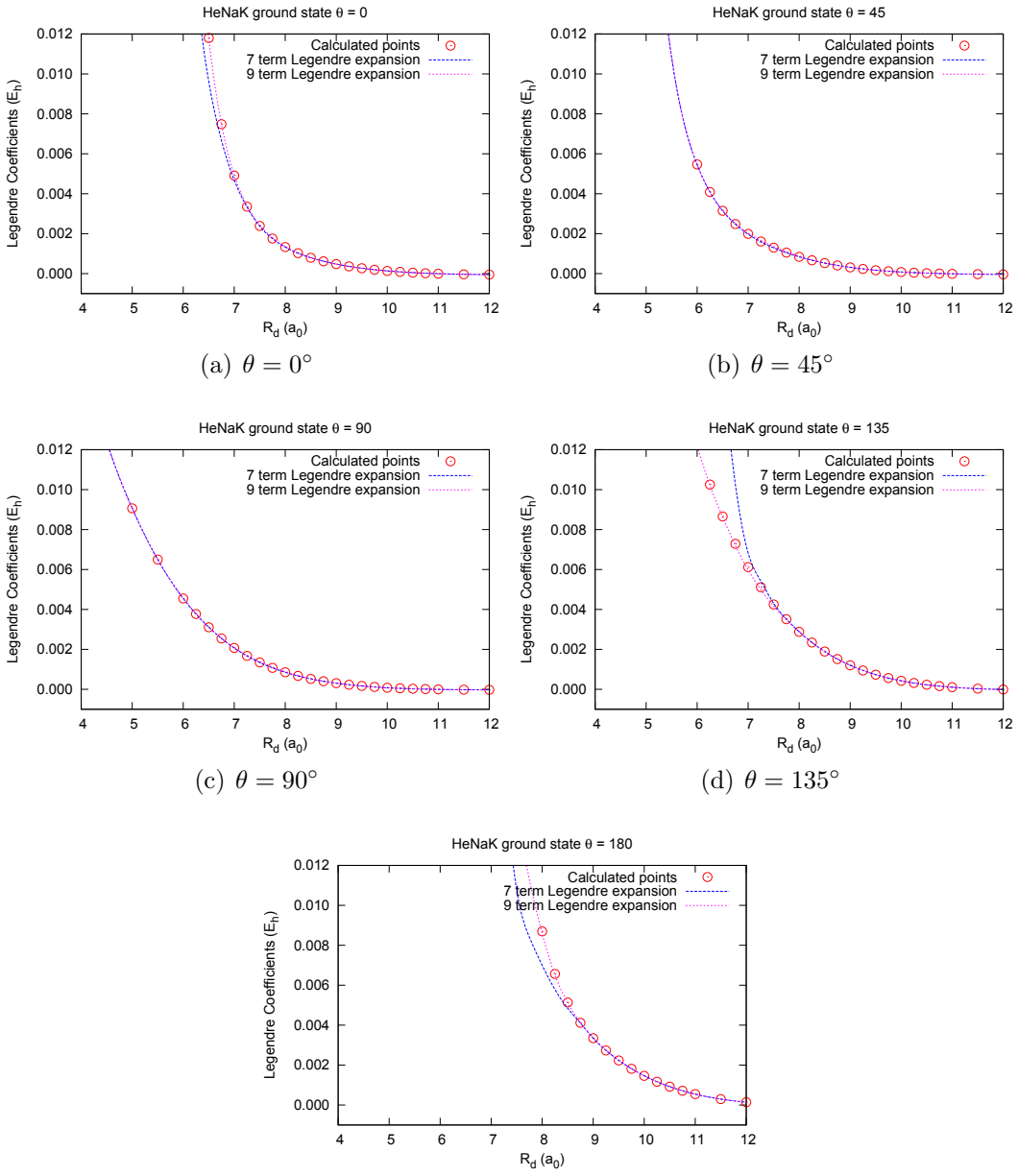


(a) $\theta = 0°$

(b) $\theta = 45°$

(c) $\theta = 90°$

(d) $\theta = 135°$

(e) $\theta = 180°$

**Figure 3.8:** Potentials generated by the seven and nine term Legendre polynomial expansion as a function of $R_{\mathrm{d}}$, for several values of $\theta$. The potentials produced by both expansions fit the calculated values for $E \leq 0.004$ $\mathrm{E_h}$, and the values of the potential produced by the nine term expansion are in agreement for energies up to $E = 0.012$ $\mathrm{E_h}$.

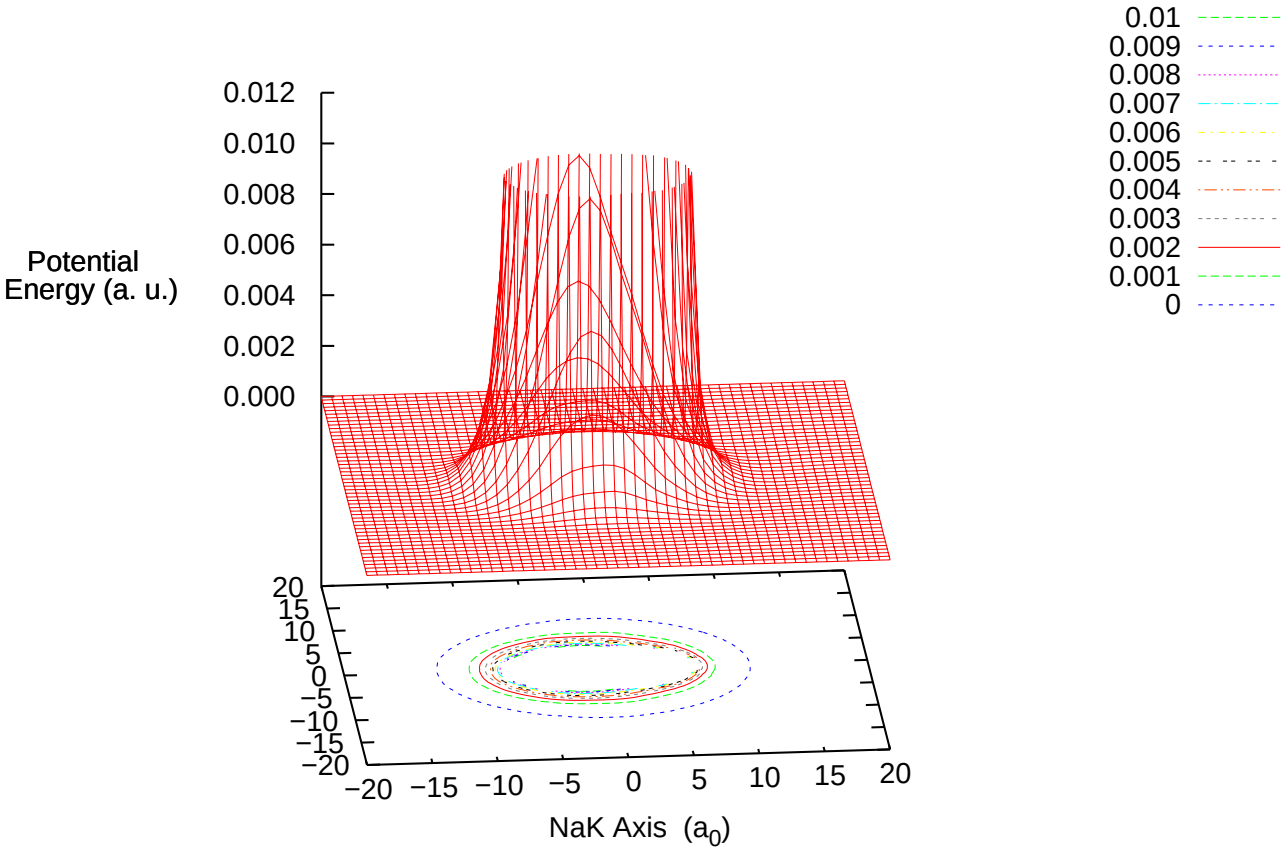


**Figure 3.9:** Potential surface for the nine term Legendre polynomial expansion of the ground state. Cubic splines were used to interpolate the Legendre polynomial expansion at each of the $R_{\mathrm{d}}$ values used in calculations. The splines were used to determine the potential on a cartesian grid that made a surface easy to visualze. The potential is also shown as contours on the $xy$-plane with the energy value of each contour line shown in $\mathrm{E_h}$ in the legend in the upper right.

coefficients do exhibit this behavior.

To be useful for scattering calculations, the PES cannot abruptly end at the edge of the grid defined by the GAMESS calculations. Thus, finding ways to extrapolate reasonably beyond the values of $R_{\mathrm{d}}$ used in the GAMESS calculations was necessary. Legendre coefficients for long range interactions (large $R_{\mathrm{d}}$) are fit with functional forms that have the desired asymptotic behavior, which is less angularly dependent. Thus, the higher order Legendre coefficients fall off more quickly and contribute less

**Table 3.3:** Values of the constants used for the exponentials fit to higher order Legendre coefficients of the ground state. The range of $R_{\rm d}$ and the rms deviation of the fits are given.

| $\lambda$ | ${R_{\rm d}}^{\rm init}$ | ${R_{\rm d}}^{\rm final}$ | $a_\lambda$ (a.u.) | $b_\lambda$ (a.u.) | rms deviation |
|---|---|---|---|---|---|
| 3 | 24 | 26 | 259.1019770 | $-.8981269$ | $1.0 \times 10^{-9}$ |
| 4 | 24 | 26 | $-351.3897962$ | $-.9203303$ | $2.6 \times 10^{-10}$ |
| 5 | 23 | 25 | 26.44405166 | $-.8359791$ | $2.2 \times 10^{-9}$ |
| 6 | 24 | 26 | $-6.149757903$ | $-.7873475$ | $1.2 \times 10^{-9}$ |

to the total potential. For $R_{\rm d} \geq 27.00\ a_0$, the potential could have been fit well by a four or five term Legendre polynomial expansion. For the nine term fit, $v_7$ and $v_8$ at $R_{\rm d} = 25\ a_0$ were $10^6$ times less than their values at $R_{\rm d} = 4.00\ a_0$. Thus, the $v_7$ and $v_8$ coefficients were set to zero for $R_{\rm d}$ larger than 25 $a_0$. The Legendre polynomial expansion coefficients $v_3, v_4, v_5$ and $v_6$ of the seven term expansion were fit at long range with an exponential function of the form

$$v_\lambda(R_{\rm d}) = a_\lambda \exp(b_\lambda R_{\rm d}) \tag{3.1.3}$$

in the ranges of $R_{\rm d}$ given in Table 3.3. The values obtained for coefficients $a_\lambda$ and $b_\lambda$ and the rms deviation of the fits are also given in Table 3.3. The remaining Legendre coefficents, $v_0, v_1$ and $v_2$, were fit at long range by an inverse power expansion of the form

$$v_\lambda(R_{\rm d}) = -\frac{C_6}{R_{\rm d}^6} + \frac{C_8}{R_{\rm d}^8}. \tag{3.1.4}$$

Calculated Legendre coefficients at $R_{\rm d} = 26.00$ and $27.50\ a_0$ were fit using this form to obtain the $C_6$ and $C_8$ constants for $v_0$ and $v_1$. Legendre expansion coefficients at $R_{\rm d} = 25.00$ and $30.00\ a_0$ were fit to obtain the $C_6$ and $C_8$ constants for $v_2$. The values of the $C_6$ and $C_8$ constants are given in Table 3.4.

**Table 3.4:** Values of the constants used for the inverse power expansion fit to $v_0$, $v_1$, and $v_2$ Legendre coefficients of the ground state.

| $\lambda$ | $C_6$ (a.u.) | $C_8$ (a.u.) |
|---|---|---|
| 0 | 37.86456146 | -9110.614558 |
| 1 | 21.33587097 | 24279.68622 |
| 2 | 15.62298730 | -25857.19567 |

These fits were then used to generate points for $R_\mathrm{d}$ larger than 25 $a_0$. The recursive function

$$(R_\mathrm{d})^{n+1} = 1.05 * (R_\mathrm{d})^n, \tag{3.1.5}$$

where $(R_\mathrm{d})^n$ is the $n^{th}$ value of $R_\mathrm{d}$, was used to generate a set of $R_\mathrm{d}$ values separated by increasing intervals, starting with $R_\mathrm{d} = 25.0\ a_0$ and continuing to $R_\mathrm{d} \approx 80.6\ a_0$. All the values of $R_\mathrm{d}$ generated by Eq. 3.1.5 and the Legendre expansion coefficients calculated from Eq. 3.1.3 and 3.1.4 for these positions are given in Appendix B.

Finally, it is important that the potential increase in a smooth, monotonic fashion for small values of $R_\mathrm{d}$. To ensure this behavior, the Legendre polynomial coefficients determined in the regions of the GAMESS calculations must be extrapolated to smaller values of $R_\mathrm{d}$. We used the interpolated values of each $v_\lambda$ coefficient near $R_\mathrm{d} = 4.00\ a_0$ to extrapolate linearly to smaller values of $R_\mathrm{d}$. This linear function was then used to generate coefficients for $R_\mathrm{d} = 0.00$, 1.00, 2.00, and 3.00 $a_0$. The values of all the Legendre polynomial expansion coefficients for both the seven and nine term expansions of the ground state, calculated and extrapolated, are given in Appendices B and C.

## 3.2 Excited State of NaK

### 3.2.1 Electronic Structure Calculations of the Excited State

For the $A^1\Sigma^+$ state of NaK plus helium, we used the same basis set listed in Table 3.1. Using the GAMESS code, we first performed a restricted Hartree-Fock calculation. Then multi-configuration self-consistent field calculations (MCSCF) and configuration interaction (CI) calculations were performed. The MCSCF calculations have two active space orbitals and the CI calculations have eight active space orbitals. As with the ground state, the six lowest orbitals were frozen and the six highest orbitals of the virtual space were closed to excitation. Single and double excitations were allowed from the reference state resulting in 3,458,067 CSFs.

The NaK separation, $r_{\mathrm{v}}$, was held fixed at the first excited state equilibrium distance 7.935 $a_0$, which was found experimentatlly by Ross *et al.* [27]. Again, this is a reasonable approximation for the $v = 0$ vibrational state. The calculations were performed for systematic combinations of $R_{\mathrm{d}}$ and $\theta$. Due to the larger number of CSFs, the calculations for the excited state were considerably more costly in terms of computer time than the ground state calculations. Thus, only a subset of the $R_{\mathrm{d}}$ and $\theta$ combinations used for the ground state calculations were performed for the excited state. The $R_{\mathrm{d}}$ values were calculated in 0.50 $a_0$ increments for $R_{\mathrm{d}}$ = 3.00–7.00 $a_0$ and 1.0 $a_0$ increments for $R_{\mathrm{d}}$ = 8.00–12.00 $a_0$. Additional points were calculated at $R_{\mathrm{d}}$ = 15.00, 17.50, 20.00, 22.50, 25.00, 27.50, and 30.00 $a_0$. As before, the angular dependence of the potential is greater for smaller $R_{\mathrm{d}}$ and calculations were performed for more angles $\theta$ between 0° and 180° in these regions. The results of all the calculations performed for the first excited state can be found in

Appendix D. A calculation at $R_{\mathrm{d}} = 10000.00\ a_0$ yielded the asymptotic limit of $-764.164448090\ \mathrm{E_h}$. For use in the scattering calculations, this energy was subtracted from all the calculated values to obtain potential energies relative to the asymptotic limit.

### 3.2.2 Legendre Expansion of the Excited State Potential

When fitting the first excited state, the same considerations discussed in Section 3.1.2 have to be taken into account; which energy ranges were pertinent to the comparison with experiment and how many terms to include in the Legendre expansion. A procedure similar to the one described for the ground state was used to fit the excited state calculations. For fixed $R_{\mathrm{d}}$, a seven term polynomial function of $\cos\theta$ was fit to potential energies up to $0.004\ \mathrm{E_h}$. At smaller values of $R_{\mathrm{d}}$, the potential at some angular positions was greater than $0.0040\ \mathrm{E_h}$. These angles were omitted from the fit at that $R_{\mathrm{d}}$. For $R_{\mathrm{d}} \leq 6.00\ a_0$, all the calculated values of the potential were above $0.0040\ \mathrm{E_h}$. The same angular range used for $R_{\mathrm{d}} = 6.00\ a_0$ was used to fit $R_{\mathrm{d}} \leq 6.00\ a_0$. All the calculated potentials were less than $0.004\ \mathrm{E_h}$ for $R_{\mathrm{d}} \geq 10.00\ a_0$. To fit the repulsive regions of the potential up to energies of $0.012\ \mathrm{E_h}$, a second eleven term fit was done. The angular ranges included in each of these fits are given in Table 3.5. Figure 3.10 graphically shows the calculated values included in the seven and eleven term fits. Both fits can be used for scattering calculations with energies lower than $0.004\ \mathrm{E_h}$, and the eleven term fit can be used for higher energy calculations up to $0.012\ \mathrm{E_h}$.

The calculated points were then fit with the same Legendre polynomial expansion in Eq. 3.1.1. Both the seven and eleven term fits were used to generate equally

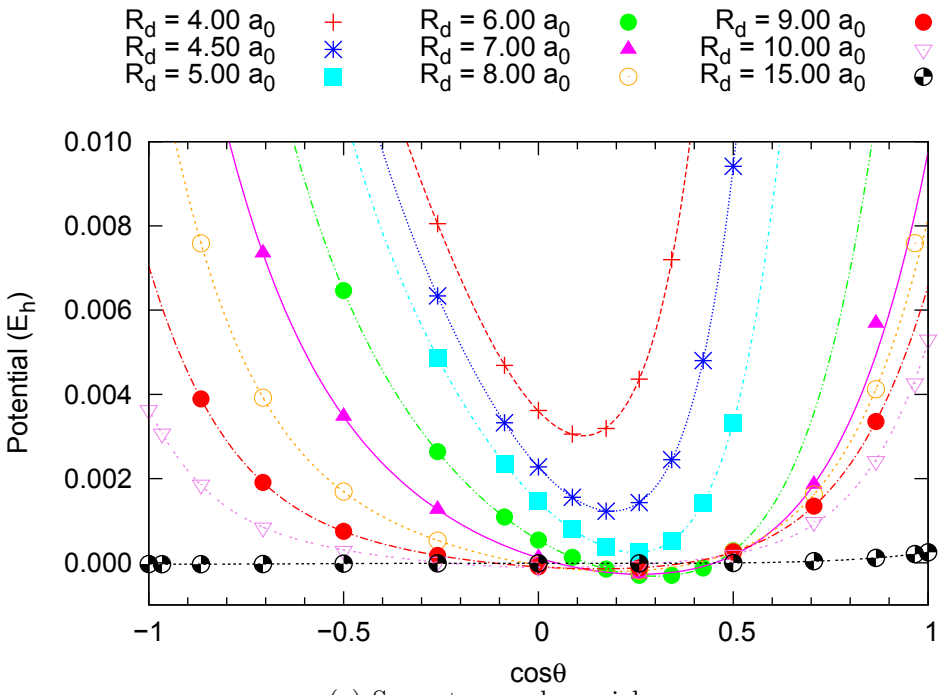


(a) Seven term polynomial

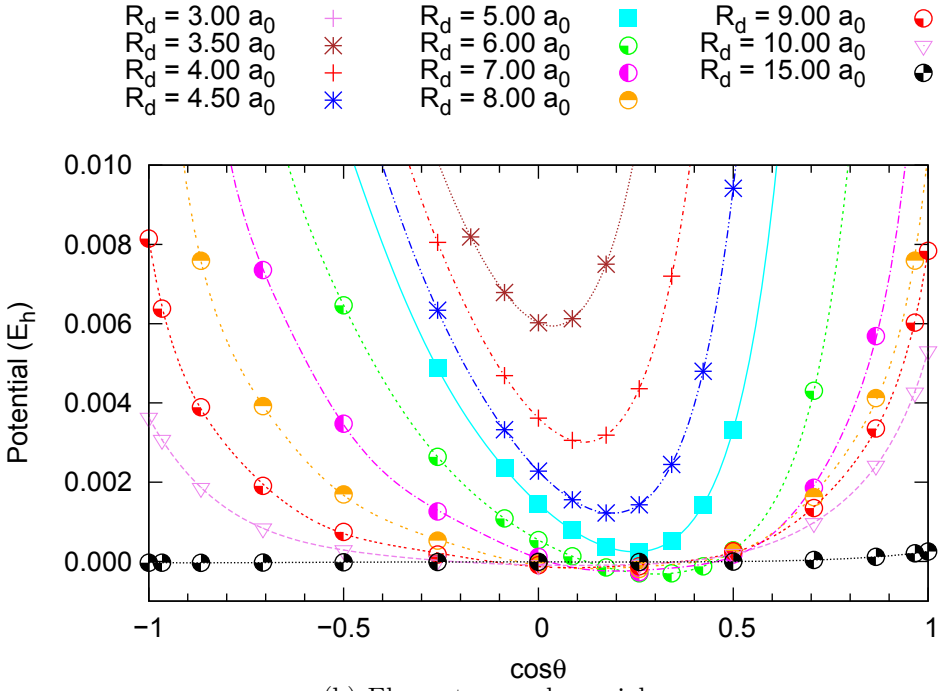


(b) Eleven term polynomial

**Figure 3.10:** Calculated values of the excited state potential within the desired energy ranges that were included in the seven and eleven term polynomial fits. The points indicate the calculated values included in the fit, and the lines represent the polynomial fits.

**Table 3.5:** Range of $\theta$ used to fit the excited state potential with seven and eleven term polynomials for each $R_d$. $R_d$ is given in $a_0$, $\theta$ in degrees and rms deviation in $cm^{-1}$.

| | | 7 Term Expansion | | 11 Term Expansion | |
|---|---|---|---|---|---|
| $R_d$ | $\Delta\theta$ | $\theta$ Range | rms deviation | $\theta$ Range | rms deviation |
| 3.00 | 5 | — | — | 60–135 | 0.043 |
| 3.50 | 5 | — | — | 60–135 | 0.022 |
| 4.00 | 5 | 60–120 | 2.8 | 45–135 | 0.014 |
| 4.50 | 5 | 60–120 | 1.4 | 45–135 | 0.014 |
| 5.00 | 5 | 60–120 | 0.068 | 45–150 | 0.12 |
| 5.50 | 5 | 60–120 | 0.27 | 30–150 | 0.10 |
| 6.00 | 5 | 60–120 | 0.10 | 30–150 | 0.08 |
| 6.50 | 5 | 45–135 | 0.59 | 15–150 | 0.28 |
| 7.00 | 15 | 45–135 | $1.1\times10^{-13}$ | 0–150 | 25.7 |
| 7.50 | 15 | — | — | 0–165 | 5.7 |
| 8.00 | 15 | 30–150 | 0.67 | 0–165 | 10.4 |
| 9.00 | 15 | 30–150 | 0.47 | 0–180 | 7.8 |
| 10.00 | 15 | 0–180 | 8.1 | 0–180 | 1.7 |

spaced points as a function of $\cos\theta$, which were then fit exactly by a Legendre expansion. The conversion from the polynomial fits to the Legendre expansion was checked using Eq. 3.1.2, and again both methods produced the same expansions.

As before, a cubic spline was used to interpolate the Legendre polynomial expansion coefficients $v_\lambda$ between $R_d$ values used in GAMESS calculations. The Legendre polynomial coefficients of the two fits are shown in Figs. 3.11 and 3.12 as a function of $R_d$. The (b) panels show the coefficents over a larger range of $R_d$. The points represent coefficients determined at $R_d$ values for which GAMESS calculations were performed. The lines correspond to the cubic splines. The Legendre expansion coefficients for the two different expansions of the excited state are more similar than those of the ground state. For the excited state, both expansions have coefficients that are mostly greater than zero except for shallow wells around $R_d = 6.00\ a_0$. The

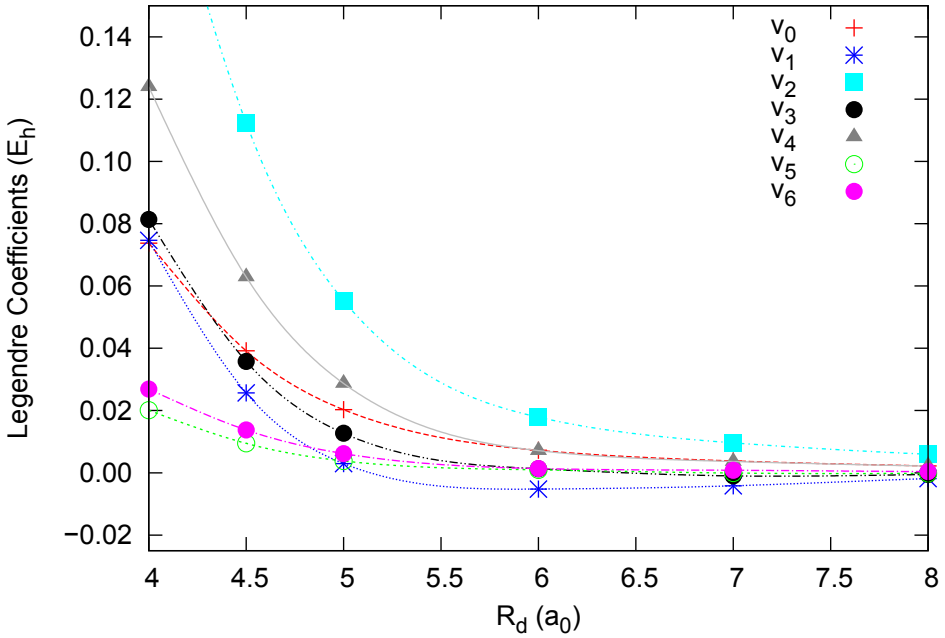


(a) Seven term Legendre polynomial expansion coefficients of the excited state

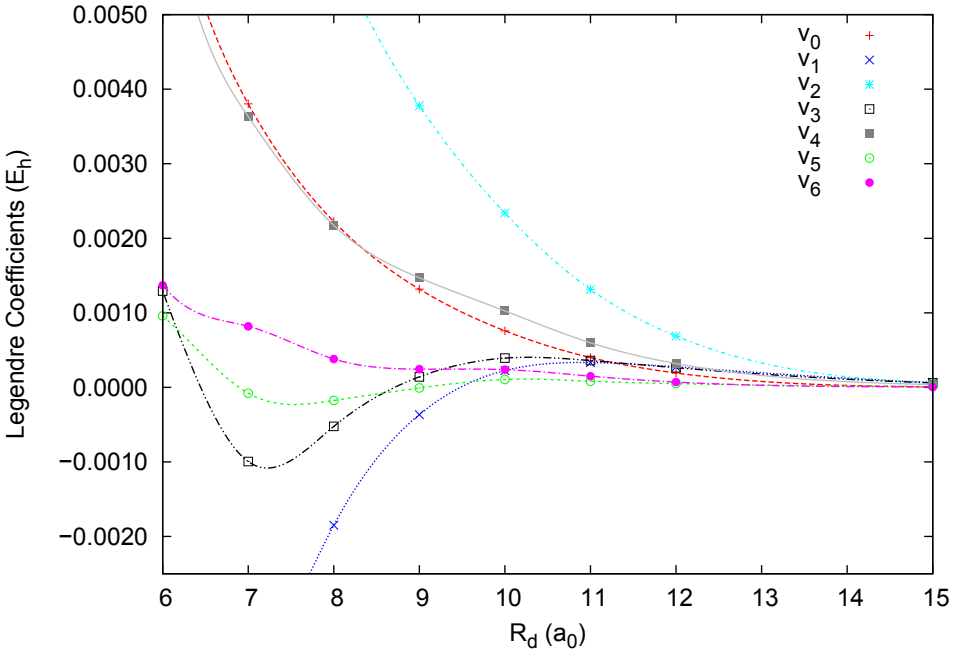


(b) Seven term Legendre polynomial expansion coefficients of the excited state: Long range

**Figure 3.11:** Seven term Legendre polynomial expansion coefficients of the excited state as a function of $R_{\mathrm{d}}$. The points represent Legendre coefficients for calculated points. The lines are the cubic splines between the data. The coefficients are given in atomic units.

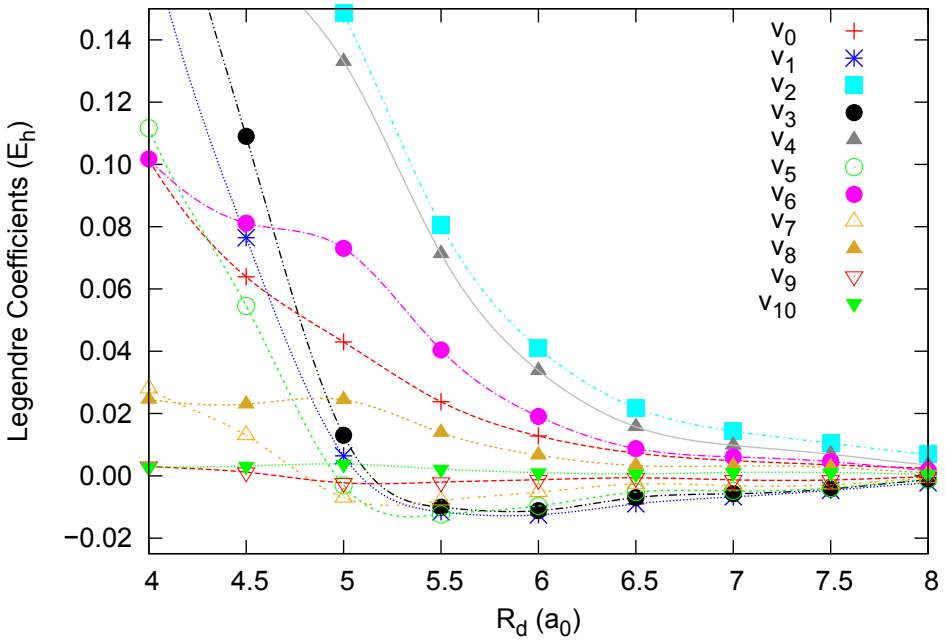


(a) Eleven term Legendre polynomial expansion coefficients of the excited state

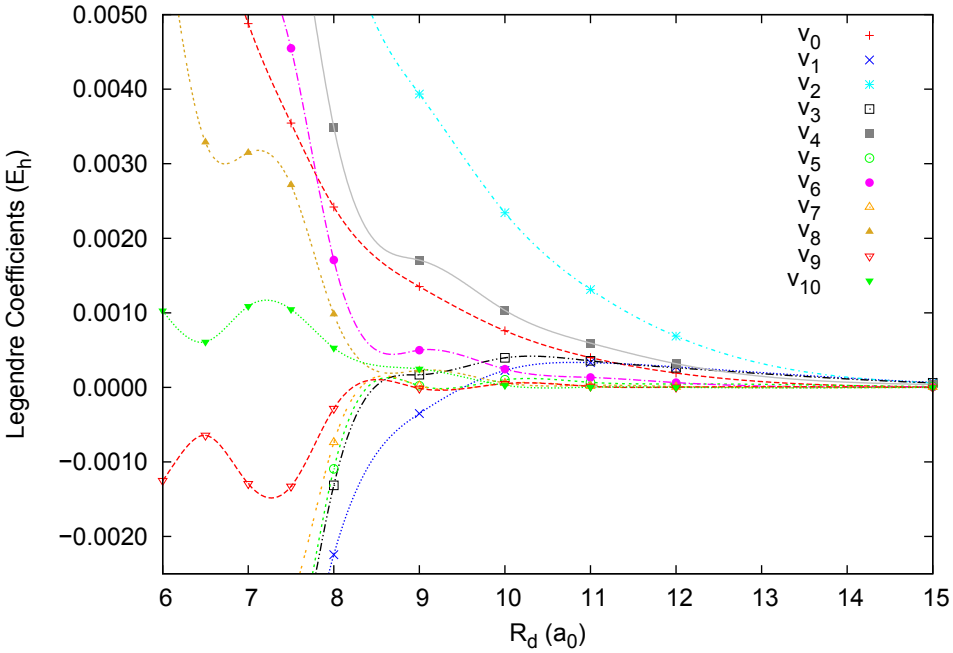


(b) Eleven term Legendre polynomial expansion coefficients of the excited state: Long range

**Figure 3.12:** Eleven term Legendre polynomial expansion coefficients of the excited state as a function of $R_{\mathrm{d}}$. The points represent Legendre coefficients for calculated points. The lines are the cubic splines between the data. The coefficients are given in atomic units.

two highest order coefficients of the eleven term expansion, $v_9$ and $v_{10}$, are relatively small compared to the other $v_\lambda$.

The splines of the $v_\lambda$ coefficients can then be used in Eq. 3.1.1 to generate coefficients for any $R_\mathrm{d}$ value, which will be needed for the scattering calculations. In the same process discussed in Section 3.1.3, the interpolations can be used to evaluate the potential for $R_\mathrm{d}$ and $\theta$ corresponding to positions $x$ and $y$ on a rectangular cartesian grid. Fig. 3.13 shows a representation of the surface generated from the eleven term Legendre polynomial expansion. Again, as the He is closer to the NaK molecule and $R_\mathrm{d}$ decreases, the potential becomes very repulsive. However, there

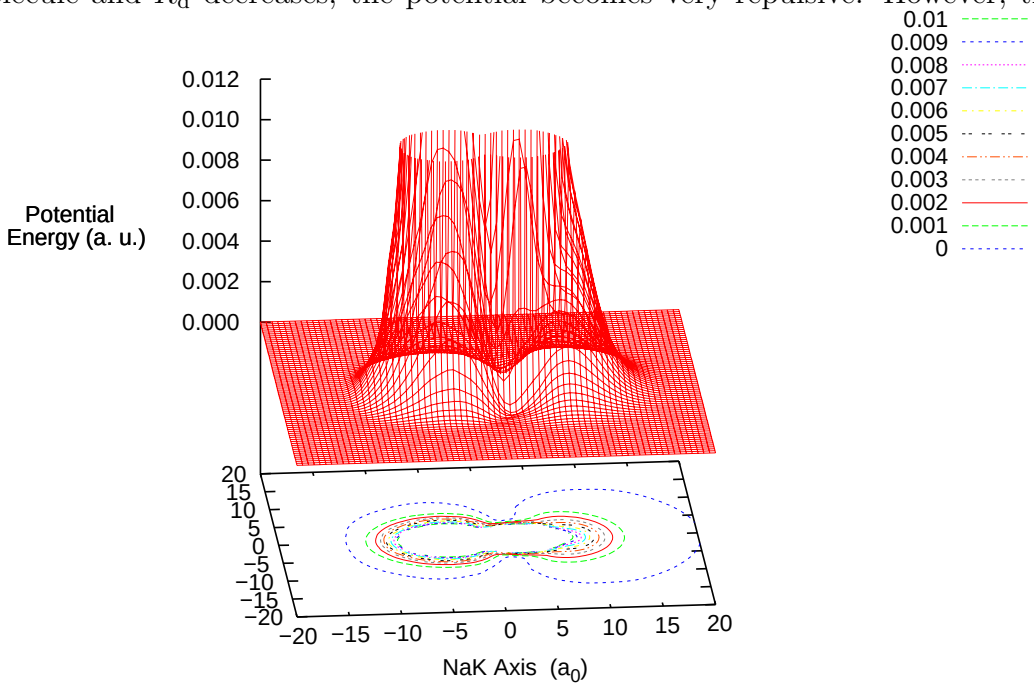


**Figure 3.13:** Potential surface for the eleven term Legendre polynomial expansion of the first excited state. Cubic splines were used to interpolate the Legendre polynomial expansion at each of the $R_\mathrm{d}$ values used in calculations. The splines were used to determine the potential on a cartesian grid that made a surface easy to visualize. The potential is also shown as contours on the $xy$-plane with the energy value of each contour line shown in $\mathrm{E_h}$ in the legend in the upper right.

is a marked difference between the excited state PES and the ground state PES shown in Fig. 3.9. Around $\theta = 90°$, the excited state potential has an area where the repulsive wall begins at relatively small $R_{\rm d}$ in comparison to other $\theta$. This causes the potential to look "pinched in" in this region.

As with the ground state, a reasonable extrapolation of the PES beyond the positions used in the GAMESS calculations was necessary for scattering calculations. For long range $R_{\rm d}$, the coefficients were again fit with functional forms that produced the desired asymptotic behavior. At large helium separations, the potential has less angular dependence and the higher order coefficients contributed negligibly to the potential. At $R_{\rm d} = 17.5\ a_0$, $v_7$, $v_8$, $v_9$, and $v_{10}$ of the eleven term fit were at least a factor of $10^6$ times less than their values at $R_{\rm d}$ =3.00 $a_0$ and fell off rapidly. For $R_{\rm d} \geq 20.0\ a_0$, $v_7$, $v_8$, $v_9$, and $v_{10}$ were set to zero.

The Legendre coefficients, $v_3$, $v_4$, $v_5$, and $v_6$, from the seven term fit were fit with the same exponential form as Eq. 3.1.3 using the potential energies at $R_{\rm d} = 20.00, 22.50$, and $25.00\ a_0$ to obtain the coefficient values in Table 3.6. To extrapolate the $v_0, v_1$, and $v_2$ coefficients of the seven term expansion, the potential energies at $R_{\rm d} = 27.50$ and $30.0\ a_0$ were fit with a three term polynomial function, which had an rms deviation well within that specified in the GAMESS calculations. The three

**Table 3.6:** Values of the constants used for the exponentials fit to higher order Legendre coefficients of the excited state. The rms deviation of the fits are given.

| $\lambda$ | $a_\lambda$ (a.u.) | $b_\lambda$ (a.u.) | rms deviation |
|---|---|---|---|
| 3 | 65.4854085 | −.8302992934 | $1.2\times10^{-7}$ |
| 4 | .104862642 | −.5565878502 | $1.0\times10^{-7}$ |
| 5 | .703830725 | −.6517641039 | $7.0\times10^{-8}$ |
| 6 | .005323882 | −.4826679190 | $1.1\times10^{-7}$ |

**Table 3.7:** Values of the constants used for the inverse power expansion fit $v_0, v_1$, and $v_2$ Legendre coefficients of the excited state. The rms deviations are also given.

| $\lambda$ | $C_6$ (a.u.) | $C_8$ (a.u.) | rms deviation |
|---|---|---|---|
| 0 | 58.5037147 | −17751.00260 | $3.5\times10^{-9}$ |
| 1 | 31.3515956 | 30120.52809 | $6.7\times10^{-9}$ |
| 2 | −9.0031635 | −57736.76543 | $3.9\times10^{-9}$ |

term polynomial was used to generate a three term Legendre polynomial expansion, with $v_0, v_1$, and $v_2$ coefficients. The Legendre polynomial coefficients for $R_\mathrm{d} = 25.00$, 27.50, and 30.00 $a_0$ were fit with the same inverse power expansion in Eq. 3.1.4 to obtain the $C_6$ and $C_8$ constants given in Table 3.7 . These fits were used to generate points for $25.0 \leq R_\mathrm{d} \leq 80.6$ $a_0$ at values given by Eq. 3.1.5.

A smooth extrapolation of the potential for $R_\mathrm{d}$ smaller than the calculated points was also needed to ensure the potential increases monotonically. For the seven term fit, a cubic spline was used to interpolate the values of the coefficients near $R_\mathrm{d} =$ 4.00 $a_0$. This spline was linearly extrapolated to generate points for $R_\mathrm{d} = 0.00$, 1.00, and 2.00 $a_0$. With these fits, Legendre polynomial expansion coefficients of the seven term expansion could be calculated for any $R_\mathrm{d}$ value needed for scattering calculations. The values of all the Legendre polynomial expansion coefficients of the seven term expansion are given in Appendix E.

For the eleven term fit, the Legendre polynomial expansion coefficients also had to be extrapolated smoothly for values of $R_\mathrm{d}$ less than 3.00 $a_0$. The Legendre polynomial expansion coefficients $v_0$, $v_2$, $v_4$, $v_5$, $v_6$, $v_7$, and $v_8$ were extrapolated

**Table 3.8:** Values of the constants used for the exponential expansion fit to Legendre coefficients of smaller $R_{\mathrm{d}}$ of the excited state.

| $\lambda$ | $c_\lambda$ | $d_\lambda$ |
|---|---|---|
| 0 | 1.970909 | 0.7132539 |
| 2 | 4.884395 | 0.6424510 |
| 4 | 2.242581 | 0.5179611 |
| 5 | 1.698092 | 0.6153261 |
| 6 | 0.5044582 | 0.3701183 |
| 7 | 0.3225516 | 0.5328718 |
| 8 | 0.06031066 | 0.2048104 |

using an exponential fit of the coefficent values at $R_{\mathrm{d}} = 3.00$ and 3.50 $a_0$

$$v_\lambda(R_{\mathrm{d}}) = c_\lambda \exp(d_\lambda R_{\mathrm{d}}). \tag{3.2.1}$$

The coefficients of these fits are listed in Table 3.8. The remaining Legendre polynomial coefficients, $v_1$, $v_3$, $v_9$ and $v_{10}$, were extrapolated with a linear function

$$v_\lambda = w_\lambda R_{\mathrm{d}} \ + t_\lambda \tag{3.2.2}$$

fit to the coefficients at $R_{\mathrm{d}} = 3.00$ and 3.50 $a_0$. The constants used in the liner fit are given in Table 3.9. These extrapolations were used to generate Legendre polynomial expansion coefficients at $R_{\mathrm{d}} = 0.0$, 0.5, 1.0, 1.5, 2.0, and 2.5 $a_0$. The

**Table 3.9:** Values of the constants used for the linear expansion fit to Legendre coefficients of smaller $R_{\mathrm{d}}$ of the excited state.

| $\lambda$ | $w_\lambda$ (a.u.) | $t_\lambda$ (a.u.) |
|---|---|---|
| 1 | −0.3544316 | 1.5753729 |
| 3 | −0.3553723 | 1.651716 |
| 9 | −0.002976065 | 0.01612675 |
| 10 | −0.0000073894 | 0.002869960 |

fitting methods described in this section were used to generate coefficients for the seven and eleven term Legendre polynomial expansion coefficients for $R_{\mathrm{d}}$ from 0.0 to 80.6 $a_0$ given in Appendices E and F.

## 3.3 Comparison of Ground and Excited State PES

There are several differences between the ground and excited state PES that should be noted. From Figs. 3.5 and 3.10 it can be seen that smaller values of $R_{\mathrm{d}}$ are in the available energy range for the excited state than the ground state. In the seven term Legendre expansion coefficients, the odd $v_\lambda$ of the ground state are negative and have roughly the same magnitude as the even $v_\lambda$. All the Legendre coefficients of the excited state are mostly positive. However, the even $v_\lambda$ are larger in magnitude than the odd coefficients in most instances. This may cause the propensity for even $\Delta j$ at certain energies and correspond to experimental observations.

# Chapter 4

# Coupled Channel Scattering Calculations

## 4.1 Scattering Theory

This chapter will discuss the coupled channel scattering method used in the majority of this work. We will begin with a brief discussion of classical scattering as a means of introducing quantum mechanical scattering. We will then move on to a formal discussion of the theory of Arthurs and Dalgarno [28] for scattering by a rigid rotator, which is used to calculate quantum mechanical cross sections. We have also extended the calculations so that we can determine preservation of the orientation, alignment, and higher moments describing the distribution of the angular momentum quantum number $m$. The final section will report the results of using this method to study inelastic scattering of He with NaK, including a comparison with experimental results.

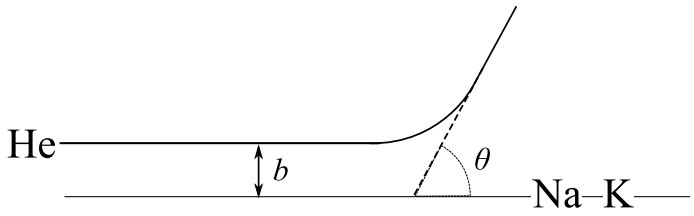


**Figure 4.1:** Basic diagram of scattering where He is the projectile and NaK is the target.

### 4.1.1 Introduction to Scattering

In classical scattering, the incident particle, in the present case helium, moves towards the target, the NaK molecule. Figure 4.1 shows a diagram of the classical scattering system, in which $b$ is the impact parameter and $\theta$ is the angle at which the projectile is scattered. The goal of scattering calculations is to determine a cross section, which is related to the effective size that the target presents to the incident particle. The cross sections depends on the forces exerted on one particle by the other. Quantum mechanics treats the system using wave functions to represent particles. The present work calculates quantum mechanical cross sections.

### 4.1.2 Scattering by a Rigid Rotator

This section will describe the formalism for the scattering calculations that was developed by Arthurs and Dalgarno [28]. The goal of this work is to determine how angular momentum from the incident He atom is imparted to the NaK molecule during a collision. Arthurs and Dalgarno use a coupled angular momentum representation. The total angular momentum is $\vec{J} = \vec{j} + \vec{l}$, where $\vec{j}$ is the rotational angular momentum of the target and $\vec{l}$ is the orbital angular momentum of the

incident particle with respect to the target. The combinations of $\vec{j}$ and $\vec{l}$ that can produce $\vec{J}$ are referred to as a channels. The projection of $\vec{l}$ onto a space-fixed axis is labeled $m_l$ to distinguish it from the projection of $\vec{j}$, which is labeled $m$ as defined in Section 1.3. The projection of the total angular momentum $\vec{J}$ onto the $z$-axis is labeled $M$. Using the total angular momentum $\vec{J}$ is advantageous because the total angular momentum must be conserved throughout the collision that does not change the vibrational state.

Figure 4.2 shows the space-fixed coordinate system used in this formalism. This work considers collisions in which the vibrational state does not change. Therefore, the internuclear separation of the Na and K, $r'$, can be held fixed, as in the calculations of the interaction potentials, and the NaK molecule is treated as a rigid rotator with moment of inertia $I$. The orientation of the internuclear axis of the diatomic with respect to a space-fixed axis is represented as $\hat{r}' = (\theta', \phi')$. The position of the helium is described using $\hat{r} = (\theta'', \phi'')$. The angle between $\hat{r}'$ and $\hat{r}$ is the same as the angle $\theta$ described by the Jacobi coordinates in Chapter 3. The eigenfunctions of the rotational Hamiltonian are spherical harmonics $Y_{jm}(\hat{r}')$

$$\hat{H}_{\text{rot}} Y_{jm}(\hat{r}') = \frac{\hbar^2}{2I} j(j+1) Y_{jm}(\hat{r}'). \tag{4.1.1}$$

The angular functions that describe the orbital motion are also spherical harmonics, $Y_{lm_l}(\hat{r})$.

The total Hamiltonian can be written as a sum of terms corresponding to the rigid rotator, the kinetic energy of the incident particle, and the interaction between the atoms:

$$\hat{H} = \hat{H}_{\text{rot}} + \hat{H}_{\text{inc}} = \hat{H}_{\text{rot}} - \frac{\hbar^2}{2\mu} \nabla_r^2 + V(r, \theta), \tag{4.1.2}$$

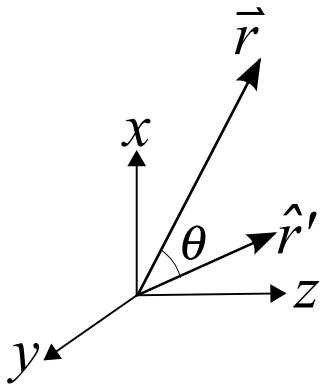


**Figure 4.2:** Coordinate system used for the rigid rotator formalism. $\hat{r}'$ represents the orientation of the internuclear axis of the rigid rotator. $\vec{r}$ represents the position of the incident particle. The angle between these is label $\theta$.

where $\mu$ is the reduced mass of He + NaK. By using Clebsch-Gordan coefficients $(jlmm_l|jlJM)$, Arthurs and Dalgarno defined the coupled angular momentum functions

$$\mathcal{Y}^M_{Jjl}(\hat{r}', \hat{r}) = \sum_{m_l=-l}^{l} \sum_{m=-j}^{j} (jlmm_l|jlJM) Y_{lm_l}(\hat{r}) Y_{jm}(\hat{r}'). \tag{4.1.3}$$

These coupled functions can be used as basis functions for an expansion of the total wave function

$$\Psi^{JM}_{jl}(\hat{r}', \hat{r}) = \sum_{j'} \sum_{l'} \frac{1}{r} u^{Jjl}_{j'l'}(r) \mathcal{Y}^M_{Jj'l'}(\hat{r}', \hat{r}). \tag{4.1.4}$$

Using this form of the wave function guarantees that the wave function will be an eigenfunction of the total angular momentum. For an exact solution, the summations over $j'$ and $l'$ would have to be infinite. However, convergence can normally be achieved by truncating the sum after a finite number of terms. Section 4.2 will discuss how to determine the number of channels that should be included in a calculation.

The total energy of the system is the sum of the rotational energy of NaK in a

given rotational state $j$ and the kinetic energy of the incident particle $KE$

$$E = KE + \frac{\hbar^2}{2I} j(j+1). \tag{4.1.5}$$

The total wave function is an eigenvector of the Schrödinger equation

$$\hat{H}\Psi^{JM}_{jm}(\hat{r}', \hat{r}) = E\Psi^{JM}_{jm}(\hat{r}', \hat{r}). \tag{4.1.6}$$

The total wave function is substituted into Eq. 4.1.6. By using Eqs. 4.1.2, 4.1.1, and 4.1.5, multiplying by the total wave function and integrating over $\hat{r}'$ and $\hat{r}$, one can obtain the coupled equations

$$\frac{\hbar^2}{2\mu}\left[-\frac{d^2}{dr^2} + \frac{l'(l'+1)}{r^2} - k^2_{j'}\right] u^{Jjl}_{j'l'}(r) + \sum_{j''}\sum_{l''}\langle j''l''; J|V|j'l'; J\rangle u^{Jjl}_{j'l'}(r) = 0, \tag{4.1.7}$$

where

$$k^2_{j'} = \frac{2\mu}{\hbar^2}\left[E - \frac{\hbar^2}{2I} j'(j'+1)\right] \tag{4.1.8}$$

and

$$\langle j''l''; J|V|j'l'; J\rangle = \iint \mathcal{Y}^M_{Jj''l''}(\hat{r}', \hat{r}) V \, \mathcal{Y}^M_{Jj'l'}(\hat{r}', \hat{r}) \mathrm{d}\hat{r}\mathrm{d}\hat{r}', \tag{4.1.9}$$

in which $|j'l'; J\rangle$ represents the coupled angular momentum basis function $\mathcal{Y}^M_{Jj'l'}$. The matrix elements in Eq. 4.1.9 are independent of $M$, so it can be omitted from the notation. The matrix elements can be easily evaluted if the potential can be expressed as a sum of Legendre polynomials that depend on $\theta$, the angle between $\hat{r}'$ and $\hat{r}$

$$V(r, \theta) = \sum_{\lambda=0}^{\lambda_{\max}} V_\lambda(r) P_\lambda(\cos\theta). \tag{4.1.10}$$

One can use the addition theorem of spherical harmonics [29]:

$$\frac{2\lambda+1}{4\pi}P_\lambda(\cos\theta)=\sum_{\mu=-\lambda}^{\lambda}Y^*_{\lambda\mu}(\hat{r})Y_{\lambda\mu}(\hat{r}') \tag{4.1.11}$$

and the Legendre polynomial expansion of the potential to write the matrix elements of Eq. 4.1.9 in terms of the Percival-Seaton coefficients [30]:

$$\begin{aligned} f_\lambda(jl,j'l';J) &= \langle jl;J|P_\lambda(\cos\theta)|j'l';J\rangle \\ &= (-1)^{j+j'-J}\sqrt{(2j+1)(2j'+1)(2l+1)(2l'+1)} \\ &\qquad \begin{pmatrix} l & l' & \lambda \\ 0 & 0 & 0 \end{pmatrix} \begin{pmatrix} j & j' & \lambda \\ 0 & 0 & 0 \end{pmatrix} \begin{Bmatrix} j & j' & \lambda \\ l & l' & J \end{Bmatrix}, \end{aligned} \tag{4.1.12}$$

where $\left(\begin{smallmatrix} l & l' & \lambda \\ 0 & 0 & 0 \end{smallmatrix}\right)$ and $\left(\begin{smallmatrix} j & j' & \lambda \\ 0 & 0 & 0 \end{smallmatrix}\right)$ are $3j$ coefficients and $\left\{\begin{smallmatrix} j & j' & \lambda \\ l & l' & J \end{smallmatrix}\right\}$ is a $6j$ coefficient. Using the fact that

$$f_0(jl,j'l';J)=\delta_{jj'}\delta_{ll'} \tag{4.1.13}$$

one can explicitly separate the spherically symmetric part of the potential, $V_0(r)$, and write the coupled equations as

$$\begin{aligned} &\frac{\hbar^2}{2\mu}\left[-\frac{d^2}{dr^2}+\frac{l'(l'+1)}{r^2}-k^2_{j'}+\frac{2\mu}{\hbar^2}V_0(r)\right]u^{Jjl}_{j'l'}(r) \\ &\qquad +\sum_{j''}\sum_{l''}\sum_{\lambda=1}^{\lambda_{\max}}f_\lambda(jl,j'l';J)V_\lambda(r)u^{Jjl}_{j'l'}(r)=0. \end{aligned} \tag{4.1.14}$$

This set of coupled equations must be solved numerically. There are $N$ linearly independent solutions, where $N$ is the number of channels $(j'l')$. The solutions can be represented by a matrix with columns denoted by $(jl)$ and rows by $(j'l')$.

The next section will discuss the appropriate boundary conditions that must be applied to the solution for scattering calculations and how they are used to determine $(jmlm_l) \rightarrow (j'm'l'm'_l)$ cross sections.

### 4.1.3 Application of Boundary Conditions

By taking appropriate linear combinations of the solutions determined numerically in Section 4.1.2, one can construct solutions that satisfy

$$u^{Jjl}_{j'l'}(r) = \delta_{jj'}\delta_{ll'} \exp\left[-i\left(k_j r - \frac{l\pi}{2}\right)\right] - \left(\frac{k_j}{k_{j'}}\right)^{\frac{1}{2}} S^J_{jl,j'l'} \exp\left[-i\left(k_{j'} r - \frac{l'\pi}{2}\right)\right]. \tag{4.1.15}$$

This form determines the scattering matrix $\mathbf{S}^J$ and the related transition matrix $\mathbf{T}^J$, which has elements

$$T^J_{jl,j'l'} = \delta_{jj'}\delta_{ll'} - S^J_{jl,j'l'}. \tag{4.1.16}$$

Partial cross sections for all the possible scattering processes for a particular total angular momentum can be written in terms of the $\mathbf{T}$-matrix elements

$$\sigma^J(j \rightarrow j') = \frac{\pi}{k_j^2}(2J+1) \sum_l \sum_{l'} \left|T^J_{jl\rightarrow j'l'}\right|^2. \tag{4.1.17}$$

A summation over all the total angular momenta yields the total cross section for a $(j \rightarrow j')$ transition,

$$\sigma(j \rightarrow j') = \sum_J \sigma^J(j \rightarrow j') = \frac{\pi}{k_j^2} \sum_J (2J+1) \sum_l \sum_{l'} \left|T^J_{jl\rightarrow j'l'}\right|^2. \tag{4.1.18}$$

Cross sections can also be determined for $(jm \rightarrow j'm')$ transitions. These cross sections are calculated using the Grawert coefficients [31], labeled $B_\lambda$, which are

derived from the **T**-matrix elements:

$$B_\lambda(j,j') = \sum_l \sum_{l'} \left| \sum_J (2J+1)(-1)^J \begin{Bmatrix} j' & j & \lambda \\ l & l' & J \end{Bmatrix} T^J_{jl\to j'l'} \right|^2 . \tag{4.1.19}$$

Note that the Grawert coefficients sum over all the **T**-matrix elements for all the partial waves and then square this sum, as opposed to Eqs. 4.1.17 and 4.1.18 which square the elements of $\mathbf{T}^J$ before the summation. The computer code used to calculate the $B_\lambda$ values must store a great deal of information in memory. The Grawert coefficients can then be used to calculate cross sections for a $(jm \to j'm')$ transition. For cell-like experiments that use a circularly polarized laser, which define the $z$-axis along the direction of laser beam propagation, the $\sigma(jm \to j'm')$ are given by the expression [32]

$$\sigma(jm \to j'm') = \frac{\pi}{k_j^2} \sum_\lambda (2\lambda+1) \begin{pmatrix} j' & j & \lambda \\ m' & -m & m-m' \end{pmatrix}^2 B_\lambda(j,j'). \tag{4.1.20}$$

Once the calculations have been performed for all values of $J$, the code can produce the cross section for any $(jm \to j'm')$ transition. The next section will describe transformations necessary to consider $m$ changing collisions using the moment expansion instead of specific $(jm \to j'm')$ cross sections.

The cross section for a $(j \to j')$ transition can also be found by calculating the average over inital $m$ and sum over final $m'$ of the $(jm \to j'm')$ cross sections in Eq. 4.1.20

$$\sigma(j \to j') = \frac{1}{2j+1} \sum_{m=-j}^{j} \sum_{m'=-j'}^{j'} \sigma(j, m \to j'm'). \tag{4.1.21}$$

The cross section obtained by Eq. 4.1.21 is independent of $m$ and is therefore valid

for both beam and cell experiments. Substituting Eq. 4.1.20 into Eq. 4.1.21 yields

$$\sigma(j \to j') = \frac{\pi}{(2j+1)k_j^2} \sum_{\lambda=|j-j'|}^{j+j'} (2\lambda+1) B_\lambda(j, j'). \tag{4.1.22}$$

Equation 4.1.19 for the Grawert coefficients can be substituted into this equation to recover the cross section in terms of $\mathbf{T}^J$.

### 4.1.4 Vibrational Dependence of the Scattering

The rigid rotator model that we have described does not include the vibrational motion of the molecule. To account for the vibrational motion of NaK, the dependence of the potential on the NaK bond length $r_\mathrm{v}$ must be included. If the full potential $V(r_\mathrm{v}, R_\mathrm{d}, \theta)$ is known, one can write it in the form

$$V(r_\mathrm{v}, R_\mathrm{d}, \theta) = \sum_\lambda V_\lambda(r_\mathrm{v}, R_\mathrm{d}) P_\lambda(\cos\theta). \tag{4.1.23}$$

For the case that only one vibrational level is included in the coupled channel expansion, one must average the potential in Eq. 4.1.23 using the square of the vibrational wave function as a weighting function. The result is that one replaces the Legendre components in Eq. 4.1.10 by

$$V_\lambda(R_\mathrm{d}) = \int V_\lambda(r_\mathrm{v}, R_\mathrm{d}) \left|\chi_v(r_\mathrm{v})\right|^2 dr_\mathrm{v}. \tag{4.1.24}$$

(We have neglected the small dependence of the wave function on the rotational quantum number $j$.) One must evaluate a different average potential for each vibrational state, and then perform a set of calculations using that potential.

For the work described in this chapter, we calculated the NaK potential surface only at the equilibrium value of the NaK bond length, $r_{\rm v}^0$. Using the Legendre expansion determined for this surface, Eq. 4.1.10, corresponds approximately to considering the $v = 0$ vibrational state. We are then essentially assuming that the vibrational wave function for $v = 0$ is so strongly peaked at $r_{\rm v}^0$ that

$$V_\lambda(R_{\rm d}) = \int V_\lambda(r_{\rm v}, R_{\rm d}) \left|\chi_0(r_{\rm v})\right|^2 dr_{\rm v} \approx V_\lambda(r_{\rm v}^0, R_{\rm d}). \tag{4.1.25}$$

### 4.1.5 Multipole Expansion of $m$-Changing Collisions

Section 1.3 of the Introduction discussed an alternative method for describing collisionally induced changes in the $m$-sublevel populations. One uses a multipole moment expansion of the population in the $m$-sublevels. This is advantageous because the experiments of Dr. Huennekens' group [2] directly measure changes in orientation and alignment, the second and third moments of the expansion. This method of expressing the population of the $m$ sublevels requires a transformation to a new basis. The description of the process in this section will follow that of Greene and Zare [12].

Let the row vector $\mathbf{N} = (N_{-j}, \cdots, N_j)$ represent the populations of each of the $m$ magnetic sublevels of a particular level $j$. For a particular $(j \rightarrow j')$ transition, the probability that population is transferred from a $m$ to $m'$ can be represented by a transition probability matrix, $\boldsymbol{\mathcal{P}}$. The elements of the rectangular transition probability matrix can be calculated from the $(jm \rightarrow j'm')$ cross sections in Eq. 4.1.20.

The population of the final $m'$ sublevels is given by

$$(N_{-j}, \cdots, N_j) \begin{pmatrix} \mathcal{P}_{-j,-j'} & \cdot & \mathcal{P}_{-j,j'} \\ \vdots & \ddots & \vdots \\ \mathcal{P}_{j,-j'} & \cdot & \mathcal{P}_{j,j'} \end{pmatrix} = (N_{-j'}, \cdots, N_{j'}). \tag{4.1.26}$$

Instead of representing the $m$ distribution using the population of the individual $m$ sublevels, we transform to a different vector, which gives the multipole moments of the magnetic sublevels. The old labeling index $m = -j$ to $j$ is replaced by the new index for the multipole moment basis $q = 0$ to $2j$. The first moment ($q = 0$) corresponds to population, the second to orientation and the third to alignment. The $m$ basis is transformed to the $q$ multipole moment basis by the matrix $\mathbf{Z}^j$, which has elements given by

$$Z^j_{mq} = (-1)^{q+m+j} \sqrt{2q+1} \begin{pmatrix} j & q & j \\ m & 0 & -m \end{pmatrix}. \tag{4.1.27}$$

The transformation matrix $\mathbf{Z}$ can be used to define a new vector $\mathbf{n}$

$$\sum_m N_m Z^j_{mq} = n(q). \tag{4.1.28}$$

Equation 4.1.28 can also be used to transform the population vector $\mathbf{N}'$ of the final $m'$ sublevels to $\mathbf{n}'$ in the $q'$ multipole basis of the final $j'$ state. For values of $j \gg q$, the transformation in Eq. 4.1.27 can be approximated with Legendre polynomials

using a relation from Edmonds [33]

$$Z^j_{mq} \approx \sqrt{\frac{2q+1}{2j+1}} P_q\left(\frac{m}{\sqrt{j(j+1)}}\right). \tag{4.1.29}$$

For $j \gg q$, the Legendre polynomial approximation from Eq. 4.1.29 leads to a simple interpretation in which the moments are the Legendre components of the distribution of $m$ values. Figure 4.3 shows a comparison of exact transformation the multipole basis and the Legendre polynomial approximation for $j = 2$ as a function of $m/\sqrt{j(j+1)}$. The approximation is exact for $q = 1$ and fairly good for the higher moments. The correlation between the moment expansion and the examples of $m$ distributions shown in Fig. 1.5 is clear; $q = 1$ corresponds to orientation, $q = 2$ corresponds to alignment, etc.

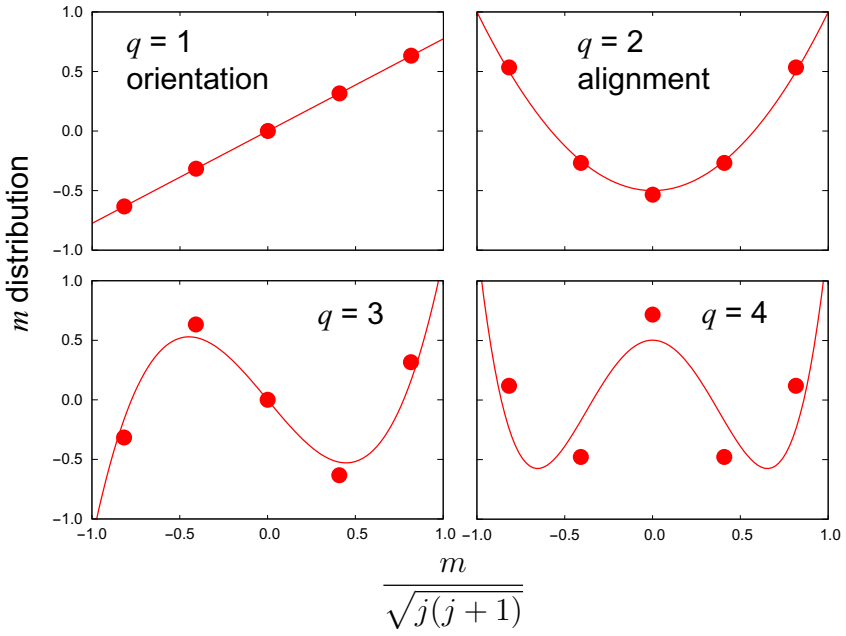


**Figure 4.3:** Comparison of exact and approximate transformation to the multipole basis for $j = 2$ as a function of $m/\sqrt{j(j+1)}$. The exact values are represented as points and the approximate values are shown as lines.

The **N** vector components are treated as continuous and the summation is replaced by an integral to yield

$$\sqrt{\frac{2q+1}{2j+1}}\int_{-j-\frac{1}{2}}^{j+\frac{1}{2}} N(m)P_q\left(\frac{m}{\sqrt{j(j+1)}}\right)dm = n(q). \tag{4.1.30}$$

The probability matrix can also be transformed to the multipole moment basis with the expression

$$(\mathbf{Z}^j)^\dagger \boldsymbol{\mathcal{P}} \mathbf{Z}^{j'} = \mathbf{Q}. \tag{4.1.31}$$

The matrix **Q** represents the transformation from the initial multipole state $q$ to the final state $q'$. **Q** is a rectangular $(2j+1)\times(2j'+1)$ matrix comprised of a diagonal square matrix with side length $2j+1$ $(2j'+1)$ for $j<j'$ $(j>j')$ and a remaining rectangular matrix in which all the elements are zero. For $j'>j$, **Q** has the form

$$\begin{pmatrix} Q_{0,0} & \cdots & Q_{0,2j'} \\ \vdots & \ddots & \vdots \\ Q_{2j,0} & \cdots & Q_{2j,2j'} \end{pmatrix} = \left(\begin{array}{ccccc|c} d_0 & 0 & \cdots & \cdots & 0 & \\ 0 & d_1 & \cdots & \vdots & \vdots & \\ \vdots & \vdots & \ddots & \vdots & \vdots & \mathbf{0} \\ \vdots & \vdots & \vdots & d_{q-1} & 0 & \\ 0 & \cdots & \cdots & 0 & d_q & \end{array}\right). \tag{4.1.32}$$

The elements of the diagonal matrix $d_0, d_1, \ldots, d_q$ give the probability for transfer of population, orientation, alignment, etc. The zero matrix represents moments that are not present in both the $j$ and $j'$ levels. For example, if $j>j'$, the largest moment in the inital state is $q=2j$ and the largest moment in the final state is $q'=2j'$. In this case, some of the moments available in the initial state are not available

in the final state. Also, if $j < j'$ then there will be higher moments available in the final state that will not be collisionally populated because the original level did not have these moments. The elements $d_q$ can be given in terms of the Grawert coefficients [34]

$$d_q = \sum_{\lambda=|j-j'|}^{j+j'} (-1)^{j+j'+\lambda+q}(2\lambda+1) \begin{Bmatrix} \lambda & j & j \\ q & j' & j \end{Bmatrix} B_\lambda(j,j'), \tag{4.1.33}$$

where the $B_\lambda(j,j')$ are given in Eq. 4.1.19. The code written for the coupled channel calculations computes the Grawert coefficients, allowing the multipole moment method to be implemented. This transformation allows us to understand how collisions change the distribution of molecules in the various $m$ sublevels without focusing on each $m \rightarrow m'$ transfer individually.

## 4.2 Results of Coupled Channel Calculations

This section will discuss the results of the coupled channel calculations. First, we will report the cross sections calculated using the coupled channel method. The results for changes in orientation and alignment obtained with the coupled channel calculations will then be reported. Finally, the results for $(j \rightarrow j')$ transitions will be compared with experimental measurements. Though the calculations produce rate constants that have roughly the same magnitude as the experimental rate constants, the experiments show a propensity for even $\Delta j$ transitions that is not present in the calculated values. We will discuss possible reasons for this discrepancy.

### 4.2.1 Convergence of Coupled Channel Calculations

Before any results are presented, there are several specifics of the calculations that must be discussed. The cross sections given in Eq. 4.1.20 depend on the Grawert coefficients, which include a summation over the total angular momentum values $J$. It is reasonable to only include values of the total angular momentum that contribute significantly to the cross sections. A semi-classical argument can be made to relate the impact parameter to energy and total angular momentum $b \approx J/\sqrt{2mE}$. At a very large impact parameter, the effect of the incident particle on the target will be negligible and there will be no significant contribution to the cross section at this range. If we consider this very large, fixed impact parameter, the number of $J$ values that contribute to the cross section depends on the total energy of the system.

We must be sure that enough $J$ values have been included such that the cross section is converged at each energy. We checked the calculations at various energies in both the ground and excited state for convergence with respect to $J$. Figures 4.4, 4.5, 4.6, 4.7, 4.8 and 4.9 demonstrate the convergence of the cross sections for transitions from $j = 0$ to various final $j'$ in the (a) panels and transitions from various initial $j$ to $j' = j + 1$ in the (b) panels. For both the ground and excited states, calculations at $E = 0.0005, 0.0020$, and $0.0040$ $\mathrm{E_h}$ show that the contributions to the cross sections becomes very small well before $J = 95, 127$, and 191, respectively. Note that th experiments are conducted at termperatures of 600K so that the mean thermal energy is $0.0020$ $\mathrm{E_h}$. In the (a) panels, one can see that the cross sections are largest when $j$ only changes by 1 or 2. The (b) panels show that the cross sections are larger for large initial $j$ values. Initial $j = 15$ is the highest value

shown, which is close to the typical initial values of $j$ in transitions investigated experimentally. In all cases, we have included enough values of $J$ for convergence.

Another important consideration is the number of channels to include in the calculation. The total wave function given in Eq 4.1.4 includes a summation over levels $j'$ and $l'$. To be sure enough channels were included, calculations were performed for several ranges of $j$ ranging from 0 to a maximum value, called $j_{\max}$, and checked for convergence. Experimental measurements investigated transitions from initial $j = 14$, so it is important that calculations for transitions from these levels are converged. Figures 4.10, 4.11, 4.12, 4.13, 4.14 and 4.15 show calculated cross sections for $j = 5, 10$, and 15 with various $j_{\max}$ for the first excited state at $E = 0.0005, 0.0020$, and $0.0040$ $\mathrm{E_h}$. The ground state rotational level spacing is larger than that of the first excited state, therefore $j_{\max}$ convergence of cross sections in the first excited state should be sufficient for the ground state. For each range of $j$, the cross sections for transitions to $j' = j_{\max} - 2$ to $j_{\max}$ are not reliable and have been omitted. Truncation artifacts cause this unreliability, but there are no implications of this effect on any other aspect of this work. The cross sections for $E = 0.0005$ $\mathrm{E_h}$ are very similar for $j_{\max} = 25$ and 30, indicating convergence with $j_{\max} = 25$. At $E = 0.0020$ $\mathrm{E_h}$, cross sections are nearly identical for $j_{\max} = 30$ and 35, again indicating convergence. The cross sections calculated at $E = 0.0040$ $\mathrm{E_h}$ are converged at $j_{\max} = 30$ for inital $j = 5$ and 10, however the cross sections for intial $j = 15$ are not the same for $j_{\max} = 25$ and 30. An additional calulation for $j = 15$ at $E = 0.0040$ $\mathrm{E_h}$ should be done with $j_{\max} = 35$ to ensure convergence of the cross sections, however current computational constraints have made this large job impossible.

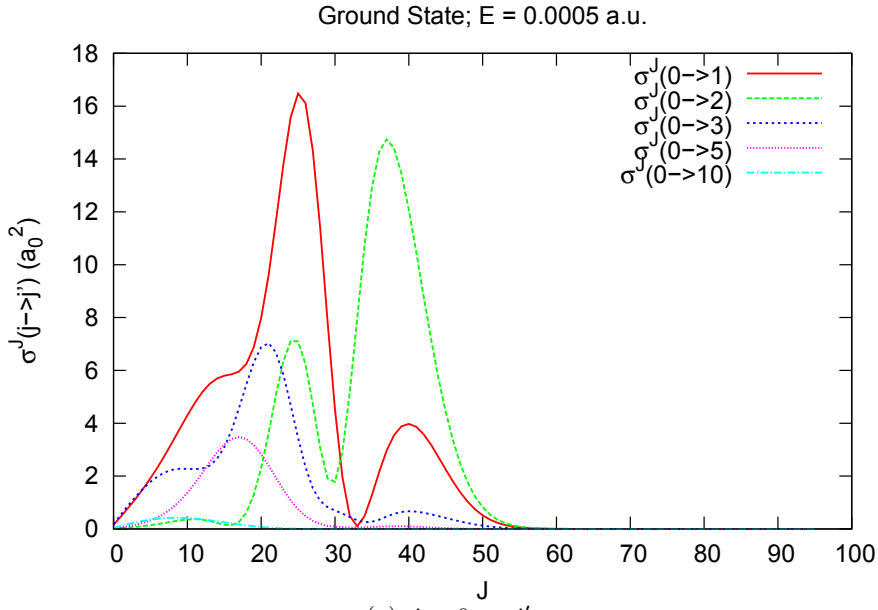


(a) $j = 0 \rightarrow j'$

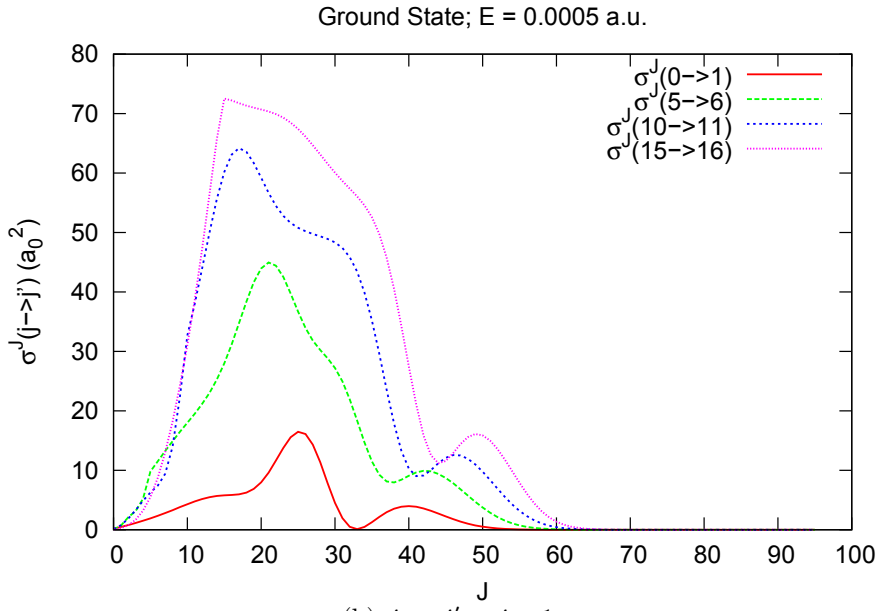


(b) $j \rightarrow j' = j + 1$

**Figure 4.4:** Convergence of cross sections with respect to the number of partial waves $J$. These figures show the partial cross section given in Eq. 4.1.17 as a function of $J$ for $\mathrm{He} + \mathrm{NaK}(X^1\Sigma^+)$ calculations at $E = 0.0005$ $\mathrm{E_h}$. Panel (a) shows cross sections for transitions from initial $j = 0$ to various final $j'$. Panel (b) shows cross sections for transistions for various initial $j$ to final $j' = j + 1$. For these calculations we included partial waves up to $J = 95$, and that was clearly sufficient for convergence of the cross sections.

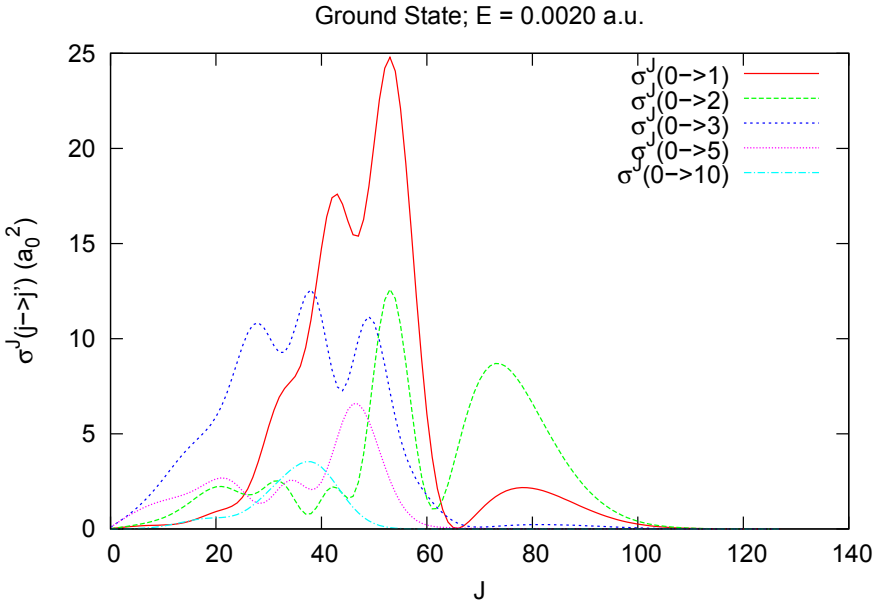


(a) $j = 0 \rightarrow j'$

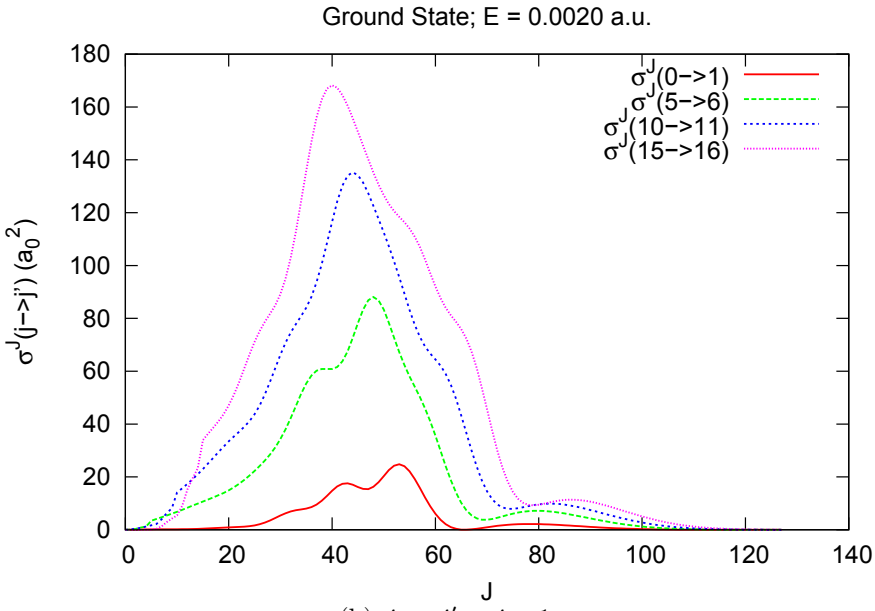


(b) $j \rightarrow j' = j + 1$

**Figure 4.5:** Convergence of cross sections with respect to the number of partial waves $J$. These figures show the partial cross section given in Eq. 4.1.17 as a function of $J$ for $\mathrm{He} + \mathrm{NaK}(X^1\Sigma^+)$ calculations at $E = 0.0020\ \mathrm{E_h}$. Panel (a) shows cross sections for transitions from initial $j = 0$ to various final $j'$. Panel (b) shows cross sections for transistions for various initial $j$ to final $j' = j + 1$. For these calculations we included partial waves up to $J = 127$, and that was clearly sufficient for convergence of the cross sections.

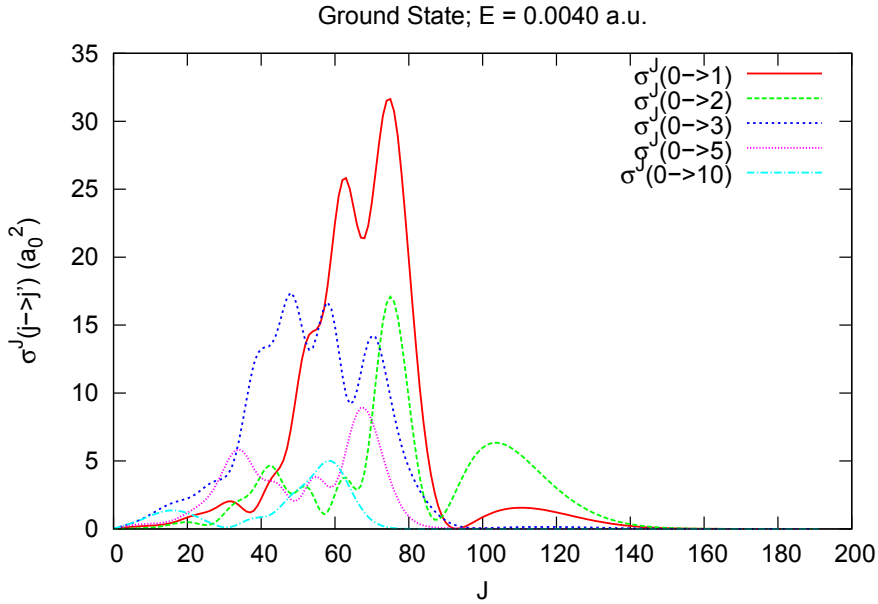


(a) $j = 0 \rightarrow j'$

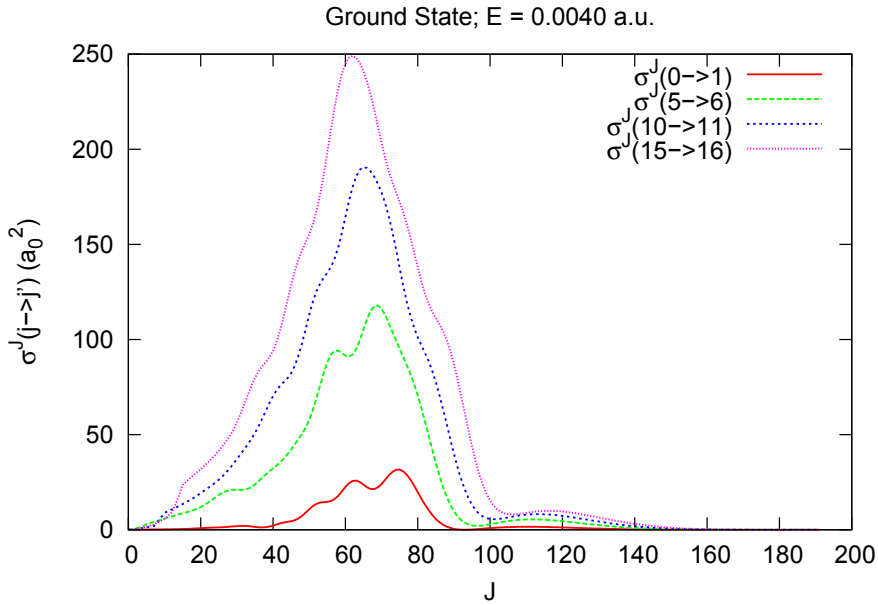


(b) $j \rightarrow j' = j + 1$

**Figure 4.6:** Convergence of cross sections with respect to the number of partial waves $J$. These figures show the partial cross section given in Eq. 4.1.17 as a function of $J$ for $\mathrm{He} + \mathrm{NaK}(X^1\Sigma^+)$ calculations at $E = 0.0040\ \mathrm{E_h}$. Panel (a) shows cross sections for transitions from initial $j = 0$ to various final $j'$. Panel (b) shows cross sections for transistions for various initial $j$ to final $j' = j + 1$. For these calculations we included partial waves up to $J = 191$, and that was clearly sufficient for convergence of the cross sections.

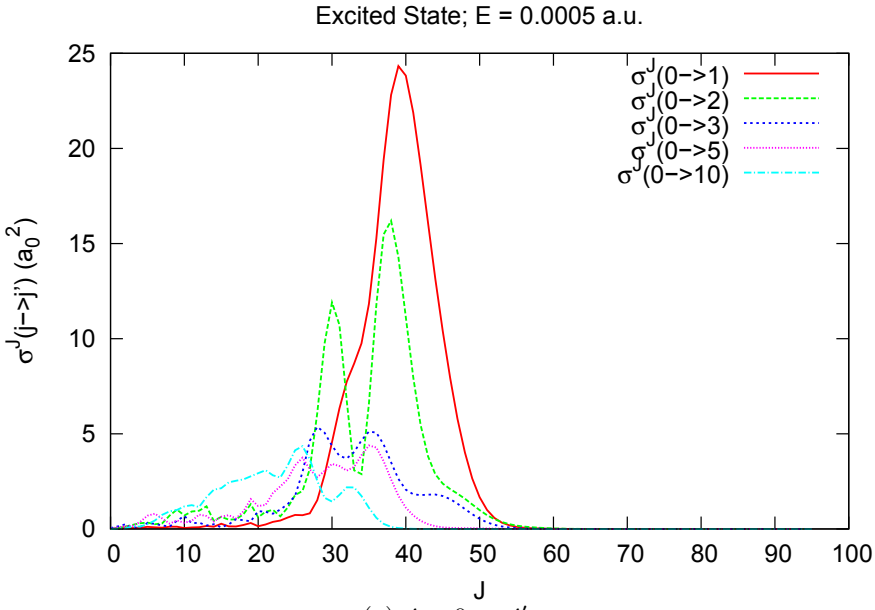


(a) $j = 0 \rightarrow j'$

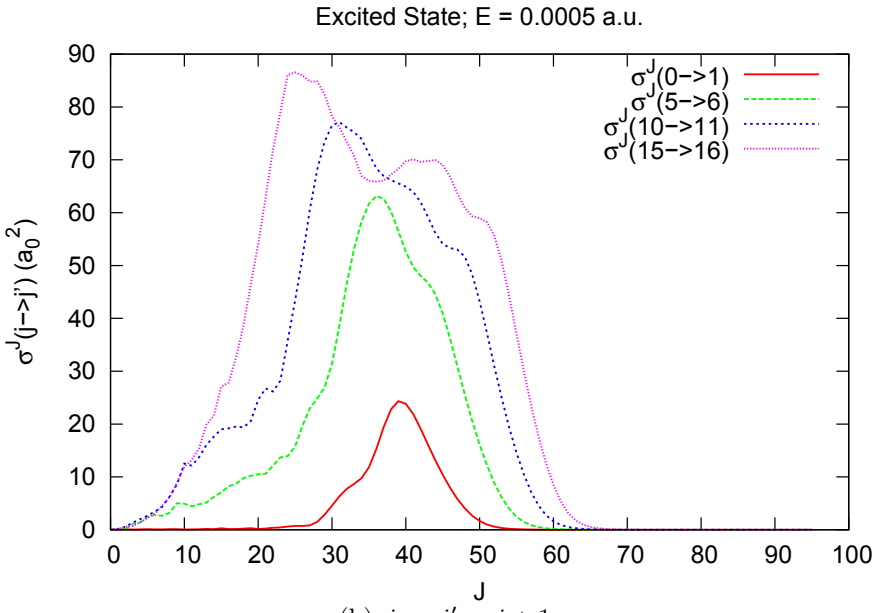


(b) $j \rightarrow j' = j + 1$

**Figure 4.7:** Convergence of cross sections with respect to the number of partial waves $J$. These figures show the partial cross section given in Eq. 4.1.17 as a function of $J$ for $\mathrm{He} + \mathrm{NaK}(A^1\Sigma^+)$ calculations at $E = 0.0005$ $\mathrm{E_h}$. Panel (a) shows cross sections for transitions from initial $j = 0$ to various final $j'$. Panel (b) shows cross sections for transistions for various initial $j$ to final $j' = j + 1$. For these calculations we included partial waves up to $J = 95$, and that was clearly sufficient for convergence of the cross sections.

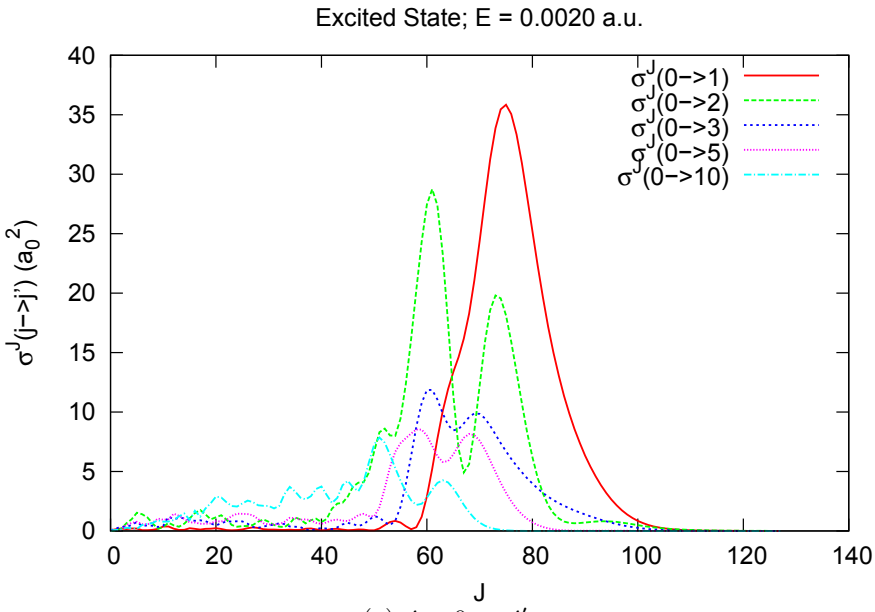


(a) $j = 0 \rightarrow j'$

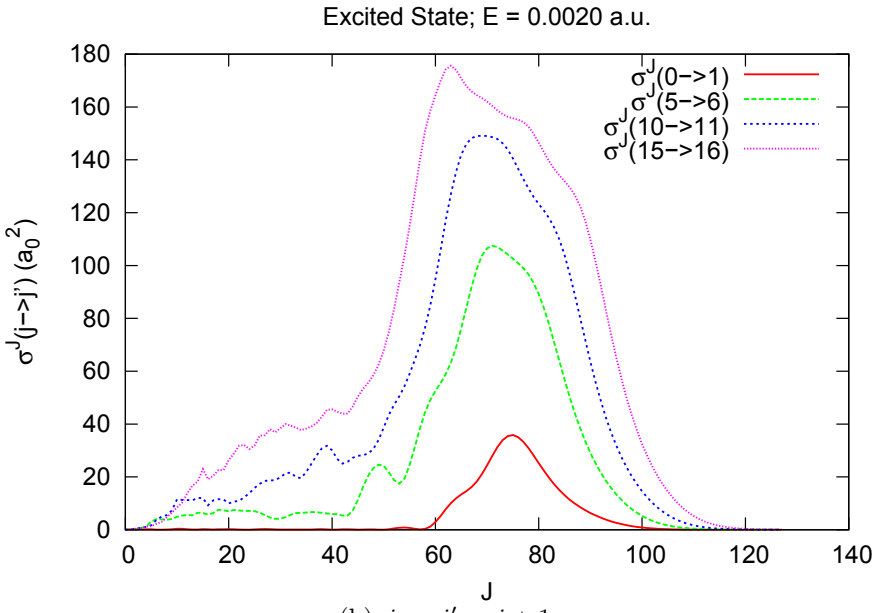


(b) $j \rightarrow j' = j + 1$

**Figure 4.8:** Convergence of cross sections with respect to the number of partial waves $J$. These figures show the partial cross section given in Eq. 4.1.17 as a function of $J$ for He + NaK($A^1\Sigma^+$) calculations at $E = 0.0020$ $E_h$. Panel (a) shows cross sections for transitions from initial $j = 0$ to various final $j'$. Panel (b) shows cross sections for transistions for various initial $j$ to final $j' = j + 1$. For these calculations we included partial waves up to $J = 127$, and that was clearly sufficient for convergence of the cross sections.

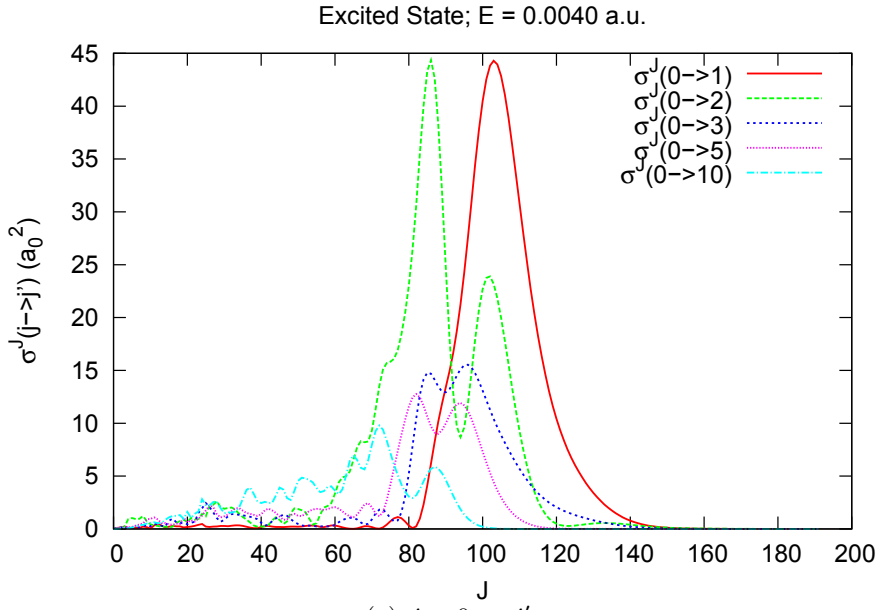


(a) $j = 0 \rightarrow j'$

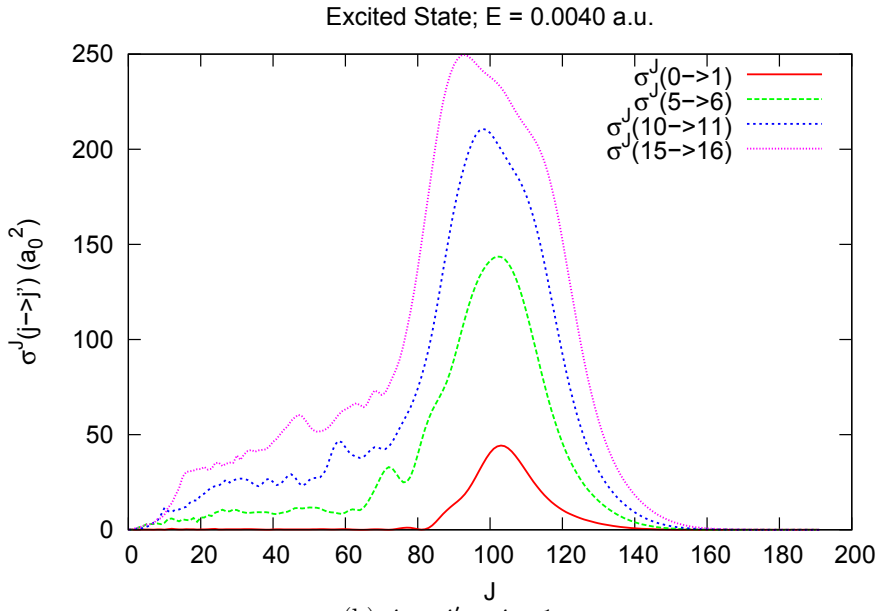


(b) $j \rightarrow j' = j + 1$

**Figure 4.9:** Convergence of cross sections with respect to the number of partial waves $J$. These figures show the partial cross section given in Eq. 4.1.17 as a function of $J$ for He + NaK($A^1\Sigma^+$) calculations at $E = 0.0040$ $E_h$. Panel (a) shows cross sections for transitions from initial $j = 0$ to various final $j'$. Panel (b) shows cross sections for transistions for various initial $j$ to final $j' = j + 1$. For these calculations we included partial waves up to $J = 191$, and that was clearly sufficient for convergence of the cross sections.

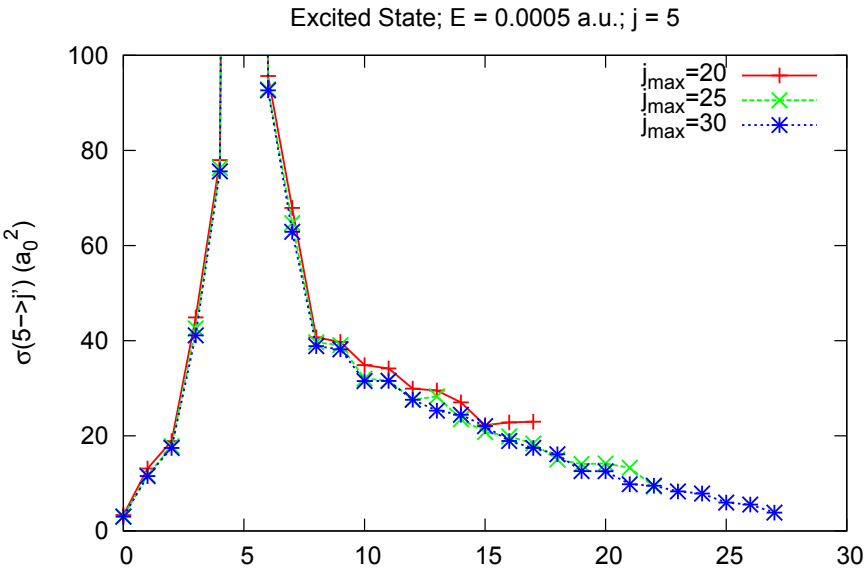


(a) $j = 5 \rightarrow j'$

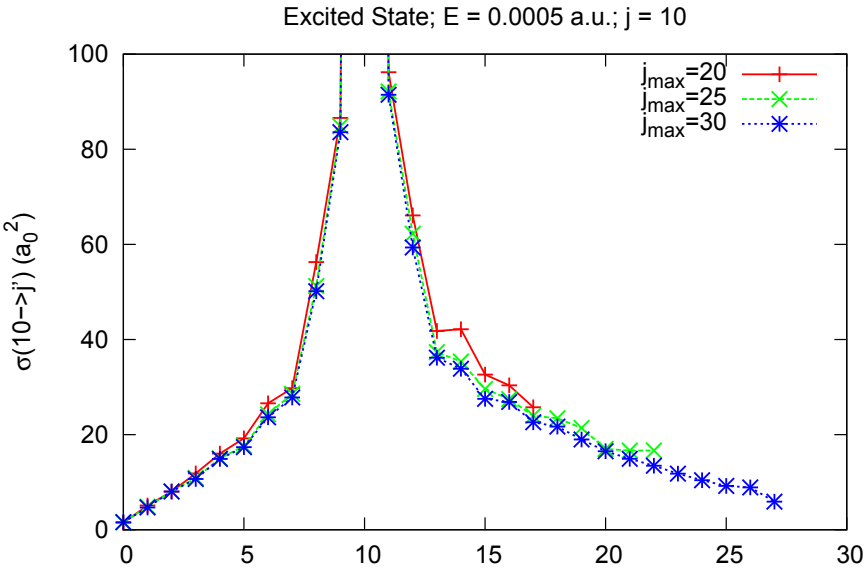


(b) $j = 10 \rightarrow j'$

**Figure 4.10:** Convergence with respect to the number of channels. These figures show the cross section for specific transitions for coupled channel calculations of three different sizes. The cross sections are shown for transitions from intial $j = 5$ or 10 to several final levels $j'$ for $\mathrm{He} + \mathrm{NaK}(A^1\Sigma^+)$ at $E = 0.0005$ $\mathrm{E_h}$. Each calculation included all the channels corresponding to rotational levels between 0 and a maximum value $j_{\max}$, where $j_{\max} = 20, 25$, or 30. The convergence of these cross sections is generally satisfactory for $j_{\max} = 25$ or 30.

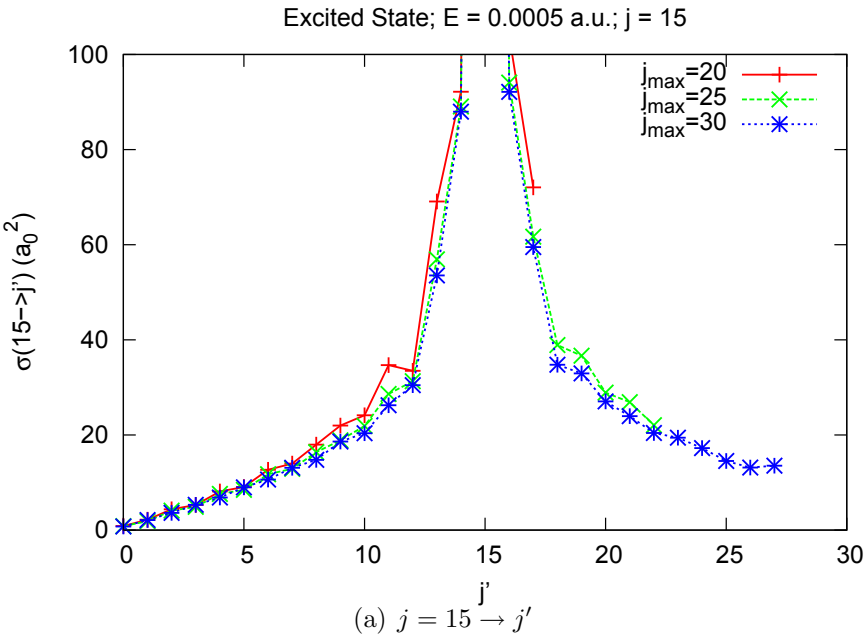


(a) $j = 15 \rightarrow j'$

**Figure 4.11:** Convergence with respect to the number of channels. This figure shows the cross section for specific transitions for coupled channel calculations of three different sizes. The cross sections are shown for transitions from intial $j = 15$ to several final levels $j'$ for $\mathrm{He} + \mathrm{NaK}(A^1\Sigma^+)$ at $E = 0.0005$ $\mathrm{E_h}$. Each calculation included all the channels corresponding to rotational levels between 0 and a maximum value $j_{\max}$, where $j_{\max} = 20, 25$, or 30. The convergence of these cross sections is generally satisfactory for $j_{\max} = 25$ or 30.

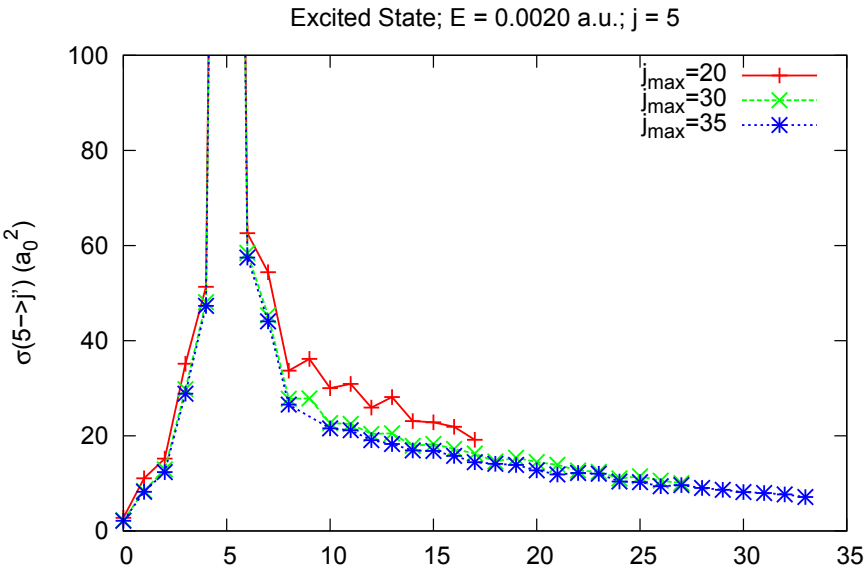


(a) $j = 5 \rightarrow j'$

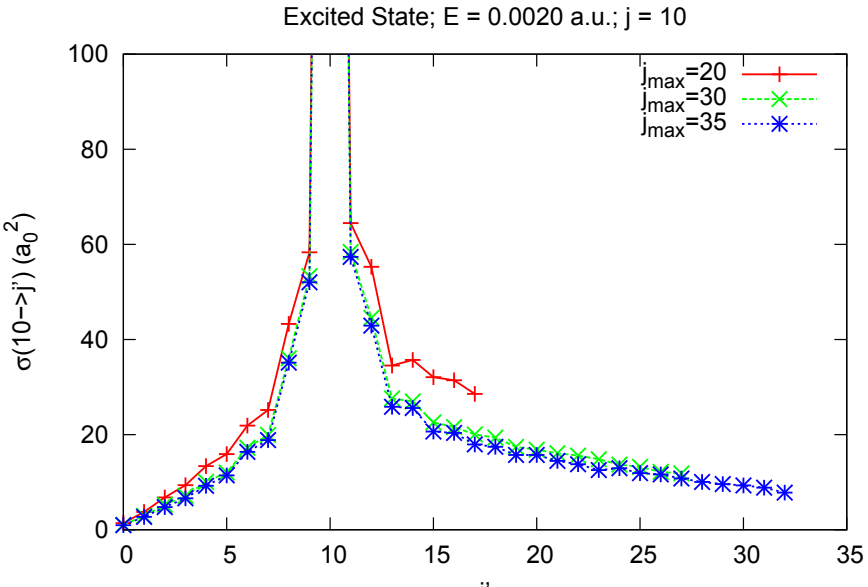


(b) $j = 10 \rightarrow j'$

**Figure 4.12:** Convergence with respect to the number of channels. These figures show the cross section for specific transitions for coupled channel calculations of three different sizes. The cross sections are shown for transitions from intial $j = 5$ or 10 to several final levels $j'$ for $\mathrm{He} + \mathrm{NaK}(A^1\Sigma^+)$ at $E = 0.0020$ $\mathrm{E_h}$. Each calculation included all the channels corresponding to rotational levels between 0 and a maximum value $j_{\max}$, where $j_{\max} = 20, 30$, or 35. The convergence of these cross sections is generally satisfactory for $j_{\max} = 30$ or 35.

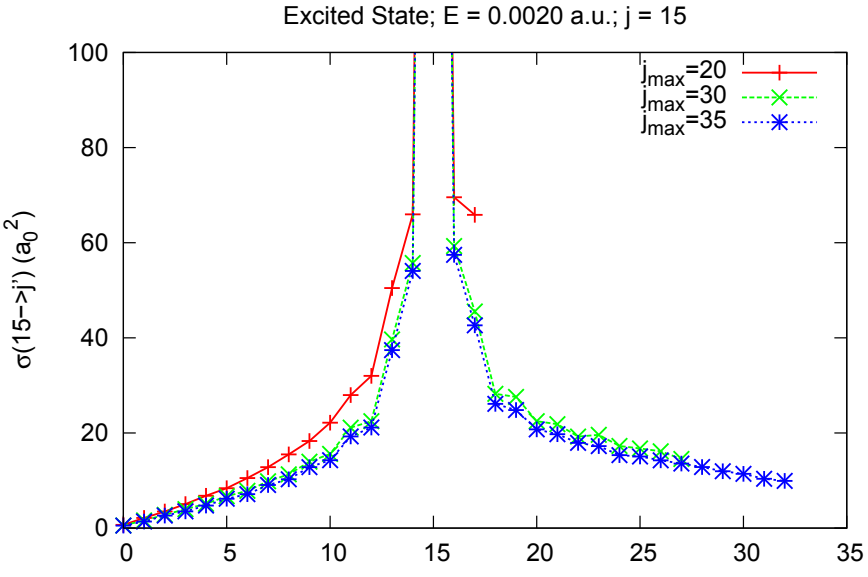


(a) $j = 15 \rightarrow j'$

**Figure 4.13:** Convergence with respect to the number of channels. This figure shows the cross section for specific transitions for coupled channel calculations of three different sizes. The cross sections are shown for transitions from intial $j = 15$ to several final levels $j'$ for $\mathrm{He} + \mathrm{NaK}(A^1\Sigma^+)$ at $E = 0.0020$ $\mathrm{E_h}$. Each calculation included all the channels corresponding to rotational levels between 0 and a maximum value $j_{\max}$, where $j_{\max} = 20, 30$, or 35. The convergence of these cross sections is generally satisfactory for $j_{\max} = 30$ or 35.

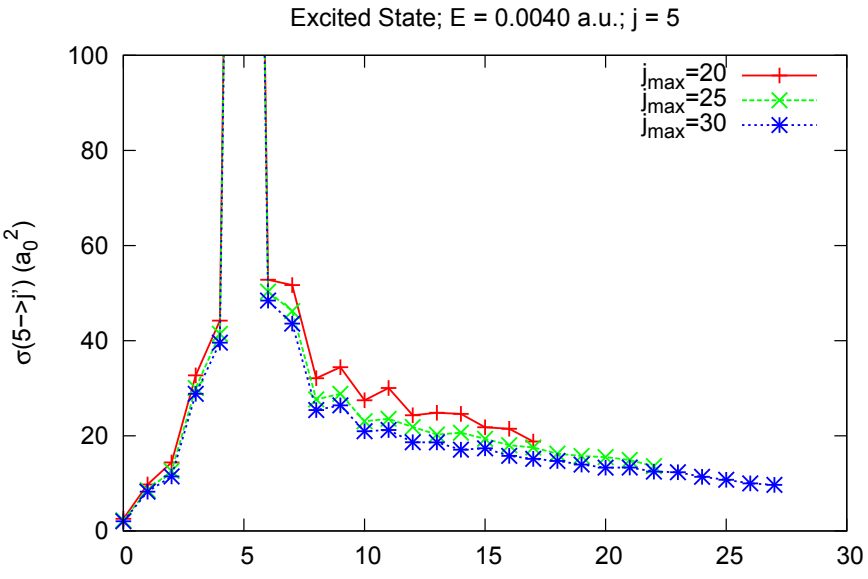


(a) $j = 5 \rightarrow j'$

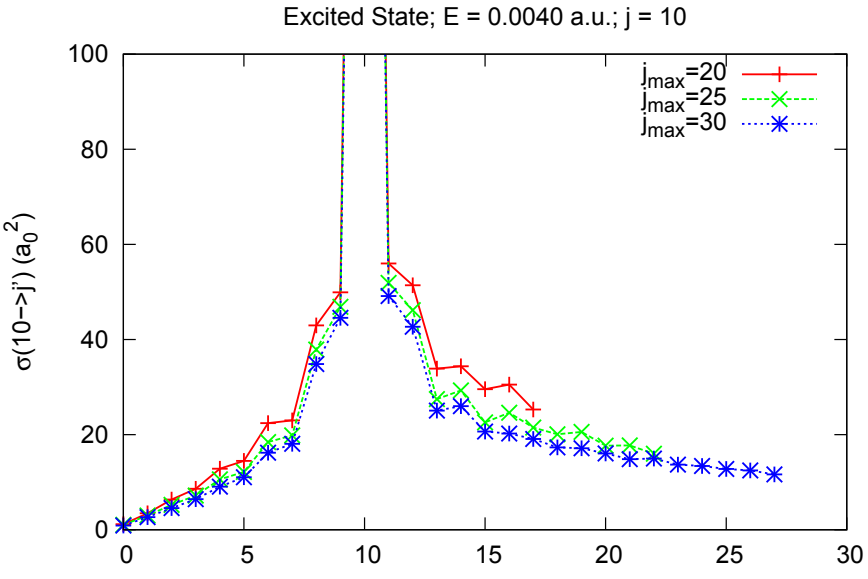


(b) $j = 10 \rightarrow j'$

**Figure 4.14:** Convergence with respect to the number of channels. These figures show the cross section for specific transitions for coupled channel calculations of three different sizes. The cross sections are shown for transitions from intial $j = 5$ or 10 to several final levels $j'$ for $\mathrm{He} + \mathrm{NaK}(A^1\Sigma^+)$ at $E = 0.0040$ $\mathrm{E_h}$. Each calculation included all the channels corresponding to rotational levels between 0 and a maximum value $j_{\max}$, where $j_{\max} = 20, 25$, or 30. The convergence of these cross sections is generally satisfactory for $j_{\max} = 25$ or 30.

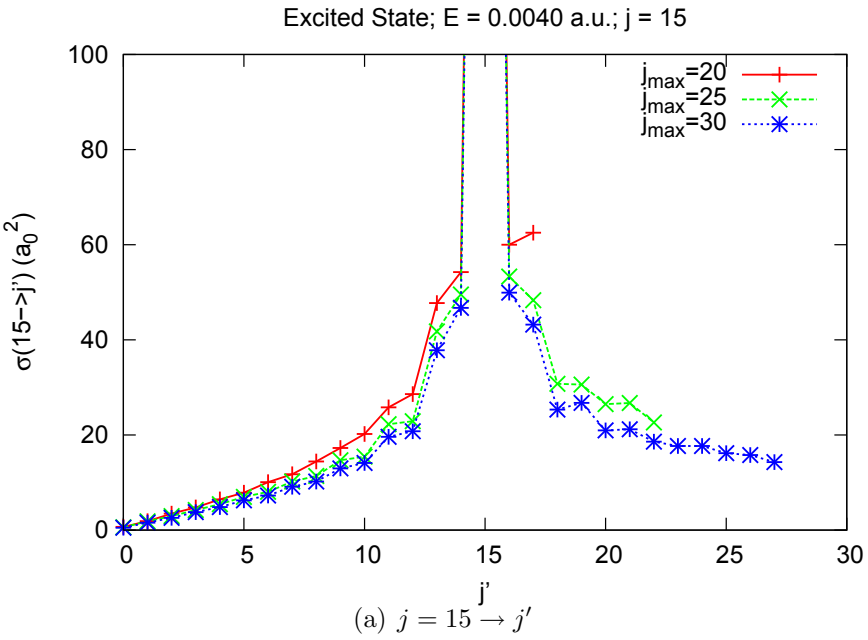


(a) $j = 15 \rightarrow j'$

**Figure 4.15:** Convergence with respect to the number of channels. This figure shows the cross section for specific transitions for coupled channel calculations of three different sizes. The cross sections are shown for transitions from intial $j = 15$ to several final levels $j'$ for $\mathrm{He} + \mathrm{NaK}(A^1\Sigma^+)$ at $E = 0.0040$ $\mathrm{E_h}$. Each calculation included all the channels corresponding to rotational levels between 0 and a maximum value $j_{\max}$, where $j_{\max} = 20, 30$, or 35. The convergence of these cross sections is generally not satisfactory for $j_{\max} = 30$ or 35.

We have also performed calculations to check for convergence of the Legendre expansion of the potential. Coupled channel calculations were performed for $\mathrm{He} + \mathrm{NaK}(A^1\Sigma^+)$ at $E = 0.0016$ $\mathrm{E_h}$ using the seven term Legendre expansion including all seven terms ($\lambda = 0 - 6$), and the first five and six ($\lambda = 0 - 4$ and $0 - 5$) terms of the expansion. Figures 4.16 and 4.17 show the cross sections for $j = 0, 5, 10$ and 15 for each of these expansions. In each case, the cross sections are reasonably converged for the $\lambda = 0 - 6$ expansion of the potential. The same procedure was used to check the cross sections for convergence of the eleven term expansion. Figures 4.18 and 4.19 show the cross sections for $j = 0, 5, 10$ and 15 using the eleven term Legendre expansion including all eleven terms ($\lambda = 0 - 10$), and the first ten and nine ($\lambda = 0 - 9$ and $0 - 8$) terms of the expansion.

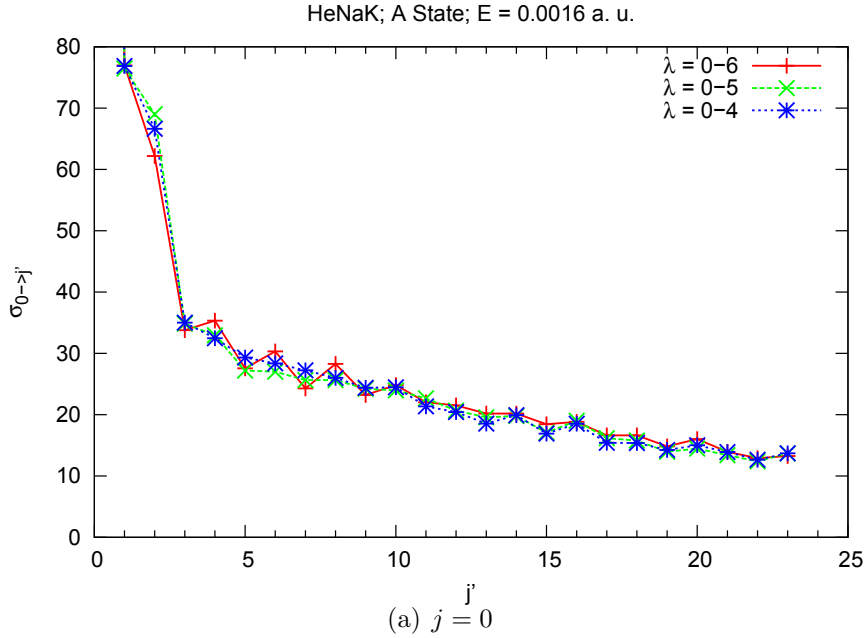


(a) $j = 0$

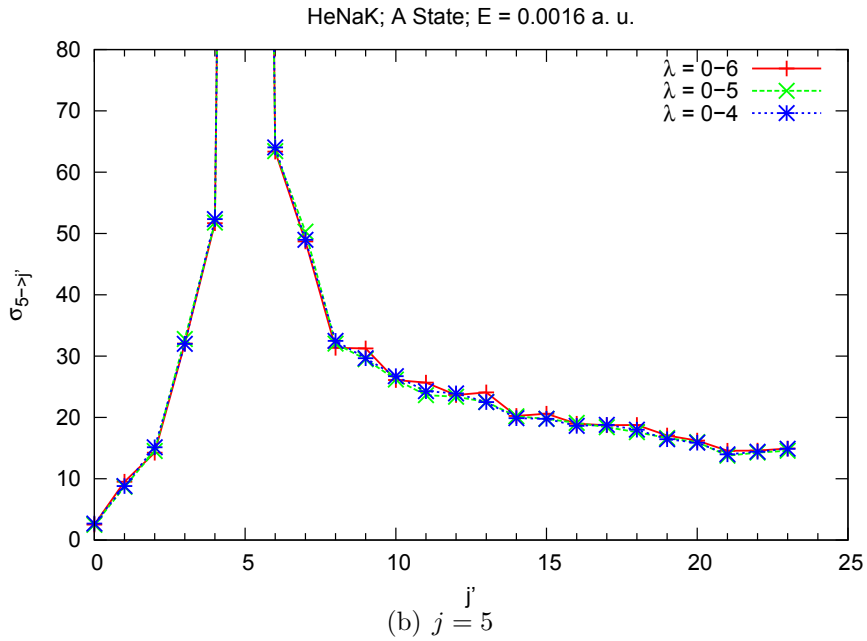


(b) $j = 5$

**Figure 4.16:** Convergence with respect to the number of terms in the Legendre expansion of the potential. The cross sections are shown for transitions from intial $j = 0$ or 5 to several final levels $j'$ for $\mathrm{He} + \mathrm{NaK}(A^1\Sigma^+)$ at $E = 0.0016$ $\mathrm{E_h}$. Each calculation included $\lambda = 0-4, 0-5$, or $0-6$ terms of the seven term expansion. The cross sections are converged for the $\lambda = 0-6$ expansion of the potential.

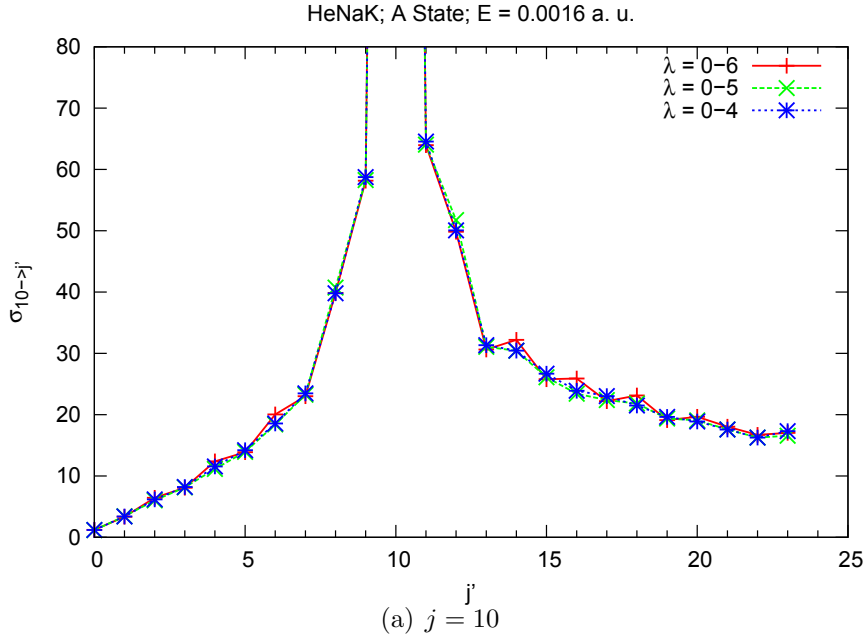


(a) $j = 10$

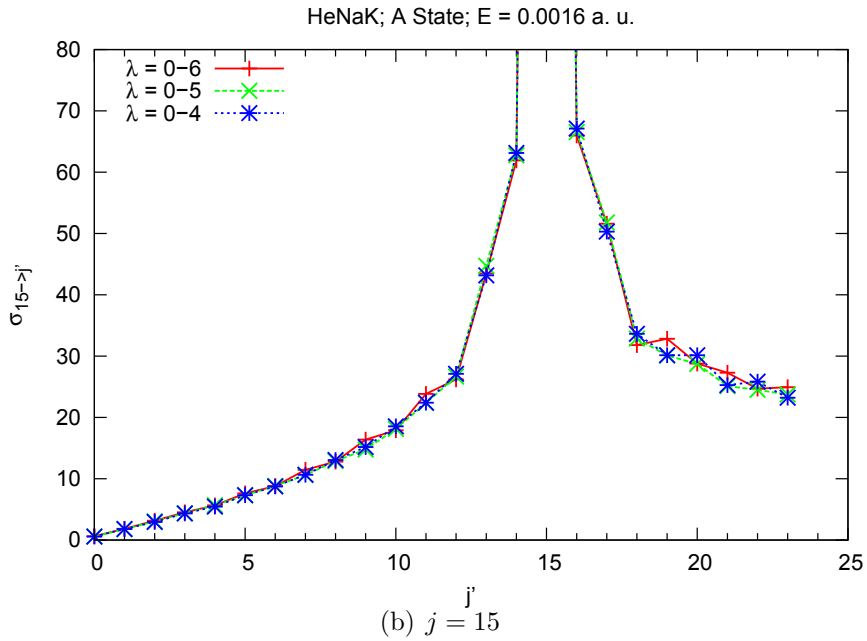


(b) $j = 15$

**Figure 4.17:** Convergence with respect to the number of terms in the Legendre expansion of the potential. The cross sections are shown for transitions from intial $j = 10$ or 15 to several final levels $j'$ for $\mathrm{He} + \mathrm{NaK}(A^1\Sigma^+)$ at $E = 0.0016\ \mathrm{E_h}$. Each calculation included $\lambda = 0-4, 0-5$, or $0-6$ terms of the seven term expansion. The cross sections are converged for the $\lambda = 0-6$ expansion of the potential.

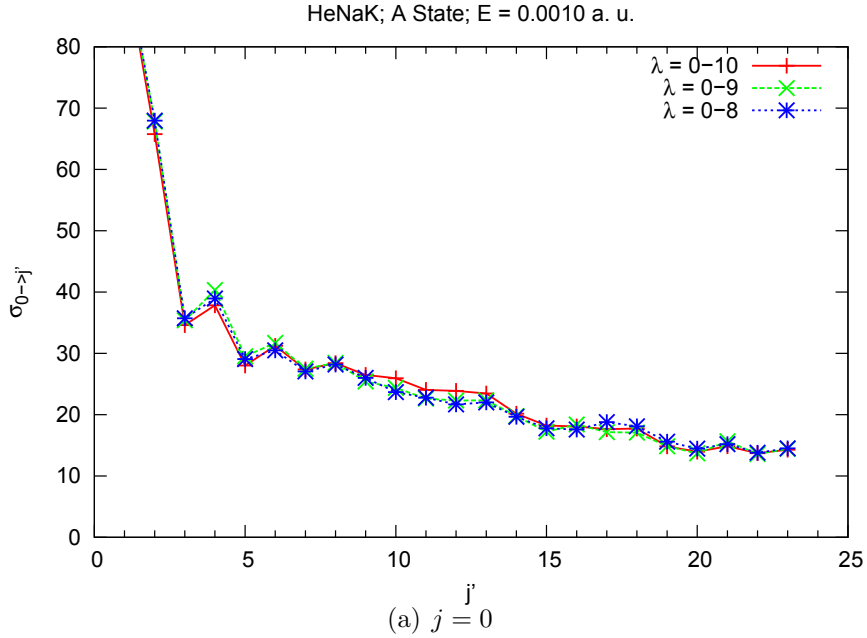


(a) $j = 0$

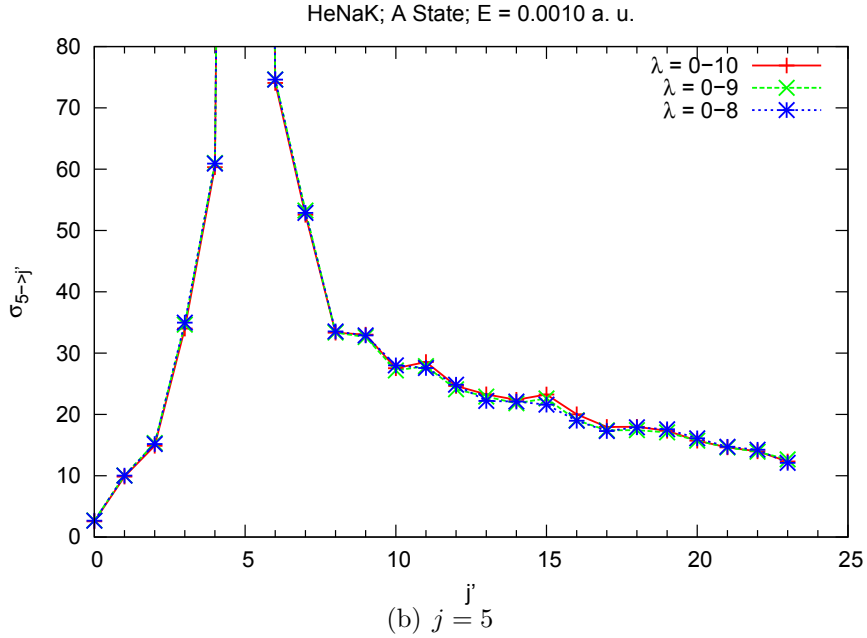


(b) $j = 5$

**Figure 4.18:** Convergence with respect to the number of terms in the Legendre expansion of the potential. The cross sections are shown for transitions from intial $j = 0$ or 5 to several final levels $j'$ for $\mathrm{He} + \mathrm{NaK}(A^1\Sigma^+)$ at $E = 0.0016\ \mathrm{E_h}$. Each calculation included $\lambda = 0 - 10, 0 - 9$, or $0 - 8$ terms of the eleven term expansion. The cross sections are converged for the $\lambda = 0 - 10$ expansion of the potential.

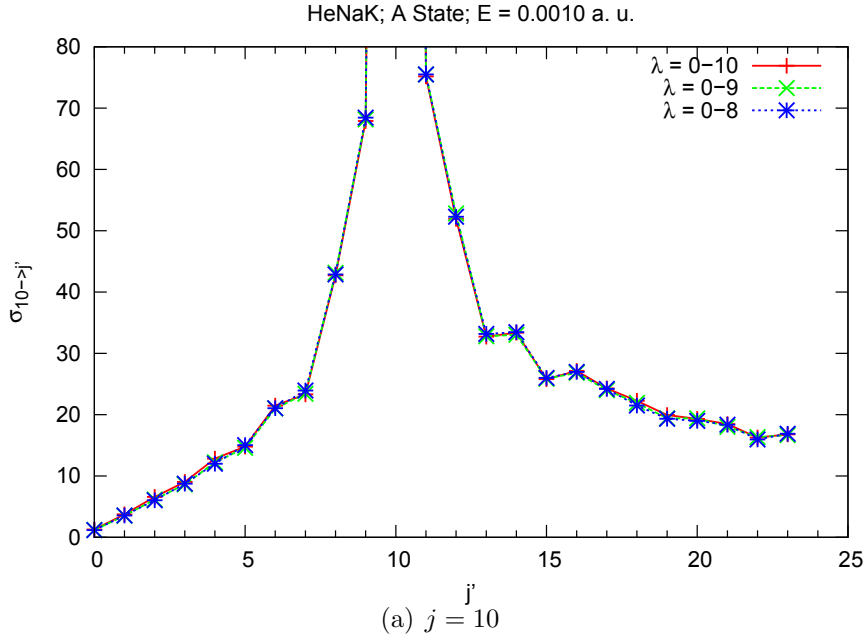


(a) $j = 10$

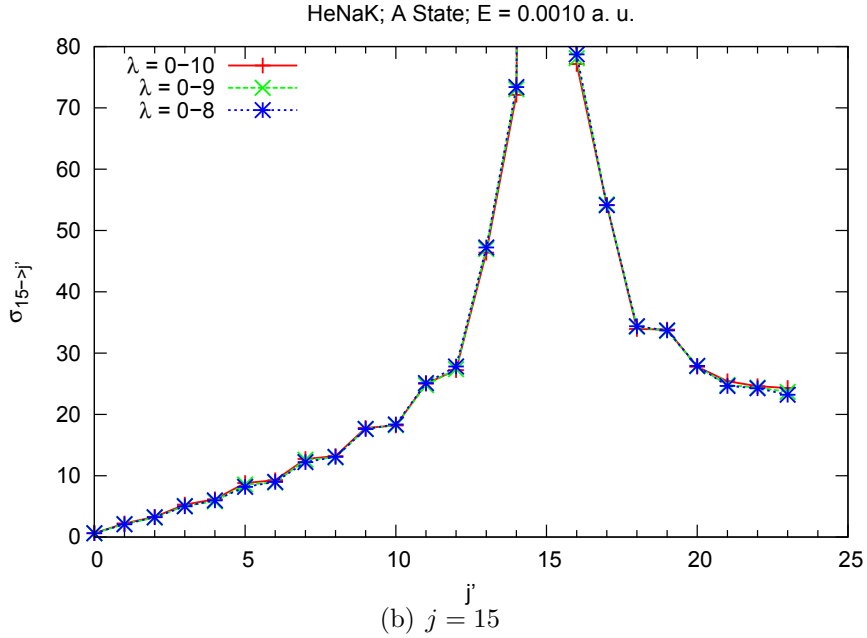


(b) $j = 15$

**Figure 4.19:** Convergence with respect to the number of terms in the Legendre expansion of the potential. The cross sections are shown for transitions from intial $j = 10$ or 15 to several final levels $j'$ for $\mathrm{He} + \mathrm{NaK}(A^1\Sigma^+)$ at $E = 0.0016\ \mathrm{E_h}$. Each calculation included $\lambda = 0 - 10, 0 - 9$, or $0 - 8$ terms of the eleven term expansion. The cross sections are converged for the $\lambda = 0 - 10$ expansion of the potential.

### 4.2.2 He + NaK($X^1\Sigma^+$)

Figures 4.20 and 4.21 show the cross sections for collisions of He with NaK in the $X^1\Sigma^+$ state with $v = 0$. The cross sections are given for various energies and initial $j$ levels as a function of $j'$. The cross sections calculated for the lowest energy, $E = 0.0005$ $E_h$, fall off faster as a function of $j'$ than the cross sections for $E = 0.0020$ and $0.0040$ $E_h$. This trend can best be seen in panel (a) of Fig 4.20 when the initial level is $j = 0$. Lower total energies for the system mean that the He cannot transfer as much energy and the NaK cannot make a transition to levels with higher rotational energy. For low enough energies, higher rotational levels are above the available energy, and transitions to these levels are forbidden resulting in a cross section = 0.

The probability that the orientation will be preserved in a collision that changes $j$ to $j'$ is shown in Figs. 4.22 and 4.23 as a function of the average of $j$ and $j'$, $\overline{j} = (j + j')/2$, for several different values of $\Delta j = j' - j$. (This probability depends only on the absolute values of $\Delta j$.) For $E = 0.0005$ $E_h$, shown in panel (a) of Fig. 4.22, nearly 80% of the orientation is preserved for many of the transitions. As the energy increases, less orientation is preserved. At all energies, the orientation is better preserved for larger $\overline{j}$ for fixed $\Delta j$. For constant values of $\overline{j}$, smaller values of $\Delta j$ tend to better preserve the orientation. There is a grouping of $\Delta j = 2$ and 3 and $\Delta j = 4$ and 6 for $E = 0.0020$ and $0.0040$ $E_h$. Figures 4.24 and 4.25 show the probability that the alignment will be preserved as a function of the average of $\overline{j}$. Again, the probability is shown for several different values of $\Delta j = j' - j$ and is independent of the sign of $\Delta j$. Similar trends to those described for the preservation of orientation can be observed in the preservation of alignment.

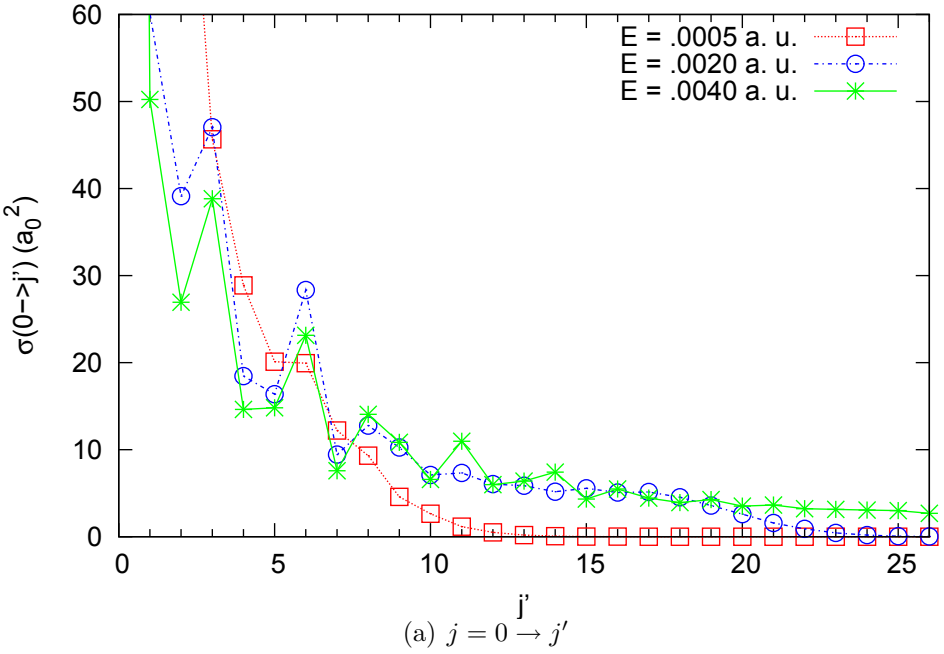


(a) $j = 0 \rightarrow j'$

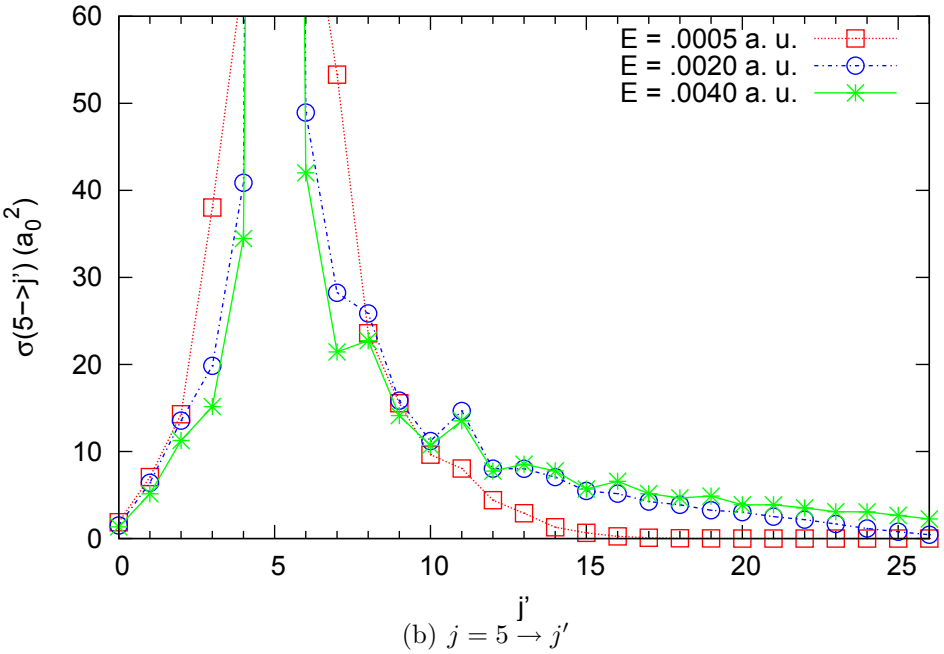


(b) $j = 5 \rightarrow j'$

**Figure 4.20:** Cross sections for $\mathrm{He} + \mathrm{NaK}(X^1\Sigma^+)$ for $E = 0.0005, 0.0020$, and $0.0040$ $\mathrm{E_h}$. The initial level is $j = 0$ and 5 in panels (a) and (b), respectively.

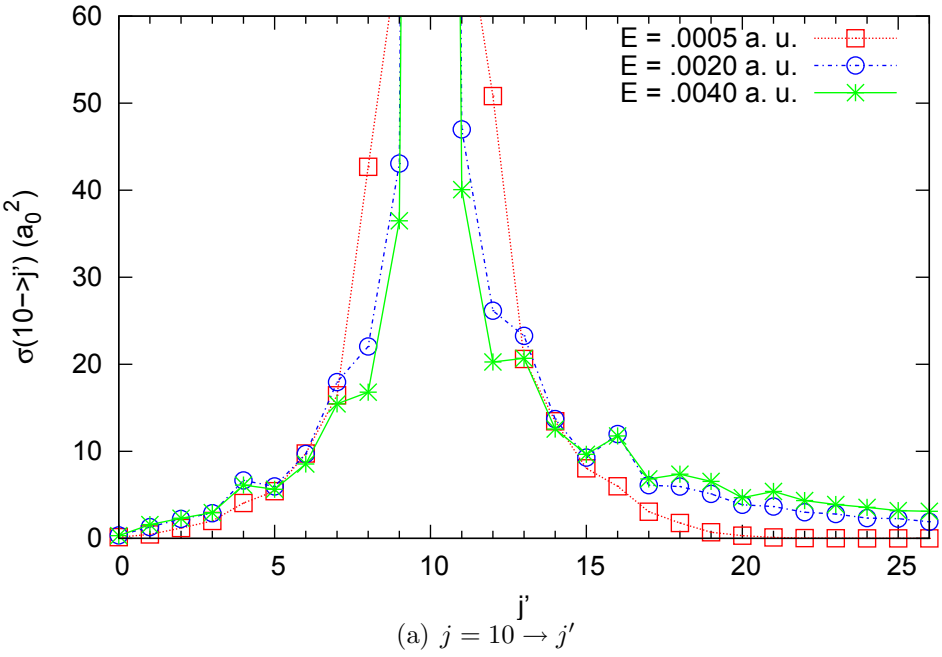


(a) $j = 10 \rightarrow j'$

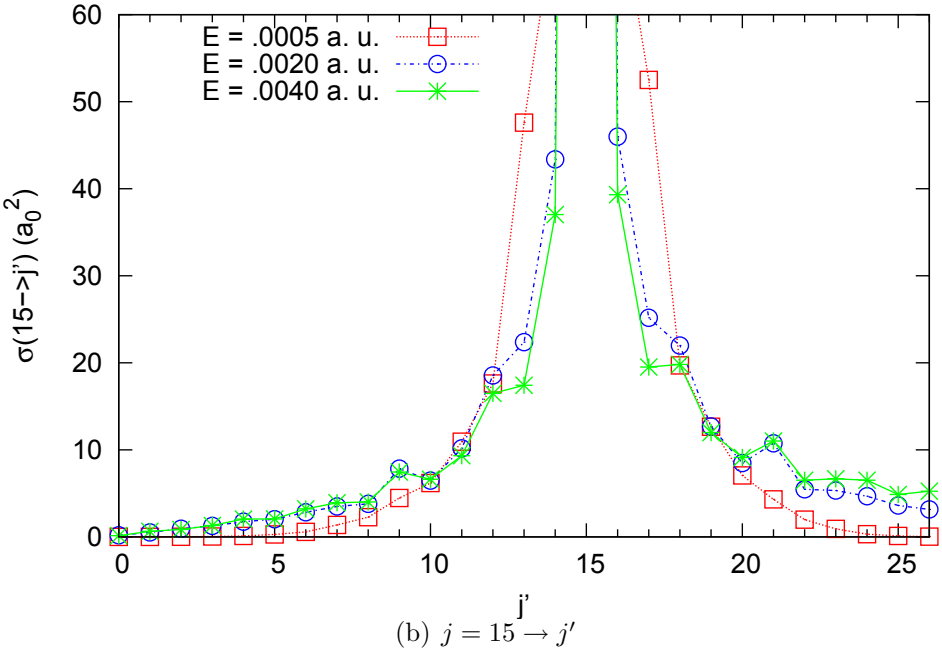


(b) $j = 15 \rightarrow j'$

**Figure 4.21:** Cross sections for $\mathrm{He} + \mathrm{NaK}(X^1\Sigma^+)$ for $E = 0.0005, 0.0020$, and $0.0040$ $\mathrm{E_h}$. The initial level is $j = 10$ and 15 in panels (a)and (b), respectively.

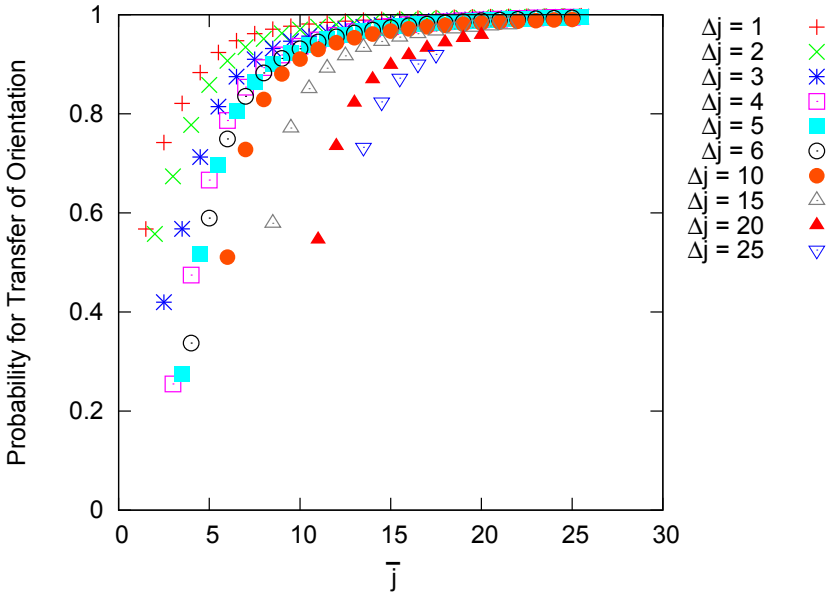


(a) $E = 0.0005$ $E_h$

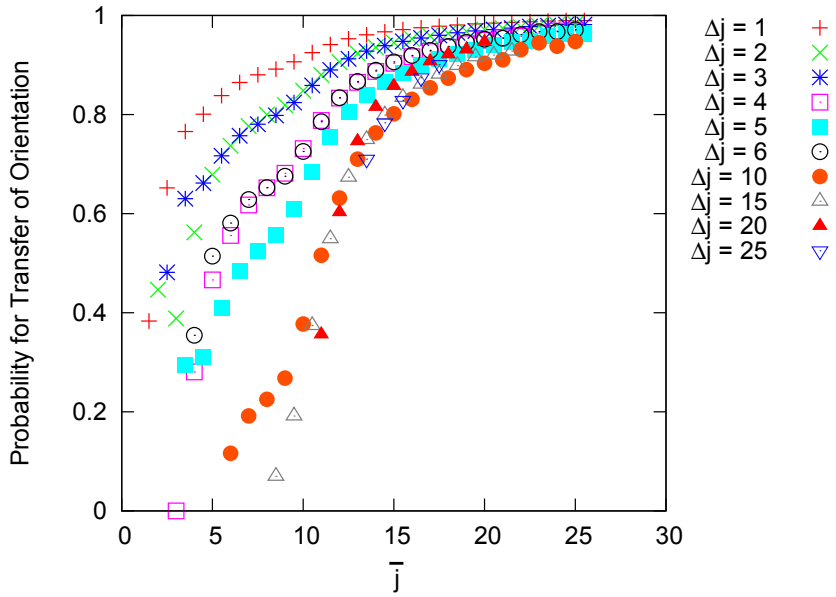


(b) $E = 0.0020$ $E_h$

**Figure 4.22:** Probability that orientation will be transferred during a collision of He with NaK($X^1\Sigma^+$) as a function of the average value of $j$ and $j'$, $\bar{j} = (j + j')/2$. Each series corresponds to a specific $\Delta j = j - j'$. The probability is independent of the sign of $\Delta j$. Panels (a) and (b) show calculations for total energy $E = 0.0005$ and $0.0020$ $E_h$, respectively.

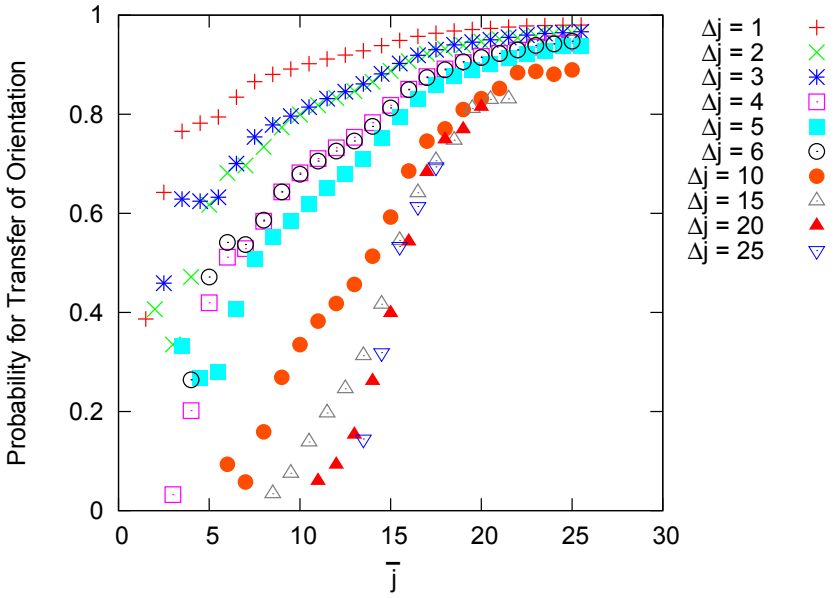


(a) $E = 0.0040$ $E_h$

**Figure 4.23:** Probability that orientation will be transferred during a collision of He with NaK($X^1\Sigma^+$) as a function of the average value of $j$ and $j'$, $\overline{j} = (j + j')/2$. Each series corresponds to a specific $\Delta j = j - j'$. The total energy of the calculation is 0.0040 $E_h$.

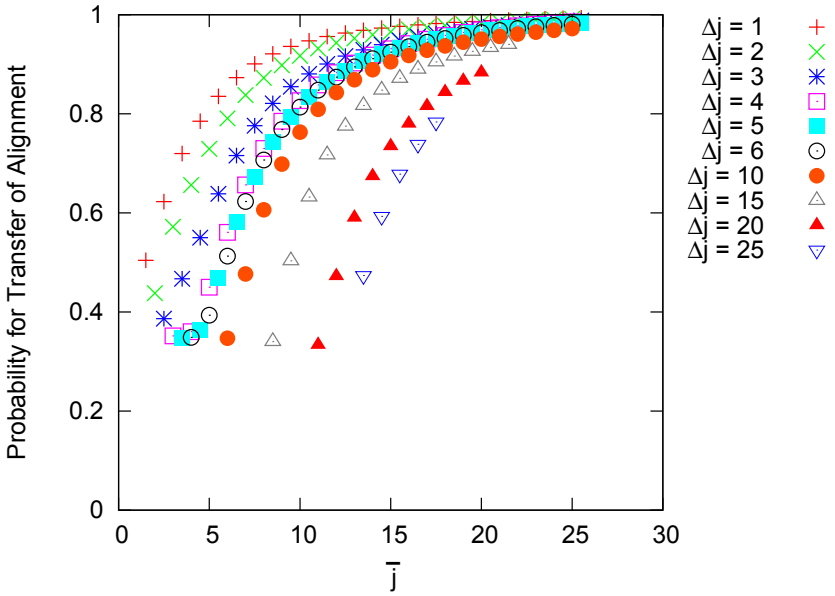


(a) $E = 0.0005$ $E_h$

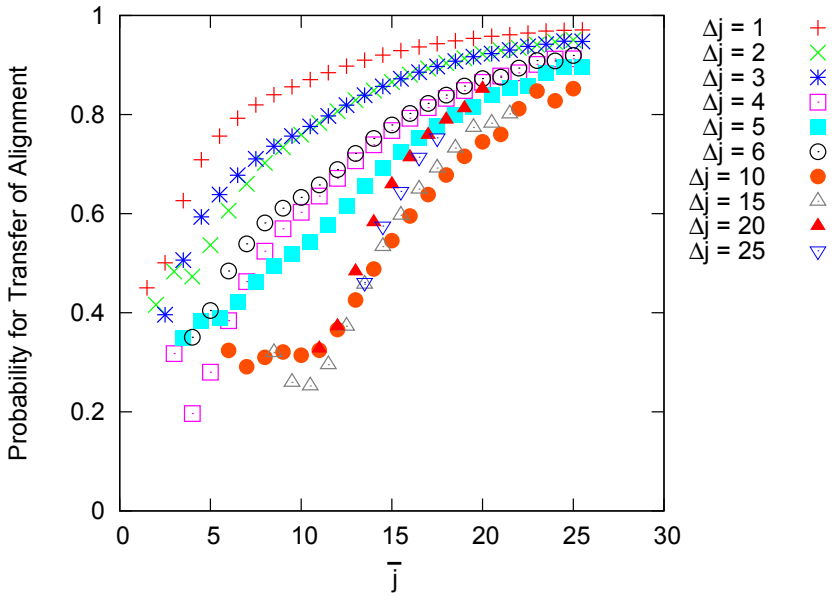


(b) $E = 0.0020$ $E_h$

**Figure 4.24:** Probability that alignment will be transferred during a collision of He with NaK($X^1\Sigma^+$) as a function of the average value of $j$ and $j'$, $\overline{j} = (j + j')/2$. Each series corresponds to a specific $\Delta j = j - j'$. The probability is independent of the sign of $\Delta j$. Panels (a) and (b) show calculations for total energy $E = 0.0005$ and $0.0020$ $E_h$, respectively.

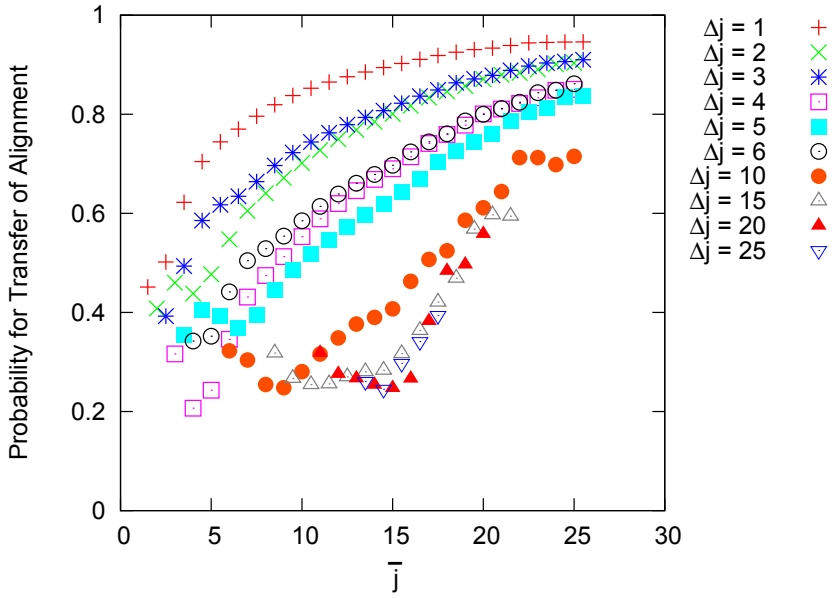


(a) $E = 0.0040$ $E_h$

**Figure 4.25:** Probability that alignment will be transferred during a collision of He with NaK($X^1\Sigma^+$) as a function of the average value of $j$ and $j'$, $\overline{j} = (j + j')/2$. Each series corresponds to a specific $\Delta j = j - j'$. The total energy of the calculation is $E = 0.0040$ $E_h$.

### 4.2.3 He + NaK($A^1\Sigma^+$)

Figures 4.26 and 4.27 show selected cross sections for collisions of He with NaK in the first excited state and the $v = 0$ vibrational state. The cross sections are again shown for various energies and initial $j$ values. The cross sections for collisions with excited state NaK are larger and fall off more slowly as a function of $\Delta j$ than the cross sections for collisions with ground state NaK. This may have to do with the fact that the rotational levels of the first excited state have smaller separations, and thus transitions to $j'$ farther from initial $j$ are easier than for the ground state where the rotational levels are more widely spaced.

The probability that the orientation will be preserved in a collision that changes $j$ to $j'$ is shown in Figs. 4.28 and 4.29 as a function of $\overline{j}$. Overall, the probability that the orientation will be preserved is much smaller than for ground state NaK. Again, larger values of $\overline{j}$ have a higher probability to preserve orientation for a fixed $\Delta j$, although not as effectively as larger $\overline{j}$ in the ground state. For constant values of $\overline{j}$, larger values of $\Delta j$ tend to destroy the orientation, even more so than in the ground state, and the probabilities are spread out more over the various $\Delta j$. A similar grouping as seen in the ground state occurs for $\Delta j = 3$ and 4 and $\Delta j = 5$ and 6 seen in the ground state is present in the excited state as well. As the energy increases the probability that orientation will be transferred decreases. Figures 4.30 and 4.31 show the probability that the alignment will be preserved during a collision that changes $j$ as a function of the average of $j$ and $j'$. Again, there are many similarities to trends described for the changes in orientation. Compared to ground state NaK, the alignment is not as effectively transferred for collisions with excited state NaK.

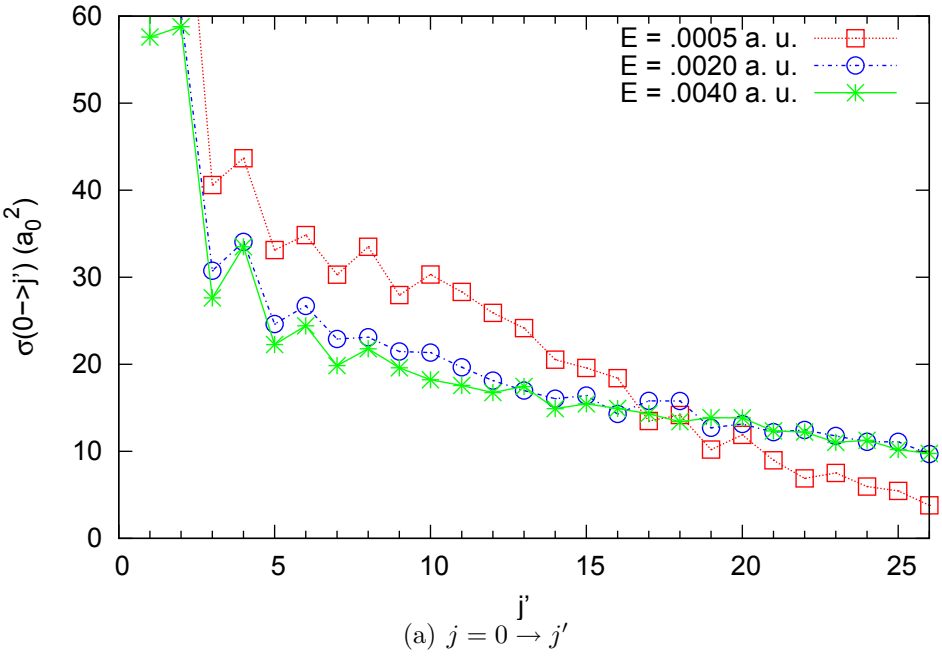


(a) $j = 0 \rightarrow j'$

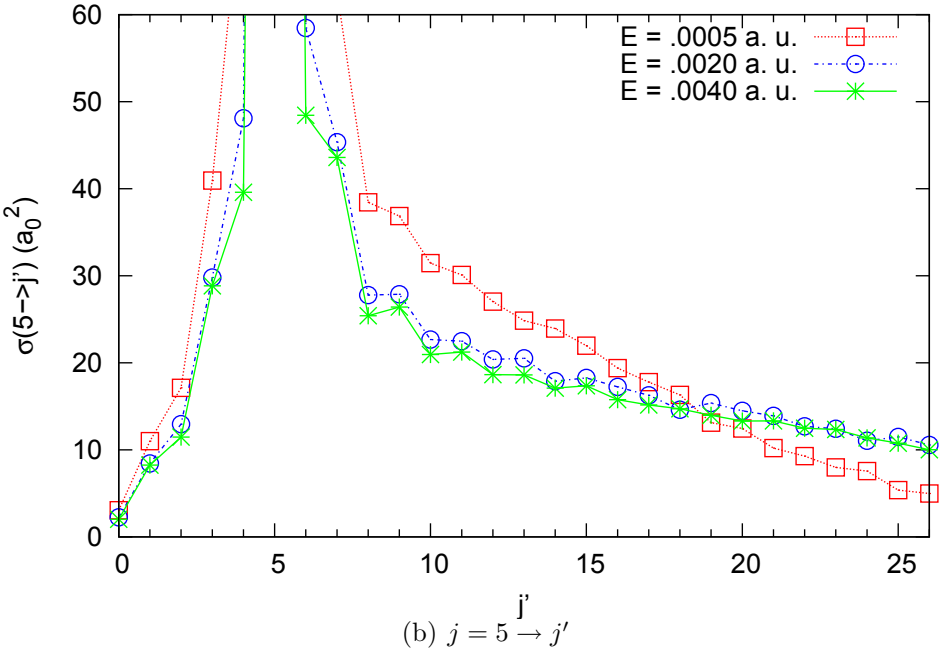


(b) $j = 5 \rightarrow j'$

**Figure 4.26:** Cross sections for $\mathrm{He} + \mathrm{NaK}(A^1\Sigma^+)$ for $E = 0.0005, 0.0020$, and $0.0040$ $\mathrm{E_h}$. The initial level is $j = 0$ and 5 in panels (a) and (b), respectively.

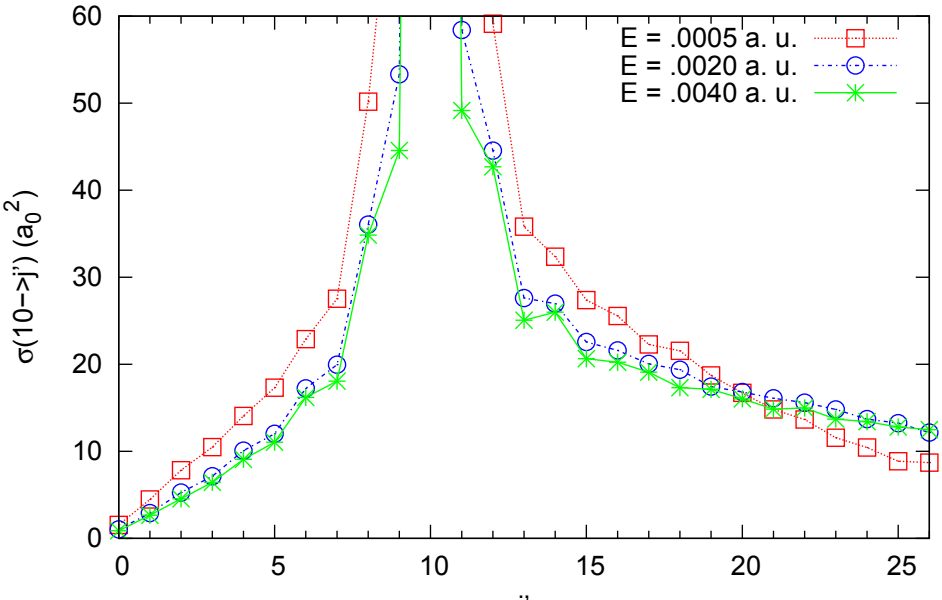


(a) $j = 10 \rightarrow j'$

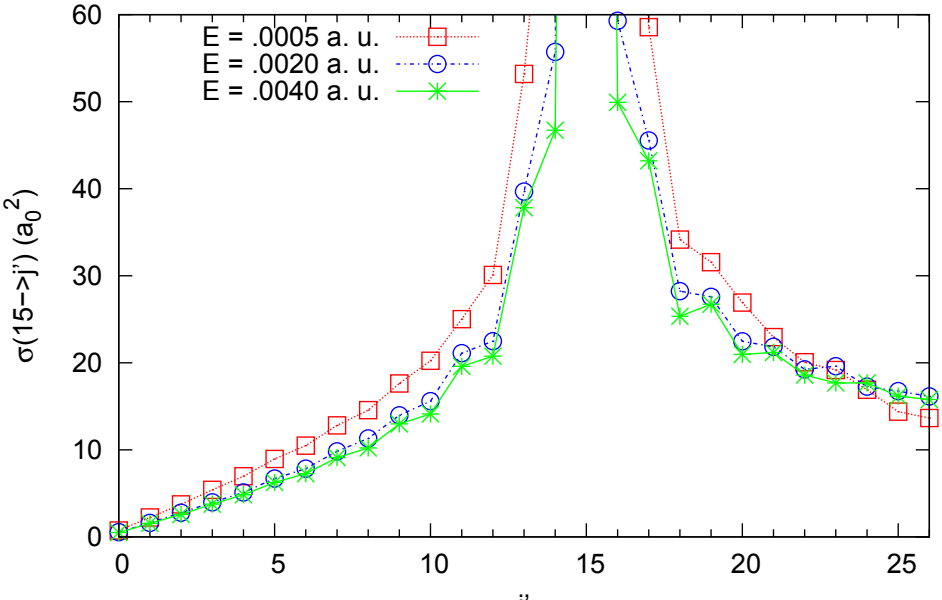


(b) $j = 15 \rightarrow j'$

**Figure 4.27:** Cross sections for $\mathrm{He} + \mathrm{NaK}(A^1\Sigma^+)$ for $E = 0.0005, 0.0020$, and $0.0040$ $\mathrm{E_h}$. The initial level is $j = 10$ and 15 in panels (a) and (b), respectively.

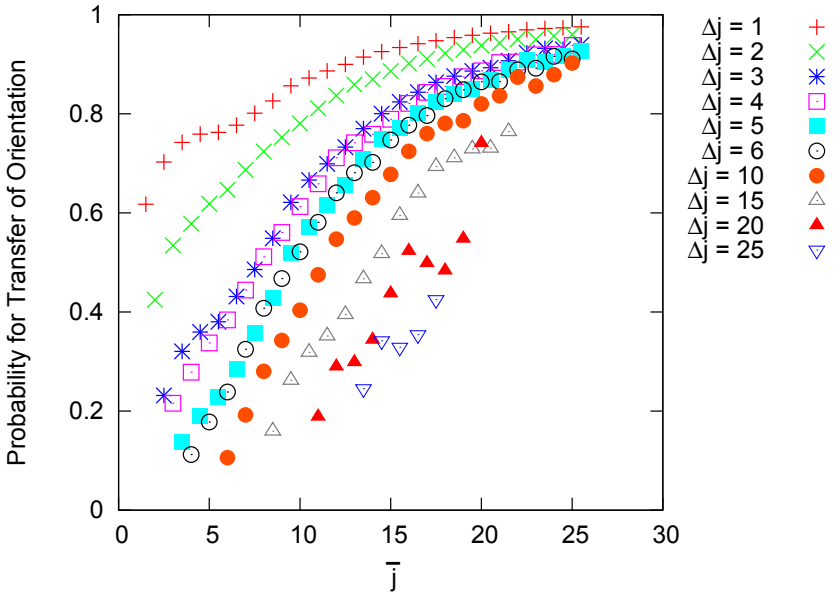


(a) $E = 0.0005$ $E_h$

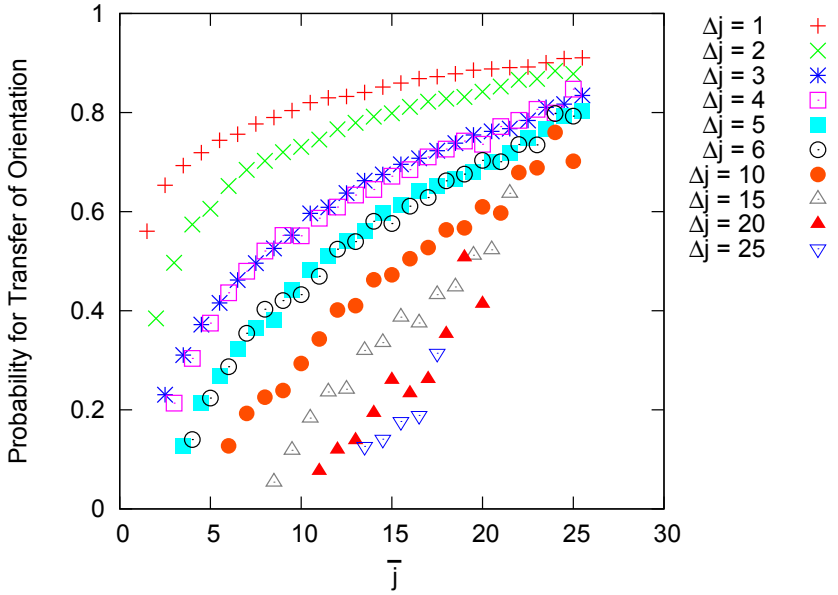


(b) $E = 0.0020$ $E_h$

**Figure 4.28:** Probability that orientation will be transferred during a collision of He with NaK($A^1\Sigma^+$) as a function of the average value of $j$ and $j'$, $\bar{j} = (j + j')/2$. Each series corresponds to a specific $\Delta j = j - j'$. The probability is independent of the sign of $\Delta j$. Panels (a) and (b) show calculations for total energy $E = 0.0005$ and $0.0020$ $E_h$, respectively.

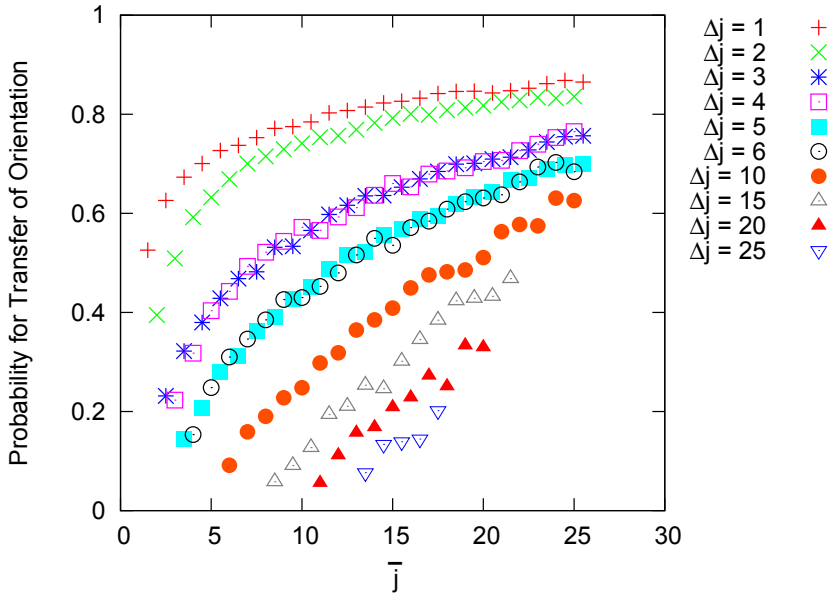


(a) $E = 0.0040$ $E_h$

**Figure 4.29:** Probability that orientation will be transferred during a collision of He with NaK($A^1\Sigma^+$) as a function of the average value of $j$ and $j'$, $\overline{j} = (j + j')/2$. Each series corresponds to a specific $\Delta j = j - j'$. The total energy of the calculation is 0.0040 $E_h$.

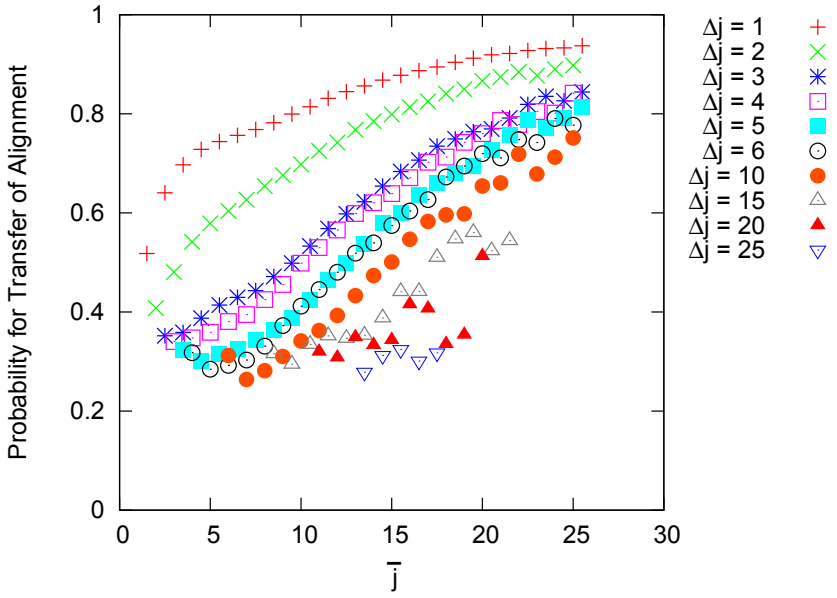


(a) $E = 0.0005$ $E_h$

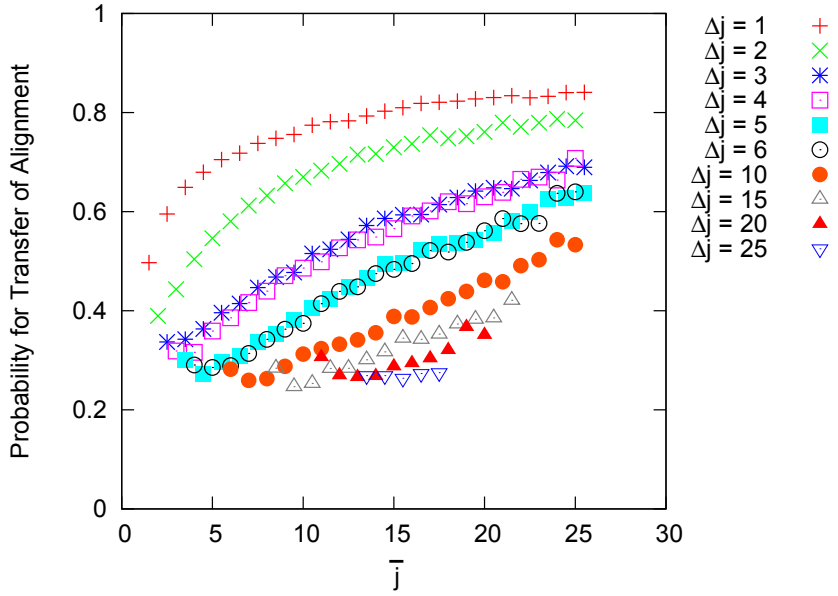


(b) $E = 0.0020$ $E_h$

**Figure 4.30:** Probability that alignment will be transferred during a collision of He with NaK($A^1\Sigma^+$) as a function of the average value of $j$ and $j'$, $\bar{j} = (j + j')/2$. Each series corresponds to a specific $\Delta j = j - j'$. The probability is independent of the sign of $\Delta j$. Panels (a) and (b) show calculations for total energy $E = 0.0005$ and $0.0020$ $E_h$, respectively.

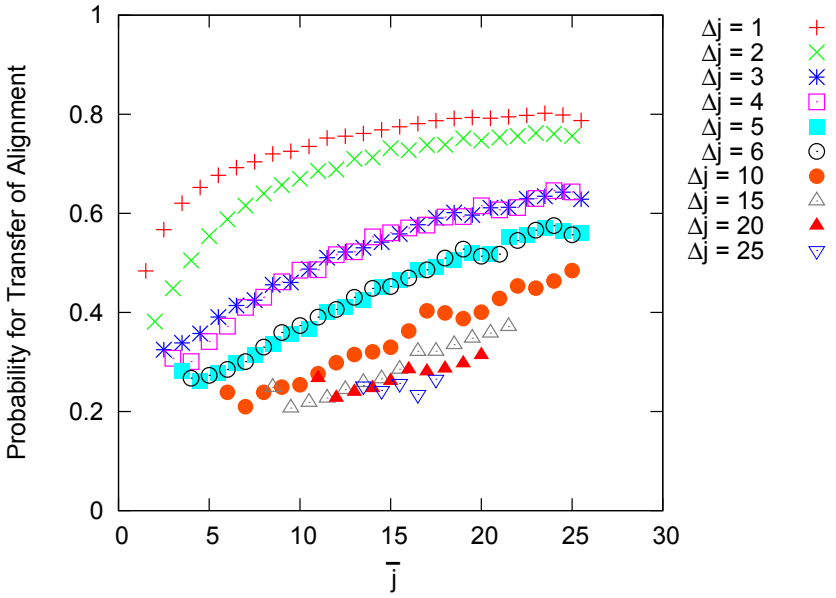


(a) $E = 0.0040$ $E_h$

**Figure 4.31:** Probability that alignment will be transferred during a collision of He with NaK($A^1\Sigma^+$) as a function of the average value of $j$ and $j'$, $\overline{j} = (j + j')/2$. Each series corresponds to a specific $\Delta j = j - j'$. The total energy of the calculation is $E = 0.0040$ $E_h$.

### 4.2.4 Comparison with Experimental Results

No measurements are currently available for He collisions with NaK($X^1\Sigma^+$). Experiments are underway for He collisions with NaK($A^1\Sigma^+$) in low $v$ vibrational levels, but preliminary experimental results are already available for He collisions with NaK($A^1\Sigma^+$, $v = 16$) and obtained rate constants for transitions from initial $j = 14$ [19]. Note that these results are not directly comparable to the coupled channel calculations, which correspond to the $v = 0$ vibrational state, as discussed in Section 4.1.4. To compare with these results, rate constants must be estimated from the cross sections obtained by the coupled channel calculations. The rate constant is expressed as the product of the thermal average of the velocity and the cross section [35]

$$k = \langle \sigma v \rangle \approx \overline{\sigma}\,\overline{v} \tag{4.2.1}$$

where $\overline{v} = \sqrt{\frac{8kT}{\pi\mu}} \approx \sqrt{\frac{8kT}{\pi m_{\mathrm{He}}}}$. We used cross sections calculated at the mean thermal energy within the heat pipe, $E = 0.0020$ $\mathrm{E_h}$, for $\overline{\sigma}$. Table 4.1 shows a comparison of rate constants measured experimentally and estimated from the cross sections obtained with coupled channel calculations. Figure 4.32 shows the comparison graphically. The numbers reported up to this point have been in atomic units, but the rate constants are given in units of $\mathrm{cm^3/s}$. The experimental results show a clear propensity for even $\Delta j$ transitions, for both positive and negative $\Delta j$. The calculations do not show this propensity.

There are several reasons that may explain this difference. The first explanation is the difference between the vibrational states. The coupled channel calculations were done at the NaK equilibrium separation, corresponding approximately to the

**Table 4.1:** Comparison of the experimental and calculated rate constants for $He + NaK(A^1\Sigma^+)$ transitions from the $j = 14$ level. The experiments used NaK in $v = 16$. Panel (a) shows the positive $\Delta j$ rate constants and Panel (b) shows rate constants for negative $\Delta j$.

(a) Positive $\Delta j$

| | $k(10^{-10}$ cm$^3$·s$^{-1})$ | |
|---|---|---|
| $j'$ | Experimental | Theoretical |
| 13 | 0.163 | 2.49 |
| 12 | 2.12 | 1.71 |
| 11 | 0.199 | 0.978 |
| 10 | 0.920 | 0.891 |

(b) Negative $\Delta j$

| | $k(10^{-10}$ cm$^3$·s$^{-1})$ | |
|---|---|---|
| $j'$ | Experimental | Theoretical |
| 15 | 0.285 | 2.66 |
| 16 | 2.24 | 1.98 |
| 17 | 0.134 | 1.19 |
| 18 | 1.46 | 1.18 |

$v = 0$ vibrational state. The experimental data are from transitions in the $v = 16$ vibrational state. Currently, GAMESS calculations are being performed for other

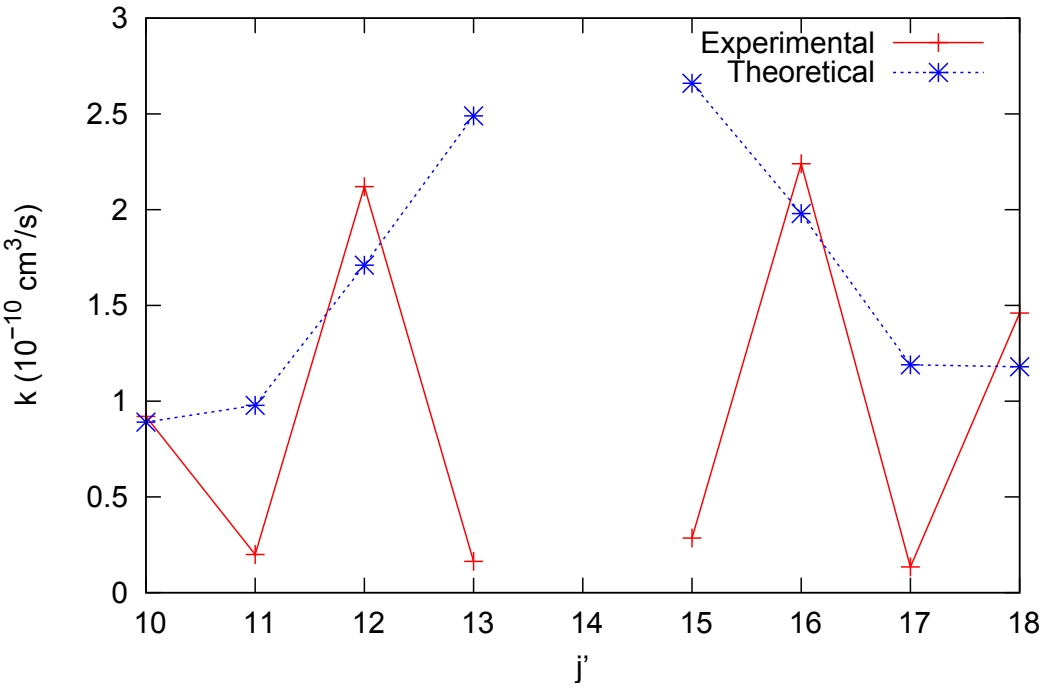


**Figure 4.32:** Comparison of rate constants for $He + NaK(A^1\Sigma^+)$ measured experimentally and calculated theoretically. Experimental measurements indicate a clear propensity for $\Delta j$ even transitions, which is not present in the theoretical calculations.

NaK internuclear separations and it has been found that the potential is sensitive to the value of $r_{\mathrm{v}}$. An average of the $v_\lambda$ coefficients weighted by the square of the wave function of the vibrational state as shown in Eq. 4.1.24 may improve the agreement. Future work of this nature will be discussed more thoroughly in Chapter 6. Current experimental work is focusing on collisions with He that cause $j$ changing transitions in the $A^1\Sigma^+$ $(v = 0)$ state of NaK.

Another explanation may relate to the procedure for estimating rate constants from the cross sections. The theoretical rate constants were estimated from cross sections at an energy corresponding to the mean thermal energy. Instead, the cross sections should be calculated as a function of energy and convoluted with a Maxwellian energy distribution [35]. However, as was discussed in Section 4.2.1, higher energy calculations include more channels and have not been checked for convergence yet due to the large amounts of computational resources required. Test calculations have been done for higher energies and seem to show that cross sections for $\Delta j = 2$ become slightly larger than those of $\Delta j = 1$ as energy increases. This trend may result in a $\Delta j$ even propensity if the rate constants are calculated from the convoluted cross sections. Figures 4.33 and 4.34 show cross sections for transitions from $j = 0, 5, 10$ and 15 to several values of $j'$ which are converged for the energies $E = 0.0005, 0.0020$, and $0.0040$ $\mathrm{E_h}$. Cross sections from test calculations not checked for convergence are shown for several other energies as well.

At this time there are no definitive experimental results for probabilty of orientation transfer during $\mathrm{He} + \mathrm{NaK}(A^1\Sigma^+)$ collisions. However results from Wolfe *et al.* [2] showed that collisions of K with $\mathrm{NaK}(A^1\Sigma^+)$ almost completely destroy orientation, while collisions of Ar with $\mathrm{NaK}(A^1\Sigma^+)$ for $\Delta j = \pm 1 - 4$ preserve roughly

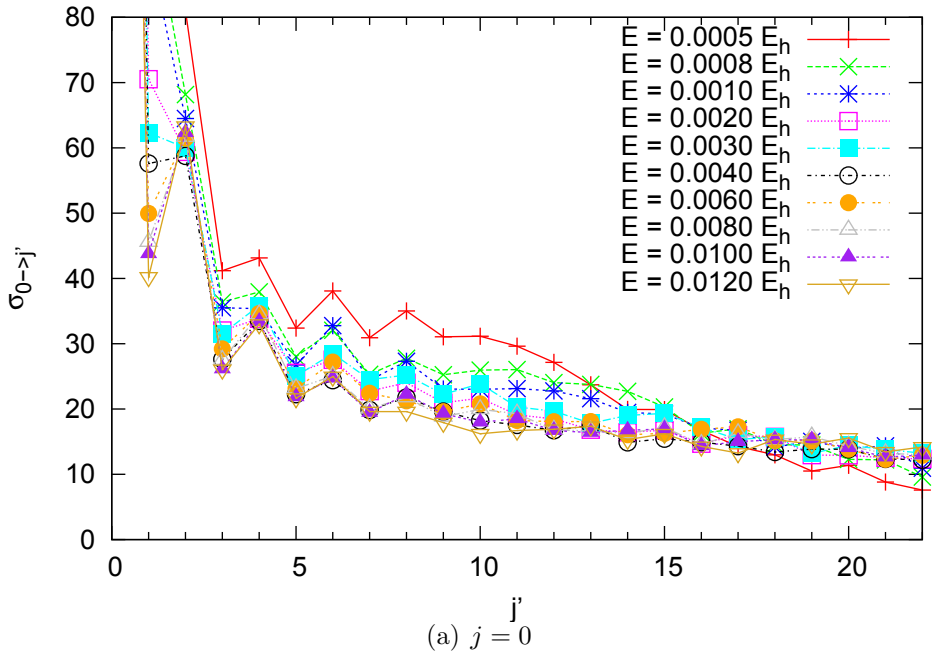


(a) $j = 0$

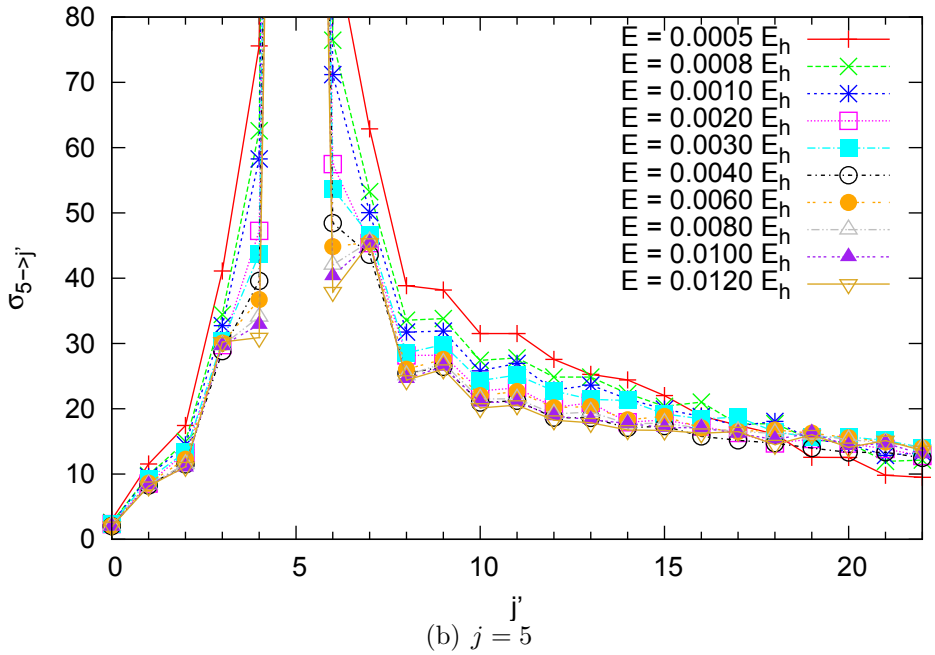


(b) $j = 5$

**Figure 4.33:** Cross sections for various energies (of which $E = 0.0005, 0.0020.$ and 0.0040 $E_h$ have been checked for convergence) as a functions of $j'$. Panels (a) and (b) show calculations for $j = 0$ and 5, respectively. Note that as the energy increases the $\Delta j = 1$ cross sections decrease while the $\Delta j = 2$ cross sections are fairly constant which may result in a $\Delta j$ even propensity.

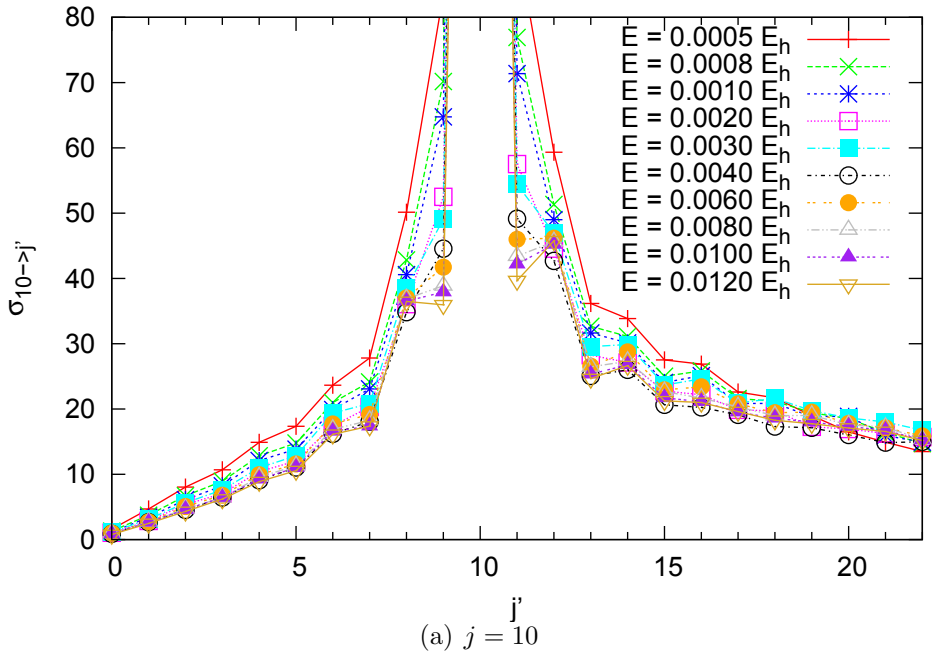


(a) $j = 10$

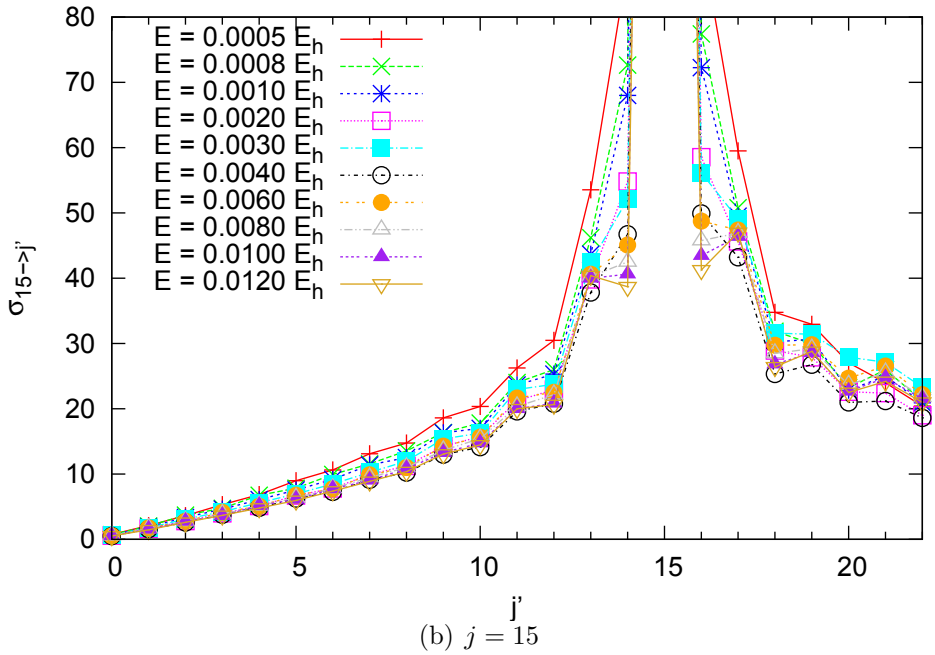


(b) $j = 15$

**Figure 4.34:** Cross sections for various energies (of which $E = 0.0005, 0.0020.$ and 0.0040 $E_h$ have been checked for convergence) as a functions of $j'$. Panels (a) and (b) show calculations for $j = 10$ and 15, respectively. Though not as dramatic as the change seen in Fig. 4.33, as the energy increases the $\Delta j = 1$ cross sections decrease while the $\Delta j = 2$ cross sections are fairly constant which may result in a $\Delta j$ even propensity.

$40\% - 75\%$ of orientation. The results shown in Figs. 4.28 and 4.29 of Section 4.2.3 show that the probability that orientation is transferred during collisions of He with NaK($A^1\Sigma^+$) is larger than 50% for $\Delta j = 1 - 4$ for most $\bar{j}$. While this is not a direct comparison, He and Ar are both rare gases and the similiarity of the results is encouraging.

## 4.3 Energy Sudden Approximation

Until now, we have presented exact calculations of the cross sections. However, valuable insights can often be obtained by considering simpler models of the collision process. A very useful model for the present situation is known as the energy sudden approximation [36]. The energy sudden approximation assumes that all the rotational energy levels are degenerate, allowing extremely simple formulas for the cross sections to be derived. Figure 4.35 shows the rotational energy levels of ground state NaK. The lower rotational levels have very small spacings compared to the energies present within the heat pipe. The mean thermal energy of the molecules in the heat pipe oven, $E = 0.0020$ $\mathrm{E_h}$, is roughly 160 times the spacing between the $j = 14$ and 15 rotational levels.

The result of the energy sudden (ES) approximation is that the cross sections for all transitions can be constructed from a knowledge of the cross sections $\sigma(0 \to \lambda)$ for transitions from the ground state, $j = 0$, to a final level with $j' = \lambda$:

$$\sigma^{\mathrm{ES}}(jm \to j'm') = \left(\frac{k_0}{k_j}\right)^2 (2j+1)(2j'+1) \sum_{\lambda=|j-j'|}^{j+j'} \sum_{\mu=-\lambda}^{\lambda} \begin{pmatrix} j & j' & \lambda \\ -m & m' & \mu \end{pmatrix}^2 \begin{pmatrix} j & j' & \lambda \\ 0 & 0 & 0 \end{pmatrix}^2 \sigma(0 \to \lambda). \quad (4.3.1)$$

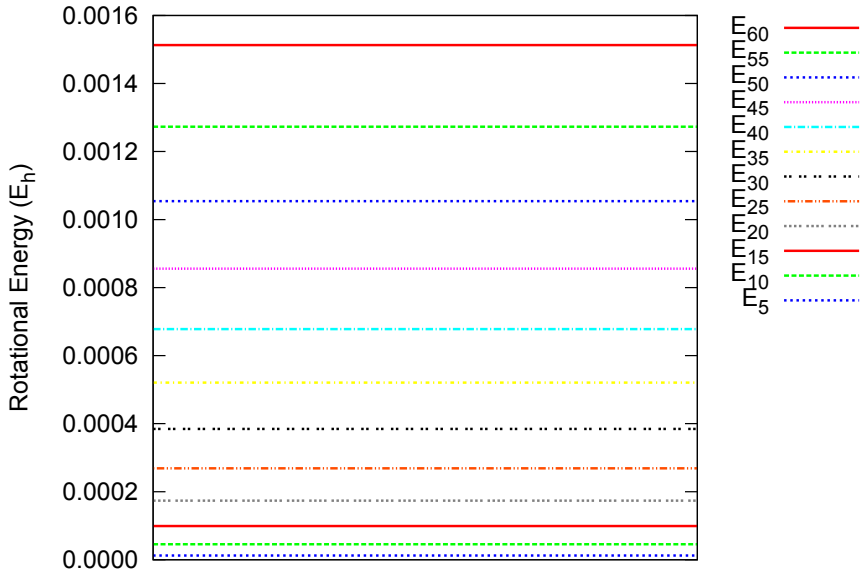


**Figure 4.35:** Rotational energy levels of NaK($X^1\Sigma^+$).

Averaging over the initial $m$ and summing over the final $m'$ leads to

$$\sigma^{\mathrm{ES}}(j \to j') = \left(\frac{k_0}{k_j}\right)^2 (2j'+1) \sum_{\lambda=|j-j'|}^{j+j'} \begin{pmatrix} j & j' & \lambda \\ 0 & 0 & 0 \end{pmatrix}^2 \sigma(0 \to \lambda). \tag{4.3.2}$$

These results support a picture in which the key factor in the collision is the transfer of angular momentum from the projectile to the target, rather than the transfer of energy [9]. For the transition $j = 0$ to $j' = \lambda$, the magnitude of the angular momentum transferred is $\lambda\hbar$, and so one can interpret $\sigma(0 \to \lambda)$ as a cross section for angular momentum transfer. Then the cross section for a transition between any initial and final states can be represented as a sum of terms corresponding to the transfer of various amounts of angular momentum; each term is weighted by the appropriate $3j$ coefficient. Figure 4.36 shows a vector representation of the

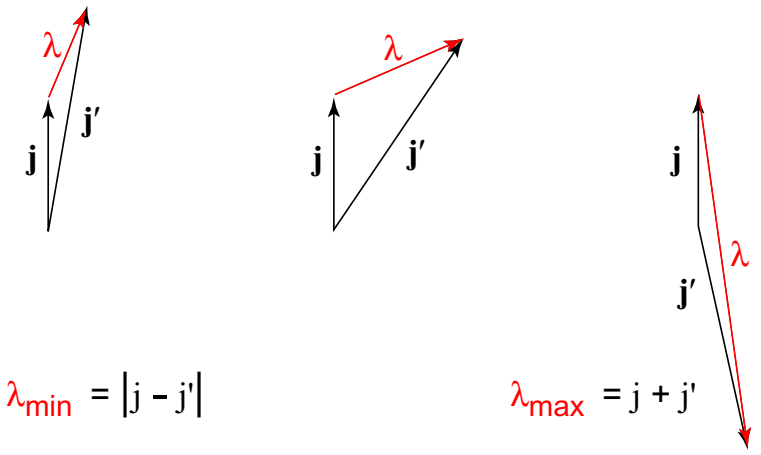


**Figure 4.36:** Vector diagram describing how the same ($j \rightarrow j'$) transition can result from different transfers of angular momentum.

different amounts of angular momentum $\lambda\hbar$ that can be transferred in a transition from $j$ to a particular $j'$.

### 4.3.1 Accuracy of the Approximation

In order to assess the accuracy of the energy sudden approximation, it is useful to compare the ES result with the exact result from Eq. 4.1.22 used for the coupled channel calculations, which is repeated here:

$$\sigma(j \rightarrow j') = \frac{\pi}{(2j+1)k_j^2} \sum_{\lambda=|j-j'|}^{j+j'} (2\lambda+1) B_\lambda(j,j'). \tag{4.3.3}$$

By equating corresponding terms in the sums over $\lambda$ in Eqs. 4.3.2 and 4.3.3, one can relate the values of $\sigma(0 \rightarrow \lambda)$ and the Grawert coefficients:

$$\sigma^{\text{eff}}(0 \rightarrow \lambda) = \left(\frac{\pi}{k_0^2}\right) \frac{2\lambda+1}{(2j+1)(2j'+1)} \begin{pmatrix} j' & j & \lambda \\ 0 & 0 & 0 \end{pmatrix}^{-2} B_\lambda(j,j'). \tag{4.3.4}$$

Equation 4.3.4 is only as accurate as the energy sudden approximation, but one can exploit it to determine an "effective" $\sigma^{\text{eff}}(0 \rightarrow \lambda)$ from each Grawert coefficient $B_\lambda(j, j')$. If many different Grawert coefficients lead to an accurate value of $\sigma^{\text{eff}}(0 \rightarrow \lambda)$, one can conclude that the ES approximation is valid. Note that the $3j$ symbol in Eq. 4.3.4 is zero if $j + j' + \lambda$ is odd, so if $j + j'$ is even (odd), only even (odd) values of $\lambda$ can be determined.

Figures 4.37 and 4.38 compare the effective cross sections $\sigma^{\text{eff}}(0 \rightarrow \lambda)$ determined using Eq. 4.3.4 for several values of $j$ and $j'$ with the accurate values of $\sigma(0 \rightarrow \lambda)$ obtained with the coupled channel calculations. These calculations were performed for $\text{He} + \text{NaK}(X^1\Sigma^+)$ at $E = 0.0005$, 0.0010, 0.0020 and 0.0040 $\text{E}_\text{h}$, where 0.0020 $\text{E}_\text{h}$ is approximately the average thermal energy within the heat pipe. The cross sections are plotted as a function of the average value of $j$ and $j'$, $\overline{j} = (j + j')/2$. The exact cross sections for the $(0 \rightarrow \lambda)$ transition are given as straight lines. Effective cross sections are shown for $\lambda = 2, 3$ and 4, which can be formed from various combinations of $j$ and $j'$. The plot includes $j$ and $j'$ ranging from $0 - 24$. Comparison of all the panels shows that the effective cross section is closer to the exact cross section for higher energies. The approximation is better for higher energies because the splitting between the rotational levels is smaller compared to the kinetic energy of the projectile. For fixed $\lambda$, the approximation is better for smaller values of average $j$ and $j'$. The approximate values were within 10% of the exact cross sections when the energy gap between the $j$ and $j'$ rotational levels was below 5% of the total energy of the calculation.

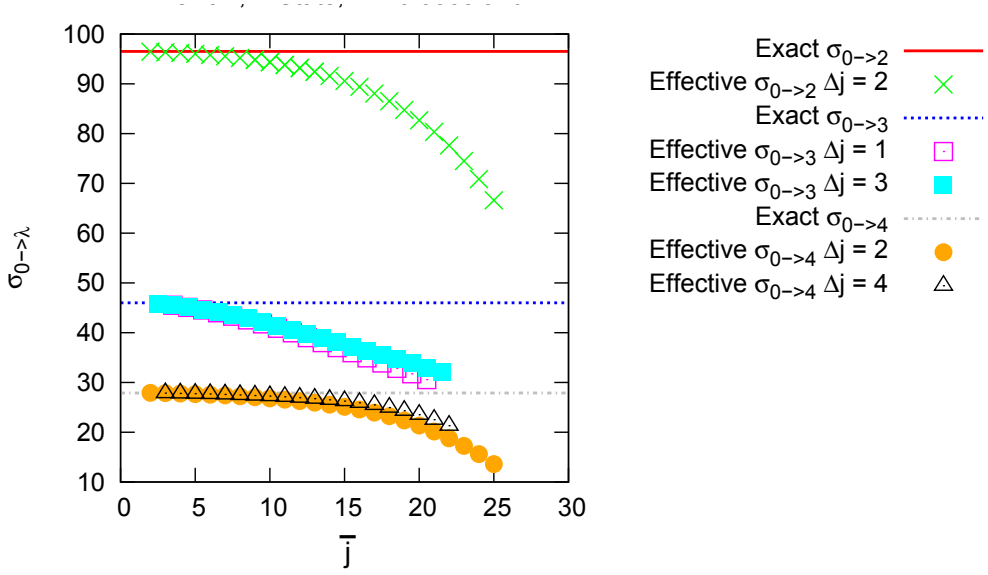


(a) $E = 0.0005$ $E_h$

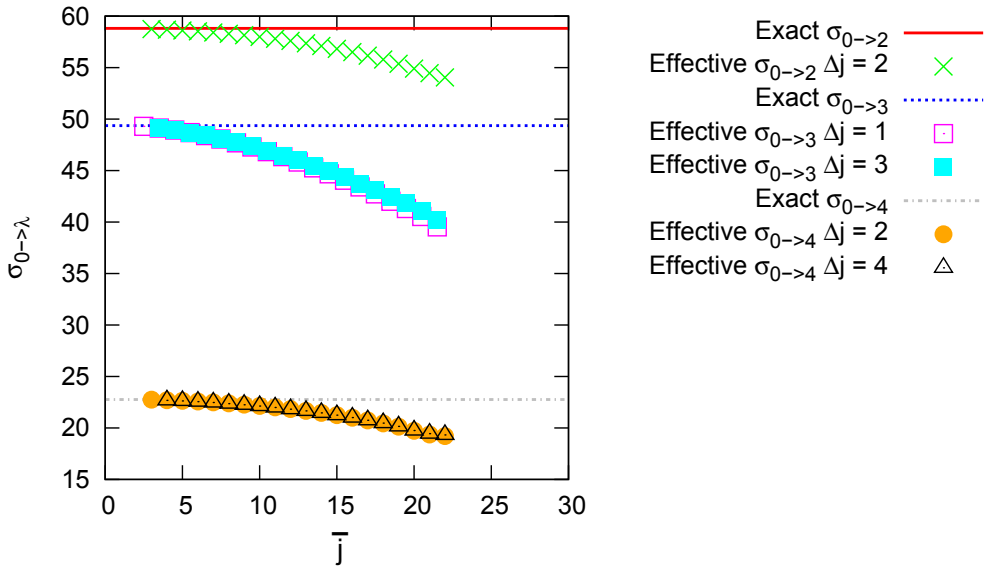


(b) $E = 0.0010$ $E_h$

**Figure 4.37:** Comparison of exact $(0 \rightarrow \lambda)$ cross sections calculated with coupled channel calculations shown as lines and effective cross sections for $\lambda = 2, 3, 4$ calculated from the Grawert coefficients as a function of $\overline{j} = (j + j')/2$. Panel (a) is for calculations at $E = 0.0005$ $E_h$ and Panel (b) $E = 0.0010$ $E_h$. As expected, the approximation is better for the higher energy calculations.

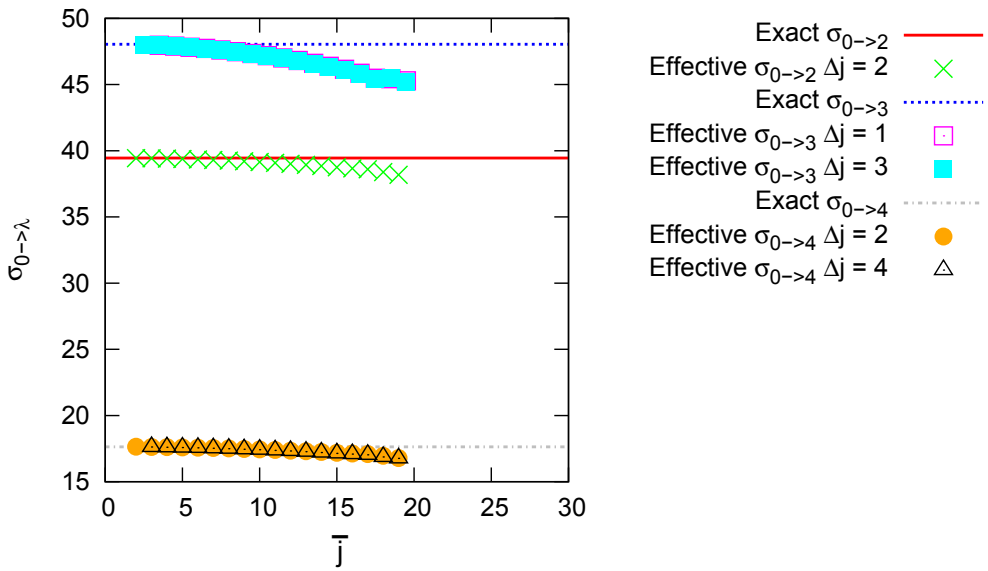


(a) $E = 0.0020$ $E_h$

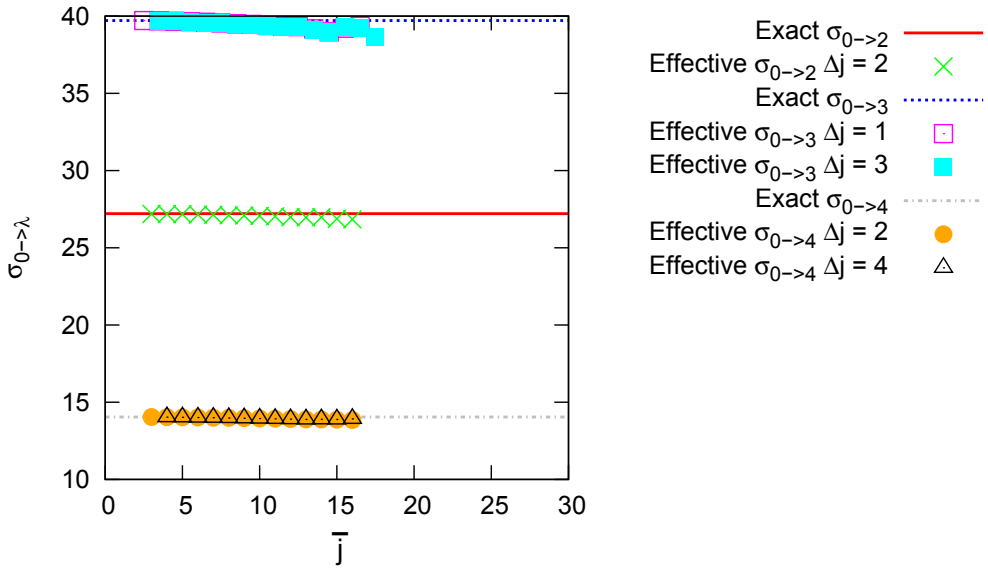


(b) $E = 0.0040$ $E_h$

**Figure 4.38:** Comparison of exact $(0 \rightarrow \lambda)$ cross sections calculated with coupled channel calculations shown as lines and effective cross sections for $\lambda = 2, 3, 4$ calculated from the Grawert coefficients as a function of $\overline{j} = (j + j')/2$. Panel (a) is for calculations at $E = 0.0020$ $E_h$ and Panel (b) $E = 0.0040$ $E_h$. As expected, the approximation is better for the higher energy calculations.

### 4.3.2 Reduction of Computer Resources Needed

The energy sudden approximation will also be very helpful should the need to conserve computer resources arise. Table 4.2 illustrates the computer resources needed for calculations of various sizes. Calculations were performed for various energies in both the ground and excited electronic states. The number of channels in each calculation and the time in processor hours on the Blacklight supercomputer at Pittsburgh Supercomputing Center is given as a function of the included $j$ rotational states. The computer time in processor hours scales roughly as the number of channels cubed.

The form of the total wavefunction given in Eq. 4.1.4 depends on a summation of the $j$ values included in the coupled channel calculation. Reducing the number of terms in this summation would vastly reduce computational requirements. Also, for each $j$ level, there are $(2j + 1)$ magnetic sublevels $m$ that must be taken into account. Using fewer and smaller $j$ values would help reduce the time needed for orientation and alignment calculations as well. The energy sudden approximation provides a way to use fewer $j$ values because this approximation would only require

**Table 4.2:** Time in processor hours on the Blacklight supercomputer for calculations at various energies and in both electronic states as a function of the number of included rotational levels.

| | 0.00025 $E_h$ (Ground State) | | 0.0005 $E_h$ (Ground State) | | 0.0020 $E_h$ (Excited State) | |
|---|---|---|---|---|---|---|
| $j$ | max. # channels | processor hours | max. # channels | processor hours | max. # channels | processor hours |
| $0-20$ | — | — | — | — | 231 | 141 |
| $0-25$ | 351 | 168 | — | — | 351 | 531 |
| $0-30$ | 496 | 504 | 496 | 710 | 496 | 1702 |
| $0-35$ | 666 | 1834 | 666 | 2304 | — | — |

that $j_{\max}$ be large enough such that all the $(0 \rightarrow \lambda)$ transitions be converged.

As was discussed in Section 4.2.1, higher energy calculations must include more partial waves, greatly increasing the computational resources required. Therefore, the fact that the approximation is more accurate for higher energies is very useful. The energy sudden approximation would allow use of fewer channels and less computer resources to obtain the same information, even with a high energy and large number of partial waves.

# Chapter 5

# Multi-Configuration Time-Dependent Hartree Scattering Calculations

## 5.1 Dynamics Calculations

This chapter will compare results from the Multi-Configuration Time-Dependent Hartree (MCTDH) wave packet dynamics calculations to those resulting from the coupled channel scattering calculations. The dynamics calculations performed using the MCTDH method were implemented with the powerful MCTDH code written by the Heidelberg group [37]. Unlike the coupled channel method which is time-independent, the wave packet method solves the time-dependent Schrödinger equation. Collisions can be treated by calculating the evolution of a wave packet representing the incident particle's position with respect to the target on a model potential surface. For the purposes of this comparison, we have developed a model

potential that will be used by both types of calculations. The dynamics calculations provide detailed cross sections for the scattering process which are directly comparable to the cross sections calculated using the coupled channel method.

This chapter begins by discussing the MCTDH method in general. We then discuss the specifics of applying the wave packet method to collisions of He atoms with NaK molecules. This section includes a description of the model potential developed for this comparison. Finally, cross sections resulting from both the wave packet and coupled channel methods are presented and compared.

### 5.1.1 Standard Method for Wavepacket Propagation

The wave function can be determined by solving the time-dependent Schrödinger equation (TDSE). A straight forward method, known as the standard solution, is to expand the wave functions in terms of sums of products of fixed basis functions:

$$\Psi(Q_1, Q_2, ...; t) = \sum_{p_1=1}^{N_1} \sum_{p_2=1}^{N_2} \cdots \sum_{p_k=1}^{N_k} C_{p_1,p_2,...}(t) \chi_{p_1}^{(1)}(Q_1) \chi_{p_2}^{(2)}(Q_2) \cdots , \tag{5.1.1}$$

where $Q_i$ are the nuclear coordinates, $\chi_{p_i}^{(i)}(Q_i)$ are called primitive basis functions, and $C_{p_1,p_2,...}(t)$ are time-dependent coefficients [37]. Each degree of freedom $Q_i$ is described by $N_i$ basis functions. The ellipsis indicates a summation for each degree of freedom over all the basis functions used to describe that degree of freedom. The primitive basis functions are time-independent. The only dependence on time appears in the coefficients $C_{p_1,p_2,...}(t)$. Using a matrix form of the Schrödinger equation one can solve for these coefficients

$$\hat{H}\mathbf{C} = i\frac{d}{dt}\mathbf{C}. \tag{5.1.2}$$

The matrices of Eq. 5.1.2 have dimension $N \times N$ where $N$ is the product of the number of basis functions of each degree of freedom:

$$N = N_1 \times N_2 \times \cdots \times N_k. \tag{5.1.3}$$

As the number of degrees of freedom grows, the amount of computer time and memory needed to solve the problem grows exponentially. The exact method is usually not feasible for systems with greater than four degrees of freedom.

### 5.1.2 Multi-Configuration Time-Dependent Hartree Method

Using a different *ansatz* for the wave function can make solving the TDSE easier and decrease the computational resources necessary. The multi-configuration time-dependent Hartree (MCTDH) method uses a wave function of the form [38]

$$\Psi(Q_1, Q_2, ...; t) = \sum_{p_1=1}^{n_1} \sum_{p_2=1}^{n_2} \dots A_{p_1,p_2,\dots}(t) \varphi_{p_1}^{(1)}(Q_1, t) \varphi_{p_2}^{(2)}(Q_2, t) \cdots \tag{5.1.4}$$

where $\varphi_{p_i}^{(i)}(Q_i, t)$ are called single particle functions (SPF) and $A_{p_1,p_2,\dots}(t)$ are the coefficients. In this scheme the single particle functions are expressed as time dependent linear combinations of the primitive basis functions [39]

$$\varphi_{p_i}^{(i)}(Q_i, t) = \sum_{p_i=1}^{N_i} c_{p_i}(t) \chi_{p_i}^{(i)}(Q_i). \tag{5.1.5}$$

Since both the SPFs and the coefficients, $A_{p_1,p_2,\dots}(t)$, are time dependent, the wave function is not necessarily unique. To guarantee uniqueness, a constraint is imposed on the single particle functions that ensures normalization.

At each time step, several sets of coupled equations must be solved to obtain the SPFs and the coefficients. The single particle functions are optimized by using a mean field approximation which allows each single particle function $\varphi_{p_i}^{(i)}(Q_i, t)$ to be solved for individually [39]. This procedure reduces solving for the SPFs for each $Q_i$ to a problem of $N_i$ dimensions. The matrix equation used to solve for the $A_{p_1,p_2,\ldots}(t)$ coefficients at each time step is similar to Eq. 5.1.2:

$$\hat{H}\mathbf{A} = i\frac{d}{dt}\mathbf{A}. \tag{5.1.6}$$

The dimensions of these matrices is again $N \times N$, however this time $N$ is given by

$$N = n_1 \times n_2 \times \cdots . \tag{5.1.7}$$

Usually, $n_i < N_i$, significantly decreasing the computational resources required for the calculation.

The MCTDH method is particularly advantageous if the Hamiltonian can be written in a separable form. In separable form, the Hamiltonian is written as the sum of products of single particle operators. The matrix elements of a separable Hamiltonian are the product of many one-dimensional integrals, as opposed to multi-dimensional integrals. This form of the Hamiltonian matrix elements greatly increases the efficiency of the computational requirements. When written in the Jacobi coordinates shown in Fig. 3.1, the kinetic energy of this system is a separable expression, which is the prime motivation to use this coordinate system for calculations with MCTDH. Then the total Hamiltonian will be separable if the potential energy can be expressed as a Legendre polynomial expansion as was done

previously in Eq 3.1.1 of Section 3.1.2.

## 5.2 Scattering Calculations with MCTDH

The powerful, widely available MCTDH computer program was used to perform the wave packet calculations in this work. The wave packet describes the position of the incident atom relative to the target molecule. The calculations assume that the internuclear separation of the target, $r_{\mathrm{v}}$, has a fixed value, as in the coupled channel calculations. Thus, the wave packet in the MCTDH calculations has two degrees of freedom, $R_{\mathrm{d}}$ and $\theta$. The incident particle is positioned far from the target at large $R_{\mathrm{d}}$ with some initial momentum. The wave packet is propagated until it has interacted with the target and moved away again. Throughout this process, the code monitors how the interaction changes the wave packet and quantum numbers.

The kinetic energy Hamiltonian for a fixed value of $J$ used in the calculations for this system [40] was built into the MCTDH code and has the form

$$\begin{aligned}\hat{H}_{\mathrm{KE}} = &-\frac{1}{2\mu_{\mathrm{He+NaK}}}\frac{\partial^2}{\partial R_{\mathrm{d}}^2} + \frac{J(J+1)-2K^2+j^2}{2\mu_{\mathrm{He+NaK}}R_{\mathrm{d}}^2} + Bj^2 \\ &- \frac{\sqrt{J(J+1)-K(K+1)}}{2\mu_{\mathrm{He+NaK}}R_{\mathrm{d}}^2}j_+ - \frac{\sqrt{J(J+1)-K(K-1)}}{2\mu_{\mathrm{He+NaK}}R_{\mathrm{d}}^2}j_- \end{aligned} \quad (5.2.1)$$

where

$$j_\pm = \mp\frac{\partial}{\partial\theta} - K\cot\theta, \quad (5.2.2)$$

$\mu$ is the reduced mass of the specified particles, $K$ is the projection of the total angular momentum $J$ onto $R_{\mathrm{d}}$, and $B$ is the NaK rotational constant. Because the Hamiltonian is dependent on $J$, a separate wave packet calculation must be

done for each state $(J, j, m)$. For this comparison with the coupled channel method, only calculations for inital states $(j = 0, m = 0)$ were performed. In the future, the energy sudden approximation discussed in Section 4.3 may be employed and Eq. 4.3.2 may be used to calculate $(j \rightarrow j')$ cross sections where $j \neq 0$ from the MCTDH results for $j = 0$.

For the purposes of comparison with the coupled channel results, a model potential was used that roughly represents the interaction of He with NaK in the ground state. Preliminary *ab initio* electronic structure calculations were performed using GAMESS for $r_{\mathrm{v}}$ fixed at 6.77 $a_0$ and various $R_{\mathrm{d}}$ and $\theta$ geometries. The $\theta$ grid extended from $0^\circ - 180^\circ$ and the $R_{\mathrm{d}}$ grid from $8 - 79$ $a_0$. A calculation at long range yielded an asymptotic limit of $-763.87$ $\mathrm{E_h}$ which was subtracted from all other calculated values. To ensure the separability of the Hamiltonian, the potential was expressed as a five term sum of products of Legendre polynomials and exponential functions of the form

$$V(R_{\mathrm{d}}, \theta) = \sum_{\lambda=0}^{4} a_\lambda \exp(-b_\lambda R_{\mathrm{d}}) P_\lambda(\cos\theta). \tag{5.2.3}$$

This form does not describe the potential determined by the GAMESS calculations exactly, but it is smoothly varying and easily incorporated into the coupled channel code. The $a_\lambda$ constants are given in Table 5.1.

To define the wave function that is the solution to the time-dependent Schrödinger equation, the basis set for each degree of freedom must be specified. The angular basis is a set of normalized associated Legendre functions. The $R_{\mathrm{d}}$ basis is a set of normalized Gaussian functions. The initial wave packet is specified by a po-

**Table 5.1:** Values of the constants used for the exponential functions in the expansion of the model potential.

| $\lambda$ | $a_\lambda$ | $b_\lambda$ |
|---|---|---|
| 0 | 1.26100 | 0.798340 |
| 1 | −0.99356 | 0.752171 |
| 2 | 0.8018727 | 0.717405 |
| 3 | −01.0 | 0.817900 |
| 4 | 1.0 | 0.879588 |

sition, width and momentum. For scattering calculations the initial wave packet must appear as though it has undergone free motion towards the scattering center from infinity. Propagating the wave packet from distances where the interaction is truly zero would require extremely long propagation times. Instead, the wave packet can be started closer to the scattering center, but must be corrected so that it seems to have traveled from infinitely far away [37]. Thus, the initial position must be choosen with care to ensure that the interaction is sufficiently small at the starting position, allowing for this correction. For these calculations, we found that $R_{\mathrm{d}} = 64.0\ a_0$ was sufficiently far from the scattering center.

The momentum given to the incident particle for these calculations was 4.0 a.u. which is equivalent to a center of mass energy of 0.0011 $\mathrm{E_h}$. However, the initial wave packet can be expressed as a linear combination of incoming waves of different momenta

$$\Psi(Q_k) = \frac{1}{\sqrt{2\pi\hbar}} \int_{-\infty}^{\infty} \phi(p) \exp(ipQ_k/\hbar) dp. \tag{5.2.4}$$

Coordinate-momentum Fourier transformation of the initial wavepacket gives the initial energy distribution of the wave packet. The results of the calculation are reliable at the energies within this distribution. Figure 5.1 shows the energy distribution for the initial wave packet specified for these calculations.

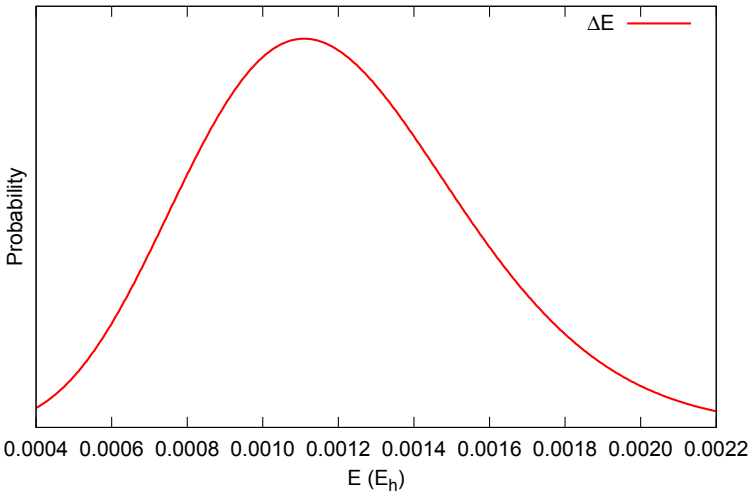


**Figure 5.1:** This figure shows the energy distribution for the initial wave packet with momentum 4.0 a.u.

MCTDH provides a means of introducing a complex absorbing potential (CAP) at the end of the $R_{\mathrm{d}}$ grid, which absorbs the wave packet as it reaches the edge of the grid and eliminates unphysical reflections. The CAP turns on gradually as $R_{\mathrm{d}}$ approaches the end of the integration grid. The analytic form of the CAP is given by [39]

$$-iW(R_{\mathrm{d}}) = -i\eta|R_{\mathrm{d}} - R_{\mathrm{d}}^{0}|^{b}\Theta\left(\pm\left(R_{\mathrm{d}} - R_{\mathrm{d}}^{0}\right)\right), \tag{5.2.5}$$

where $R_{\mathrm{d}}^{0}$ is the starting point of the CAP, $\eta$ is the strength, $b$ is the order of the CAP and $\Theta$ is a Heaviside's step function. The MCTDH program has built-in routines to determine which CAP parameters are best suited for a particular calculation. The $R_{\mathrm{d}}^{0}$, $\eta$ and $b$ parameters used for these calculations were 69.0 $a_0$, 0.0000043824 $\mathrm{E_h}/a_0$, and 4, respectively. As the wave packet interacts with the CAP, MCTDH determines the contribution of each final state of the system to the absorbed wave packet, which is referred to as the quantum flux. MCTDH uses the

flux to calculate the reaction probabilities $P(j=0, m=0 \rightarrow j', m')$ for the final states of the system.

From these probabilities, one can compute cross sections [40]

$$\sigma^{J}_{0,0\rightarrow j'm'}(E) = \frac{\pi}{k_j^2}\frac{2J+1}{2j+1}P(0,0\rightarrow j', m'). \tag{5.2.6}$$

To obtain total cross sections for a particular initial $(j, m)$ state, one must sum over all total angular momenta values $J$. Thus, a wave packet scattering calculation must be performed for every $J$. An approximation can be made by including only $J$ values that contribute significantly to the $(j, m \rightarrow j', m')$ cross section. A suitable $J_{\max}$ is chosen and a calculation must be performed for every $J = 0$ to $J_{\max}$. The total $(j = 0, m = 0 \rightarrow j'm')$ cross section is

$$\sigma_{0,0\rightarrow j'm'}(E) = \sum_{J=0}^{J_{\max}} \sigma^{J}_{0,0\rightarrow j'm'}(E). \tag{5.2.7}$$

Once the MCTDH scattering calculations for every $J$ have been performed, one can obtain cross sections for any energy within the range defined by the inital wave packet's energy distribution. Conversely, each coupled channel scattering calculation provides cross sections for all included $J$ values for a single specified energy.

To determine cross sections for $(j \rightarrow j')$ transitions, one would have to average over all the initial $m$ values and sum over all the final $m'$ values. Since the initial $j = 0$ in these calculations, the first step has essentially already been done and the cross sections are given by

$$\sigma_{0\rightarrow j'}(E) = \sum_{m'=-j'}^{j'} \sigma_{0,0\rightarrow j'm'}(E). \tag{5.2.8}$$

## 5.3 Comparison of MCTDH and Coupled Channel Results

In this section we compare the cross sections for a model interaction of He with NaK($X^1\Sigma^+$) resulting from the wave packet and coupled channel methods. The MCTDH calculations were performed for an inital momentum of 4.0 a.u. corresponding to an energy of 0.0011 $E_h$, which is at the peak of the energy distribution shown in Fig. 5.1. The total angular momentum, $J$, included in both the MCTDH and coupled channel calculations ranged from $0-79$. Coupled channel calculations were performed at energies of 0.0011 and 0.0014 $E_h$ and included $j = 0-28$, which was sufficiently converged for transitions from $j = 0$ to $j' = 1-10$. Only the initial state $j = 0$ was investigated with MCTDH due to the limitation mentioned earlier; $2j+1$ calculations must be performed (one for every possible initial state $(j, m)$) to obtain $j \rightarrow j'$ cross sections. For $j \neq 0$ the number of initial states can add up quickly, requiring many calculations and a great deal of computer time. Table 5.2 shows the excellent agreement of the cross sections $\sigma_{0\rightarrow j'}$ obtained by the two different methods for 0.0011 $E_h$. The agreement of the MCTDH with coupled channel at $E = 0.0008$ and 0.0014 $E_h$ is not as good as at the peak of the energy distribution, but is still within 10% of the coupled channel cross section. For $E = 0.0017$ $E_h$ which is nearer the tail of the energy distribution, the agreement with the coupled channel cross section is worse. These same results can be seen graphically in Figs. 5.2, 5.3, 5.4 and 5.5.

**Table 5.2:** Values of the cross sections $\sigma_{0\to j'}$ obtained by the multi-configuration time-dependent Hartree (MCTDH) and the coupled channel (CC) methods.

| | $E = 0.0008$ $E_h$ | | $E = 0.0011$ $E_h$ | | $E = 0.0014$ $E_h$ | | $E = 0.0017$ $E_h$ | |
|---|---|---|---|---|---|---|---|---|
| $j'$ | MCTDH | CC | MCTDH | CC | MCTDH | CC | MCTDH | CC |
| 1 | 74.48104 | 80.20 | 77.42588 | 78.42 | 82.91642 | 77.51 | 89.62784 | 76.26 |
| 2 | 61.54547 | 65.08 | 58.29261 | 57.74 | 59.14251 | 53.76 | 61.30280 | 50.17 |
| 3 | 83.64850 | 87.74 | 83.79782 | 82.19 | 83.72427 | 77.33 | 85.44810 | 74.07 |
| 4 | 16.97689 | 18.21 | 18.39406 | 19.68 | 20.42743 | 20.75 | 22.24276 | 22.58 |
| 5 | 28.73922 | 29.98 | 26.40028 | 26.15 | 24.85310 | 22.67 | 23.29145 | 19.90 |
| 6 | 30.76616 | 32.41 | 29.54074 | 31.00 | 30.09425 | 32.05 | 30.92808 | 31.35 |
| 7 | 10.61924 | 11.23 | 10.70287 | 11.28 | 10.76221 | 11.08 | 10.91099 | 12.13 |
| 8 | 18.95955 | 20.02 | 17.57178 | 17.41 | 15.72153 | 15.35 | 15.17234 | 13.95 |
| 9 | 12.03645 | 12.70 | 13.45037 | 14.62 | 13.76140 | 14.50 | 13.26394 | 14.33 |
| 10 | 9.14720 | 9.534 | 8.71614 | 8.491 | 8.31846 | 7.686 | 8.12050 | 7.385 |

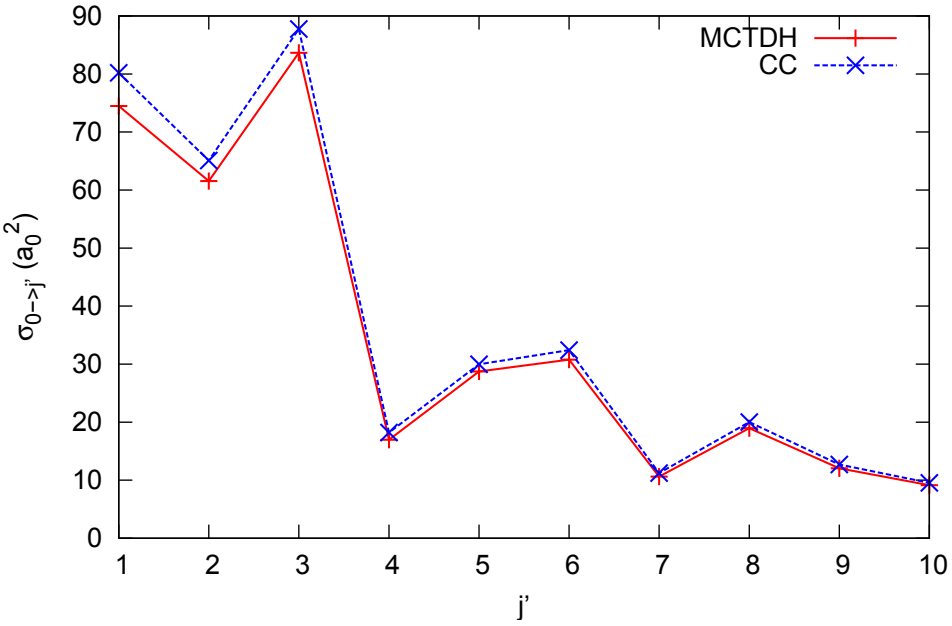


**Figure 5.2:** Comparison of the cross sections $\sigma_{0\to j'}$ obtained by the two different methods for $E = 0.0008$ $E_h$.

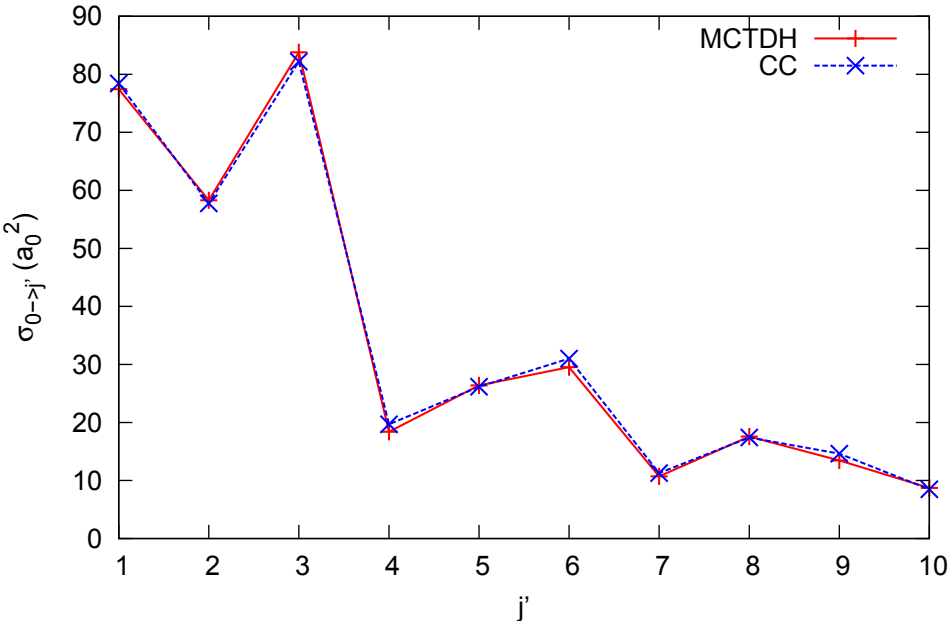


**Figure 5.3:** Comparison of the cross sections $\sigma_{0\to j'}$ obtained by the two different methods for $E = 0.0011$ $E_h$. This energy is at the center of the distribution shown in Fig. 5.1

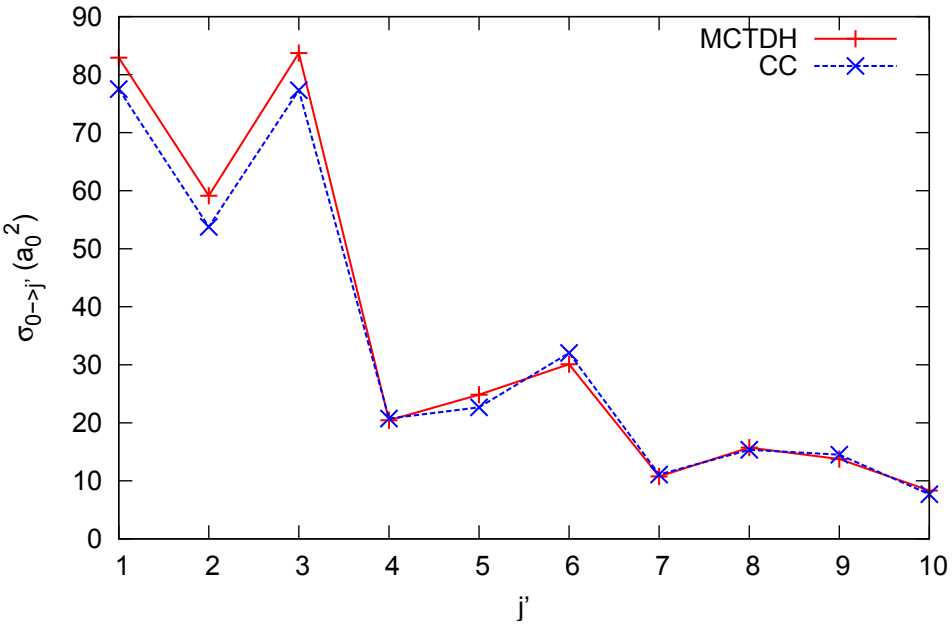


**Figure 5.4:** Comparison of the cross sections $\sigma_{0\to j'}$ obtained by the two different methods for $E = 0.0014$ $E_h$.

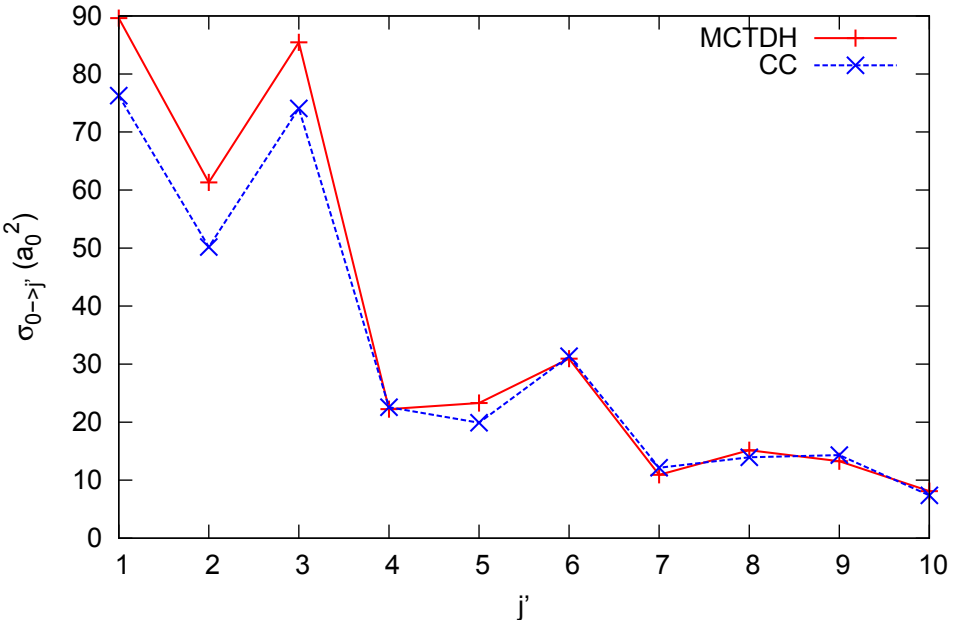


**Figure 5.5:** Comparison of the cross sections $\sigma_{0\to j'}$ obtained by the two different methods for $E = 0.0017$ $\mathrm{E_h}$.

# Chapter 6

# Conclusions, Very Recent Results, and Future Work

## 6.1 Conclusions

This dissertation presents theoretical scattering calculations of an atomic perturber with a diatomic molecule, specifically He + NaK. The work has considered primarily the $v = 0$ vibrational state of the target molecule. GAMESS calculations were performed for He + NaK($X^1\Sigma^+$) and He + NaK($A^1\Sigma^+$), and a method for fitting these potentials with Legendre polynomial expansions was developed. As expected, the potentials of the two different states have considerably different features. Scattering calculations were performed with the coupled channel method for both electronic states of NaK and cross sections and information about the probability of orientation and alignment preservation were obtained. The alternative MCTDH method was also investigated as tool for scattering calculations using a model potential and it gave excellent agreement with the couple channel results.

There is currently no definitive experimental data concerning the probabilty of orientation transfer during $He + NaK(A^1\Sigma^+)$ collisions. Wolfe *et al.* [2] reported that collisions of K with $NaK(A^1\Sigma^+)$ effectively destroy orientation, while collisions of Ar with $NaK(A^1\Sigma^+)$ for $\Delta j = \pm 1, \pm 2, \pm 3$, and $\pm 4$ have a $40\% - 75\%$ probability of preserving orientation. The results of the coupled channel calculations show collisions of He with $NaK(A^1\Sigma^+)$ have a probability of transferring orientation that is greater than 50% for $\Delta j = 1 - 4$ for most $\bar{j}$. This similarity may be related to the fact that both He and Ar are rare gases.

The rate constants obtained experimentally have shown a propensity for even $\Delta j$ transitions in collisions of $He + NaK(A^1\Sigma^+, v = 16, j = 14)$ [19]. The scattering calculations for $He + NaK(A^1\Sigma^+, v = 0)$ presented in Fig. 4.32 do not show this propensity. Very recent calculations (to be described in the next section) have confirmed that the different ranges of $r_v$ in different vibrational levels of the NaK molecule can account for this difference. The earlier calculations correspond to $v = 0$, while the experiments measured rates for $v = 16$. Recent calculations with $v = 15$ show a much greater propensity for even $\Delta j$. At this time, experiments are being developed to measure rate constants for $He + NaK(A^1\Sigma^+, v = 0)$ and $He + NaK(X^1\Sigma^+, v = 0)$, but there is no conclusive data for these collisions at this time.

Future work will have two main thrusts. Currently, work is underway to investigate the effect different vibrational levels of NaK have on the propensity for even $\Delta j$ transitions. Other future work will study collisions of NaK with different atomic alkali perturbers, particularly Ar for which there already exists experimental data.

## 6.2 Preliminary Results for Vibrational Dependence

To account for the vibrational motion of the NaK, the dependence of the potential on the NaK bond length, $r_{\rm v}$, must be included. One can write

$$V(r_{\rm v}, R_{\rm d}, \theta) = \sum_{\lambda} V_{\lambda}(r_{\rm v}, R_{\rm d}) P_{\lambda}(\cos\theta). \tag{6.2.1}$$

We showed in Section 4.1.4 that the initial vibrational state of NaK can be taken into account by averaging this potential over the range of $r_{\rm v}$ appropriate to the state of interest:

$$V_{\lambda}(R_{\rm d}) = \int v_{\lambda}(r_{\rm v}, R_{\rm d}) |\chi_v(r_{\rm v})|^2 dr_{\rm v} \tag{6.2.2}$$

where $\chi_v(r_{\rm v})$ is the vibrational wave function. This new form of the potential allows us to perform scattering calculations for He + NaK in which the vibrational quantum number $v$ is varied. The calculations reported in Chapter 4 correspond approximately to the $v = 0$ vibrational state of NaK. However, experimental data were taken for $j \rightarrow j'$ transitions in the $v = 16$ vibrational state. A comparison of the probability densities of the NaK vibrational states for $v = 0$ and 16 is shown in Fig. 6.1. The probability density of $v = 0$ is strongly peaked about $r_{\rm v} = 7.935\ a_0$. Thus, fixing $r_{\rm v}$ at the equilibrium separation of NaK is a reasonable approximation for $v = 0$. The probability density of the $v = 16$ vibrational state is spread out over a range of $r_{\rm v} = 6 - 11 a_0$. This figure clearly shows that to obtain an accurate potential for higher vibrational levels, a constant value of $r_{\rm v}$ is not sufficient.

Other members of Dr. Hickman's group have very recently performed GAMESS

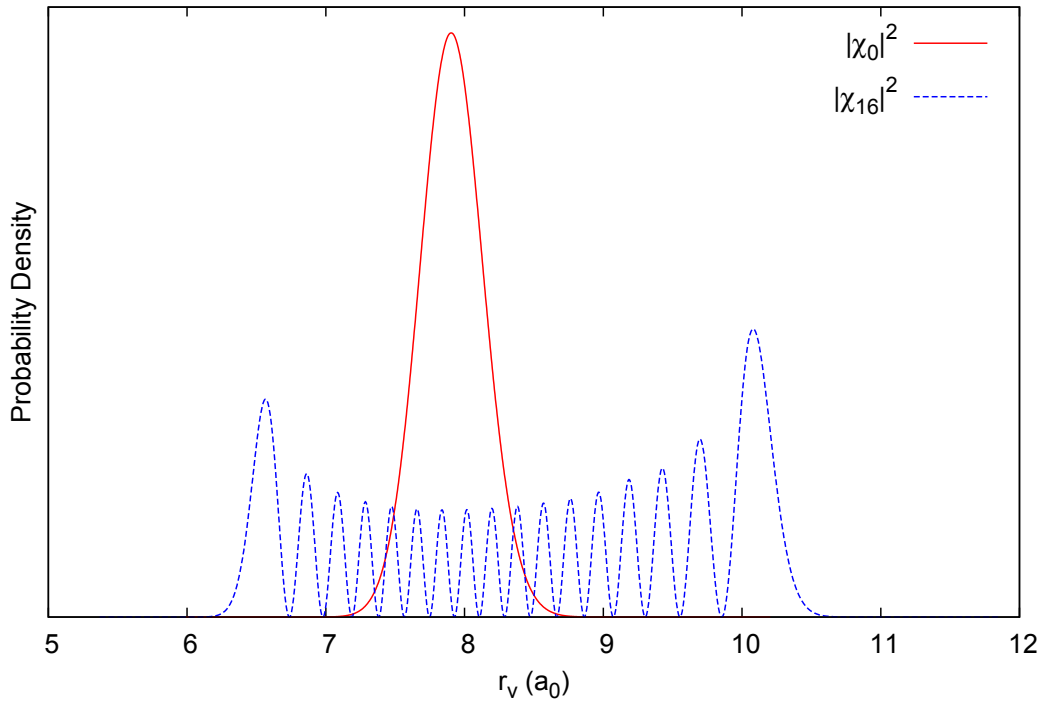


**Figure 6.1:** Probability density function of NaK($A^1\Sigma^+$) for the $v = 0$ and 16 vibrational states. The $v = 0$ probability density is peaked about 7.935 $a_0$, while the $v = 16$ probability density is spread over a range of $r_v = 6-11$ $a_0$.

calculations for various He + NaK geometries, which includes varying $r_v$ from 6 to 11 $a_0$ in 1 $a_0$ increments [41]. These values of $r_v$ span the range of the $v = 16$ probability density shown in Fig. 6.1. For each $r_v$ separation, GAMESS calculations were done for 15° increments of $\theta$ and $R_d$ = 5 to 12 $a_0$ in 1 $a_0$ increments and additionally at $R_d$ = 15 $a_0$. For each fixed value of the NaK internuclear separation, $r_v$, the potential was fit with a 21 term Legendre polynomial expansion of the same form as Eq. 3.1.1 to obtain the $v_\lambda(r_v, R_d)$ coefficients. The $v_\lambda(r_v, R_d)$ coefficients were then weighted with the $v = 15$ vibrational wave function using Eq. 6.2.2 to produce $V_\lambda(R_d)$ coefficients for the Legendre expansion in Eq. 6.2.1. From these coefficients a potential surface was generated.

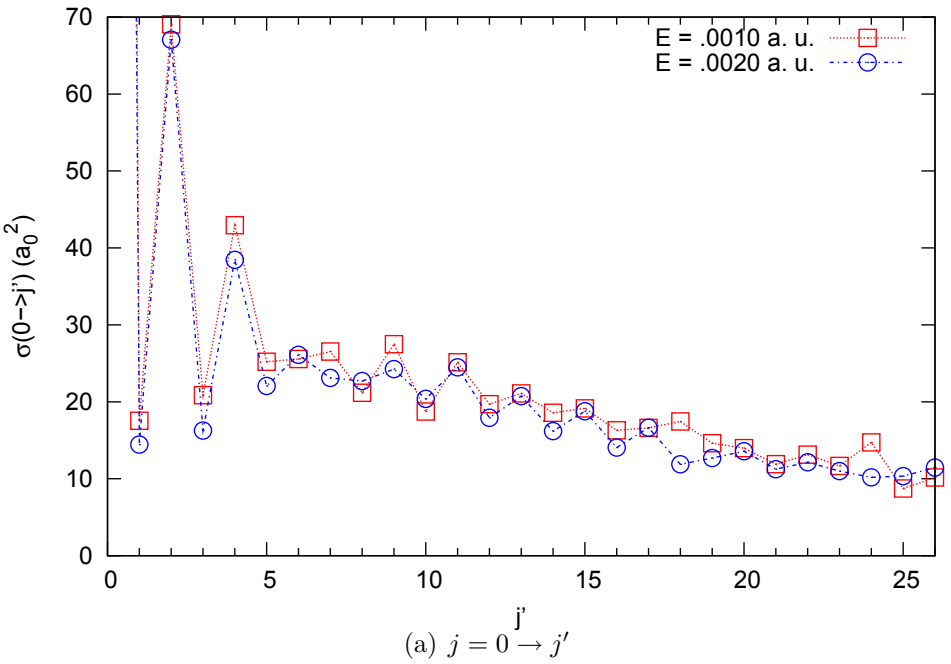


(a) $j = 0 \rightarrow j'$

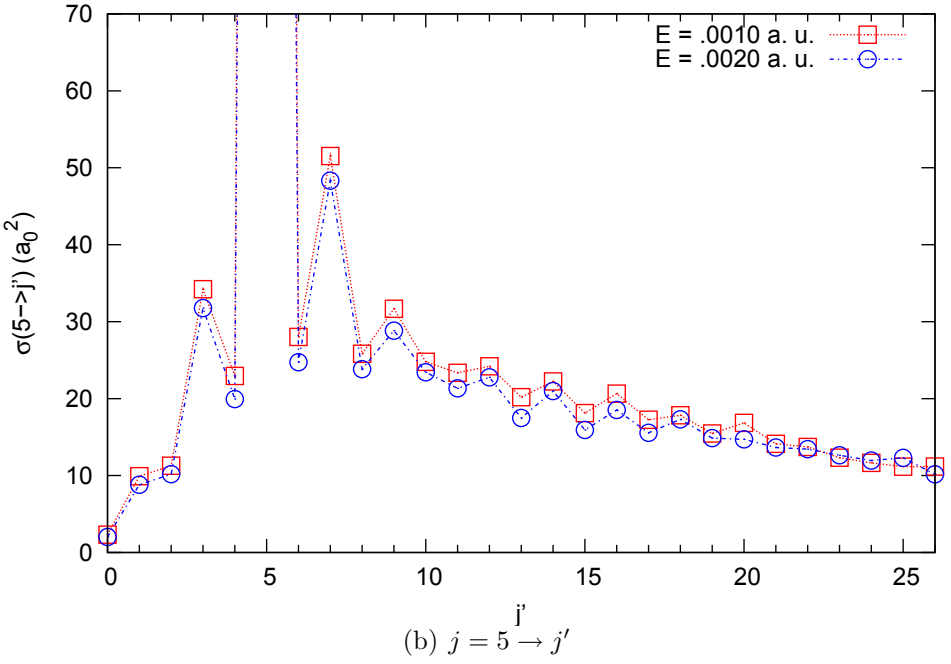


(b) $j = 5 \rightarrow j'$

**Figure 6.2:** Preliminary calculated cross sections for $\mathrm{He} + \mathrm{NaK}(A^1\Sigma^+, v = 15)$ for $E = 0.0010$ and $0.0020$ $\mathrm{E_h}$ using the vibrationally averaged potential. The initial level is $j = 0$ and 5 in panels (a) and (b), respectively. In both cases, the $\Delta j = 2$ cross section is larger than the $\Delta j = 1$ cross section and the $\Delta j = 4$ cross section is larger than the $\Delta j = 3$ cross section. This propensity for even $\Delta j$ is similar to that seen experimentally.

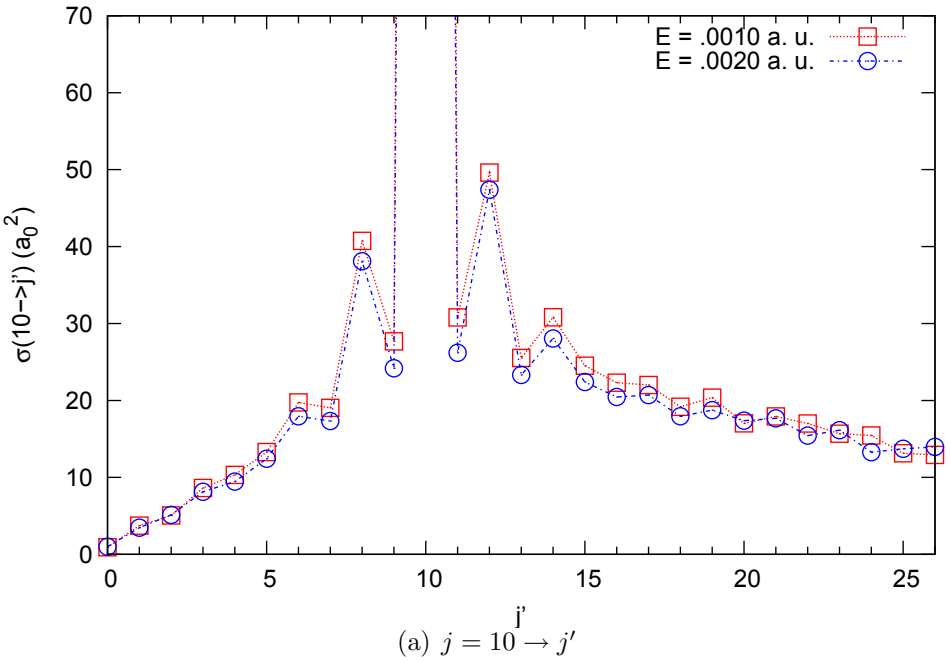


(a) $j = 10 \rightarrow j'$

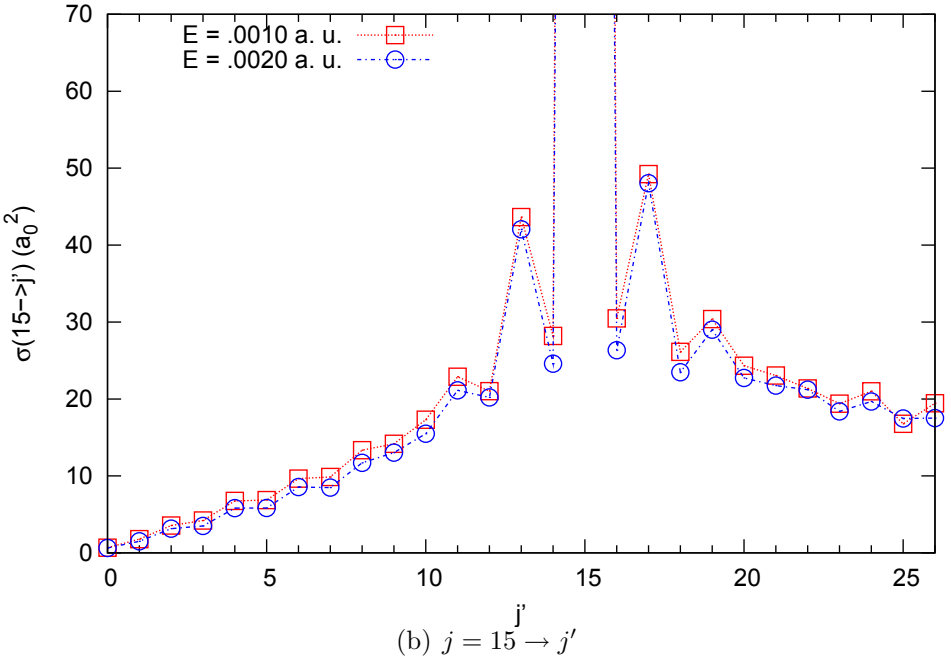


(b) $j = 15 \rightarrow j'$

**Figure 6.3:** Preliminary calculated cross sections for $\mathrm{He} + \mathrm{NaK}(A^1\Sigma^+, v = 15)$ for $E = 0.00010$ and $0.0020$ $\mathrm{E_h}$ using the vibrationally averaged potential. The initial level is $j = 10$ and 15 in panels (a) and (b), respectively. In both cases, the $\Delta j = 2$ cross section is larger than the $\Delta j = 1$ cross section and the $\Delta j = 4$ cross section is larger than the $\Delta j = 3$ cross section. This propensity for even $\Delta j$ is similar to that seen experimentally.

Preliminary scattering calculations have been performed using the vibrationally dependent $A^1\Sigma^+$, $v = 15$ potential for energies at 0.0010 and 0.0020 $E_h$. The expansion was truncated because at the time only the first eleven terms of the 21 term expansion were available. The values of $j$ range from 0 to $j_{max} = 30$. Figures 6.2 and 6.3 show the cross sections for collisions of He with NaK ($A^1\Sigma^+$, $v = 15$) for $j = 0$, 5, 10 and 15 as a function of $j'$. In both energy cases, the $\Delta j = 2$ cross section is larger than the $\Delta j = 1$ cross section and the the $\Delta j = 4$ cross section is larger than the $\Delta j = 3$ cross section. The $v = 15$ vibrational state clearly shows a propensity for even $\Delta j$ transitions that was not present in the $v = 0$ vibrational state. The theory predicts that the vibrational level of the target will have a large effect on the change in $j$ during collision.

By using the cross sections calculated for NaK($A^1\Sigma^+, v = 15$) to estimate rate constants as discussed in Section 4.2.4, the results can be compared to the experimental results for NaK($A^1\Sigma^+, v = 16$). Table 6.1 shows a comparison of rate constants measured experimentally and estimated from the cross sections obtained with coupled channel calculations. Figure 6.4 shows the comparison graphically. Both the experimental results and theoretical calculations show a clear propensity for even $\Delta j$ transitions, for both positive and negative $\Delta j$. This propensity was not present in calculations for NaK($A^1\Sigma^+$, $v = 0$), suggesting that $j$ changing transitions have a strong dependence on the vibrational state.

**Table 6.1:** Comparison of the experimental and calculated rate constants for $He + NaK(A^1\Sigma^+)$ transitions from the $j = 14$ level. The vibrational state of NaK used for the experiments was $v = 16$. The calculations were performed for NaK $v = 15$. Panel (a) shows the positive $\Delta j$ rate constants and Panel (b) shows rate constants for negative $\Delta j$.

(a) Positive $\Delta j$

| $j'$ | $k(10^{-10}$ cm$^3$·s$^{-1})$ Experimental | Theoretical |
|---|---|---|
| 13 | 0.163 | 1.08 |
| 12 | 2.12 | 1.89 |
| 11 | 0.199 | 0.850 |
| 10 | 0.920 | 0.935 |

(b) Negative $\Delta j$

| $j'$ | $k(10^{-10}$ cm$^3$·s$^{-1})$ Experimental | Theoretical |
|---|---|---|
| 15 | 0.285 | 1.19 |
| 16 | 2.24 | 2.18 |
| 17 | 0.134 | 1.08 |
| 18 | 1.46 | 1.31 |

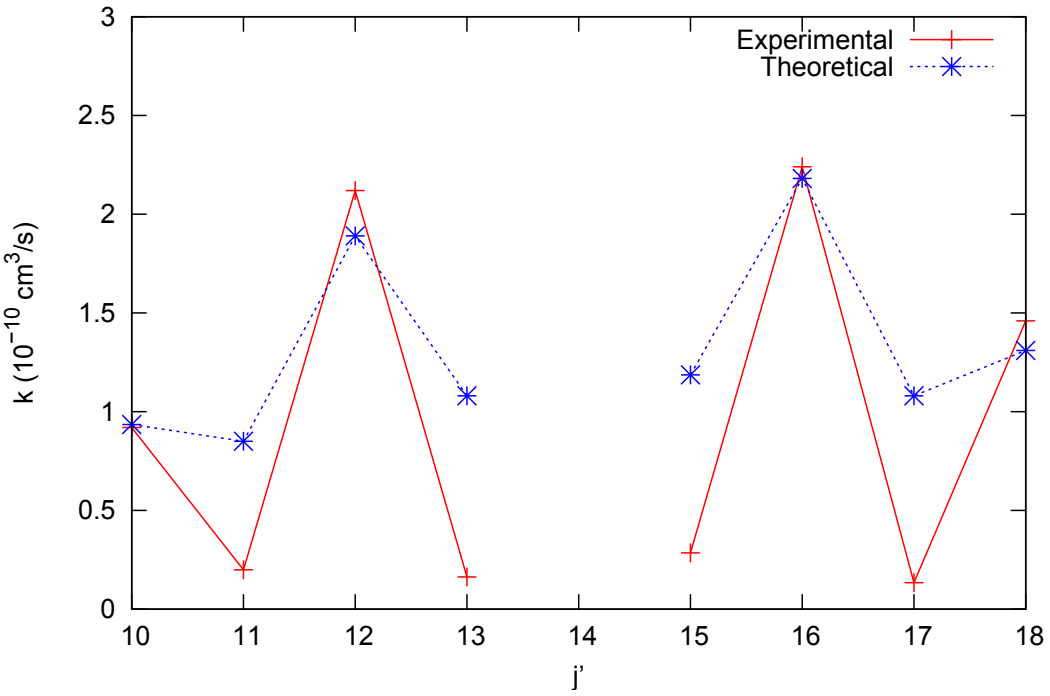


**Figure 6.4:** Comparison of rate constants for $He + NaK(A^1\Sigma^+)$ measured experimentally and calculated theoretically. The vibrational state of NaK used for the experiments was $v = 16$. The calculations were performed for NaK $v = 15$. There is a clear propensity for $\Delta j$ even transitions in both the experimental data and the theoretical calculations.

The probability that the orientation will be preserved in a collision that changes $j$ to $j'$ is shown in Fig. 6.5 as a function of the average of $j$ and $j'$, $\overline{j} = (j + j')/2$, for several different values of $\Delta j = j' - j$. (This probability depends only on the absolute values of $\Delta j$.) There is a $\Delta j$ even propensity observed in the probability of orientation preservation, which can be seen as the probability of orientation transfer of $\Delta j = 2$ is larger than that of $\Delta j = 1$. The same trend is observed for $\Delta j = 4$ and 3. This propensity was not observed in the $v = 0$ probability of preserving orientation. Note that because we are looking at the fraction of orientation transferred during a collision, the $\Delta j$ even propensity of population transfer does not necessarily affect the orientation transfer probability. Figure 6.6 shows the probability that the alignment will be preserved as a function of the average of $\overline{j}$. Again, the probability is shown for several different values of $\Delta j = j' - j$ and is independent of the sign of $\Delta j$. The same even $\Delta j$ propensity is observed in the probability of preservation of alignment.

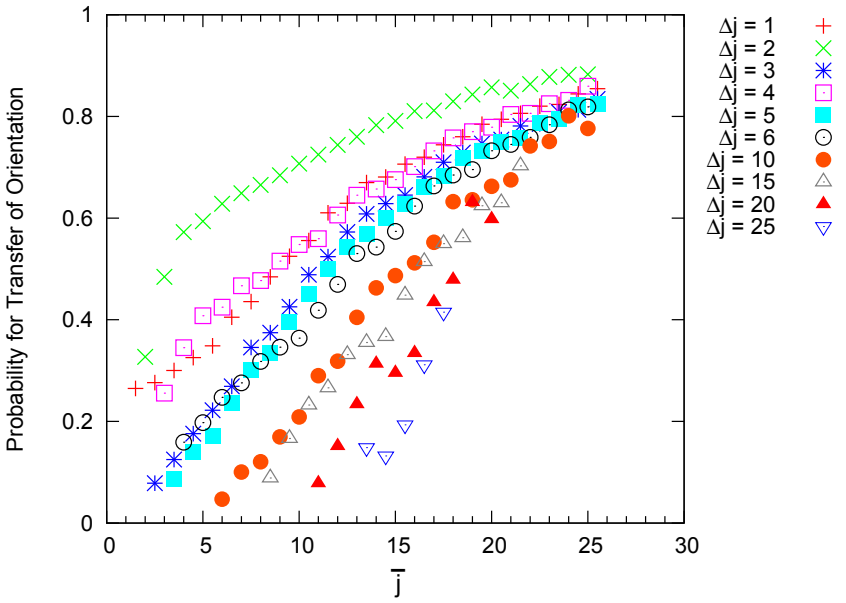


(a) $E = 0.0010$ $E_h$

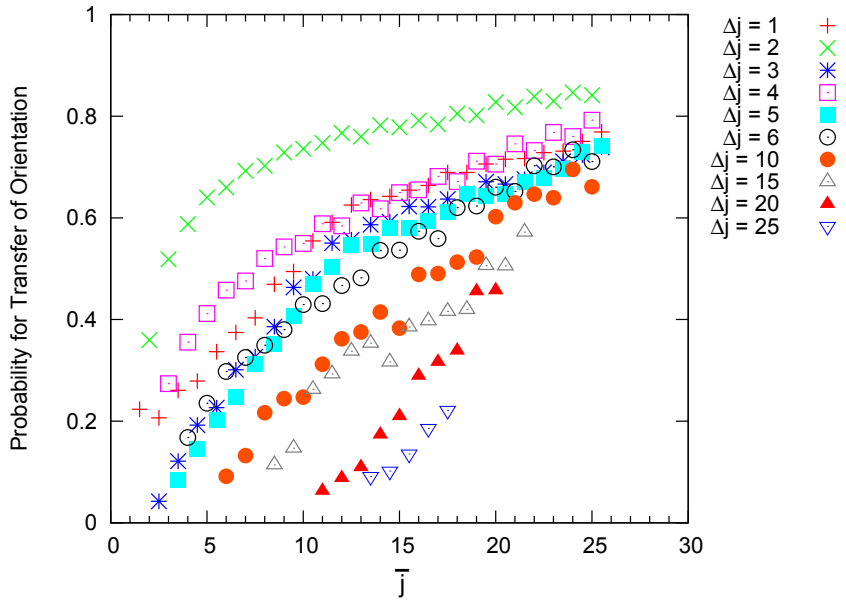


(b) $E = 0.0020$ $E_h$

**Figure 6.5:** Probability that orientation will be transferred during a collision of He with NaK($A^1\Sigma^+$, $v = 15$) as a function of the average value of $j$ and $j'$, $\bar{j} = (j + j')/2$. Each series corresponds to a specific $\Delta j = j - j'$. The probability is independent of the sign of $\Delta j$. Panels (a) and (b) show calculations for total energy $E = 0.0010$ and $0.0020$ $E_h$, respectively. The probability of orientation transfer of $\Delta j = 2$ is larger than that of $\Delta j = 1$, and a similar trend is seen for $\Delta j = 4$ and 3.

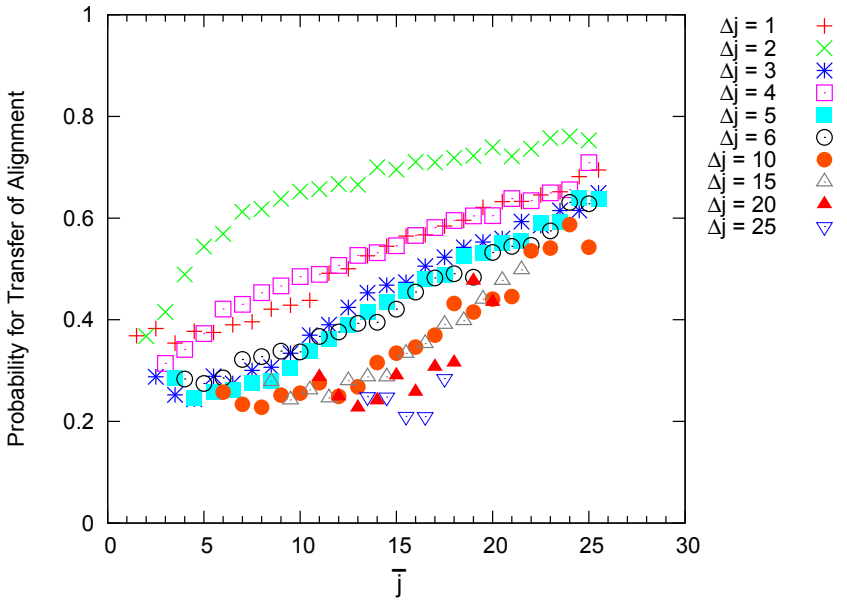


(a) $E = 0.0010$ $E_h$

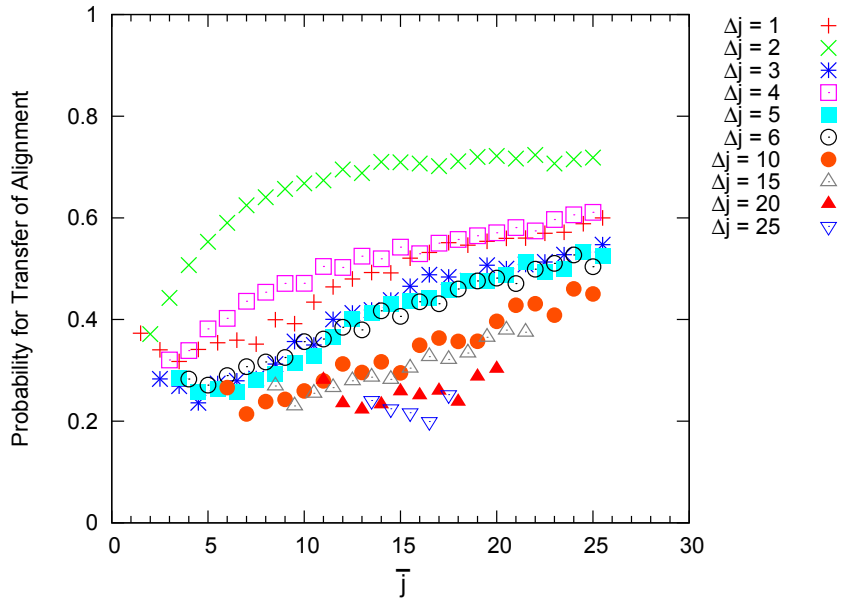


(b) $E = 0.0020$ $E_h$

**Figure 6.6:** Probability that alignment will be transferred during a collision of He with NaK($A^1\Sigma^+$, $v = 15$) as a function of the average value of $j$ and $j'$, $\bar{j} = (j + j')/2$. Each series corresponds to a specific $\Delta j = j - j'$. The probability is independent of the sign of $\Delta j$. Panels (a) and (b) show calculations for total energy $E = 0.0010$ and $0.0020$ $E_h$, respectively. The probability of alignment transfer of $\Delta j = 2$ is larger than that of $\Delta j = 1$. The same is true fo the probability of alignment transfer for $\Delta j = 4$ and 3.

## 6.3 Future Work

The results of these calculations show that the propensity for transitions with even $\Delta j$ in collisions of He with NaK may be strongly dependent on the vibrational state of the NaK target. Further scattering calculations with the potentials adjusted to include vibrational state dependences will be performed to compare directly with experimental data. A great deal has been learned about the procedures for determining potentials and conducting scattering calculations that will be valuable as this project continues.

Once calculations have been completed for the He + NaK system, they can be used as a model for calculations of other alkali perturbers. New GAMESS calculations will have to be conducted for NaK collisions with any other collisional partner. The next perturber to be investigated will likely be Ar for comparison with the readily available experimental data. Dr. Huennekens' group also hopes to investigate NaK collisions with Xe, so this is another likely candidate for calculations. The potentials will be fit with the methods described above and scattering calculations will be performed to compare with experimental results.

# Appendix A

# Ground State Potential

**Table A.1:** $He + NaK(X^1\Sigma^+)$ potential calculations

| $R_d$ | $\theta$ | Energy | $R_d$ | $\theta$ | Energy |
|---|---|---|---|---|---|
| 4.00 | 0 | −762.863357255 | 4.00 | 130 | −764.181476326 |
| 4.00 | 5 | −762.915744606 | 4.00 | 135 | −764.171088962 |
| 4.00 | 10 | −763.056251303 | 4.00 | 140 | −764.148404876 |
| 4.00 | 15 | −763.247863322 | 4.00 | 145 | −764.096413833 |
| 4.00 | 20 | −763.453660256 | 4.00 | 150 | −763.975854233 |
| 4.00 | 25 | −763.646036556 | 4.00 | 155 | −763.697365728 |
| 4.00 | 30 | −763.808360211 | 4.00 | 160 | −763.069925422 |
| 4.00 | 35 | −763.934563027 | 4.00 | 165 | −761.796840498 |
| 4.00 | 40 | −764.026584975 | 4.00 | 170 | −758.891280455 |
| 4.00 | 45 | −764.090451838 | 4.00 | 175 | −744.549167492 |
| 4.00 | 50 | −764.133094893 | 4.00 | 180 | −744.549167492 |
| 4.00 | 55 | −764.160668518 | 4.50 | 50 | −764.178834414 |
| 4.00 | 60 | −764.177981760 | 4.50 | 55 | −764.190440570 |
| 4.00 | 65 | −764.188511986 | 4.50 | 60 | −764.197507264 |
| 4.00 | 70 | −764.194647826 | 4.50 | 65 | −764.201594345 |
| 4.00 | 75 | −764.197973507 | 4.50 | 70 | −764.203772554 |
| 4.00 | 80 | −764.199512925 | 4.50 | 75 | −764.204745165 |
| 4.00 | 85 | −764.199913001 | 4.50 | 80 | −764.204955783 |
| 4.00 | 90 | −764.199573524 | 4.50 | 85 | −764.204673333 |
| 4.00 | 95 | −764.198736580 | 4.50 | 90 | −764.204054361 |
| 4.00 | 100 | −764.197546176 | 5.00 | 0 | −763.985205681 |
| 4.00 | 105 | −764.196084644 | 5.00 | 5 | −763.993304943 |
| 4.00 | 110 | −764.194387094 | 5.00 | 10 | −764.015670557 |
| 4.00 | 115 | −764.192426839 | 5.00 | 15 | −764.047342809 |
| 4.00 | 120 | −764.190049692 | 5.00 | 20 | −764.082305780 |
| 4.00 | 125 | −764.186798702 | 5.00 | 25 | −764.115434444 |

He + NaK($X^1\Sigma^+$) potential calculations continued

| $R_d$ | $\theta$ | Energy | $R_d$ | $\theta$ | Energy |
|---|---|---|---|---|---|
| 5.00 | 30 | −764.143547080 | 5.50 | 75 | −764.210898367 |
| 5.00 | 35 | −764.165448805 | 5.50 | 80 | −764.210686177 |
| 5.00 | 40 | −764.181373922 | 5.50 | 85 | −764.210369280 |
| 5.00 | 45 | −764.192300168 | 5.50 | 90 | −764.209955535 |
| 5.00 | 50 | −764.199417019 | 5.50 | 95 | −764.209441709 |
| 5.00 | 55 | −764.203820599 | 5.50 | 100 | −764.208818855 |
| 5.00 | 60 | −764.206388770 | 5.50 | 105 | −764.208076330 |
| 5.00 | 65 | −764.207762598 | 5.50 | 110 | −764.207204460 |
| 5.00 | 70 | −764.208378026 | 5.50 | 115 | −764.206194432 |
| 5.00 | 75 | −764.208514072 | 5.50 | 120 | −764.205031347 |
| 5.00 | 80 | −764.208339267 | 5.50 | 125 | −764.203668861 |
| 5.00 | 85 | −764.207948767 | 5.50 | 130 | −764.201955949 |
| 5.00 | 90 | −764.207391250 | 6.00 | 0 | −764.185051355 |
| 5.00 | 95 | −764.206687601 | 6.00 | 5 | −764.186031120 |
| 5.00 | 100 | −764.205843635 | 6.00 | 10 | −764.188753844 |
| 5.00 | 105 | −764.204858300 | 6.00 | 15 | −764.192653076 |
| 5.00 | 110 | −764.203727476 | 6.00 | 20 | −764.197016853 |
| 5.00 | 115 | −764.202440762 | 6.00 | 25 | −764.201206664 |
| 5.00 | 120 | −764.200962091 | 6.00 | 30 | −764.204796074 |
| 5.00 | 125 | −764.199170184 | 6.00 | 35 | −764.207599971 |
| 5.00 | 130 | −764.196701421 | 6.00 | 40 | −764.209624410 |
| 5.00 | 135 | −764.192541497 | 6.00 | 45 | −764.210986276 |
| 5.00 | 140 | −764.183963199 | 6.00 | 50 | −764.211840916 |
| 5.00 | 145 | −764.163931392 | 6.00 | 55 | −764.212335151 |
| 5.00 | 150 | −764.115212079 | 6.00 | 60 | −764.212585847 |
| 5.00 | 155 | −763.997989614 | 6.00 | 65 | −764.212675834 |
| 5.00 | 160 | −763.727174796 | 6.00 | 70 | −764.212658265 |
| 5.00 | 165 | −763.153403414 | 6.00 | 75 | −764.212563484 |
| 5.00 | 170 | −762.164728242 | 6.00 | 80 | −764.212405538 |
| 5.00 | 175 | −760.956167518 | 6.00 | 85 | −764.212187407 |
| 5.00 | 180 | −760.223645687 | 6.00 | 90 | −764.211904740 |
| 5.50 | 35 | −764.195758603 | 6.00 | 95 | −764.211548376 |
| 5.50 | 40 | −764.201610161 | 6.00 | 100 | −764.211106150 |
| 5.50 | 45 | −764.205586734 | 6.00 | 105 | −764.210564665 |
| 5.50 | 50 | −764.208127791 | 6.00 | 110 | −764.209911332 |
| 5.50 | 55 | −764.209648862 | 6.00 | 115 | −764.209135993 |
| 5.50 | 60 | −764.210484008 | 6.00 | 120 | −764.208229954 |
| 5.50 | 65 | −764.210874208 | 6.00 | 125 | −764.207177768 |
| 5.50 | 70 | −764.210979480 | 6.00 | 130 | −764.205929110 |

He + NaK($X^1\Sigma^+$) potential calculations continued

| $R_d$ | $\theta$ | Energy | $R_d$ | $\theta$ | Energy |
|---|---|---|---|---|---|
| 6.00 | 135 | −764.204319931 | 6.25 | 145 | −764.201254501 |
| 6.00 | 140 | −764.201880236 | 6.25 | 150 | −764.195223492 |
| 6.00 | 145 | −764.197389359 | 6.25 | 155 | −764.182787341 |
| 6.00 | 150 | −764.187937851 | 6.25 | 160 | −764.158289744 |
| 6.00 | 155 | −764.167431004 | 6.25 | 165 | −764.115903703 |
| 6.00 | 160 | −764.125477356 | 6.25 | 170 | −764.056814819 |
| 6.00 | 165 | −764.050141763 | 6.25 | 175 | −763.999064376 |
| 6.00 | 170 | −763.940799328 | 6.25 | 180 | −763.974112347 |
| 6.00 | 175 | −763.829880914 | 6.50 | 0 | −764.204653750 |
| 6.00 | 180 | −763.780856056 | 6.50 | 5 | −764.204974883 |
| 6.25 | 0 | −764.197354878 | 6.50 | 10 | −764.205869869 |
| 6.25 | 5 | −764.197918057 | 6.50 | 15 | −764.207157865 |
| 6.25 | 10 | −764.199485276 | 6.50 | 20 | −764.208607566 |
| 6.25 | 15 | −764.201734906 | 6.50 | 25 | −764.210007306 |
| 6.25 | 20 | −764.204259065 | 6.50 | 30 | −764.211212586 |
| 6.25 | 25 | −764.206688095 | 6.50 | 35 | −764.212158446 |
| 6.25 | 30 | −764.208772369 | 6.50 | 40 | −764.212844253 |
| 6.25 | 35 | −764.210401874 | 6.50 | 45 | −764.213307159 |
| 6.25 | 40 | −764.211578426 | 6.50 | 50 | −764.213597744 |
| 6.25 | 45 | −764.212368966 | 6.50 | 55 | −764.213764021 |
| 6.25 | 50 | −764.212863105 | 6.50 | 60 | −764.213843875 |
| 6.25 | 55 | −764.213145580 | 6.50 | 65 | −764.213863295 |
| 6.25 | 60 | −764.213283587 | 6.50 | 70 | −764.213837639 |
| 6.25 | 65 | −764.213324168 | 6.50 | 75 | −764.213773994 |
| 6.25 | 70 | −764.213296572 | 6.50 | 80 | −764.213673492 |
| 6.25 | 75 | −764.213216245 | 6.50 | 85 | −764.213533111 |
| 6.25 | 80 | −764.213088754 | 6.50 | 90 | −764.213346775 |
| 6.25 | 85 | −764.212912884 | 6.50 | 95 | −764.213105933 |
| 6.25 | 90 | −764.212682765 | 6.50 | 100 | −764.212799820 |
| 6.25 | 95 | −764.212389142 | 6.50 | 105 | −764.212415861 |
| 6.25 | 100 | −764.212020245 | 6.50 | 110 | −764.211940724 |
| 6.25 | 105 | −764.211562766 | 6.50 | 115 | −764.211362258 |
| 6.25 | 110 | −764.211003461 | 6.50 | 120 | −764.210671389 |
| 6.25 | 115 | −764.210331112 | 6.50 | 125 | −764.209861461 |
| 6.25 | 120 | −764.209537299 | 6.50 | 130 | −764.208920087 |
| 6.25 | 125 | −764.208612697 | 6.50 | 135 | −764.207801292 |
| 6.25 | 130 | −764.207531183 | 6.50 | 140 | −764.206353094 |
| 6.25 | 135 | −764.206201794 | 6.50 | 145 | −764.204163992 |
| 6.25 | 140 | −764.204349618 | 6.50 | 150 | −764.200276309 |

He + NaK($X^1\Sigma^+$) potential calculations continued

| $R_d$ | $\theta$ | Energy | $R_d$ | $\theta$ | Energy |
|---|---|---|---|---|---|
| 6.50 | 155 | −764.192773102 | 6.75 | 165 | −764.178155883 |
| 6.50 | 160 | −764.178648983 | 6.75 | 170 | −764.161237251 |
| 6.50 | 165 | −764.155104382 | 6.75 | 175 | −764.145615847 |
| 6.50 | 170 | −764.123413644 | 6.75 | 180 | −764.139090318 |
| 6.50 | 175 | −764.093375909 | 7.00 | 0 | −764.211544553 |
| 6.50 | 180 | −764.080636271 | 7.00 | 5 | −764.211647602 |
| 6.75 | 0 | −764.208973415 | 7.00 | 10 | −764.211936243 |
| 6.75 | 5 | −764.209155480 | 7.00 | 15 | −764.212355494 |
| 6.75 | 10 | −764.209663908 | 7.00 | 20 | −764.212833379 |
| 6.75 | 15 | −764.210398267 | 7.00 | 25 | −764.213302117 |
| 6.75 | 20 | −764.211228837 | 7.00 | 30 | −764.213713653 |
| 6.75 | 25 | −764.212035502 | 7.00 | 35 | −764.214044598 |
| 6.75 | 30 | −764.212735001 | 7.00 | 40 | −764.214292220 |
| 6.75 | 35 | −764.213288688 | 7.00 | 45 | −764.214466383 |
| 6.75 | 40 | −764.213694520 | 7.00 | 50 | −764.214581784 |
| 6.75 | 45 | −764.213972303 | 7.00 | 55 | −764.214652601 |
| 6.75 | 50 | −764.214149865 | 7.00 | 60 | −764.214689791 |
| 6.75 | 55 | −764.214253790 | 7.00 | 65 | −764.214700345 |
| 6.75 | 60 | −764.214304864 | 7.00 | 70 | −764.214687617 |
| 6.75 | 65 | −764.214316909 | 7.00 | 75 | −764.214652059 |
| 6.75 | 70 | −764.214297473 | 7.00 | 80 | −764.214591929 |
| 6.75 | 75 | −764.214249196 | 7.00 | 85 | −764.214503777 |
| 6.75 | 80 | −764.214171135 | 7.00 | 90 | −764.214382684 |
| 6.75 | 85 | −764.214059729 | 7.00 | 95 | −764.214222240 |
| 6.75 | 90 | −764.213909350 | 7.00 | 100 | −764.214014320 |
| 6.75 | 95 | −764.213712477 | 7.00 | 105 | −764.213748817 |
| 6.75 | 100 | −764.213459640 | 7.00 | 110 | −764.213413746 |
| 6.75 | 105 | −764.213139397 | 7.00 | 115 | −764.212996352 |
| 6.75 | 110 | −764.212738872 | 7.00 | 120 | −764.212485537 |
| 6.75 | 115 | −764.212245357 | 7.00 | 125 | −764.211874512 |
| 6.75 | 120 | −764.211648731 | 7.00 | 130 | −764.211160740 |
| 6.75 | 125 | −764.210942871 | 7.00 | 135 | −764.210338337 |
| 6.75 | 130 | −764.210122399 | 7.00 | 140 | −764.209373857 |
| 6.75 | 135 | −764.209167437 | 7.00 | 145 | −764.208152891 |
| 6.75 | 140 | −764.208000921 | 7.00 | 150 | −764.206394006 |
| 6.75 | 145 | −764.206397846 | 7.00 | 155 | −764.203554935 |
| 6.75 | 150 | −764.203830286 | 7.00 | 160 | −764.198848183 |
| 6.75 | 155 | −764.199266631 | 7.00 | 165 | −764.191668978 |
| 6.75 | 160 | −764.191148409 | 7.00 | 170 | −764.182635530 |

He + NaK($X^1\Sigma^+$) potential calculations continued

| $R_d$ | $\theta$ | Energy | $R_d$ | $\theta$ | Energy |
|---|---|---|---|---|---|
| 7.00 | 175 | −764.174495438 | 7.50 | 0 | −764.214070329 |
| 7.00 | 180 | −764.171139933 | 7.50 | 5 | −764.214103927 |
| 7.25 | 0 | −764.213100748 | 7.50 | 10 | −764.214199106 |
| 7.25 | 5 | −764.213159289 | 7.50 | 15 | −764.214340346 |
| 7.25 | 10 | −764.213324012 | 7.50 | 20 | −764.214506281 |
| 7.25 | 15 | −764.213565341 | 7.50 | 25 | −764.214675518 |
| 7.25 | 20 | −764.213843775 | 7.50 | 30 | −764.214831595 |
| 7.25 | 25 | −764.214121197 | 7.50 | 35 | −764.214965065 |
| 7.25 | 30 | −764.214369674 | 7.50 | 40 | −764.215072782 |
| 7.25 | 35 | −764.214574653 | 7.50 | 45 | −764.215155744 |
| 7.25 | 40 | −764.214733107 | 7.50 | 50 | −764.215216864 |
| 7.25 | 45 | −764.214849235 | 7.50 | 55 | −764.215259327 |
| 7.25 | 50 | −764.214930194 | 7.50 | 60 | −764.215285619 |
| 7.25 | 55 | −764.214983085 | 7.50 | 65 | −764.215297128 |
| 7.25 | 60 | −764.215013367 | 7.50 | 70 | −764.215294076 |
| 7.25 | 65 | −764.215024335 | 7.50 | 75 | −764.215275654 |
| 7.25 | 70 | −764.215017218 | 7.50 | 80 | −764.215240164 |
| 7.25 | 75 | −764.214991515 | 7.50 | 85 | −764.215185084 |
| 7.25 | 80 | −764.214945344 | 7.50 | 90 | −764.215107023 |
| 7.25 | 85 | −764.214875665 | 7.50 | 95 | −764.215001560 |
| 7.25 | 90 | −764.214778336 | 7.50 | 100 | −764.214862935 |
| 7.25 | 95 | −764.214647999 | 7.50 | 105 | −764.214683658 |
| 7.25 | 100 | −764.214477792 | 7.50 | 110 | −764.214454187 |
| 7.25 | 105 | −764.214258966 | 7.50 | 115 | −764.214163160 |
| 7.25 | 110 | −764.213980699 | 7.50 | 120 | −764.213798901 |
| 7.25 | 115 | −764.213630722 | 7.50 | 125 | −764.213352438 |
| 7.25 | 120 | −764.213197362 | 7.50 | 130 | −764.212820623 |
| 7.25 | 125 | −764.212672689 | 7.50 | 135 | −764.212206286 |
| 7.25 | 130 | −764.212054523 | 7.50 | 140 | −764.211511649 |
| 7.25 | 135 | −764.211343551 | 7.50 | 145 | −764.210720909 |
| 7.25 | 140 | −764.210530166 | 7.50 | 150 | −764.209771516 |
| 7.25 | 145 | −764.209563634 | 7.50 | 155 | −764.208529786 |
| 7.25 | 150 | −764.208302705 | 7.50 | 160 | −764.206812175 |
| 7.25 | 155 | −764.206470390 | 7.50 | 165 | −764.204513900 |
| 7.25 | 160 | −764.203679505 | 7.50 | 170 | −764.201863418 |
| 7.25 | 165 | −764.199666643 | 7.50 | 175 | −764.199601218 |
| 7.25 | 170 | −764.194811506 | 7.50 | 180 | −764.198693262 |
| 7.25 | 175 | −764.190544953 | 7.75 | 0 | −764.214699191 |
| 7.25 | 180 | −764.188808428 | 7.75 | 5 | −764.214718842 |

He + NaK($X^1\Sigma^+$) potential calculations continued

| $R_d$ | $\theta$ | Energy | $R_d$ | $\theta$ | Energy |
|---|---|---|---|---|---|
| 7.75 | 10 | −764.214775053 | 8.00 | 75 | −764.215706937 |
| 7.75 | 15 | −764.214859991 | 8.00 | 90 | −764.215601514 |
| 7.75 | 20 | −764.214962333 | 8.00 | 105 | −764.215325395 |
| 7.75 | 25 | −764.215070078 | 8.00 | 120 | −764.214725079 |
| 7.75 | 35 | −764.215265433 | 8.00 | 135 | −764.213575663 |
| 7.75 | 40 | −764.215343391 | 8.00 | 150 | −764.211887047 |
| 7.75 | 45 | −764.215406426 | 8.00 | 165 | −764.209583140 |
| 7.75 | 50 | −764.215455169 | 8.00 | 180 | −764.207758656 |
| 7.75 | 55 | −764.215490728 | 8.25 | 0 | −764.215432861 |
| 7.75 | 60 | −764.215514053 | 8.25 | 15 | −764.215497353 |
| 7.75 | 65 | −764.215525580 | 8.25 | 30 | −764.215646717 |
| 7.75 | 70 | −764.215525121 | 8.25 | 45 | −764.215785976 |
| 7.75 | 75 | −764.215511878 | 8.25 | 60 | −764.215862945 |
| 7.75 | 80 | −764.215484474 | 8.25 | 75 | −764.215866949 |
| 7.75 | 85 | −764.215440919 | 8.25 | 90 | −764.215783763 |
| 7.75 | 90 | −764.215378504 | 8.25 | 105 | −764.215563296 |
| 7.75 | 95 | −764.215293598 | 8.25 | 120 | −764.215074139 |
| 7.75 | 100 | −764.215181369 | 8.25 | 135 | −764.214110783 |
| 7.75 | 105 | −764.215035424 | 8.25 | 150 | −764.212676127 |
| 7.75 | 110 | −764.214847476 | 8.25 | 165 | −764.210992999 |
| 7.75 | 115 | −764.214607336 | 8.25 | 180 | −764.209891650 |
| 7.75 | 120 | −764.214303894 | 8.50 | 0 | −764.215661542 |
| 7.75 | 125 | −764.213927603 | 8.50 | 15 | −764.215705853 |
| 7.75 | 130 | −764.213473888 | 8.50 | 30 | −764.215816921 |
| 7.75 | 135 | −764.212945189 | 8.50 | 45 | −764.215928800 |
| 7.75 | 140 | −764.212348494 | 8.50 | 60 | −764.215993216 |
| 7.75 | 145 | −764.211685785 | 8.50 | 75 | −764.215997383 |
| 7.75 | 150 | −764.210937298 | 8.50 | 90 | −764.215931968 |
| 7.75 | 155 | −764.210046828 | 8.50 | 105 | −764.215757530 |
| 7.75 | 160 | −764.208934193 | 8.50 | 120 | −764.215361659 |
| 7.75 | 165 | −764.207565371 | 8.50 | 135 | −764.214561968 |
| 7.75 | 170 | −764.206077201 | 8.50 | 150 | −764.213340097 |
| 7.75 | 175 | −764.204852302 | 8.50 | 165 | −764.212033990 |
| 7.75 | 180 | −764.204369056 | 8.50 | 180 | −764.211319029 |
| 8.00 | 0 | −764.215127021 | 8.75 | 0 | −764.215838772 |
| 8.00 | 15 | −764.215226372 | 8.75 | 15 | −764.215870915 |
| 8.00 | 30 | −764.215436913 | 8.75 | 30 | −764.215956332 |
| 8.00 | 45 | −764.215613784 | 8.75 | 45 | −764.216046728 |
| 8.00 | 60 | −764.215704756 | 8.75 | 60 | −764.216099676 |

He + NaK($X^1\Sigma^+$) potential calculations continued

| $R_d$ | $\theta$ | Energy | $R_d$ | $\theta$ | Energy |
|---|---|---|---|---|---|
| 8.75 | 75 | −764.216103080 | 9.50 | 75 | −764.216311063 |
| 8.75 | 90 | −764.216051905 | 9.50 | 90 | −764.216287540 |
| 8.75 | 105 | −764.215915292 | 9.50 | 105 | −764.216226468 |
| 8.75 | 120 | −764.215597081 | 9.50 | 120 | −764.216068421 |
| 8.75 | 135 | −764.214939471 | 9.50 | 135 | −764.215720928 |
| 8.75 | 150 | −764.213902368 | 9.50 | 150 | −764.215120159 |
| 8.75 | 165 | −764.212841375 | 9.50 | 165 | −764.214480742 |
| 8.75 | 180 | −764.212337701 | 9.50 | 180 | −764.214222883 |
| 9.00 | 0 | −764.215979618 | 9.75 | 0 | −764.216260352 |
| 9.00 | 15 | −764.216003920 | 9.75 | 15 | −764.216271446 |
| 9.00 | 30 | −764.216070805 | 9.75 | 30 | −764.216302370 |
| 9.00 | 45 | −764.216143436 | 9.75 | 45 | −764.216336013 |
| 9.00 | 60 | −764.216186005 | 9.75 | 60 | −764.216355084 |
| 9.00 | 75 | −764.216188265 | 9.75 | 75 | −764.216354313 |
| 9.00 | 90 | −764.216148495 | 9.75 | 90 | −764.216336331 |
| 9.00 | 105 | −764.216042706 | 9.75 | 105 | −764.216290916 |
| 9.00 | 120 | −764.215788713 | 9.75 | 120 | −764.216167958 |
| 9.00 | 135 | −764.215252725 | 9.75 | 135 | −764.215891424 |
| 9.00 | 150 | −764.214379049 | 9.75 | 150 | −764.215401693 |
| 9.00 | 165 | −764.213491996 | 9.75 | 165 | −764.214860748 |
| 9.00 | 180 | −764.213109086 | 9.75 | 180 | −764.214641257 |
| 9.25 | 0 | −764.216093239 | 9.80 | 0 | −764.216273510 |
| 9.25 | 15 | −764.216112031 | 9.80 | 15 | −764.216283976 |
| 9.25 | 30 | −764.216164552 | 9.80 | 30 | −764.216313115 |
| 9.25 | 45 | −764.216222080 | 9.80 | 45 | −764.216344792 |
| 9.25 | 60 | −764.216255482 | 9.80 | 60 | −764.216362722 |
| 9.25 | 75 | −764.216256567 | 9.80 | 75 | −764.216361806 |
| 9.25 | 90 | −764.216225885 | 9.80 | 90 | −764.216344763 |
| 9.25 | 105 | −764.216144968 | 9.80 | 105 | −764.216302040 |
| 9.25 | 120 | −764.215943763 | 9.80 | 120 | −764.216185257 |
| 9.25 | 135 | −764.215510501 | 9.80 | 135 | −764.215921329 |
| 9.25 | 150 | −764.214781901 | 9.80 | 150 | −764.215451834 |
| 9.25 | 165 | −764.214029835 | 9.80 | 165 | −764.214929246 |
| 9.25 | 180 | −764.213721314 | 9.80 | 180 | −764.214716523 |
| 9.50 | 0 | −764.216185487 | 10.00 | 0 | −764.216320768 |
| 9.50 | 15 | −764.216200053 | 10.00 | 15 | −764.216328902 |
| 9.50 | 30 | −764.216240840 | 10.00 | 30 | −764.216351473 |
| 9.50 | 45 | −764.216285442 | 10.00 | 45 | −764.216376006 |
| 9.50 | 60 | −764.216311003 | 10.00 | 60 | −764.216389865 |

He + NaK($X^1\Sigma^+$) potential calculations continued

| $R_d$ | $\theta$ | Energy | $R_d$ | $\theta$ | Energy |
|---|---|---|---|---|---|
| 10.00 | 75 | −764.216388424 | 10.75 | 75 | −764.216451571 |
| 10.00 | 90 | −764.216374635 | 10.75 | 90 | −764.216444543 |
| 10.00 | 105 | −764.216341419 | 10.75 | 105 | −764.216433274 |
| 10.00 | 120 | −764.216246837 | 10.75 | 120 | −764.216394229 |
| 10.00 | 135 | −764.216028606 | 10.75 | 135 | −764.216293882 |
| 10.00 | 150 | −764.215633699 | 10.75 | 150 | −764.216098652 |
| 10.00 | 165 | −764.215180583 | 10.75 | 165 | −764.215852080 |
| 10.00 | 180 | −764.214992924 | 10.75 | 180 | −764.215741251 |
| 10.25 | 0 | −764.216369063 | 11.00 | 0 | −764.216459778 |
| 10.25 | 15 | −764.216374652 | 11.00 | 15 | −764.216459968 |
| 10.25 | 30 | −764.216390222 | 11.00 | 30 | −764.216461591 |
| 10.25 | 45 | −764.216407361 | 11.00 | 45 | −764.216464936 |
| 10.25 | 60 | −764.216417136 | 11.00 | 60 | −764.216467120 |
| 10.25 | 75 | −764.216415118 | 11.00 | 75 | −764.216463382 |
| 10.25 | 90 | −764.216404411 | 11.00 | 90 | −764.216457323 |
| 10.25 | 105 | −764.216380592 | 11.00 | 105 | −764.216450081 |
| 10.25 | 120 | −764.216308819 | 11.00 | 120 | −764.216422486 |
| 10.25 | 135 | −764.216138246 | 11.00 | 135 | −764.216347506 |
| 10.25 | 150 | −764.215822985 | 11.00 | 150 | −764.216196265 |
| 10.25 | 165 | −764.215448168 | 11.00 | 165 | −764.215999910 |
| 10.25 | 180 | −764.215288612 | 11.00 | 180 | −764.215909795 |
| 10.50 | 0 | −764.216407206 | 11.50 | 0 | −764.216489975 |
| 10.50 | 15 | −764.216410634 | 11.50 | 15 | −764.216488183 |
| 10.50 | 30 | −764.216420452 | 11.50 | 30 | −764.216485038 |
| 10.50 | 45 | −764.216431746 | 11.50 | 45 | −764.216483818 |
| 10.50 | 60 | −764.216438355 | 11.50 | 60 | −764.216482991 |
| 10.50 | 75 | −764.216435790 | 11.50 | 75 | −764.216477967 |
| 10.50 | 90 | −764.216427270 | 11.50 | 90 | −764.216472854 |
| 10.50 | 105 | −764.216410609 | 11.50 | 105 | −764.216470789 |
| 10.50 | 120 | −764.216357071 | 11.50 | 120 | −764.216459240 |
| 10.50 | 135 | −764.216225285 | 11.50 | 135 | −764.216420839 |
| 10.50 | 150 | −764.215975990 | 11.50 | 150 | −764.216333907 |
| 10.50 | 165 | −764.215670032 | 11.50 | 165 | −764.216213633 |
| 10.50 | 180 | −764.215536005 | 11.50 | 180 | −764.216156923 |
| 10.75 | 0 | −764.216436934 | 12.00 | 0 | −764.216506118 |
| 10.75 | 15 | −764.216438569 | 12.00 | 15 | −764.216503226 |
| 10.75 | 30 | −764.216443780 | 12.00 | 30 | −764.216497475 |
| 10.75 | 45 | −764.216450558 | 12.00 | 45 | −764.216493507 |
| 10.75 | 60 | −764.216454705 | 12.00 | 60 | −764.216490346 |

He + NaK($X^1\Sigma^+$) potential calculations continued

| $R_d$ | $\theta$ | Energy | $R_d$ | $\theta$ | Energy |
|---|---|---|---|---|---|
| 12.00 | 75 | −764.216484133 | 13.50 | 75 | −764.216479424 |
| 12.00 | 90 | −764.216479341 | 13.50 | 90 | −764.216475542 |
| 12.00 | 105 | −764.216480048 | 13.50 | 105 | −764.216478626 |
| 12.00 | 120 | −764.216478208 | 13.50 | 120 | −764.216487169 |
| 12.00 | 135 | −764.216462725 | 13.50 | 135 | −764.216497873 |
| 12.00 | 150 | −764.216417211 | 13.50 | 150 | −764.216503160 |
| 12.00 | 165 | −764.216347549 | 13.50 | 165 | −764.216499485 |
| 12.00 | 180 | −764.216314192 | 13.50 | 180 | −764.216497379 |
| 12.50 | 0 | −764.216513520 | 14.00 | 0 | −764.216508660 |
| 12.50 | 15 | −764.216510064 | 14.00 | 15 | −764.216505076 |
| 12.50 | 30 | −764.216502914 | 14.00 | 30 | −764.216497172 |
| 12.50 | 45 | −764.216497133 | 14.00 | 45 | −764.216489303 |
| 12.50 | 60 | −764.216492122 | 14.00 | 60 | −764.216482119 |
| 12.50 | 75 | −764.216485066 | 14.00 | 75 | −764.216475358 |
| 12.50 | 90 | −764.216480472 | 14.00 | 90 | −764.216471995 |
| 12.50 | 105 | −764.216482620 | 14.00 | 105 | −764.216475054 |
| 12.50 | 120 | −764.216486478 | 14.00 | 120 | −764.216484045 |
| 12.50 | 135 | −764.216484857 | 14.00 | 135 | −764.216496742 |
| 12.50 | 150 | −764.216465360 | 14.00 | 150 | −764.216506884 |
| 12.50 | 165 | −764.216428559 | 14.00 | 165 | −764.216510175 |
| 12.50 | 180 | −764.216410685 | 14.00 | 180 | −764.216511319 |
| 13.00 | 0 | −764.216515279 | 14.50 | 0 | −764.216502568 |
| 13.00 | 15 | −764.216511579 | 14.50 | 15 | −764.216499258 |
| 13.00 | 30 | −764.216503724 | 14.50 | 30 | −764.216491839 |
| 13.00 | 45 | −764.216496728 | 14.50 | 45 | −764.216484226 |
| 13.00 | 60 | −764.216490404 | 14.50 | 60 | −764.216477373 |
| 13.00 | 75 | −764.216482991 | 14.50 | 75 | −764.216471391 |
| 13.00 | 90 | −764.216478685 | 14.50 | 90 | −764.216468583 |
| 13.00 | 105 | −764.216481524 | 14.50 | 105 | −764.216471442 |
| 13.00 | 120 | −764.216488540 | 14.50 | 120 | −764.216480180 |
| 13.00 | 135 | −764.216494936 | 14.50 | 135 | −764.216493421 |
| 13.00 | 150 | −764.216491170 | 14.50 | 150 | −764.216505880 |
| 13.00 | 165 | −764.216475072 | 14.50 | 165 | −764.216512745 |
| 13.00 | 180 | −764.216467050 | 14.50 | 180 | −764.216515444 |
| 13.50 | 0 | −764.216513237 | 15.00 | 0 | −764.216495795 |
| 13.50 | 15 | −764.216509511 | 15.00 | 15 | −764.216492837 |
| 13.50 | 30 | −764.216501433 | 15.00 | 30 | −764.216486133 |
| 13.50 | 45 | −764.216493749 | 15.00 | 45 | −764.216479118 |
| 13.50 | 60 | −764.216486709 | 15.00 | 60 | −764.216472923 |

He + NaK($X^1\Sigma^+$) potential calculations continued

| $R_d$ | $\theta$ | Energy | $R_d$ | $\theta$ | Energy |
|---|---|---|---|---|---|
| 15.00 | 75 | −764.216467842 | 16.50 | 75 | −764.216460503 |
| 15.00 | 90 | −764.216465572 | 16.50 | 90 | −764.216459492 |
| 15.00 | 105 | −764.216468128 | 16.50 | 105 | −764.216460979 |
| 15.00 | 120 | −764.216476178 | 16.50 | 120 | −764.216466015 |
| 15.00 | 135 | −764.216489054 | 16.50 | 135 | −764.216475346 |
| 15.00 | 150 | −764.216502332 | 16.50 | 150 | −764.216487004 |
| 15.00 | 165 | −764.216510819 | 16.50 | 165 | −764.216495927 |
| 15.00 | 180 | −764.216514098 | 16.50 | 180 | −764.216499161 |
| 15.50 | 0 | −764.216488981 | 17.00 | 0 | −764.216472005 |
| 15.50 | 15 | −764.216486424 | 17.00 | 15 | −764.216470588 |
| 15.50 | 30 | −764.216480565 | 17.00 | 30 | −764.216467295 |
| 15.50 | 45 | −764.216474368 | 17.00 | 45 | −764.216463806 |
| 15.50 | 60 | −764.216469012 | 17.00 | 60 | −764.216460986 |
| 15.50 | 75 | −764.216464844 | 17.00 | 75 | −764.216459040 |
| 15.50 | 90 | −764.216463064 | 17.00 | 90 | −764.216458304 |
| 15.50 | 105 | −764.216465261 | 17.00 | 105 | −764.216459483 |
| 15.50 | 120 | −764.216472377 | 17.00 | 120 | −764.216463546 |
| 15.50 | 135 | −764.216484338 | 17.00 | 135 | −764.216471449 |
| 15.50 | 150 | −764.216497546 | 17.00 | 150 | −764.216481949 |
| 15.50 | 165 | −764.216506618 | 17.00 | 165 | −764.216490468 |
| 15.50 | 180 | −764.216510007 | 17.00 | 180 | −764.216493600 |
| 16.00 | 0 | −764.216482588 | 17.50 | 0 | −764.216467964 |
| 16.00 | 15 | −764.216480435 | 17.50 | 15 | −764.216466851 |
| 16.00 | 30 | −764.216475468 | 17.50 | 30 | −764.216464265 |
| 16.00 | 45 | −764.216470191 | 17.50 | 45 | −764.216461539 |
| 16.00 | 60 | −764.216465731 | 17.50 | 60 | −764.216459380 |
| 16.00 | 75 | −764.216462413 | 17.50 | 75 | −764.216457940 |
| 16.00 | 90 | −764.216461053 | 17.50 | 90 | −764.216457418 |
| 16.00 | 105 | −764.216462887 | 17.50 | 105 | −764.216458331 |
| 16.00 | 120 | −764.216468964 | 17.50 | 120 | −764.216461531 |
| 16.00 | 135 | −764.216479687 | 17.50 | 135 | −764.216468059 |
| 16.00 | 150 | −764.216492289 | 17.50 | 150 | −764.216477274 |
| 16.00 | 165 | −764.216501424 | 17.50 | 165 | −764.216485224 |
| 16.00 | 180 | −764.216504755 | 17.50 | 180 | −764.216488233 |
| 16.50 | 0 | −764.216476886 | 18.00 | 0 | −764.216464713 |
| 16.50 | 15 | −764.216475119 | 18.00 | 15 | −764.216463857 |
| 16.50 | 30 | −764.216471024 | 18.00 | 30 | −764.216461869 |
| 16.50 | 45 | −764.216466671 | 18.00 | 45 | −764.216459785 |
| 16.50 | 60 | −764.216463075 | 18.00 | 60 | −764.216458170 |

He + NaK($X^1\Sigma^+$) potential calculations continued

| $R_d$ | $\theta$ | Energy | $R_d$ | $\theta$ | Energy |
|---|---|---|---|---|---|
| 18.00 | 75 | −764.216457123 | 19.50 | 75 | −764.216455768 |
| 18.00 | 90 | −764.216456763 | 19.50 | 90 | −764.216455667 |
| 18.00 | 105 | −764.216457456 | 19.50 | 105 | −764.216455951 |
| 18.00 | 120 | −764.216459924 | 19.50 | 120 | −764.216456959 |
| 18.00 | 135 | −764.216465186 | 19.50 | 135 | −764.216459370 |
| 18.00 | 150 | −764.216473067 | 19.50 | 150 | −764.216463581 |
| 18.00 | 165 | −764.216480294 | 19.50 | 165 | −764.216468120 |
| 18.00 | 180 | −764.216483132 | 19.50 | 180 | −764.216470107 |
| 18.50 | 0 | −764.216462157 | 20.00 | 0 | −764.216457629 |
| 18.50 | 15 | −764.216461513 | 20.00 | 15 | −764.216457379 |
| 18.50 | 30 | −764.216460015 | 20.00 | 30 | −764.216456799 |
| 18.50 | 45 | −764.216458458 | 20.00 | 45 | −764.216456210 |
| 18.50 | 60 | −764.216457271 | 20.00 | 60 | −764.216455780 |
| 18.50 | 75 | −764.216456523 | 20.00 | 75 | −764.216455535 |
| 18.50 | 90 | −764.216456282 | 20.00 | 90 | −764.216455473 |
| 18.50 | 105 | −764.216456801 | 20.00 | 105 | −764.216455681 |
| 18.50 | 120 | −764.216458665 | 20.00 | 120 | −764.216456407 |
| 18.50 | 135 | −764.216462811 | 20.00 | 135 | −764.216458191 |
| 18.50 | 150 | −764.216469374 | 20.00 | 150 | −764.216461434 |
| 18.50 | 165 | −764.216475758 | 20.00 | 165 | −764.216465090 |
| 18.50 | 180 | −764.216478366 | 20.00 | 180 | −764.216466737 |
| 19.00 | 0 | −764.216460198 | 21.00 | 0 | −764.216456252 |
| 19.00 | 15 | −764.216459721 | 21.00 | 15 | −764.216456127 |
| 19.00 | 30 | −764.216458613 | 21.00 | 30 | −764.216455842 |
| 19.00 | 45 | −764.216457468 | 21.00 | 45 | −764.216455550 |
| 19.00 | 60 | −764.216456610 | 21.00 | 60 | −764.216455343 |
| 19.00 | 75 | −764.216456087 | 21.00 | 75 | −764.216455231 |
| 19.00 | 90 | −764.216455929 | 21.00 | 90 | −764.216455214 |
| 19.00 | 105 | −764.216456314 | 21.00 | 105 | −764.216455326 |
| 19.00 | 120 | −764.216457695 | 21.00 | 120 | −764.216455693 |
| 19.00 | 135 | −764.216460891 | 21.00 | 135 | −764.216456618 |
| 19.00 | 150 | −764.216466216 | 21.00 | 150 | −764.216458413 |
| 19.00 | 165 | −764.216471684 | 21.00 | 165 | −764.216460580 |
| 19.00 | 180 | −764.216474000 | 21.00 | 180 | −764.216461604 |
| 19.50 | 0 | −764.216458723 | 22.00 | 0 | −764.216455545 |
| 19.50 | 15 | −764.216458375 | 22.00 | 15 | −764.216455486 |
| 19.50 | 30 | −764.216457568 | 22.00 | 30 | −764.216455346 |
| 19.50 | 45 | −764.216456741 | 22.00 | 45 | −764.216455207 |
| 19.50 | 60 | −764.216456130 | 22.00 | 60 | −764.216455108 |

He + NaK($X^1\Sigma^+$) potential calculations continued

| $R_d$ | $\theta$ | Energy | $R_d$ | $\theta$ | Energy |
|---|---|---|---|---|---|
| 22.00 | 75 | −764.216455059 | 25.00 | 75 | −764.216454828 |
| 22.00 | 90 | −764.216455058 | 25.00 | 90 | −764.216454833 |
| 22.00 | 105 | −764.216455121 | 25.00 | 105 | −764.216454850 |
| 22.00 | 120 | −764.216455303 | 25.00 | 120 | −764.216454883 |
| 22.00 | 135 | −764.216455756 | 25.00 | 135 | −764.216454938 |
| 22.00 | 150 | −764.216456670 | 25.00 | 150 | −764.216455031 |
| 22.00 | 165 | −764.216457825 | 25.00 | 165 | −764.216455145 |
| 22.00 | 180 | −764.216458389 | 25.00 | 180 | −764.216455202 |
| 23.00 | 0 | −764.216455187 | 26.00 | 0 | −764.216454837 |
| 23.00 | 15 | −764.216455158 | 26.00 | 15 | −764.216454833 |
| 23.00 | 30 | −764.216455092 | 26.00 | 30 | −764.216454821 |
| 23.00 | 45 | −764.216455023 | 26.00 | 45 | −764.216454807 |
| 23.00 | 60 | −764.216454974 | 26.00 | 60 | −764.216454796 |
| 23.00 | 75 | −764.216454951 | 26.00 | 75 | −764.216454791 |
| 23.00 | 90 | −764.216454956 | 26.00 | 90 | −764.216454795 |
| 23.00 | 105 | −764.216454994 | 26.00 | 105 | −764.216454807 |
| 23.00 | 120 | −764.216455088 | 26.00 | 120 | −764.216454829 |
| 23.00 | 135 | −764.216455305 | 26.00 | 135 | −764.216454862 |
| 23.00 | 150 | −764.216455738 | 26.00 | 150 | −764.216454908 |
| 23.00 | 165 | −764.216456303 | 26.00 | 165 | −764.216454960 |
| 23.00 | 180 | −764.216456584 | 26.00 | 180 | −764.216454985 |
| 24.00 | 0 | −764.216455002 | 27.50 | 0 | −764.216454780 |
| 24.00 | 15 | −764.216454988 | 27.50 | 30 | −764.216454770 |
| 24.00 | 30 | −764.216454954 | 27.50 | 60 | −764.216454755 |
| 24.00 | 45 | −764.216454918 | 27.50 | 90 | −764.216454754 |
| 24.00 | 60 | −764.216454891 | 27.50 | 120 | −764.216454776 |
| 24.00 | 75 | −764.216454879 | 27.50 | 150 | −764.216454815 |
| 24.00 | 90 | −764.216454884 | 27.50 | 180 | −764.216454843 |
| 24.00 | 105 | −764.216454909 | 29.00 | 0 | −764.216454744 |
| 24.00 | 120 | −764.216454962 | 29.00 | 15 | −764.216454742 |
| 24.00 | 135 | −764.216455068 | 29.00 | 30 | −764.216454738 |
| 24.00 | 150 | −764.216455267 | 29.00 | 45 | −764.216454732 |
| 24.00 | 165 | −764.216455524 | 29.00 | 60 | −764.216454727 |
| 24.00 | 180 | −764.216455653 | 29.00 | 75 | −764.216454725 |
| 25.00 | 0 | −764.216454900 | 29.00 | 90 | −764.216454726 |
| 25.00 | 15 | −764.216454892 | 29.00 | 105 | −764.216454732 |
| 25.00 | 30 | −764.216454873 | 29.00 | 120 | −764.216454741 |
| 25.00 | 45 | −764.216454852 | 29.00 | 135 | −764.216454753 |
| 25.00 | 60 | −764.216454836 | 29.00 | 150 | −764.216454765 |

He + NaK($X^1\Sigma^+$) potential calculations continued

| $R_d$ | $\theta$ | Energy | $R_d$ | $\theta$ | Energy |
|---|---|---|---|---|---|
| 29.00 | 165 | −764.216454775 | 40.00 | 90 | −764.216454664 |
| 29.00 | 180 | −764.216454779 | 40.00 | 180 | −764.216454669 |
| 30.00 | 0 | −764.216454727 | 50.00 | 0 | −764.216454657 |
| 30.00 | 15 | −764.216454726 | 50.00 | 90 | −764.216454657 |
| 30.00 | 30 | −764.216454722 | 50.00 | 180 | −764.216454658 |
| 30.00 | 45 | −764.216454717 | 60.00 | 0 | −764.216454655 |
| 30.00 | 60 | −764.216454713 | 60.00 | 90 | −764.216454655 |
| 30.00 | 75 | −764.216454712 | 60.00 | 180 | −764.216454655 |
| 30.00 | 90 | −764.216454713 | 100.00 | 0 | −764.216454654 |
| 30.00 | 105 | −764.216454717 | 100.00 | 90 | −764.216454654 |
| 30.00 | 120 | −764.216454725 | 100.00 | 180 | −764.216454654 |
| 30.00 | 135 | −764.216454734 | 300.00 | 0 | −764.216454654 |
| 30.00 | 150 | −764.216454743 | 300.00 | 90 | −764.216454654 |
| 30.00 | 165 | −764.216454750 | 300.00 | 180 | −764.216454654 |
| 30.00 | 180 | −764.216454752 | 10000.00 | 0 | −764.216454654 |
| 35.00 | 0 | −764.216454682 | 10000.00 | 45 | −764.216454654 |
| 35.00 | 90 | −764.216454677 | 10000.00 | 90 | −764.216454654 |
| 35.00 | 180 | −764.216454690 | 10000.00 | 135 | −764.216454654 |
| 40.00 | 0 | −764.216454667 | 10000.00 | 180 | −764.216454654 |

# Appendix B

# Seven Term Legendre Expansion of the Ground State Potential

**Table B.1:** He + NaK($X^1\Sigma^+$) Legendre Expansion coefficients $v_0, v_1$, and $v_2$

| $R_\mathrm{d}$ | $v_0$ | $v_1$ | $v_2$ |
|---|---|---|---|
| 0.00 | 4.2546600000 | −8.7565900000 | 12.7925000000 |
| 1.00 | 3.3685430000 | −6.9310500000 | 10.1222800000 |
| 2.00 | 2.4824260000 | −5.1055100000 | 7.4520600000 |
| 3.00 | 1.5963090000 | −3.2799700000 | 4.7818400000 |
| 4.00 | 0.7101874723 | −1.4544151303 | 2.1115533583 |
| 4.50 | 0.3168558409 | −0.6442522218 | 0.9269802408 |
| 5.00 | 0.1342293409 | −0.2688913642 | 0.3802575697 |
| 5.50 | 0.0560303155 | −0.1089603343 | 0.1494045265 |
| 6.00 | 0.0231210374 | −0.0418887062 | 0.0551489872 |
| 6.25 | 0.0146197398 | −0.0246214232 | 0.0322165285 |
| 6.75 | 0.0060165669 | −0.0078364166 | 0.0100548006 |
| 7.00 | 0.0041032242 | −0.0045272830 | 0.0055754039 |
| 7.25 | 0.0032180607 | −0.0034999173 | 0.0041122736 |
| 7.50 | 0.0024926299 | −0.0026013419 | 0.0029076899 |
| 7.75 | 0.0019970142 | −0.0021003618 | 0.0022939714 |
| 8.00 | 0.0016193942 | −0.0017556968 | 0.0019123549 |
| 8.25 | 0.0013052755 | −0.0014548700 | 0.0015894526 |
| 8.50 | 0.0010482049 | −0.0012070151 | 0.0013298405 |
| 8.75 | 0.0008365450 | −0.0009997212 | 0.0011133756 |
| 9.00 | 0.0006594645 | −0.0008161861 | 0.0009160599 |
| 9.25 | 0.0005146112 | −0.0006636887 | 0.0007504146 |
| 9.50 | 0.0003964670 | −0.0005366526 | 0.0006104164 |
| 9.75 | 0.0003005701 | −0.0004310128 | 0.0004921665 |
| 10.00 | 0.0002232403 | −0.0003435655 | 0.0003928285 |
| 10.25 | 0.0001613443 | −0.0002716537 | 0.0003099936 |

He + NaK($X^1\Sigma^+$) Legendre Expansion coefficients $v_0, v_1$, and $v_2$ continued

| $R_\mathrm{d}$ | $v_0$ | $v_1$ | $v_2$ |
|---|---|---|---|
| 10.50 | 0.0001122252 | −0.0002129531 | 0.0002415020 |
| 10.75 | 0.0000736137 | −0.0001654425 | 0.0001853485 |
| 11.00 | 0.0000435878 | −0.0001272883 | 0.0001396286 |
| 11.50 | 0.0000030468 | −0.0000728694 | 0.0000728187 |
| 12.00 | −0.0000193298 | −0.0000392500 | 0.0000298911 |
| 12.50 | −0.0000302341 | −0.0000189907 | 0.0000029843 |
| 13.00 | −0.0000340746 | −0.0000070060 | −0.0000131317 |
| 13.50 | −0.0000337410 | −0.0000000473 | −0.0000219623 |
| 14.00 | −0.0000311276 | 0.0000039145 | −0.0000259352 |
| 14.50 | −0.0000274384 | 0.0000060988 | −0.0000267859 |
| 15.00 | −0.0000234280 | 0.0000071978 | −0.0000257256 |
| 15.50 | −0.0000195398 | 0.0000076094 | −0.0000235757 |
| 16.00 | −0.0000160009 | 0.0000075583 | −0.0000209124 |
| 16.50 | −0.0000129154 | 0.0000071855 | −0.0000180622 |
| 17.00 | −0.0000102987 | 0.0000065985 | −0.0000152751 |
| 17.50 | −0.0000081267 | 0.0000058678 | −0.0000126489 |
| 18.00 | −0.0000063580 | 0.0000050634 | −0.0000102730 |
| 18.50 | −0.0000049301 | 0.0000042420 | −0.0000081877 |
| 19.00 | −0.0000037989 | 0.0000034659 | −0.0000063988 |
| 19.50 | −0.0000029097 | 0.0000027566 | −0.0000049021 |
| 20.00 | −0.0000022198 | 0.0000021365 | −0.0000036861 |
| 21.00 | −0.0000012942 | 0.0000012023 | −0.0000019850 |
| 22.00 | −0.0000007642 | 0.0000006268 | −0.0000009923 |
| 23.00 | −0.0000004796 | 0.0000003136 | −0.0000004869 |
| 24.00 | −0.0000003175 | 0.0000001579 | −0.0000002259 |
| 25.00 | −0.0000002268 | 0.0000000808 | −0.0000001180 |

He + NaK($X^1\Sigma^+$) Legendre Expansion coefficients $v_0, v_1$, and $v_2$ continued

| $R_\mathrm{d}$ | $v_0$ | $v_1$ | $v_2$ |
|---|---|---|---|
| 26.25 | −1.561452333E−07 | 4.248518784E−08 | −6.694401986E−08 |
| 27.5625 | −1.137143344E−07 | 2.423142444E−08 | −4.199752871E−08 |
| 28.940625 | −8.295777131E−08 | 1.302473700E−08 | −2.595350401E−08 |
| 30.38765625 | −6.061998514E−08 | 6.296398032E−09 | −1.572165153E−08 |
| 31.9070390625 | −4.436624658E−08 | 2.381741926E−09 | −9.264487876E−09 |
| 33.502391015625 | −3.251838652E−08 | 2.092403163E−10 | −5.243371204E−09 |
| 35.1775105664063 | −2.386747533E−08 | −9.051810912E−10 | −2.782408416E−09 |
| 36.9363860947266 | −1.754072944E−08 | −1.393802838E−09 | −1.311260777E−09 |
| 38.7832053994629 | −1.290672159E−08 | −1.526279800E−09 | −4.606905649E−10 |
| 40.7223656694361 | −9.507711263E−09 | −1.468014586E−09 | 6.687895710E−12 |
| 42.7584839529079 | −7.011222305E−09 | −1.318190128E−09 | 2.421972824E−10 |
| 44.8964081505533 | −5.175312999E−09 | −1.134409613E−09 | 3.412821534E−10 |
| 47.1412285580809 | −3.823610094E−09 | −9.485514083E−10 | 3.633371069E−10 |
| 49.4982899859850 | −2.827321797E−09 | −7.768866543E−10 | 3.446779203E−10 |
| 51.9732044852842 | −2.092250814E−09 | −6.264693323E−10 | 3.069856259E−10 |
| 54.5718647095484 | −1.549397845E−09 | −4.991196122E−10 | 2.627715841E−10 |
| 57.3004579450259 | −1.148149140E−09 | −3.938649561E−10 | 2.188897515E−10 |
| 60.1654808422772 | −8.513278999E−10 | −3.084020792E−10 | 1.787745964E−10 |
| 63.1737548843910 | −6.315928831E−10 | −2.399444792E−10 | 1.438518415E−10 |
| 66.3324426286106 | −4.688128181E−10 | −1.856901261E−10 | 1.144157281E−10 |
| 69.6490647600411 | −3.481489872E−10 | −1.430589507E−10 | 9.016489119E−11 |
| 73.1315179980432 | −2.586527425E−10 | −1.097945886E−10 | 7.052185990E−11 |
| 76.7880938979453 | −1.922381198E−10 | −8.398922046E−11 | 5.481707130E−11 |
| 80.6274985928426 | −1.429281600E−10 | −6.406753172E−11 | 4.238936275E−11 |

**Table B.2:** He + NaK($X^1\Sigma^+$) Legendre Expansion coefficients $v_3, v_4, v_5$, and $v_6$

| $R_\mathrm{d}$ | $v_3$ | $v_4$ | $v_5$ | $v_6$ |
|---|---|---|---|---|
| 0.00 | −8.5683000000 | 6.6507100000 | −2.1858900000 | 0.9524140000 |
| 1.00 | −6.7794500000 | 5.2625400000 | −1.7293290000 | 0.7537410000 |
| 2.00 | −4.9906000000 | 3.8743700000 | −1.2727680000 | 0.5550680000 |
| 3.00 | −3.2017500000 | 2.4862000000 | −0.8162070000 | 0.3563950000 |
| 4.00 | −1.4129189254 | 1.0980241795 | −0.3596504336 | 0.1577220046 |
| 4.50 | −0.6195967266 | 0.4820253454 | −0.1572165913 | 0.0695189472 |
| 5.00 | −0.2544187453 | 0.1969942146 | −0.0642057351 | 0.0285116242 |
| 5.50 | −0.1001960273 | 0.0762727073 | −0.0249552819 | 0.0109796912 |
| 6.00 | −0.0365805460 | 0.0272536972 | −0.0088943200 | 0.0038936199 |
| 6.25 | −0.0210679726 | 0.0160695987 | −0.0052960260 | 0.0024520353 |
| 6.75 | −0.0058964984 | 0.0049743428 | −0.0016281848 | 0.0009812838 |
| 7.00 | −0.0028090315 | 0.0024882724 | −0.0007388877 | 0.0005828813 |
| 7.25 | −0.0020680996 | 0.0016899695 | −0.0005288701 | 0.0004114832 |
| 7.50 | −0.0013411834 | 0.0009725253 | −0.0002565122 | 0.0002002814 |
| 7.75 | −0.0010546373 | 0.0006811007 | −0.0001704493 | 0.0001041192 |
| 8.00 | −0.0009202976 | 0.0005612942 | −0.0001574963 | 0.0000676100 |
| 8.25 | −0.0007891479 | 0.0004663321 | −0.0001383691 | 0.0000439670 |
| 8.50 | −0.0006858056 | 0.0004051555 | −0.0001311718 | 0.0000356607 |
| 8.75 | −0.0006008770 | 0.0003633303 | −0.0001405240 | 0.0000482308 |
| 9.00 | −0.0005063028 | 0.0003072993 | −0.0001119285 | 0.0000287929 |
| 9.25 | −0.0004276161 | 0.0002630139 | −0.0000967932 | 0.0000229762 |
| 9.50 | −0.0003600393 | 0.0002250477 | −0.0000870705 | 0.0000225205 |
| 9.75 | −0.0003011748 | 0.0001911755 | −0.0000790347 | 0.0000233396 |
| 10.00 | −0.0002497618 | 0.0001606470 | −0.0000711839 | 0.0000235670 |
| 10.25 | −0.0002051050 | 0.0001333914 | −0.0000631051 | 0.0000226409 |

He + NaK($X^1\Sigma^+$) Legendre Expansion coefficients $v_3, v_4, v_5$, and $v_6$ continued

| $R_\mathrm{d}$ | $v_3$ | $v_4$ | $v_5$ | $v_6$ |
|---|---|---|---|---|
| 10.50 | −0.0001666727 | 0.0001094952 | −0.0000549730 | 0.0000206429 |
| 10.75 | −0.0001339598 | 0.0000889573 | −0.0000471262 | 0.0000179661 |
| 11.00 | −0.0001064491 | 0.0000716566 | −0.0000398812 | 0.0000150423 |
| 11.50 | −0.0000647497 | 0.0000455528 | −0.0000277941 | 0.0000096824 |
| 12.00 | −0.0000370791 | 0.0000282012 | −0.0000188789 | 0.0000056836 |
| 12.50 | −0.0000194451 | 0.0000168505 | −0.0000125155 | 0.0000029719 |
| 13.00 | −0.0000087107 | 0.0000095118 | −0.0000081404 | 0.0000012613 |
| 13.50 | −0.0000024809 | 0.0000048525 | −0.0000052799 | 0.0000003067 |
| 14.00 | 0.0000009850 | 0.0000019356 | −0.0000035206 | −0.0000000899 |
| 14.50 | 0.0000028427 | 0.0000001188 | −0.0000024745 | −0.0000001435 |
| 15.00 | 0.0000038208 | −0.0000010388 | −0.0000018230 | −0.0000000280 |
| 15.50 | 0.0000043300 | −0.0000017769 | −0.0000013571 | 0.0000000887 |
| 16.00 | 0.0000045557 | −0.0000022649 | −0.0000009402 | 0.0000001660 |
| 16.50 | 0.0000045981 | −0.0000025673 | −0.0000005457 | 0.0000001568 |
| 17.00 | 0.0000044751 | −0.0000027027 | −0.0000001839 | 0.0000001002 |
| 17.50 | 0.0000042169 | −0.0000026870 | 0.0000001262 | −0.0000000125 |
| 18.00 | 0.0000038305 | −0.0000025552 | 0.0000003683 | −0.0000001077 |
| 18.50 | 0.0000033625 | −0.0000023170 | 0.0000005277 | −0.0000001890 |
| 19.00 | 0.0000028535 | −0.0000020245 | 0.0000005917 | −0.0000002327 |
| 19.50 | 0.0000023444 | −0.0000016991 | 0.0000005888 | −0.0000002553 |
| 20.00 | 0.0000018697 | −0.0000013777 | 0.0000005387 | −0.0000002476 |
| 21.00 | 0.0000010770 | −0.0000008214 | 0.0000003840 | −0.0000001721 |
| 22.00 | 0.0000005594 | −0.0000004366 | 0.0000002220 | −0.0000001146 |
| 23.00 | 0.0000002652 | −0.0000002076 | 0.0000001155 | −0.0000000576 |
| 24.00 | 0.0000001115 | −0.0000000901 | 0.0000000534 | −0.0000000396 |
| 25.00 | 0.0000000470 | −0.0000000355 | 0.0000000217 | −0.0000000162 |

He + NaK($X^1\Sigma^+$) Legendre Expansion coefficients $v_3, v_4, v_5$, and $v_6$ continued

| $R_\mathrm{d}$ | $v_3$ | $v_4$ | $v_5$ | $v_6$ |
|---|---|---|---|---|
| 26.25 | 1.494917971E−08 | −1.131910040E−08 | 7.797825535E−09 | −6.500032667E−09 |
| 27.5625 | 4.599119506E−09 | −3.382307203E−09 | 2.602889852E−09 | −2.312695287E−09 |
| 28.940625 | 1.333935692E−09 | −9.514462213E−10 | 8.224550656E−10 | −7.814144447E−10 |
| 30.38765625 | 3.636788971E−10 | −2.511967410E−10 | 2.453304124E−10 | −2.500820990E−10 |
| 31.9070390625 | 9.291385302E−11 | −6.204763653E−11 | 6.888466625E−11 | −7.560383666E−11 |
| 33.502391015625 | 2.217231078E−11 | −1.429131028E−11 | 1.815149025E−11 | −2.152921159E−11 |
| 35.1775105664063 | 4.925246474E−12 | −3.058695142E−12 | 4.474468975E−12 | −5.757535591E−12 |
| 36.9363860947266 | 1.014789187E−12 | −6.060710584E−13 | 1.028400257E−12 | −1.441469846E−12 |
| 38.7832053994629 | 1.932062121E−13 | −1.107542156E−13 | 2.196108967E−13 | −3.367463825E−13 |
| 40.7223656694361 | 3.385701018E−14 | −1.859040374E−14 | 4.341303814E−14 | −7.315182830E−14 |
| 42.7584839529079 | 5.438229081E−15 | −2.854064643E−15 | 7.913794870E−15 | −1.472290614E−14 |
| 44.8964081505533 | 7.971808115E−16 | −3.989767041E−16 | 1.324913815E−15 | −2.734955847E−15 |
| 47.1412285580809 | 1.061600567E−16 | −5.054817240E−17 | 2.028526147E−16 | −4.670409215E−16 |
| 49.4982899859850 | 1.278161297E−17 | −5.775655401E−18 | 2.827634297E−17 | −7.300956827E−17 |
| 51.9732044852842 | 1.384335670E−18 | −5.920956630E−19 | 3.571724912E−18 | −1.040173699E−17 |
| 54.5718647095484 | 1.341621297E−19 | −5.416540773E−20 | 4.068230049E−19 | −1.344368292E−18 |
| 57.3004579450259 | 1.157012110E−20 | −4.396617257E−21 | 4.156802385E−20 | −1.568560495E−19 |
| 60.1654808422772 | 8.827368638E−22 | −3.147640581E−22 | 3.789491591E−21 | −1.643741180E−20 |
| 63.1737548843910 | 5.921739386E−23 | −1.975126589E−23 | 3.064739707E−22 | −1.538800102E−21 |
| 66.3324426286106 | 3.470549303E−24 | −1.079158473E−24 | 2.185731822E−23 | −1.279671258E−22 |
| 69.6490647600411 | 1.764999526E−25 | −5.098589283E−26 | 1.366030257E−24 | −9.397458913E−24 |
| 73.1315179980432 | 7.734073346E−27 | −2.067916854E−27 | 7.432192250E−26 | −6.056448887E−25 |
| 76.7880938979453 | 2.898378933E−28 | −7.145296736E−29 | 3.495878917E−27 | −3.403188917E−26 |
| 80.6274985928426 | 9.216995729E−30 | −2.086564554E−30 | 1.411294995E−28 | −1.655912789E−27 |

# Appendix C

# Nine Term Legendre Expansion of the Ground State Potential

**Table C.1:** He + NaK($X^1\Sigma^+$) Legendre Expansion coefficients $v_0, v_1$, and $v_2$

| $R_\mathrm{d}$ | $v_0$ | $v_1$ | $v_2$ |
|---|---|---|---|
| 0.00 | 0.4707843743 | 0.7356761744 | 1.316314678 |
| 0.50 | 0.4228271743 | 0.6572111444 | 1.179454338 |
| 1.00 | 0.3748699743 | 0.5787461144 | 1.042593998 |
| 1.50 | 0.3269127743 | 0.5002810844 | 0.905733658 |
| 2.00 | 0.2789555743 | 0.4218160544 | 0.768873318 |
| 2.50 | 0.2309983743 | 0.3433510244 | 0.632012978 |
| 3.00 | 0.1830411743 | 0.2648859944 | 0.495152638 |
| 3.50 | 0.1350839743 | 0.1864209644 | 0.358292298 |
| 4.00 | 0.0871266143 | 0.1079559344 | 0.2214319584 |
| 4.50 | 0.0452417121 | 0.0383407043 | 0.1035698352 |
| 5.00 | 0.0266983440 | 0.0074732004 | 0.0568471350 |
| 5.50 | 0.0149839693 | −0.0022443844 | 0.0265862896 |
| 6.00 | 0.0094601848 | −0.0059396012 | 0.0150886475 |
| 6.25 | 0.0076437404 | −0.0062516747 | 0.0117699009 |
| 6.50 | 0.0059398405 | −0.0052021166 | 0.0081801166 |
| 6.75 | 0.0048332802 | −0.0047254065 | 0.0065027774 |
| 7.00 | 0.0039322647 | −0.0041087831 | 0.0052080736 |
| 7.25 | 0.0031792284 | −0.0034332339 | 0.0041220693 |
| 7.50 | 0.0025561337 | −0.0027975908 | 0.0032316798 |
| 8.00 | 0.0016449176 | −0.0018336373 | 0.0020329496 |
| 8.25 | 0.0013175590 | −0.0014920174 | 0.0016465923 |
| 8.50 | 0.0010526321 | −0.0012203085 | 0.0013505287 |
| 8.75 | 0.0008364720 | −0.0009990052 | 0.0011129567 |
| 9.00 | 0.0006595191 | −0.0008160633 | 0.0009163680 |
| 9.25 | 0.0005147012 | −0.0006637066 | 0.0007509071 |

He + NaK($X^1\Sigma^+$) Legendre Expansion coefficients $v_0, v_1$, and $v_2$ continued

| $R_\mathrm{d}$ | $v_0$ | $v_1$ | $v_2$ |
|---|---|---|---|
| 9.50 | 0.0003965466 | −0.0005366239 | 0.0006108817 |
| 9.75 | 0.0003006282 | −0.0004308779 | 0.0004924908 |
| 10.00 | 0.0002232709 | −0.0003433310 | 0.0003930011 |
| 10.25 | 0.0001613487 | −0.0002713538 | 0.0003100255 |
| 10.50 | 0.0001122192 | −0.0002126355 | 0.0002414580 |
| 10.75 | 0.0000735977 | −0.0001651289 | 0.0001852491 |
| 11.00 | 0.0000435652 | −0.0001270047 | 0.0001395117 |
| 11.50 | 0.0000030297 | −0.0000726499 | 0.0000727192 |
| 12.00 | −0.0000193428 | −0.0000390995 | 0.0000298236 |
| 12.50 | −0.0000302416 | −0.0000188786 | 0.0000029345 |
| 13.00 | −0.0000340768 | −0.0000069417 | −0.0000131436 |
| 13.50 | −0.0000337449 | −0.0000000052 | −0.0000219706 |
| 14.00 | −0.0000311235 | 0.0000039438 | −0.0000259256 |
| 14.50 | −0.0000274411 | 0.0000061214 | −0.0000267994 |
| 15.00 | −0.0000234279 | 0.0000072146 | −0.0000257227 |
| 15.50 | −0.0000195398 | 0.0000076279 | −0.0000235826 |
| 16.00 | −0.0000160014 | 0.0000075757 | −0.0000209085 |
| 16.50 | −0.0000129179 | 0.0000072072 | −0.0000180797 |
| 17.00 | −0.0000102969 | 0.0000066105 | −0.0000152681 |
| 17.50 | −0.0000081282 | 0.0000058718 | −0.0000126501 |
| 18.00 | −0.0000063553 | 0.0000050707 | −0.0000102797 |
| 18.50 | −0.0000049301 | 0.0000042490 | −0.0000081915 |
| 19.00 | −0.0000038026 | 0.0000034671 | −0.0000064116 |
| 19.50 | −0.0000029088 | 0.0000027563 | −0.0000049021 |
| 20.00 | −0.0000022188 | 0.0000021382 | −0.0000036807 |
| 21.00 | −0.0000012938 | 0.0000011988 | −0.0000019771 |

He + NaK($X^1\Sigma^+$) Legendre Expansion coefficients $v_0, v_1$, and $v_2$ continued

| $R_\mathrm{d}$ | $v_0$ | $v_1$ | $v_2$ |
|---|---|---|---|
| 22.00 | −0.0000007638 | 0.0000006263 | −0.0000009901 |
| 23.00 | −0.0000004826 | 0.0000003103 | −0.0000004853 |
| 24.00 | −0.0000003194 | 0.0000001544 | −0.0000002290 |
| 25.00 | −0.0000002264 | 0.0000000844 | −0.0000001154 |
| 26.25 | −1.561452333E−07 | 4.248518784E−08 | −6.694401986E−08 |
| 27.5625 | −1.137143344E−07 | 2.423142444E−08 | −4.199752871E−08 |
| 28.940625 | −8.295777131E−08 | 1.302473700E−08 | −2.595350401E−08 |
| 30.38765625 | −6.061998514E−08 | 6.296398032E−09 | −1.572165153E−08 |
| 31.9070390625 | −4.436624658E−08 | 2.381741926E−09 | −9.264487876E−09 |
| 33.502391015625 | −3.251838652E−08 | 2.092403163E−10 | −5.243371204E−09 |
| 35.1775105664063 | −2.386747533E−08 | −9.051810912E−10 | −2.782408416E−09 |
| 36.9363860947266 | −1.754072944E−08 | −1.393802838E−09 | −1.311260777E−09 |
| 38.7832053994629 | −1.290672159E−08 | −1.526279800E−09 | −4.606905649E−10 |
| 40.7223656694361 | −9.507711263E−09 | −1.468014586E−09 | 6.687895710E−12 |
| 42.7584839529079 | −7.011222305E−09 | −1.318190128E−09 | 2.421972824E−10 |
| 44.8964081505533 | −5.175312999E−09 | −1.134409613E−09 | 3.412821534E−10 |
| 47.1412285580809 | −3.823610094E−09 | −9.485514083E−10 | 3.633371069E−10 |
| 49.4982899859850 | −2.827321797E−09 | −7.768866543E−10 | 3.446779203E−10 |
| 51.9732044852842 | −2.092250814E−09 | −6.264693323E−10 | 3.069856259E−10 |
| 54.5718647095484 | −1.549397845E−09 | −4.991196122E−10 | 2.627715841E−10 |
| 57.3004579450259 | −1.148149140E−09 | −3.938649561E−10 | 2.188897515E−10 |
| 60.1654808422772 | −8.513278999E−10 | −3.084020792E−10 | 1.787745964E−10 |
| 63.1737548843910 | −6.315928831E−10 | −2.399444792E−10 | 1.438518415E−10 |
| 66.3324426286106 | −4.688128181E−10 | −1.856901261E−10 | 1.144157281E−10 |
| 69.6490647600411 | −3.481489872E−10 | −1.430589507E−10 | 9.016489119E−11 |
| 73.1315179980432 | −2.586527425E−10 | −1.097945886E−10 | 7.052185990E−11 |

He + NaK($X^1\Sigma^+$) Legendre Expansion coefficients $v_0, v_1$, and $v_2$ continued

| $R_\mathrm{d}$ | $v_0$ | $v_1$ | $v_2$ |
|---|---|---|---|
| 76.7880938979453 | −1.922381198E−10 | −8.398922046E−11 | 5.481707130E−11 |
| 80.6274985928426 | −1.429281600E−10 | −6.406753172E−11 | 4.238936275E−11 |

**Table C.2:** He + NaK($X^1\Sigma^+$) Legendre Expansion coefficients $v_3, v_4, v_5$, and $v_6$

| $R_\mathrm{d}$ | $v_3$ | $v_4$ | $v_5$ | $v_6$ |
|---|---|---|---|---|
| 0.00 | 0.7497549342 | 0.8313690701 | 0.2523575216 | 0.2527090134 |
| 0.50 | 0.6711628192 | 0.7447882701 | 0.2260518416 | 0.2263383634 |
| 1.00 | 0.5925707042 | 0.6582074701 | 0.1997461616 | 0.1999677134 |
| 1.50 | 0.5139785892 | 0.5716266701 | 0.1734404816 | 0.1735970634 |
| 2.00 | 0.4353864742 | 0.4850458701 | 0.1471348016 | 0.1472264134 |
| 2.50 | 0.3567943592 | 0.3984650701 | 0.1208291216 | 0.1208557634 |
| 3.00 | 0.2782022442 | 0.3118842701 | 0.0945234416 | 0.0944851134 |
| 3.50 | 0.1996101292 | 0.2253034701 | 0.0682177616 | 0.0681144634 |
| 4.00 | 0.1210180142 | 0.1387226701 | 0.0419120816 | 0.0417438134 |
| 4.50 | 0.0504711480 | 0.0653573343 | 0.0180215147 | 0.0201616218 |
| 5.00 | 0.0161750062 | 0.0388778012 | 0.0057138362 | 0.0142232484 |
| 5.50 | 0.0040872048 | 0.0176198690 | 0.0017831757 | 0.0068898598 |
| 6.00 | −0.0023906260 | 0.0100275405 | −0.0013178830 | 0.0045265266 |
| 6.25 | −0.0037437402 | 0.0078108772 | −0.0021850828 | 0.0037853990 |
| 6.50 | −0.0028558352 | 0.0047901905 | −0.0013623180 | 0.0022359673 |
| 6.75 | −0.0029405115 | 0.0036956381 | −0.0015073396 | 0.0018023847 |
| 7.00 | −0.0027197626 | 0.0028745960 | −0.0014631547 | 0.0014903129 |
| 7.25 | −0.0022851678 | 0.0021453855 | −0.0012209925 | 0.0011536877 |
| 7.50 | −0.0018008553 | 0.0015225094 | −0.0008899132 | 0.0007990513 |
| 8.00 | −0.0010873135 | 0.0007500415 | −0.0003846548 | 0.0002850073 |
| 8.25 | −0.0008668453 | 0.0005532316 | −0.0002406229 | 0.0001420169 |
| 8.50 | −0.0007137251 | 0.0004370789 | −0.0001678677 | 0.0000737309 |
| 8.75 | −0.0005985827 | 0.0003622221 | −0.0001306492 | 0.0000435997 |
| 9.00 | −0.0005058997 | 0.0003080685 | −0.0001101977 | 0.0000319052 |
| 9.25 | −0.0004276805 | 0.0002642904 | −0.0000970363 | 0.0000282691 |

He + NaK($X^1\Sigma^+$) Legendre Expansion coefficients $v_3, v_4, v_5$, and $v_6$ continued

| $R_\mathrm{d}$ | $v_3$ | $v_4$ | $v_5$ | $v_6$ |
|---|---|---|---|---|
| 9.50 | −0.0003599481 | 0.0002262324 | −0.0000866605 | 0.0000273527 |
| 9.75 | −0.0003007434 | 0.0001919850 | −0.0000771696 | 0.0000266816 |
| 10.00 | −0.0002490215 | 0.0001610736 | −0.0000679534 | 0.0000252536 |
| 10.25 | −0.0002041608 | 0.0001334753 | −0.0000590140 | 0.0000229655 |
| 10.50 | −0.0001656512 | 0.0001093528 | −0.0000505575 | 0.0000200475 |
| 10.75 | −0.0001329569 | 0.0000887024 | −0.0000428120 | 0.0000168800 |
| 11.00 | −0.0001055279 | 0.0000713599 | −0.0000359255 | 0.0000138121 |
| 11.50 | −0.0000640564 | 0.0000452886 | −0.0000247916 | 0.0000086115 |
| 12.00 | −0.0000365850 | 0.0000280244 | −0.0000167399 | 0.0000049461 |
| 12.50 | −0.0000191075 | 0.0000167459 | −0.0000110467 | 0.0000025416 |
| 13.00 | −0.0000084925 | 0.0000094714 | −0.0000071816 | 0.0000010577 |
| 13.50 | −0.0000023349 | 0.0000048416 | −0.0000046769 | 0.0000002733 |
| 14.00 | 0.0000010751 | 0.0000019528 | −0.0000031440 | −0.0000000453 |
| 14.50 | 0.0000029076 | 0.0000001132 | −0.0000022009 | −0.0000000688 |
| 15.00 | 0.0000038817 | −0.0000010255 | −0.0000015904 | 0.0000000046 |
| 15.50 | 0.0000043857 | −0.0000017804 | −0.0000011240 | 0.0000000874 |
| 16.00 | 0.0000046118 | −0.0000022800 | −0.0000007170 | 0.0000001208 |
| 16.50 | 0.0000046399 | −0.0000025889 | −0.0000003439 | 0.0000000917 |
| 17.00 | 0.0000045143 | −0.0000027117 | −0.0000000094 | 0.0000000104 |
| 17.50 | 0.0000042456 | −0.0000027028 | 0.0000002600 | −0.0000000799 |
| 18.00 | 0.0000038465 | −0.0000025587 | 0.0000004507 | −0.0000001635 |
| 18.50 | 0.0000033762 | −0.0000023289 | 0.0000005698 | −0.0000002233 |
| 19.00 | 0.0000028560 | −0.0000020438 | 0.0000006003 | −0.0000002487 |
| 19.50 | 0.0000023414 | −0.0000017042 | 0.0000005812 | −0.0000002641 |
| 20.00 | 0.0000018615 | −0.0000013759 | 0.0000005198 | −0.0000002467 |
| 21.00 | 0.0000010701 | −0.0000008256 | 0.0000003531 | −0.0000001765 |

He + NaK($X^1\Sigma^+$) Legendre Expansion coefficients $v_3, v_4, v_5$, and $v_6$ continued

| $R_\mathrm{d}$ | $v_3$ | $v_4$ | $v_5$ | $v_6$ |
|---|---|---|---|---|
| 22.00 | 0.0000005493 | −0.0000004314 | 0.0000002035 | −0.0000001107 |
| 23.00 | 0.0000002538 | −0.0000002089 | 0.0000001054 | −0.0000000567 |
| 24.00 | 0.0000001134 | −0.0000000878 | 0.0000000415 | −0.0000000311 |
| 25.00 | 0.0000000439 | −0.0000000378 | 0.0000000246 | −0.0000000135 |
| 26.25 | 1.494917971E−08 | −1.131910040E−08 | 7.797825535E−09 | −6.500032667E−09 |
| 27.5625 | 4.599119506E−09 | −3.382307203E−09 | 2.602889852E−09 | −2.312695287E−09 |
| 28.940625 | 1.333935692E−09 | −9.514462213E−10 | 8.224550656E−10 | −7.814144447E−10 |
| 30.38765625 | 3.636788971E−10 | −2.511967410E−10 | 2.453304124E−10 | −2.500820990E−10 |
| 31.9070390625 | 9.291385302E−11 | −6.204763653E−11 | 6.888466625E−11 | −7.560383666E−11 |
| 33.502391015625 | 2.217231078E−11 | −1.429131028E−11 | 1.815149025E−11 | −2.152921159E−11 |
| 35.1775105664063 | 4.925246474E−12 | −3.058695142E−12 | 4.474468975E−12 | −5.757535591E−12 |
| 36.9363860947266 | 1.014789187E−12 | −6.060710584E−13 | 1.028400257E−12 | −1.441469846E−12 |
| 38.7832053994629 | 1.932062121E−13 | −1.107542156E−13 | 2.196108967E−13 | −3.367463825E−13 |
| 40.7223656694361 | 3.385701018E−14 | −1.859040374E−14 | 4.341303814E−14 | −7.315182830E−14 |
| 42.7584839529079 | 5.438229081E−15 | −2.854064643E−15 | 7.913794870E−15 | −1.472290614E−14 |
| 44.8964081505533 | 7.971808115E−16 | −3.989767041E−16 | 1.324913815E−15 | −2.734955847E−15 |
| 47.1412285580809 | 1.061600567E−16 | −5.054817240E−17 | 2.028526147E−16 | −4.670409215E−16 |
| 49.4982899859850 | 1.278161297E−17 | −5.775655401E−18 | 2.827634297E−17 | −7.300956827E−17 |
| 51.9732044852842 | 1.384335670E−18 | −5.920956630E−19 | 3.571724912E−18 | −1.040173699E−17 |
| 54.5718647095484 | 1.341621297E−19 | −5.416540773E−20 | 4.068230049E−19 | −1.344368292E−18 |
| 57.3004579450259 | 1.157012110E−20 | −4.396617257E−21 | 4.156802385E−20 | −1.568560495E−19 |
| 60.1654808422772 | 8.827368638E−22 | −3.147640581E−22 | 3.789491591E−21 | −1.643741180E−20 |
| 63.1737548843910 | 5.921739386E−23 | −1.975126589E−23 | 3.064739707E−22 | −1.538800102E−21 |
| 66.3324426286106 | 3.470549303E−24 | −1.079158473E−24 | 2.185731822E−23 | −1.279671258E−22 |
| 69.6490647600411 | 1.764999526E−25 | −5.098589283E−26 | 1.366030257E−24 | −9.397458913E−24 |
| 73.1315179980432 | 7.734073346E−27 | −2.067916854E−27 | 7.432192250E−26 | −6.056448887E−25 |

He + NaK($X^1\Sigma^+$) Legendre Expansion coefficients $v_3, v_4, v_5$, and $v_6$ continued

| $R_\mathrm{d}$ | $v_3$ | $v_4$ | $v_5$ | $v_6$ |
|---|---|---|---|---|
| 76.7880938979453 | 2.898378933E−28 | −7.145296736E−29 | 3.495878917E−27 | −3.403188917E−26 |
| 80.6274985928426 | 9.216995729E−30 | −2.086564554E−30 | 1.411294995E−28 | −1.655912789E−27 |

**Table C.3:** He + NaK($X^1\Sigma^+$) Legendre Expansion coefficients $v_7$ and $v_8$

| $R_\mathrm{d}$ | $v_7$ | $v_8$ |
|---|---|---|
| 0.00 | 0.0333487165 | 0.0344039405 |
| 0.50 | 0.0298723915 | 0.0307867555 |
| 1.00 | 0.0263960665 | 0.0271695705 |
| 1.50 | 0.0229197415 | 0.0235523855 |
| 2.00 | 0.0194434165 | 0.0199352005 |
| 2.50 | 0.0159670915 | 0.0163180155 |
| 3.00 | 0.0124907665 | 0.0127008305 |
| 3.50 | 0.0090144415 | 0.0090836455 |
| 4.00 | 0.0055381165 | 0.0054664605 |
| 4.50 | 0.0023160085 | 0.0026885921 |
| 5.00 | 0.0005235734 | 0.0024028277 |
| 5.50 | 0.0001195954 | 0.0013110337 |
| 6.00 | −0.0006104551 | 0.0010999252 |
| 6.25 | −0.0009637833 | 0.0010312717 |
| 6.50 | −0.0005781178 | 0.0006343174 |
| 6.75 | −0.0007136876 | 0.0005401946 |
| 7.00 | −0.0008064696 | 0.0005306928 |
| 7.25 | −0.0007827008 | 0.0005187442 |
| 7.50 | −0.0006451005 | 0.0004566261 |
| 8.00 | −0.0003103242 | 0.0002570842 |
| 8.25 | −0.0001391594 | 0.0001133552 |
| 8.50 | −0.0000557426 | 0.0000419054 |
| 8.75 | −0.0000178777 | 0.0000082946 |
| 9.00 | −0.0000031320 | −0.0000056336 |
| 9.25 | 0.0000004535 | −0.0000095176 |

He + NaK($X^1\Sigma^+$) Legendre Expansion coefficients $v_7$ and $v_8$ continued

| $R_\mathrm{d}$ | $v_7$ | $v_8$ |
|---|---|---|
| 9.50 | −0.0000007371 | −0.0000087229 |
| 9.75 | −0.0000033748 | −0.0000060314 |
| 10.00 | −0.0000058314 | −0.0000030765 |
| 10.25 | −0.0000074005 | −0.0000005942 |
| 10.50 | −0.0000079876 | 0.0000010506 |
| 10.75 | −0.0000078101 | 0.0000019329 |
| 11.00 | −0.0000071631 | 0.0000022198 |
| 11.50 | −0.0000054329 | 0.0000019301 |
| 12.00 | −0.0000038638 | 0.0000013205 |
| 12.50 | −0.0000026563 | 0.0000007805 |
| 13.00 | −0.0000017227 | 0.0000003428 |
| 13.50 | −0.0000010923 | 0.0000000712 |
| 14.00 | −0.0000006905 | −0.0000000941 |
| 14.50 | −0.0000004969 | −0.0000000827 |
| 15.00 | −0.0000004310 | −0.0000000637 |
| 15.50 | −0.0000004222 | 0.0000000128 |
| 16.00 | −0.0000004069 | 0.0000000727 |
| 16.50 | −0.0000003707 | 0.0000001372 |
| 17.00 | −0.0000003111 | 0.0000001206 |
| 17.50 | −0.0000002322 | 0.0000001161 |
| 18.00 | −0.0000001479 | 0.0000000873 |
| 18.50 | −0.0000000835 | 0.0000000654 |
| 19.00 | −0.0000000133 | 0.0000000569 |
| 19.50 | 0.0000000178 | 0.0000000160 |
| 20.00 | 0.0000000386 | −0.0000000098 |
| 21.00 | 0.0000000541 | −0.0000000009 |

He + NaK($X^1\Sigma^+$) Legendre Expansion coefficients $v_7$ and $v_8$ continued

| $R_\mathrm{d}$ | $v_7$ | $v_8$ |
|---|---|---|
| 22.00 | 0.0000000399 | −0.0000000149 |
| 23.00 | 0.0000000289 | 0.0000000018 |
| 24.00 | 0.0000000165 | −0.0000000067 |
| 25.00 | −0.0000000010 | −0.0000000050 |
| 26.25 | 0 | 0 |
| 27.5625 | 0 | 0 |
| 28.940625 | 0 | 0 |
| 30.38765625 | 0 | 0 |
| 31.9070390625 | 0 | 0 |
| 33.502391015625 | 0 | 0 |
| 35.1775105664063 | 0 | 0 |
| 36.9363860947266 | 0 | 0 |
| 38.7832053994629 | 0 | 0 |
| 40.7223656694361 | 0 | 0 |
| 42.7584839529079 | 0 | 0 |
| 44.8964081505533 | 0 | 0 |
| 47.1412285580809 | 0 | 0 |
| 49.498289985985 | 0 | 0 |
| 51.9732044852842 | 0 | 0 |
| 54.5718647095484 | 0 | 0 |
| 57.3004579450259 | 0 | 0 |
| 60.1654808422772 | 0 | 0 |
| 63.173754884391 | 0 | 0 |
| 66.3324426286106 | 0 | 0 |
| 69.6490647600411 | 0 | 0 |
| 73.1315179980432 | 0 | 0 |

He + NaK($X^1\Sigma^+$) Legendre Expansion coefficients $v_7$ and $v_8$ continued

| $R_\mathrm{d}$ | $v_7$ | $v_8$ |
|---|---|---|
| 76.7880938979453 | 0 | 0 |
| 80.6274985928426 | 0 | 0 |

# Appendix D

# Excited State Potential

**Table D.1:** He + NaK($A^1\Sigma^+$) potential calculations

| $R_d$ | $\theta$ | Energy | $R_d$ | $\theta$ | Energy |
|---|---|---|---|---|---|
| 3.00 | 30 | −762.789938909 | 3.50 | 70 | −764.147037280 |
| 3.00 | 45 | −763.787023725 | 3.50 | 75 | −764.153587206 |
| 3.00 | 60 | −764.071927080 | 3.50 | 80 | −764.156946424 |
| 3.00 | 65 | −764.106788051 | 3.50 | 85 | −764.158322995 |
| 3.00 | 70 | −764.128107691 | 3.50 | 90 | −764.158426009 |
| 3.00 | 75 | −764.140877400 | 3.50 | 95 | −764.157662156 |
| 3.00 | 80 | −764.148243030 | 3.50 | 100 | −764.156258742 |
| 3.00 | 85 | −764.152166084 | 3.50 | 105 | −764.154337988 |
| 3.00 | 90 | −764.153856051 | 3.50 | 110 | −764.151957682 |
| 3.00 | 95 | −764.154056249 | 3.50 | 115 | −764.149135061 |
| 3.00 | 100 | −764.153217633 | 3.50 | 120 | −764.145840957 |
| 3.00 | 105 | −764.151609499 | 3.50 | 125 | −764.141959513 |
| 3.00 | 110 | −764.149390629 | 3.50 | 130 | −764.137177195 |
| 3.00 | 115 | −764.146640997 | 3.50 | 135 | −764.130709173 |
| 3.00 | 120 | −764.143379554 | 3.50 | 140 | −764.120711736 |
| 3.00 | 125 | −764.139544553 | 3.50 | 165 | −763.716401687 |
| 3.00 | 130 | −764.134935177 | 4.00 | 0 | −760.444260666 |
| 3.00 | 135 | −764.129088532 | 4.00 | 15 | −762.343570350 |
| 3.00 | 140 | −764.121057229 | 4.00 | 30 | −763.607558408 |
| 3.00 | 165 | −763.963638251 | 4.00 | 45 | −764.039285174 |
| 3.00 | 180 | −763.832918231 | 4.00 | 60 | −764.141345842 |
| 3.50 | 15 | −759.927151116 | 4.00 | 65 | −764.151633911 |
| 3.50 | 30 | −763.200641168 | 4.00 | 70 | −764.157248618 |
| 3.50 | 45 | −763.929122495 | 4.00 | 75 | −764.160088462 |
| 3.50 | 60 | −764.114896124 | 4.00 | 80 | −764.161259708 |
| 3.50 | 65 | −764.135265111 | 4.00 | 85 | −764.161391510 |

He + NaK($A^1\Sigma^+$) potential calculations continued

| $R_d$ | $\theta$ | Energy | $R_d$ | $\theta$ | Energy |
|---|---|---|---|---|---|
| 4.00 | 90 | −764.160830739 | 5.00 | 165 | −762.665237758 |
| 4.00 | 95 | −764.159760414 | 5.50 | 0 | −763.943258362 |
| 4.00 | 105 | −764.156396478 | 5.50 | 15 | −764.017131073 |
| 4.00 | 120 | −764.148441844 | 5.50 | 30 | −764.115394118 |
| 4.00 | 135 | −764.134007820 | 5.50 | 45 | −764.154447128 |
| 4.00 | 150 | −764.054607204 | 5.50 | 60 | −764.163442332 |
| 4.00 | 165 | −763.253127341 | 5.50 | 65 | −764.164241800 |
| 4.50 | 15 | −763.310703968 | 5.50 | 70 | −764.164585203 |
| 4.50 | 30 | −763.889779937 | 5.50 | 75 | −764.164625231 |
| 4.50 | 45 | −764.105909886 | 5.50 | 80 | −764.164442792 |
| 4.50 | 60 | −764.155033641 | 5.50 | 85 | −764.164074634 |
| 4.50 | 65 | −764.159647805 | 5.50 | 90 | −764.163534286 |
| 4.50 | 70 | −764.162000573 | 5.50 | 95 | −764.162819441 |
| 4.50 | 75 | −764.163018734 | 5.50 | 105 | −764.160805878 |
| 4.50 | 80 | −764.163222348 | 5.50 | 120 | −764.155973901 |
| 4.50 | 85 | −764.162891859 | 5.50 | 135 | −764.147795248 |
| 4.50 | 90 | −764.162170189 | 5.50 | 150 | −764.101700639 |
| 4.50 | 95 | −764.161122348 | 5.50 | 165 | −763.109795740 |
| 4.50 | 105 | −764.158109656 | 5.50 | 180 | −752.704262530 |
| 4.50 | 120 | −764.151095423 | 6.00 | 0 | −764.080718979 |
| 4.50 | 135 | −764.138497230 | 6.00 | 15 | −764.107556601 |
| 4.50 | 150 | −764.062516825 | 6.00 | 30 | −764.144547562 |
| 4.50 | 165 | −762.745168985 | 6.00 | 45 | −764.160141692 |
| 5.00 | 0 | −763.598547756 | 6.00 | 60 | −764.164164471 |
| 5.00 | 15 | −763.794228459 | 6.00 | 65 | −764.164571453 |
| 5.00 | 30 | −764.044050641 | 6.00 | 70 | −764.164746436 |
| 5.00 | 45 | −764.139636057 | 6.00 | 75 | −764.164745243 |
| 5.00 | 60 | −764.161120981 | 6.00 | 80 | −764.164598263 |
| 5.00 | 65 | −764.163030200 | 6.00 | 85 | −764.164317754 |
| 5.00 | 70 | −764.163924374 | 6.00 | 90 | −764.163907047 |
| 5.00 | 75 | −764.164201923 | 6.00 | 95 | −764.163361164 |
| 5.00 | 80 | −764.164076117 | 6.00 | 105 | −764.161808087 |
| 5.00 | 85 | −764.163656116 | 6.00 | 120 | −764.157984257 |
| 5.00 | 90 | −764.162990810 | 6.00 | 135 | −764.151579983 |
| 5.00 | 95 | −764.162094540 | 6.00 | 150 | −764.124674046 |
| 5.00 | 105 | −764.159573955 | 6.00 | 165 | −763.626513973 |
| 5.00 | 120 | −764.153649703 | 6.00 | 180 | −761.421601581 |
| 5.00 | 135 | −764.143326163 | 6.50 | 0 | −764.130443178 |
| 5.00 | 150 | −764.074895259 | 6.50 | 15 | −764.140835850 |

He + NaK($A^1\Sigma^+$) potential calculations continued

| $R_d$ | $\theta$ | Energy | $R_d$ | $\theta$ | Energy |
|---|---|---|---|---|---|
| 6.50 | 30 | −764.155234416 | 7.50 | 105 | −764.163616448 |
| 6.50 | 45 | −764.162043101 | 7.50 | 120 | −764.161994045 |
| 6.50 | 60 | −764.164303197 | 7.50 | 135 | −764.159024337 |
| 6.50 | 65 | −764.164592758 | 7.50 | 150 | −764.153713277 |
| 6.50 | 70 | −764.164734642 | 7.50 | 160 | −764.142284005 |
| 6.50 | 75 | −764.164751586 | 7.50 | 165 | −764.128058758 |
| 6.50 | 80 | −764.164658443 | 7.50 | 172 | −764.093694238 |
| 6.50 | 85 | −764.164461228 | 7.50 | 180 | −764.072055764 |
| 6.50 | 90 | −764.164162119 | 8.00 | 0 | −764.154090228 |
| 6.50 | 95 | −764.163757871 | 8.00 | 15 | −764.156859013 |
| 6.50 | 105 | −764.162592096 | 8.00 | 30 | −764.160326478 |
| 6.50 | 120 | −764.159647813 | 8.00 | 45 | −764.162824098 |
| 6.50 | 135 | −764.154649964 | 8.00 | 60 | −764.164183200 |
| 6.50 | 150 | −764.139825514 | 8.00 | 75 | −764.164635880 |
| 6.50 | 165 | −763.937229992 | 8.00 | 90 | −764.164498413 |
| 6.50 | 180 | −763.230359774 | 8.00 | 105 | −764.163922404 |
| 7.00 | 0 | −764.146962425 | 8.00 | 120 | −764.162756079 |
| 7.00 | 15 | −764.152056593 | 8.00 | 135 | −764.160527857 |
| 7.00 | 30 | −764.158763407 | 8.00 | 150 | −764.156860736 |
| 7.00 | 45 | −764.162586689 | 8.00 | 160 | −764.151957429 |
| 7.00 | 60 | −764.164271545 | 8.00 | 165 | −764.147243837 |
| 7.00 | 75 | −764.164719590 | 8.00 | 172 | −764.137299394 |
| 7.00 | 90 | −764.164331341 | 8.00 | 180 | −764.131517735 |
| 7.00 | 105 | −764.163184530 | 8.50 | 0 | −764.155354054 |
| 7.00 | 120 | −764.160973348 | 8.50 | 15 | −764.157631025 |
| 7.00 | 135 | −764.157095445 | 8.50 | 30 | −764.160685843 |
| 7.00 | 145 | −764.152814996 | 8.50 | 45 | −764.162942616 |
| 7.00 | 150 | −764.148634503 | 8.50 | 60 | −764.164176231 |
| 7.00 | 160 | −764.119056336 | 8.50 | 75 | −764.164598912 |
| 7.00 | 165 | −764.075219474 | 8.50 | 90 | −764.164529074 |
| 7.00 | 172 | −763.956185733 | 8.50 | 105 | −764.164133018 |
| 7.00 | 180 | −763.874144664 | 8.50 | 120 | −764.163309825 |
| 7.50 | 0 | −764.152164232 | 8.50 | 135 | −764.161678662 |
| 7.50 | 15 | −764.155602452 | 8.50 | 150 | −764.159000474 |
| 7.50 | 30 | −764.159875122 | 8.50 | 165 | −764.154647892 |
| 7.50 | 45 | −764.162736155 | 8.50 | 180 | −764.149871103 |
| 7.50 | 60 | −764.164217034 | 9.00 | 0 | −764.156611173 |
| 7.50 | 75 | −764.164677364 | 9.00 | 15 | −764.158420542 |
| 7.50 | 90 | −764.164437410 | 9.00 | 30 | −764.161094255 |

He + NaK($A^1\Sigma^+$) potential calculations continued

| $R_d$ | $\theta$ | Energy | $R_d$ | $\theta$ | Energy |
|---|---|---|---|---|---|
| 9.00 | 45 | −764.163101148 | 12.00 | 30 | −764.163535088 |
| 9.00 | 60 | −764.164190439 | 12.00 | 45 | −764.164087198 |
| 9.00 | 75 | −764.164567968 | 12.00 | 60 | −764.164386024 |
| 9.00 | 90 | −764.164540703 | 12.00 | 75 | −764.164487757 |
| 9.00 | 105 | −764.164273639 | 12.00 | 90 | −764.164496999 |
| 9.00 | 120 | −764.163702631 | 12.00 | 105 | −764.164478843 |
| 9.00 | 135 | −764.162538997 | 12.00 | 120 | −764.164440972 |
| 9.00 | 150 | −764.160557671 | 12.00 | 135 | −764.164349981 |
| 9.00 | 165 | −764.158067863 | 12.00 | 150 | −764.164157949 |
| 9.00 | 180 | −764.156302115 | 12.00 | 165 | −764.163895685 |
| 10.00 | 0 | −764.159141614 | 12.00 | 180 | −764.163765473 |
| 10.00 | 15 | −764.160183209 | 15.00 | 0 | −764.164197693 |
| 10.00 | 30 | −764.162027804 | 15.00 | 15 | −764.164240185 |
| 10.00 | 45 | −764.163475110 | 15.00 | 30 | −764.164331795 |
| 10.00 | 60 | −764.164253020 | 15.00 | 45 | −764.164410639 |
| 10.00 | 75 | −764.164525265 | 15.00 | 60 | −764.164450159 |
| 10.00 | 90 | −764.164535621 | 15.00 | 75 | −764.164460186 |
| 10.00 | 105 | −764.164420095 | 15.00 | 90 | −764.164459528 |
| 10.00 | 120 | −764.164160169 | 15.00 | 105 | −764.164460515 |
| 10.00 | 135 | −764.163607749 | 15.00 | 120 | −764.164466982 |
| 10.00 | 150 | −764.162587885 | 15.00 | 135 | −764.164476303 |
| 10.00 | 165 | −764.161373906 | 15.00 | 150 | −764.164481090 |
| 10.00 | 180 | −764.160817566 | 15.00 | 165 | −764.164479331 |
| 11.00 | 0 | −764.161191065 | 15.00 | 180 | −764.164478512 |
| 11.00 | 15 | −764.161762464 | 17.50 | 0 | −764.164418537 |
| 11.00 | 30 | −764.162891602 | 17.50 | 15 | −764.164424523 |
| 11.00 | 45 | −764.163823530 | 17.50 | 30 | −764.164437085 |
| 11.00 | 60 | −764.164326330 | 17.50 | 45 | −764.164447106 |
| 11.00 | 75 | −764.164502047 | 17.50 | 60 | −764.164451177 |
| 11.00 | 90 | −764.164517002 | 17.50 | 75 | −764.164451405 |
| 11.00 | 105 | −764.164469578 | 17.50 | 90 | −764.164450898 |
| 11.00 | 120 | −764.164361859 | 17.50 | 105 | −764.164451721 |
| 11.00 | 135 | −764.164122129 | 17.50 | 120 | −764.164455307 |
| 11.00 | 150 | −764.163656223 | 17.50 | 135 | −764.164462915 |
| 11.00 | 165 | −764.163049838 | 17.50 | 150 | −764.164473878 |
| 11.00 | 180 | −764.162763894 | 17.50 | 165 | −764.164483739 |
| 11.00 | 190 | −764.162895630 | 17.50 | 180 | −764.164487751 |
| 12.00 | 0 | −764.162581381 | 20.00 | 0 | −764.164447584 |
| 12.00 | 15 | −764.162890109 | 20.00 | 30 | −764.164448973 |

He + NaK($A^1\Sigma^+$) potential calculations continued

| $R_d$ | $\theta$ | Energy | $R_d$ | $\theta$ | Energy |
|---|---|---|---|---|---|
| 20.00 | 60 | −764.164449392 | 25.00 | 0 | −764.164448717 |
| 20.00 | 90 | −764.164448979 | 25.00 | 30 | −764.164448584 |
| 20.00 | 120 | −764.164450161 | 25.00 | 60 | −764.164448375 |
| 20.00 | 150 | −764.164457075 | 25.00 | 90 | −764.164448302 |
| 20.00 | 180 | −764.164464940 | 25.00 | 120 | −764.164448405 |
| 22.50 | 0 | −764.164449217 | 25.00 | 150 | −764.164448731 |
| 22.50 | 30 | −764.164449041 | 25.00 | 180 | −764.164449094 |
| 22.50 | 60 | −764.164448655 | 27.50 | 0 | −764.164448419 |
| 22.50 | 90 | −764.164448490 | 27.50 | 90 | −764.164448211 |
| 22.50 | 120 | −764.164448779 | 27.50 | 180 | −764.164448451 |
| 22.50 | 150 | −764.164450321 | 30.00 | 0 | −764.164448275 |
| 22.50 | 180 | −764.164452409 | 30.00 | 90 | −764.164448163 |
| 23.00 | 0 | −764.164449123 | 30.00 | 180 | −764.164448278 |
| 23.00 | 90 | −764.164448439 | 35.00 | 180 | −764.164448158 |
| 23.00 | 180 | −764.164451279 | 10000.00 | 0 | −764.164448090 |

# Appendix E

# Seven Term Legendre Expansion of the Excited State Potential

**Table E.1:** He + NaK($A^1\Sigma^+$) Legendre Expansion coefficients $v_0, v_1$, and $v_2$

| $R_\mathrm{d}$ | $v_0$ | $v_1$ | $v_2$ |
|---|---|---|---|
| 0.00 | 0.3791020000 | 0.5150490000 | 1.1346800000 |
| 1.00 | 0.3027648000 | 0.4049490000 | 0.9051280000 |
| 2.00 | 0.2264276000 | 0.2948490000 | 0.6755760000 |
| 3.00 | 0.1500904000 | 0.1847490000 | 0.4460240000 |
| 4.00 | 0.0737529195 | 0.0746499023 | 0.2164716187 |
| 4.50 | 0.0391627240 | 0.0256532955 | 0.1123612495 |
| 5.00 | 0.0202740389 | 0.0029588841 | 0.0553033347 |
| 6.00 | 0.0072220843 | −0.0052214612 | 0.0178501624 |
| 7.00 | 0.0038028693 | −0.0041674295 | 0.0096254858 |
| 8.00 | 0.0022245861 | −0.0018495802 | 0.0059538173 |
| 9.00 | 0.0013179394 | −0.0003651797 | 0.0037775826 |
| 10.00 | 0.0007590401 | 0.0002256353 | 0.0023385016 |
| 11.00 | 0.0003997655 | 0.0003330692 | 0.0013139881 |
| 12.00 | 0.0001928142 | 0.0002754035 | 0.0006878960 |
| 15.00 | 0.0000059583 | 0.0000671890 | 0.0000596930 |
| 17.50 | −0.0000050975 | 0.0000165188 | −0.0000031980 |
| 20.00 | −0.0000024883 | 0.0000036815 | −0.0000040369 |
| 22.50 | −0.0000008724 | 0.0000006006 | −0.0000012193 |
| 25.00 | −0.0000003589 | 0.0000000765 | −0.0000003448 |
| 26.25 | −2.575553400E−07 | 3.778056645E−08 | −2.285868051E−07 |
| 27.5625 | −1.867291719E−07 | 1.892333984E−08 | −1.528074470E−07 |
| 28.940625 | −1.356428883E−07 | 7.847195448E−09 | −1.020014948E−07 |
| 30.38765625 | −9.871633702E−08 | 1.609416309E−09 | −6.797556817E−08 |
| 31.9070390625 | −7.196987724E−08 | −1.673079405E−09 | −4.521526956E−08 |
| 33.502391015625 | −5.255861802E−08 | −3.193748209E−09 | −3.001152344E−08 |

He + NaK($A^1\Sigma^+$) Legendre Expansion coefficients $v_0, v_1$, and $v_2$ continued

| $R_\mathrm{d}$ | $v_0$ | $v_1$ | $v_2$ |
|---|---|---|---|
| 35.1775105664063 | −3.844411290E−08 | −3.699859797E−09 | −1.987125761E−08 |
| 36.9363860947266 | −2.816240420E−08 | −3.652043220E−09 | −1.312002899E−08 |
| 38.7832053994629 | −2.065975390E−08 | −3.328376869E−09 | −8.634184280E−09 |
| 40.7223656694361 | −1.517603326E−08 | −2.891932549E−09 | −5.660410844E−09 |
| 42.7584839529079 | −1.116174674E−08 | −2.434321883E−09 | −3.694224807E−09 |
| 44.8964081505533 | −8.218848755E−09 | −2.003550887E−09 | −2.398192074E−09 |
| 47.1412285580809 | −6.058431256E−09 | −1.621664654E−09 | −1.546924081E−09 |
| 49.498289985985 | −4.470402312E−09 | −1.295788258E−09 | −9.901077135E−10 |
| 51.9732044852842 | −3.301707810E−09 | −1.024926799E−09 | −6.276757142E−10 |
| 54.5718647095484 | −2.440654067E−09 | −8.040658356E−10 | −3.931452358E−10 |
| 57.3004579450259 | −1.805597578E−09 | −6.265720334E−10 | −2.424483106E−10 |
| 60.1654808422772 | −1.336768073E−09 | −4.855384281E−10 | −1.464521626E−10 |
| 63.173754884391 | −9.903446945E−10 | −3.744863163E−10 | −8.595657503E−11 |
| 66.3324426286106 | −7.341560160E−10 | −2.876846345E−10 | −4.835261913E−11 |
| 69.6490647600411 | −5.445528446E−10 | −2.202499509E−10 | −2.539451335E−11 |
| 73.1315179980432 | −4.041298406E−10 | −1.681274513E−10 | −1.171642470E−11 |
| 76.7880938979453 | −3.000627023E−10 | −1.280133778E−10 | −3.847159052E−12 |
| 80.6274985928426 | −2.228926251E−10 | −9.725425873E−11 | 4.428726449E−13 |

**Table E.2:** He + NaK($A^1\Sigma^+$) Legendre Expansion coefficients $v_3, v_4, v_5$, and $v_6$

| $R_\mathrm{d}$ | $v_3$ | $v_4$ | $v_5$ | $v_6$ |
|---|---|---|---|---|
| 0.00 | 0.4868470000 | 0.6607750000 | 0.1140710000 | 0.1418930000 |
| 1.00 | 0.3854690000 | 0.5265710000 | 0.0905770000 | 0.1131407000 |
| 2.00 | 0.2840910000 | 0.3923670000 | 0.0670830000 | 0.0843884000 |
| 3.00 | 0.1827130000 | 0.2581630000 | 0.0435890000 | 0.0556361000 |
| 4.00 | 0.0813354325 | 0.1239573027 | 0.0200949957 | 0.0268835796 |
| 4.50 | 0.0357633580 | 0.0628849036 | 0.0094578554 | 0.0137442818 |
| 5.00 | 0.0127009336 | 0.0286907182 | 0.0037967392 | 0.0061705950 |
| 6.00 | 0.0012926405 | 0.0071243664 | 0.0009589151 | 0.0013683213 |
| 7.00 | −0.0009946294 | 0.0036328591 | −0.0000778236 | 0.0008194833 |
| 8.00 | −0.0005234702 | 0.0021735716 | −0.0001756767 | 0.0003809178 |
| 9.00 | 0.0001415927 | 0.0014702233 | −0.0000079276 | 0.0002443900 |
| 10.00 | 0.0003927310 | 0.0010256231 | 0.0001056743 | 0.0002381057 |
| 11.00 | 0.0003596443 | 0.0005983027 | 0.0000825710 | 0.0001504481 |
| 12.00 | 0.0002636643 | 0.0003195699 | 0.0000503179 | 0.0000712156 |
| 15.00 | 0.0000604454 | 0.0000380450 | 0.0000121636 | 0.0000063318 |
| 17.50 | 0.0000148894 | 0.0000023746 | 0.0000031494 | 0.0000008384 |
| 20.00 | 0.0000036148 | −0.0000013596 | 0.0000013816 | −0.0000002871 |
| 22.50 | 0.0000006239 | −0.0000004868 | 0.0000003720 | −0.0000001450 |
| 25.00 | 0.0000000569 | −0.0000000841 | 0.0000000531 | −0.0000000257 |
| 26.25 | 2.241514245E−08 | −4.735776560E−08 | 2.613409309E−08 | −1.673798037E−08 |
| 27.5625 | 7.538090571E−09 | −2.281023314E−08 | 1.110949696E−08 | −8.883350256E−09 |
| 28.940625 | 2.400585573E−09 | −1.059266337E−08 | 4.524865797E−09 | −4.567664578E−09 |
| 30.38765625 | 7.219810926E−10 | −4.733957879E−09 | 1.762027073E−09 | −2.271786392E−09 |
| 31.9070390625 | 2.044771995E−10 | −2.032144421E−09 | 6.545454297E−10 | −1.091124852E−09 |
| 33.502391015625 | 5.437132364E−11 | −8.362213623E−10 | 2.314000100E−10 | −5.051923309E−10 |

He + NaK($A^1\Sigma^+$) Legendre Expansion coefficients $v_3, v_4, v_5$, and $v_6$ continued

| $R_\mathrm{d}$ | $v_3$ | $v_4$ | $v_5$ | $v_6$ |
|---|---|---|---|---|
| 35.1775105664063 | 1.353103988E−11 | −3.291594145E−10 | 7.766192140E−11 | −2.250702875E−10 |
| 36.9363860947266 | 3.141163235E−12 | −1.236646451E−10 | 2.467999836E−11 | −9.629919421E−11 |
| 38.7832053994629 | 6.778565610E−13 | −4.424118933E−11 | 7.406089768E−12 | −3.949047567E−11 |
| 40.7223656694361 | 1.354838306E−13 | −1.503443437E−11 | 2.092642346E−12 | −1.548836456E−11 |
| 42.7584839529079 | 2.498472729E−14 | −4.840724969E−12 | 5.550809829E−13 | −5.796881460E−12 |
| 44.8964081505533 | 4.234002567E−15 | −1.472735953E−12 | 1.377846239E−13 | −2.065583328E−12 |
| 47.1412285580809 | 6.565706210E−16 | −4.221823704E−13 | 3.189975750E−14 | −6.990100741E−13 |
| 49.498289985985 | 9.275520531E−17 | −1.136957050E−13 | 6.864411965E−15 | −2.240764347E−13 |
| 51.9732044852842 | 1.188223066E−17 | −2.867478842E−14 | 1.367918098E−15 | −6.785854980E−14 |
| 54.5718647095484 | 1.373522096E−18 | −6.750628266E−15 | 2.514720309E−16 | −1.935857485E−14 |
| 57.3004579450259 | 1.425345687E−19 | −1.478360545E−15 | 4.247572130E−17 | −5.186873188E−15 |
| 60.1654808422772 | 1.320714631E−20 | −3.000808919E−16 | 6.564087924E−18 | −1.301186326E−15 |
| 63.173754884391 | 1.086531225E−21 | −5.624309602E−17 | 9.239738881E−19 | −3.046106228E−16 |
| 66.3324426286106 | 7.889275007E−23 | −9.694862202E−18 | 1.179150588E−19 | −6.631638984E−17 |
| 69.6490647600411 | 5.024371261E−24 | −1.530515326E−18 | 1.357607800E−20 | −1.337797866E−17 |
| 73.1315179980432 | 2.788229912E−25 | −2.203172628E−19 | 1.402941718E−21 | −2.491142683E−18 |
| 76.7880938979453 | 1.339022220E−26 | −2.878524393E−20 | 1.294250078E−22 | −4.264882908E−19 |
| 80.6274985928426 | 5.524843063E−28 | −3.397014260E−21 | 1.059853160E−23 | −6.684840460E−20 |

# Appendix F

# Eleven Term Legendre Expansion of the Excited State Potential

**Table F.1:** He + NaK($A^1\Sigma^+$) Legendre Expansion coefficients $v_0, v_1$, and $v_2$

| $R_\mathrm{d}$ | $v_0$ | $v_1$ | $v_2$ |
|---|---|---|---|
| 0.00 | 1.970908951 | 1.573729205 | 4.884394840 |
| 0.50 | 1.379702505 | 1.396513401 | 3.542454719 |
| 1.00 | 0.965838124 | 1.219297597 | 2.569199634 |
| 1.50 | 0.676119147 | 1.042081793 | 1.863336946 |
| 2.00 | 0.473306127 | 0.864865989 | 1.351403188 |
| 2.50 | 0.331330196 | 0.687650185 | 0.980118266 |
| 3.00 | 0.2319244726 | 0.5104343807 | 0.7108402758 |
| 3.50 | 0.1623673861 | 0.3332185767 | 0.5155438026 |
| 4.00 | 0.1014359127 | 0.1740757173 | 0.3290632033 |
| 4.50 | 0.0638964486 | 0.0764759706 | 0.2128906954 |
| 5.00 | 0.0429741037 | 0.0064158083 | 0.1485850975 |
| 5.50 | 0.0237748487 | −0.0115606326 | 0.0804610623 |
| 6.00 | 0.0127856425 | −0.0125474047 | 0.0410240143 |
| 6.50 | 0.0072862163 | −0.0090085719 | 0.0218442633 |
| 7.00 | 0.0048792352 | −0.0067718974 | 0.0143315280 |
| 7.50 | 0.0035458709 | −0.0046703836 | 0.0104634930 |
| 8.00 | 0.0024204847 | −0.0022438364 | 0.0068541771 |
| 9.00 | 0.0013519607 | −0.0003510845 | 0.0039353686 |
| 10.00 | 0.0007598704 | 0.0002275100 | 0.0023426897 |
| 11.00 | 0.0003995043 | 0.0003317808 | 0.0013124803 |
| 12.00 | 0.0001927025 | 0.0002751036 | 0.0006872471 |
| 15.00 | 0.0000059593 | 0.0000671159 | 0.0000596835 |
| 17.50 | −0.0000050965 | 0.0000165170 | −0.0000031902 |
| 20.00 | −0.0000024883 | 0.0000036815 | −0.0000040369 |
| 22.50 | −0.0000008724 | 0.0000006006 | −0.0000012193 |

He + NaK($A^1\Sigma^+$) Legendre Expansion coefficients $v_0, v_1$, and $v_2$ continued

| $R_\mathrm{d}$ | $v_0$ | $v_1$ | $v_2$ |
|---|---|---|---|
| 25.00 | −0.0000003589 | 0.0000000765 | −0.0000003448 |
| 26.25 | −2.575553400E−07 | 3.778056645E−08 | −2.285868051E−07 |
| 27.5625 | −1.867291719E−07 | 1.892333984E−08 | −1.528074470E−07 |
| 28.940625 | −1.356428883E−07 | 7.847195448E−09 | −1.020014948E−07 |
| 30.38765625 | −9.871633702E−08 | 1.609416309E−09 | −6.797556817E−08 |
| 31.9070390625 | −7.196987724E−08 | −1.673079405E−09 | −4.521526956E−08 |
| 33.502391015625 | −5.255861802E−08 | −3.193748209E−09 | −3.001152344E−08 |
| 35.1775105664063 | −3.844411290E−08 | −3.699859797E−09 | −1.987125761E−08 |
| 36.9363860947266 | −2.816240420E−08 | −3.652043220E−09 | −1.312002899E−08 |
| 38.7832053994629 | −2.065975390E−08 | −3.328376869E−09 | −8.634184280E−09 |
| 40.7223656694361 | −1.517603326E−08 | −2.891932549E−09 | −5.660410844E−09 |
| 42.7584839529079 | −1.116174674E−08 | −2.434321883E−09 | −3.694224807E−09 |
| 44.8964081505533 | −8.218848755E−09 | −2.003550887E−09 | −2.398192074E−09 |
| 47.1412285580809 | −6.058431256E−09 | −1.621664654E−09 | −1.546924081E−09 |
| 49.4982899859850 | −4.470402312E−09 | −1.295788258E−09 | −9.901077135E−10 |
| 51.9732044852842 | −3.301707810E−09 | −1.024926799E−09 | −6.276757142E−10 |
| 54.5718647095484 | −2.440654067E−09 | −8.040658356E−10 | −3.931452358E−10 |
| 57.3004579450259 | −1.805597578E−09 | −6.265720334E−10 | −2.424483106E−10 |
| 60.1654808422772 | −1.336768073E−09 | −4.855384281E−10 | −1.464521626E−10 |
| 63.1737548843910 | −9.903446945E−10 | −3.744863163E−10 | −8.595657503E−11 |
| 66.3324426286106 | −7.341560160E−10 | −2.876846345E−10 | −4.835261913E−11 |
| 69.6490647600411 | −5.445528446E−10 | −2.202499509E−10 | −2.539451335E−11 |
| 73.1315179980432 | −4.041298406E−10 | −1.681274513E−10 | −1.171642470E−11 |
| 76.7880938979453 | −3.000627023E−10 | −1.280133778E−10 | −3.847159052E−12 |
| 80.6274985928426 | −2.228926251E−10 | −9.725425873E−11 | 4.428726449E−13 |

**Table F.2:** He + NaK($A^1\Sigma^+$) Legendre Expansion coefficients $v_3, v_4, v_5$, and $v_6$

| $R_\mathrm{d}$ | $v_3$ | $v_4$ | $v_5$ | $v_6$ |
|---|---|---|---|---|
| 0.00 | 1.651715733 | 2.242581415 | 1.698092482 | 0.504458200 |
| 0.50 | 1.474029576 | 1.730909667 | 1.248374731 | 0.419232567 |
| 1.00 | 1.296343420 | 1.335981943 | 0.917758888 | 0.348405368 |
| 1.50 | 1.118657264 | 1.031161699 | 0.674702360 | 0.289544063 |
| 2.00 | 0.940971107 | 0.795889835 | 0.496016198 | 0.240627074 |
| 2.50 | 0.763284951 | 0.614298059 | 0.364652747 | 0.199974360 |
| 3.00 | 0.5855987942 | 0.4741386161 | 0.2680792002 | 0.1661897148 |
| 3.50 | 0.4079126377 | 0.3659582251 | 0.1970819039 | 0.1381128123 |
| 4.00 | 0.2261640343 | 0.2466347057 | 0.1116267838 | 0.1017220801 |
| 4.50 | 0.1090008615 | 0.1724437478 | 0.0545536999 | 0.0811488452 |
| 5.00 | 0.0130236222 | 0.1329837344 | −0.0030618848 | 0.0730510036 |
| 5.50 | −0.0100700654 | 0.0712857035 | −0.0124095245 | 0.0404033637 |
| 6.00 | −0.0111913164 | 0.0337736686 | −0.0096908083 | 0.0190578484 |
| 6.50 | −0.0070050327 | 0.0157497698 | −0.0052062189 | 0.0087480255 |
| 7.00 | −0.0057631087 | 0.0097855865 | −0.0048397046 | 0.0060739118 |
| 7.50 | −0.0042158236 | 0.0069294198 | −0.0039110379 | 0.0045485634 |
| 8.00 | −0.0013134235 | 0.0034914514 | −0.0010932656 | 0.0017095498 |
| 9.00 | 0.0001692903 | 0.0017074066 | 0.0000223677 | 0.0004997645 |
| 10.00 | 0.0003964543 | 0.0010331881 | 0.0001021828 | 0.0002445439 |
| 11.00 | 0.0003557708 | 0.0005942760 | 0.0000680463 | 0.0001335551 |
| 12.00 | 0.0002627355 | 0.0003178810 | 0.0000466001 | 0.0000643104 |
| 15.00 | 0.0000602134 | 0.0000380317 | 0.0000112266 | 0.0000062622 |
| 17.50 | 0.0000148727 | 0.0000023721 | 0.0000030790 | 0.0000007614 |
| 20.00 | 0.0000036148 | −0.0000013596 | 0.0000013816 | −0.0000002871 |
| 22.50 | 0.0000006239 | −0.0000004868 | 0.0000003720 | −0.0000001450 |

He + NaK($A^1\Sigma^+$) Legendre Expansion coefficients $v_3, v_4, v_5$, and $v_6$ continued

| $R_\mathrm{d}$ | $v_3$ | $v_4$ | $v_5$ | $v_6$ |
|---|---|---|---|---|
| 25.00 | 0.0000000569 | −0.0000000841 | 0.0000000531 | −0.0000000257 |
| 26.25 | 2.241514245E−08 | −4.735776560E−08 | 2.613409309E−08 | −1.673798037E−08 |
| 27.5625 | 7.538090571E−09 | −2.281023314E−08 | 1.110949696E−08 | −8.883350256E−09 |
| 28.940625 | 2.400585573E−09 | −1.059266337E−08 | 4.524865797E−09 | −4.567664578E−09 |
| 30.38765625 | 7.219810926E−10 | −4.733957879E−09 | 1.762027073E−09 | −2.271786392E−09 |
| 31.9070390625 | 2.044771995E−10 | −2.032144421E−09 | 6.545454297E−10 | −1.091124852E−09 |
| 33.502391015625 | 5.437132364E−11 | −8.362213623E−10 | 2.314000100E−10 | −5.051923309E−10 |
| 35.1775105664063 | 1.353103988E−11 | −3.291594145E−10 | 7.766192140E−11 | −2.250702875E−10 |
| 36.9363860947266 | 3.141163235E−12 | −1.236646451E−10 | 2.467999836E−11 | −9.629919421E−11 |
| 38.7832053994629 | 6.778565610E−13 | −4.424118933E−11 | 7.406089768E−12 | −3.949047567E−11 |
| 40.7223656694361 | 1.354838306E−13 | −1.503443437E−11 | 2.092642346E−12 | −1.548836456E−11 |
| 42.7584839529079 | 2.498472729E−14 | −4.840724969E−12 | 5.550809829E−13 | −5.796881460E−12 |
| 44.8964081505533 | 4.234002567E−15 | −1.472735953E−12 | 1.377846239E−13 | −2.065583328E−12 |
| 47.1412285580809 | 6.565706210E−16 | −4.221823704E−13 | 3.189975750E−14 | −6.990100741E−13 |
| 49.4982899859850 | 9.275520531E−17 | −1.136957050E−13 | 6.864411965E−15 | −2.240764347E−13 |
| 51.9732044852842 | 1.188223066E−17 | −2.867478842E−14 | 1.367918098E−15 | −6.785854980E−14 |
| 54.5718647095484 | 1.373522096E−18 | −6.750628266E−15 | 2.514720309E−16 | −1.935857485E−14 |
| 57.3004579450259 | 1.425345687E−19 | −1.478360545E−15 | 4.247572130E−17 | −5.186873188E−15 |
| 60.1654808422772 | 1.320714631E−20 | −3.000808919E−16 | 6.564087924E−18 | −1.301186326E−15 |
| 63.1737548843910 | 1.086531225E−21 | −5.624309602E−17 | 9.239738881E−19 | −3.046106228E−16 |
| 66.3324426286106 | 7.889275007E−23 | −9.694862202E−18 | 1.179150588E−19 | −6.631638984E−17 |
| 69.6490647600411 | 5.024371261E−24 | −1.530515326E−18 | 1.357607800E−20 | −1.337797866E−17 |
| 73.1315179980432 | 2.788229912E−25 | −2.203172628E−19 | 1.402941718E−21 | −2.491142683E−18 |
| 76.7880938979453 | 1.339022220E−26 | −2.878524393E−20 | 1.294250078E−22 | −4.264882908E−19 |
| 80.6274985928426 | 5.524843063E−28 | −3.397014260E−21 | 1.059853160E−23 | −6.684840460E−20 |

**Table F.3:** He + NaK($A^1\Sigma^+$) Legendre Expansion coefficients $v_7$, $v_8$, $v_9$ and $v_{10}$

| $R_\mathrm{d}$ | $v_7$ | $v_8$ | $v_9$ | $v_{10}$ |
|---|---|---|---|---|
| 0.00 | 0.322551572 | 0.060310566 | 0.016126749 | 0.002869960 |
| 0.50 | 0.247108403 | 0.054440159 | 0.014638716 | 0.002866265 |
| 1.00 | 0.189311007 | 0.049141157 | 0.013150684 | 0.002862571 |
| 1.50 | 0.145032128 | 0.044357939 | 0.011662651 | 0.002858876 |
| 2.00 | 0.111109852 | 0.040040303 | 0.010174619 | 0.002855181 |
| 2.50 | 0.085121824 | 0.036142929 | 0.008686586 | 0.002851487 |
| 3.00 | 0.0652122633 | 0.0326249103 | 0.0071985533 | 0.0028477920 |
| 3.50 | 0.0499594473 | 0.0294493229 | 0.0057105207 | 0.0028440973 |
| 4.00 | 0.0280005224 | 0.0245279463 | 0.0030617179 | 0.0028187876 |
| 4.50 | 0.0129578163 | 0.0230103322 | 0.0011645935 | 0.0031387627 |
| 5.00 | −0.0070543815 | 0.0243944588 | −0.0022526737 | 0.0037956125 |
| 5.50 | −0.0080012761 | 0.0138912071 | −0.0020190665 | 0.0021690196 |
| 6.00 | −0.0052740954 | 0.0066257412 | −0.0012506485 | 0.0010280617 |
| 6.50 | −0.0026519159 | 0.0032870875 | −0.0006437310 | 0.0006107971 |
| 7.00 | −0.0031884739 | 0.0031469757 | −0.0012925042 | 0.0010882840 |
| 7.50 | −0.0028753700 | 0.0027160412 | −0.0013274098 | 0.0010466269 |
| 8.00 | −0.0007388221 | 0.0009811957 | −0.0002827605 | 0.0005302931 |
| 9.00 | 0.0000216427 | 0.0002300734 | −0.0000123103 | 0.0002482720 |
| 10.00 | 0.0000552730 | 0.0000588906 | 0.0000511085 | 0.0000275260 |
| 11.00 | 0.0000145218 | 0.0000280590 | 0.0000139717 | 0.0000032267 |
| 12.00 | 0.0000045677 | 0.0000116909 | 0.0000026649 | 0.0000008698 |
| 15.00 | 0.0000012583 | 0.0000003941 | 0.0000005428 | −0.0000003238 |
| 17.50 | 0.0000001355 | 0.0000001447 | −0.0000000045 | −0.0000000418 |
| 20.00 | 0 | 0 | 0 | 0 |
| 22.50 | 0 | 0 | 0 | 0 |

He + NaK($A^1\Sigma^+$) Legendre Expansion coefficients $v_7$, $v_8$, $v_9$ and $v_{10}$ continued

| $R_\mathrm{d}$ | $v_7$ | $v_8$ | $v_9$ | $v_{10}$ |
|---|---|---|---|---|
| 25.00 | 0 | 0 | 0 | 0 |
| 26.25 | 0 | 0 | 0 | 0 |
| 27.5625 | 0 | 0 | 0 | 0 |
| 28.940625 | 0 | 0 | 0 | 0 |
| 30.38765625 | 0 | 0 | 0 | 0 |
| 31.9070390625 | 0 | 0 | 0 | 0 |
| 33.502391015625 | 0 | 0 | 0 | 0 |
| 35.1775105664063 | 0 | 0 | 0 | 0 |
| 36.9363860947266 | 0 | 0 | 0 | 0 |
| 38.7832053994629 | 0 | 0 | 0 | 0 |
| 40.7223656694361 | 0 | 0 | 0 | 0 |
| 42.7584839529079 | 0 | 0 | 0 | 0 |
| 44.8964081505533 | 0 | 0 | 0 | 0 |
| 47.1412285580809 | 0 | 0 | 0 | 0 |
| 49.4982899859850 | 0 | 0 | 0 | 0 |
| 51.9732044852842 | 0 | 0 | 0 | 0 |
| 54.5718647095484 | 0 | 0 | 0 | 0 |
| 57.3004579450259 | 0 | 0 | 0 | 0 |
| 60.1654808422772 | 0 | 0 | 0 | 0 |
| 63.1737548843910 | 0 | 0 | 0 | 0 |
| 66.3324426286106 | 0 | 0 | 0 | 0 |
| 69.6490647600411 | 0 | 0 | 0 | 0 |
| 73.1315179980432 | 0 | 0 | 0 | 0 |
| 76.7880938979453 | 0 | 0 | 0 | 0 |
| 80.6274985928426 | 0 | 0 | 0 | 0 |

# Bibliography


[1] S. Ashman, B. McGeehan, C. M. Wolfe, C. Faust, K. Richter, J. Jones, A. P. Hickman, and J. Huennekens, "Experimental studies of the NaCs $5^3\Pi_0$ and $1(a)^3\Sigma^+$ states", J. Chem. Phys. **136**, 114313 (2012).

[2] C. M. Wolfe, S. Ashman, J. Bai, B. Beser, E. H. Ahmed, A. M. Lyyra, and J. Huennekens, "Collisional transfer of population and orientation in NaK", The J. Chem. Phys. **134**, 174301 (2011).

[3] S. J. Sweeney, E. Ahmed, P. Qi, T. Kirova, A. M. Lyyra, and J. Huennekens, "Measurement of absolute transition dipole moment functions of the $3^1\Pi \rightarrow 1(X)^1\Sigma^+$ and $3^1\Pi \rightarrow 2(A)^1\Sigma^+$ transitions in NaK using Autler-Townes spectroscopy and calibrated fluorescence", J. Chem. Phys. **129**, 154303 (2008).

[4] L. Morgus, P. Burns, R. D. Miles, A. D. Wilkins, U. Ogba, A. P. Hickman, and J. Huennekens, "Experimental study of the NaK $3^3\Pi$ double minimum state", J. Chem. Phys. **122**, 144313 (2005).

[5] P. Burns, A. D. Wilkins, A. P. Hickman, and J. Huennekens, "The NaK $1(b)^3\Pi_{\Omega=0}$ state hyperfine structure and the $1(b)^3\Pi_{\Omega=0} \sim 2(A)^1\Sigma^+$ spin-orbit interaction", J. Chem. Phys. **122**, 074306 (2005).

[6] P. Burns, L. Sibbach-Morgus, A. D. Wilkins, F. Halpern, L. Clarke, R. D. Miles, L. Li, A. P. Hickman, and J. Huennekens, "The $4^3\Sigma^+$ state of NaK: Potential energy curve and hyperfine structure", J. Chem. Phys. **119**, 4743–4754 (2003).

[7] G. Herzberg, *Molecular Spectra and Molecular Structure I. Spectra of Diatomic Molecules* (D. Van Nostrand Company, Inc., New York, NY, 1950).

[8] P. D. Magill, B. Stewart, N. Smith, and D. E. Pritchard, "Dynamics of Quasiresonant Vibration-Rotation Transfer in Atom-Diatom Scattering", Phys. Rev. Lett. **60**, 1943–1946 (1988).

[9] T. A. Brunner and D. Pritchard, in *Fitting Laws for Rotationally Inelastic Collisions*, Vol. 50 of *Advances in Chemical Physics*, edited by K. P. Lawley (John Wiley & Sons, Inc., New York, 1982), pp. 589–641.

[10] W. Demtröder, *Laser spectroscopy, Volume 2 Experimental Techniques*, 4th ed. (Springer-Verlag, Berlin, 2008).

[11] M. Rowe and A. McCaffery, "Transfer of state multipoles in excited $A^1\Sigma_u^+$ $^7Li_2$ following rotationally inelastic collisions with He: Experiment and theory", Chemical Physics **43**, 35 – 54 (1979).

[12] C. H. Greene and R. N. Zare, "Photofragment Alignment and Orientation", Ann. Rev. Phys. Chem. **33**, 119–150 (1982).

[13] E. Merzbacher, *Quantum Mechanics*, 3rd ed. (John Wiley & Sons Inc., New York, NY, 1988).

[14] M. W. Schmidt *et al.*, "General atomic and molecular electronic structure system", J. Comp. Chem. **104**, 1347–1363 (1993).

[15] W. J. Hehre, L. Radom, P. v.R. Schleyer, and J. A. Pople, *Ab Initio Molecular Theory* (Hohn Wiley & Sons, Inc., New York, NY, 1986).

[16] W. A. Harrison, *Electronic Structure and the Properties of Solids: The Physics of the Chemical Bond* (W. H. Freeman and Company, San Francisco, CA, 1980).

[17] J. A. Pople and D. L. Beveridge, *Approximate Molecular Orbital Theory* (McGraw-Hill Book Company, New York, NY, 1970).

[18] D. A. McQuarrie, *Quantum Chemistry* (University Science Books, Mill Valley, CA, 1983).

[19] J. Jones and J. Huennekens, personal communication, 2012.

[20] M. J. Frisch, J. A. Pople, and J. S. Binkley, "Self-Consistent Molecular Orbital Methods. 25. Supplementary Functions for Gaussian Basis Sets", J. Chem. Phys **80**, 3265–3269 (1984).

[21] A. D. McLean and G. S. Chandler, "Contracted Gaussian-basis sets for molecular calculations. 1. 2nd row atoms, Z=11-18", J. Chem. Phys. **72**, 5639–5648 (1980).

[22] J. P. Blaudeau, M. P. McGrath, L. A. Curtiss, and L. Radom, "Extension of Gaussian-2 (G2) theory to molecules containing third-row atoms K and Ca", J. Chem. Phys. **107**, 5016–5021 (1997).

[23] I. Russier-Antoine, A. J. Ross, M. Aubert-Frécon, F. Marin, and P. Crozet, "An improved energy curve for the ground state of NaK", J. Phys. B **33**, 2753–2762 (2000).

[24] L. F. Shampine, S. M. Davenport, and R. E. Huddleston, DPOLFT: Curve fitting by polynomials in one variable, netlib.org, 1974, url: http://www.netlib.org/slatec/src/dpolft.f.

[25] R. F. Malenda, LegInterp.cpp, 2009, computer code written to solve a set of linear algebraic equations to find the Legendre expansion coefficients.

[26] I. S. Gradshteyn and I. M. Ryzhik, in *Tables of Integrals, Series and Products*, sixth ed., edited by A. Jeffrey and D. Zwillinger (Academic Press, San Diego, 2000).

[27] A. Ross, R. Clements, and R. Barrow, "The $A(2)^1\Sigma^+$ State of NaK", J. of Molecular Spectroscopy **127**, 546–548 (1988).

[28] A. M. Arthurs and A. Dalgarno, "Theory of scattering by a rigid rotor", Proc. Roy. Soc. (London) Series A, Mathematical and Physical Sciences **256**, 540–551 (1960).

[29] A. Messiah, *Quantum Mechanics* (John Wiley & Sons, Inc., New York, NY, 1968), Vol. One.

[30] I. C. Percival and M. J. Seaton, Proc. Camb. Phil. Soc. **53**, 654–9 (1957).

[31] G. Grawert, "Zur Theorie der Stoße angeregte Alkaliatome mit Edelgasatomen [On the theory of the scattering of excited alkali atoms by inert gas atoms]", Z. Phys. **225**, 283–292 (1969).

[32] M. H. Alexander and S. L. Davis, "$M$ dependence in rotationally inelastic scattering in cell experiments: Implications of an irreducible tensor expansion for molecules in $^1\Sigma$ electronic states", J. Chem. Phys. **78**, 6754–6762 (1983).

[33] A. R. Edmonds, *Angular Momentum in Quantum Mechanics* (Princeton University Press, Princeton, N. J., 1957).

[34] J. Derouard, "Reorientation, polarization and scaling laws in rotational transfer experiments", Chem. Phys. **84**, 181–192 (1983).

[35] A. P. Hickman, D. L. Huestis, and R. P. Saxon, "Calculations of inelastic collisions of excited states of Xe with He and Ar", J. Chem. Phys. **98**, 5419 (1993).

[36] R. Goldflam, S. Green, and D. J. Kouri, "Infinite order sudden approximation for rotational energy transfer in gaseous mixtures", J. Chem. Phys **67**, 4149–4161 (1977).

[37] M. H. Beck, A. Jäckele, G. A. Worth, and H.-D. Meyer, "The multiconfiguration time-dependent hartree (MCTDH) method: A highly efficient algorithm for propogating wavepackets", Physics Reports **324**, 1–105 (2000).

[38] H.-D. Meyer, F. Gatti, and G. A. Worth, *Multidimensional Quantum Dynamics: MCTDH Theory and Applications* (Wiley-VCH Verlag GmbH & Co., Weinheim, 2009).

[39] H.-D. Meyer and G. A. Worth, "The multi-configuration time-dependent Hartree (MCTDH) algorithm: an efficient method for propagating wavepackets of several dimensions", Submitted to the Collaborative Computational Project Number 6 on Molecular Quantum Dynamics Workshop on Time-Dependent Quantum Dynamics, Bristol (2001).

[40] S. Sukiasyana and H.-D. Meyer, "Reaction cross sections for the H+$D_2(v_0 = 1)$ and D+$H2_2(v_0 = 1)$. A multiconfiguration time-dependent Hartree (MCTDH) wave packet propagation study", J. Chem. Phys. **116**, 10641 (2002).

[41] P. M. Weiser, A. K. Fragale, and A. P. Hickman, personal communication, 2012.

# Ruth Fraser Malenda


**Contact Information**

Department of Physics
Lehigh University
16 Memorial Dr. E.
Bethlehem, PA 18015 USA

*Voice:* (610) 246-5801 *cell*
*Fax:* (610)758-5730
*Voice:* (610) 758-3963 *office*
*E-mail:* rfm206@lehigh.edu


**Education**

**Lehigh University**, Bethlehem, Pennsylvania

**Ph.D.,** Theoretical Atomic and Molecular Physics, Expected July 2012
*Dissertation: Rotationally Inelastic Collisions of Helium with NaK molecules*
Advisor: A. P. Hickman

**M. S.,** Physics, September 2009

**Kutztown University**, Kutztown, Pennsylvania

**B.S.,** Physics, May 2007 (*Summa Cum Laude*)
**B.S.,** Mathematics, May 2007 (*Summa Cum Laude*)

**Honors and Awards**

**National Science Foundation**

GK-12 Teaching Fellow, August 2007–July 2009

**Kutztown University of Pennsylvania**, Kutztown, Pennsylvania

President of the Society of Physics Students (SPS), 2006–2007
Sigma Pi Sigma ($\Sigma\Pi\Sigma$) National Honor Society, April 2005
Kappa Mu Epsilon ($KME$) National Honor Society, April 2005
Dean's List Honor Roll for entire undergraduate career

**Professional Organizations**

American Association of Physics Teachers Member, May 2011
American Physical Society, December 2006
Society of Physics Students, December 2004

**Teaching Interests**

Teaching introductory physics, for both majors and non-majors, as well as higher level courses. Organizing student clubs such as SPS and $\Sigma\Pi\Sigma$ that give leadership and mentorship opportunities to physics majors. Particular interest in developing mentoring and tutoring programs with other students and possibly neighboring high schools.

**Teaching Experience**

**Lehigh University**, Bethlehem, Pennsylvania

*Teaching Assistant* **September 2009–Present**

➢ PHY-021 Introductory Physics II (second semester physics for science and engineering students) recitations. Held two 50 minute classes of $20-25$ students, twice weekly. Reviewed and clarified course materials, wrote and graded weekly quizzes, held office hours, met with students to answer questions, held review sessions before mid-term and final exams. Wrote and graded exam questions. Utilized MasteringPhysics and WileyPLUS in conjunction with textbooks for web based homework.

*GK-12 STEM Graduate Teaching Fellow* **August 2007–July 2009**

➢ Presented graduate level research to a variety of audiences including middle school students, physics undergraduates, and other graduate fellows of a variety of backgrounds. Met weekly with students in first, fourth and sixth grades for science class. Tailored prepackaged lesson kits to meet the learning and developmental needs of students, taught physics related lessons, wrote and administered evaluations of students' understanding. Assisted with grant renewal process by providing reports.

**Teaching Experience Continued**

*Research Experience for Undergraduates (REU) Teaching Assistant* **Summer 2011**

➢ Mentored and advised REU students. Welcomed and oriented students, assisted in opening student computer accounts, presented Lehigh University chemical, fire and lab safety protocols, and organized trips and activities.

**Kutztown University**, Kutztown, Pennsylvania

*Supplemental Instructor* **January 2006–May 2007**

➢ PHY 100 and 102 Introductory Physics for Science and Engineering Majors supplemental instructor. Provided one-on-one and group tutoring, organized lesson plans and study sessions, detailed examples of concepts, created study guides, handouts and equations tables.

*Tutor* **September 2005–May 2007**

➢ Introductory Mathematics and Physics, Calculus III and IV. Met with students one-on-one and in groups, developed problem solving skills, applied concepts to real life problems in students' individual fields.

**Research Interests**

Theoretical Atomic and Molecular Physics. Implementation of electronic structure calculations for polyatomic molecules, wavepacket propagation and coupled channel methods to study dissociative recombination of molecular ions with electrons; the change in rotational states of a molecule during collision with an atomic partner. Experience with Windows, Linux, C++, Fortran, BASH scripting, LaTEX, and running on TeraGrid supercomputers.

**Research Experience**

**Lehigh University**, Bethlehem, Pennsylvania USA

*Research Assistant* **August 2009 – present**

➢ **Advisor:** A. P. Hickman, Lehigh University
Ph.D. research. Implemented General Atomic & Molecular Electronic Structure System (GAMESS) program for electronic structure calculations and Multiconfiguration Time-Dependent Hartree (MCTDH) program to perform wavepacket propagation calculations. These methods were used to study the dissociative recombination (DR) of electrons with the $N_2H^+$ molecular ion and the changes in the angular momentum of the NaK molecule due to collision with an atomic partner. Created scripts and programs to run on the TeraGrid supercomputing resources. Extensive use of C++ and BASH scripting to analyze, fit and sort data.

*Graduate Research Project* **Summer 2008**

➢ **Advisor:** A. P. Hickman, Lehigh University
Investigated the DR of an electron with the $HCNH^+$ molecular ion. Developed approximate analytic solutions of the normal modes of the HCNH molecule. Wrote code to simulate the motion of the atoms based on these solutions and compared them to exact solutions. Also, used program to investigate the overlap of the $HCNH^+$ and HCNH wavefunctions.

*Summer Research Project* **Summer 2007**

➢ **Advisor:** A. P. Hickman, Lehigh University
Investigated the normal modes of the c-$C_3H_3^+$molecule as they pertained to DR. Implemented Visual Molecular Dynamics (VMD) code to visualize and aid in understanding of the motion of the molecule.

*Research Experience for Undergraduates (REU)* **Summer 2006**

➢ **Advisor:** A. P. Hickman, Lehigh University
Investigated the DR of c-$C_3H_3^+$and l-$C_3H_3^+$. Wrote a molecular dynamics program using the Lennard-Jones potential and Verlet algorithm to track the motion and interaction of the atoms in $C_3H_3^+$. GAMESS was used to calcualte a torsion force that can be adequately approximated using by a harmonic oscillator and to determine a spring constant.

**Publications**

"Calculation of dissociating autoionizing states using the block diagonalization method: Application to $N_2H$", A. P. Hickman, D. O. Kashinski, R. F. Malenda, F. Gatti and D. Talbi, J. Phys. Conf. Series **300**, 012016 (2011).

"A Comparative Study of the DR Reactions of c-$C_3H_3^+$ and l-$C_3H_3^+$: Preliminary Theoretical Studies", D. Talbi, A. .P. Hickman, D. O. Kashinski, and R. F. Malenda, J. Phys. Conf. Series **192**, 012014 (2009).

**Conference Presentations**

R. F. Malenda, D. O. Kashinski, D. Talbi, F. Gatti, and A. P. Hickman, 2011. Theoretical Studies of Dissociative Recombination of Electrons with $N_2H^+$ Ions. 42$^{\text{nd}}$ Annual Meeting of the APS Division of Atomic, Molecular, and Optical Physics, Atlanta, Georgia, USA, May, 2011.

➢ *Recieved $500.00 Student Travel Grant from DAMOP/APS.*

A. P. Hickman, D. O. Kashinski, R. F. Malenda, F. Gatti, and D. Talbi, 2010. Calculation of dissociating autoionizing states using the block diagonalization method: Application to $N_2H$. 8$^{\text{th}}$ International Conference on Dissociative Recombination (DR2010), Lake Tahoe, California, USA, August, 2010.

➢ *Recieved $1,000.00 Travel Support from NSF and NASA.*

D. O. Kashinski, R. F. Malenda, A. P. Hickman, D. Talbi, and F. Gatti 2010. Theoretical Studies of Dissociative Recombination. 41$^{\text{st}}$ Annual Meeting of the APS Division of Atomic, Molecular, and Optical Physics, Houston, Texas, USA, May, 2010.

D. O. Kashinski, R. F. Malenda, A. P. Hickman, and D. Talbi, 2009. Theoretical Studies of Dissociative Recombination. 40$^{\text{th}}$ Annual Meeting of the APS Division of Atomic, Molecular, and Optical Physics, Charlottesville, Virginia, USA, May, 2009.

D. O. Kashinski, R. F. Malenda, A. P. Hickman, and D. Talbi, 2008. Theoretical Studies of Dissociative Recombination. 39$^{\text{th}}$ Annual Meeting of the APS Division of Atomic, Molecular, and Optical Physics, State College, Pennsylvania, USA, May, 2008.

**Related Skills**

➢ Computing: GAMESS-US, MCTDH, LaTeX 2$\varepsilon$.
➢ High Performance computing using TeraGrid resources.
➢ Programming: C++, FORTRAN, Shell Scripting.
➢ Proficient in: Word, PowerPoint, Excel, WinEDT, Gnuplot, and OpenOffice.

**Professional Contacts**

Prof. A. P. Hickman
Department of Physics
Lehigh University
Bethlehem, PA 18015
Phone : (610)-758-3917
E-mail: aph2@Lehigh.edu

Prof. G. G. DeLeo
Department of Physics
Lehigh University
Bethlehem, PA 18015
Phone : (610)-758-3930
E-mail: lgd0@Lehigh.edu

Prof. J. P. Huennekens
Department of Physics
Lehigh University
Bethlehem, PA 18015
Phone : (610)-758-3926
E-mail: jph7@Lehigh.edu